Beam Constraint Model: Generalized Nonlinear Closed-form Modeling of Beam Flexures for Flexure Mechanism Design

by

Shiladitya Sen

A dissertation submitted in partial fulfillment
of the requirements for the degree of
Doctoral of Philosophy
(Mechanical Engineering)
in the University of Michigan
2013

Doctoral Committee:

Assistant Professor Shorya Awtar, Chair
Professor Carlos E. S. Cesnik
Professor Albert Shih
Professor Alan Wineman

To my mother, Ragasree Sen.

ACKNOWLEDGEMENTS

I would like to thank my advisor Professor Shorya Awtar for his guidance and support. His perseverance and constant dedication to research was a huge inspiration to me. He is directly responsible for teaching me everything I know of flexure mechanism. He developed in me the ability to physically understand a mathematical expression. Of the many positive experiences I have had during my doctoral degree I feel our brain-storming sessions were the most educational. I am truly grateful to him for believing in me.

I am grateful to my committee members, Professor Carlos Cesnik, Professor Albert Shih and Professor Alan Wineman. Their comments and suggestions were very useful. Additionally I also express my gratitude to Professor Samantha Daly and Professor Vikram Gavani for helping me develop my presentation skills.

I would like to thank my parents, Dr. Ragasree Sen and Dr. Sankar Sen for their continuous encouragement. My mother is probably the reason I started my Ph.D. degree. She is also the one who has inspired me to keep on trying even when research was tough. My father, on the other hand, was a patient listener to my problems and has always given me insight into the various goals of research.

A huge thanks has to go my wife, Titli, who made sure that I was up and functioning every day. She was always there for me in everything that I did in the past four years. My days with her in Ann Arbor are one of my most cherished memories.

Finally I would like to acknowledge the help given to me by my fellow graduate students of Precision Systems Design Laboratory, Gaurav Parmar, Kevin Shimotsu and Tristan Trutna. During my first semester, they assisted me in learning the initial skills required to run experiments and ANSYS^{TM} simulations for flexure mechanism. Later, they frequently reviewed my articles and my presentations.

TABLE OF CONTENTS

LIST OF FIGURES

LIST OF TABLES

ABSTRACT

Beam Constraint Model: Generalized Nonlinear Closed-form modeling of Beam Flexures for Flexure Mechanism Design

By

Shiladitya Sen

Chair: Shorya Awtar

Flexure mechanisms, also known as compliant mechanisms, provide guided motion via elastic deformation. Their ability to produce repeatable/precise frictionless motion makes them a common choice in precision positioning devices, frictionless bearings, biomedical devices and prosthetics. Traditionally, design of flexure mechanisms has been conducted in an intuitive manner using simplistic linear models. For flexure mechanisms where nonlinear effects that contribute to error motions and stiffness variations are present, designers have had to use computational methods such as finite elements modeling, which provides relatively limited design insight. This dissertation aims to create an alternative modeling tool that captures nonlinear effects in a simple closed form manner, so that the parametric variation of various performance attributes in flexure mechanisms can be easily studied. In order to make the design process more systematic, this approach breaks down flexure mechanisms to its building blocks that are referred to as flexure elements. The deformation mechanics of the two most common flexure elements, the flexure strip and the wire flexure, are analyzed in detail and the relations between the loads and displacements, applied and measured at the elements' end points, are determined. To ensure accuracy at an elemental level, pertinent geometric nonlinearities are captured. The effects of initial alignment errors, which are often present in flexure mechanisms in practice, are also studied in detail at the elemental as well as overall mechanism level. Furthermore, an analytical framework is provided in this dissertation that illustrates Newtonian

and energy methods to analyze flexure mechanisms constructed using multiple flexure elements. Overall, the novelty of this modeling technique lies in its ability to represent the relations between fully generalized spatial loads and spatial end-displacements (both translational and rotational displacement) over a relatively large range in a simple yet accurate manner. As a result, several complex mechanisms can be analyzed accurately without resorting to computational/numerical techniques or restricting the loading conditions.

Given the generality of the analytical models of the flexure elements, this formulation can be used in the future for optimization of flexure mechanisms in terms of shape/type/number of flexure elements as well as their spatial arrangement. Furthermore, this work can provide a foundation for a new nonlinear constraint based synthesis approach.

Chapter 1

Analysis of Flexure Mechanisms: Needs and Challenges

1.1 Flexure Mechanisms

Certain applications in Scanning Probe Microscopy (SPM) [1-3], Micro-Electro-Mechanical Systems (MEMS) [4-6], and semi-conductor wafer inspection/production instrumentation [7, 8] require motion guidance systems capable of nanometric precision/repeatability, which is difficult to achieve with mechanisms that have traditional revolute and prismatic joints (e.g. Figure 1.1(a)). The precision of such traditional motion systems, defined as the ability to move to the same commanded position repeatedly, is degraded severely by friction and backlash in the sliding joints. In comparison, a flexure mechanism, also known as a compliant mechanism, generates the required motion using elastic deformation (e.g. Figure 1.1(b)) rather than the using sliding or rolling motion in traditional joints and therefore is capable of achieving high precision by eliminating friction. Additionally when flexure mechanisms are made from elastic and low-hysteresis metals such as Aluminum (e.g. AL6061-T6) and Steel (e.g. AST), the generated motion can be highly repeatable allowing the mechanism to operate with sub-nanometer precision. Other advantages of using flexure mechanisms include minimal requirement of assembly, maintenance, and lubrication. As a result, flexure mechanisms enable nanopositioning systems that are used extensively in not only the above-mentioned applications but also in Dip-Pen Nanolithography [9, 10], Nano-shaving and Nano-grafting [11], nanometrology [2, 12] and memory storage [13]. Other than nanopositioning stages, several other application also exist such as micro-robotics [14], micromanipulation [15], micro-grippers

[16], force/torque sensors [17], MEMS gyroscopes [18] and accelerometers [19], bio-mimicking compliant fingers [20], electrostatic micro-mirrors [4, 21, 22] and energy harvesting [23]. With these target applications, this thesis focuses primarily on the 'analysis' part of the design process of flexure mechanisms. In general, the design process also includes 'synthesis' and 'optimization', which are not covered here.

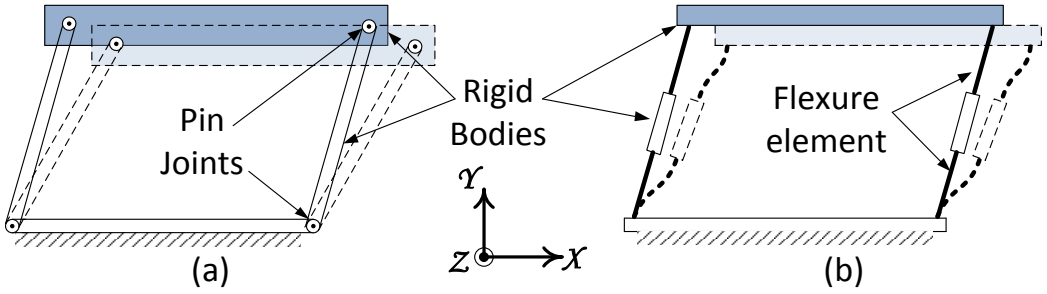

Figure 1.1: Parallelogram mechanism using (a) rigid bodies with pin joints and (b) flexure elements

Certain other flexible elements such as aircraft wings and live hinges of bottle caps require a different type of design approach to achieve their respective specifications. In the case of aircraft wings, shape optimization is the primary objective. Such a study would require an in-depth understanding of the loads due to the air flowing over the wings. In the case of live hinges, creating designs that are less susceptible to failure due to fatigue is the primary objective. This would require the appropriate use of failure mechanics. Although both these areas of research are important and should be included in the design of flexure mechanisms from an overall perspective, this dissertation focuses primarily on a different but also important requirement of a design process that is in obtaining knowledge of elastic and kinematic behavior of beam-like flexure elements. However, as will be shown later, this analysis given in this dissertation also provides a foundation of beam shape optimization.

Analysis of a flexure mechanism entails its mathematical modeling using knowledge from solid mechanics. This mathematical model provides estimates of the output motions of the flexure mechanism when subjected to actuation loads[1]. The motion of any flexure mechanism at a predetermined point of interest on a rigid motion stage may be sufficiently characterized by six independent displacements[2]. Each independent motion has an associated stiffness defined as the

[1] Throughout this dissertation, 'loads' is used in a generalized sense to mean forces and moments.
[2] Throughout this dissertation, 'displacements' is used in a generalized sense to mean translations and rotations

rate of change of load with respect to displacement along the direction of the load. Depending on the relative magnitude of the stiffness values, the independent directions are classified as Degrees of Freedom (DoF) and Degrees of Constraint (DoC) [24]. A DoF refers to a direction in which motion is intended to occur and hence the associated stiffness is designed to be relatively low. In Figure 1.1 motion along the X axis is a DoF. A DoC refers to any direction in which motion is undesired and hence the associated stiffness is designed to be relatively high. In Figure 1.1 translations along Y and Z axis as well as rotations about the X, Y and Z axes are DoCs. A quantitative estimate of the stiffness along DoFs and DoCs is of paramount importance in designing flexure-based motion guidance systems and is one of the goals of any flexure mechanism analysis technique.

In addition to accurately estimating the stiffness values in various directions, it is also important to model motions produced in all other directions in response to a load along one DoF. These motions are called error motions and are generally undesired [24]. Error motions may be further divided into 'parasitic motions' that occur along other DoCs and 'cross-axis coupling' that occurs along other DoFs. Typically, the stiffness values and error motions of a flexure mechanism together define its constraint characteristics and their accurate modeling over the entire load and displacement range of interest forms the primary focus of this dissertation.

1.2 Requirements of Analysis Techniques

In order to facilitate the analysis of any flexure mechanism, this thesis aims to develop suitable analytical models of those flexure elements that are used as building blocks in flexure mechanism design. One of the most common flexure elements is a flexure strip, shown in Figure 1.2(a), and is characterized by a length that is generally at least 20 times the thickness, while the width is of the same order of the length. For the flexure strip, the translation along Y direction and rotations about X and Z direction of its end point are regarded as DoFs. The flexure strip under planar loading, which consists of forces along X and Y and moment along Z, is also known as a simple beam flexure or cantilever beam because it deforms primarily in one plane (XY plane in Figure 1.2). Another common flexure element is the spatial beam flexure (Figure 1.2(b)) which is characterized by the length being at least being 20 times larger than both

thickness and width. This flexure element, at times known as wire flexure, provides five DoFs: two translations along Y and Z axis and three rotations about X, Y and Z axis.

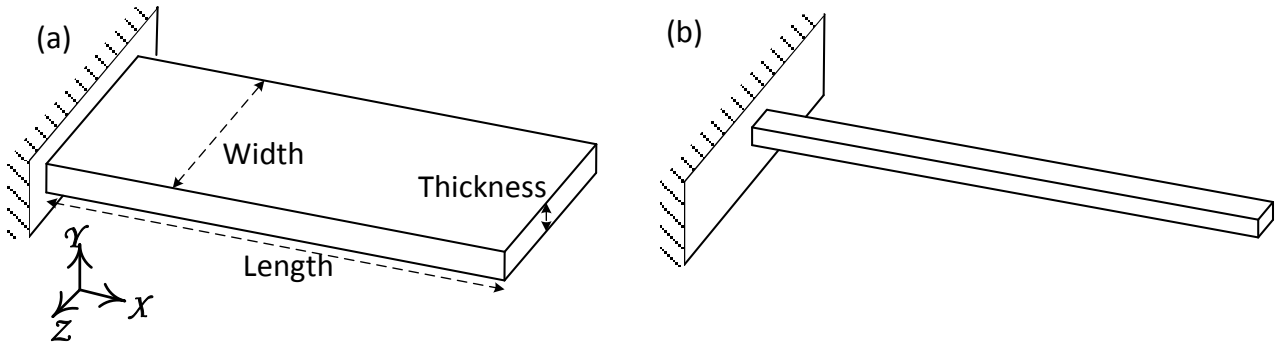

Figure 1.2: (a) Flexure Strip (b) Spatial Beam Flexure

Although the beam mechanics of either element is described via differential equations of load equilibrium and geometric compatibility in literature [25-28], this thesis aims to go a step further and obtain a model of flexure elements that provides load-displacement relations in a closed-form manner rather than using differential equations. Typically, such a model mathematically relates the resulting displacement due to an applied load using intuitive algebraic functions rather than differential equations. Essentially these models alleviate the need to start from first principles of beam mechanics and hence are more suited to technical design. However, the model should still powerful enough to analyze several complex flexure mechanisms. This can be done by combining the individual models of these flexure elements such that analytical relations between different variables (loads, displacements, geometry) pertinent to design process are derived.

Other than generality, a model should be easy to derive accurate, physical and analytical design insights of any flexure mechanism or a general mechanism topology. These insights generally include parametric dependence of constraint characteristics on the topology and various dimensions of the flexure mechanism, over a practical range of loads and displacements. An analytical model should also allow for an effective optimization of the mechanism's dimensions and provide an understanding of the various performance tradeoffs associated with its topology.

The required properties of an ideal model of a flexure element, namely closed-form load-displacement relations, accuracy, ability of capture manufacturing defects and compatible

closed-form strain energy, are discussed in more detail in the following three sub-sections. Furthermore, inadequacies of previous models of flexure elements in each of these criteria are also highlighted.

1.2.1 Closed-form Model

Design insights are most simply understood when the mathematical model of the flexure mechanism is closed-form that is the relation can be expressed in terms of a finite number of 'well-known' functions. These functions typically include algebraic functions with finite number of terms, n^{th} roots, exponents, logarithmic, trigonometric and inverse trigonometric functions. A closed-form function typically does not require computational/iterative methods, infinite series solutions or look up tables to determine its value. To gauge the importance of a closed-form model let us compare a parallelogram flexure module (Figure 1.3(a)) and a double parallelogram flexure module (Figure 1.3(b) and (c)). These two mechanisms are often used to guide straight line motion. Although the double parallelogram module generates more accurate straight line motion, its X-stiffness $K_X = dF_X / dU_X$ degrades much faster than that of the parallelogram flexure module. A comparison of the X-stiffness values of the two flexure modules is shown in Figure 1.3 (d) that is generated using analytical models in Eq. (0.1) based on Euler beam theory[3] [29, 30]. Here, the elastic modulus is given by E while the moment of area about the bending axis is given by I. The length and in-plane thickness of the flexure beams are given by L and T, respectively, while the displacement of the motion stage along the Y direction is given by U_Y.

$$K_X^P = \frac{24EI}{L\left(T^2 + 0.0014U_Y^2\right)}, \quad K_X^{DP} = \frac{12EI}{L\left(T^2 + 0.0014U_Y^2 + 0.03U_Y^2\right)} \tag{0.1}$$

The analytical expression in Eq. (0.1) shows the nonlinear variation of axial stiffness in the parallelogram and double parallelogram flexure module that occurs due to the presence of U_Y^2 terms in the denominator. To explain this variation in axial stiffness in the two flexure module in detail, we divide the source of X-displacement due to axial force $\boldsymbol{F_X}$ in three

[3] Euler beam theory assumes 'plane sections remains plane and perpendicular to the neutral axis' leads to a proportionality relation between curvature and bending moment. This assumption is fairly accurate when beam thickness is no more than 1/20 of the beam length.

fundamentally different effects, linear elastic stretching, distributed compliance of flexure elements and load-equilibrium in the deform configuration.

The first source is simply the linear elastic stretching of the beams along the X direction. This occurs in both the parallelogram and double parallelogram flexure module.

The second source of the X displacement, represented by the '$0.0014U_Y^2$' term in Eq.(0.1), is the distributed compliance of the beam flexures that are the building blocks of the two mechanisms. In order to physically understand this effect, we acknowledge the presence of an additional bending moment $\boldsymbol{F_X}\times U_Y$ when an axial load is applied to a motion stage that has already moved in the Y-direction by U_Y. This additional bending moment 'uncurls' the already deformed S-shaped beam flexures. If the Y-displacement of the beam flexure end point is kept constant, the uncurling effect solely results in an increase of the 'X-span' of the beam flexure due to conservation of arc-length, thus resulting in additional X-displacement at the end of the beam flexure. For the mechanism, the axial load causes an additional X-displacement of the motion stage in the presence of U_Y due to the uncurling of the component beam flexures. Overall, this implies a reduction in the x-stiffness of the flexure mechanism. Since this additional X displacement requires the presence of both the load $\boldsymbol{F_X}$ and the displacement U_Y, this is known as the elasto-kinematic effect [30]. Also, as uncurling is impossible for a flexure element with lumped compliance, we note that elasto-kinematic effect is fundamentally property of flexure elements with distributed compliance alone.

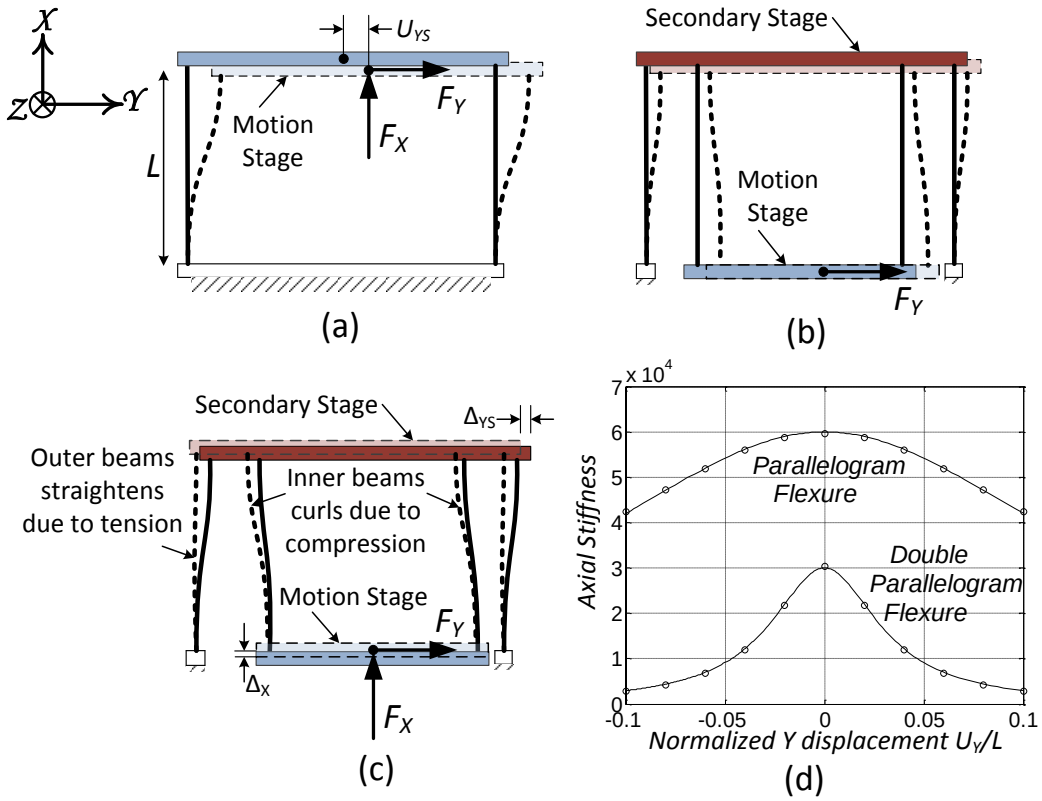

Figure 1.3: (a) A parallelogram flexure module shown in the deformed and undeformed configurations (b) A double parallelogram flexure module in the undeformed and deformed configurations (c) Change in deformation of a double parallelogram flexure module due to force along X when the Y-displacement is held fixed (d) Variation of axial stiffness of parallelogram and double parallelogram flexure modules with displacement along Y

The third source of X-displacement, represented by the '$0.03U_Y^2$' term in Eq. (0.1), is a purely kinematic effect as it results from applying the load-equilibrium in the deformed configuration. A convenient way of physically understanding this effect is to first recognize the load-stiffening effect [30] which is direct result of load equilibrium applied in the deformed configuration. It states that the Y-stiffness of a flexure element is higher when in tension and the amount of stiffening is proportional to the axial stretching force. Similarly, the Y-stiffness of a flexure element is lower when in compression. This effect is discussed in more detail in section 1.2.2.1. Using this concept of load-stiffening in the double parallelogram flexure module, we find that an application of $\boldsymbol{F_X}$ on the motion stage in the positive X direction as shown in Figure 1.3 (c), causes the inner parallelogram to be in compression while the outer parallelogram to be in tension. As a result the Y-stiffness of inner parallelogram is reduced while the Y-stiffness of the outer parallelogram is increased.

We will now use the understanding of the load-stiffening effect in the following loading condition of the double parallelogram flexure module. First a bending force $\boldsymbol{F_Y}$ is applied to the motion stage as shown in Figure 1.3(b). We notice that the motion stage moves by U_Y. Since the Y-stiffness of the inner and outer parallelogram is the same the secondary stage moves by $U_Y/2$. Additionally the secondary stage also moves in the X-direction due to the conservation of arc-length of the flexure elements. Next an axial force $\boldsymbol{F_X}$ is applied while the Y-displacement of the motion stage is held constant. As we discussed earlier, in the presence of the axial force, the Y-stiffness of inner parallelogram reduces while that of the outer parallelogram increases. This implies that the inner parallelogram bends more while the outer parallelogram straightens. The net effect is that the secondary stage moves in negative Y direction by an amount Δ_{YS} while the motion stage to move further in the positive X direction by Δ_X due to arc-length conservation. Since the original cause of this additional X-displacement is $\boldsymbol{F_X}$, this effect is another source of drop in the axial stiffness. Such an effect is not possible in a parallelogram flexure module due to the absence of a secondary stage.

Now, as an alternative, let's try to analyze the same problem using finite element analysis (FEA). By running multiple simulations and monitoring the displacements of the motion stage, one may arrive at the expressions of Eq. (0.1) using regression techniques. However, it is impossible to separate the '$0.0014U_Y^2$' and the '$0.03U_Y^2$' terms in such a procedure, and to recognize that these two terms arise from two fundamentally different sources. The elasto-kinematic and kinematic sources that lead to the drop in axial stiffness in this case are numerically combined in the data and do not give the reader any insight into ways to deal with them individually. The only way to derive insights via FEA is to look at the Y displacement of the secondary stage rather than the motion stage. However, this is not obvious and depends on the intuition and experience of the designer. Herein lies the advantage of a closed form model, which makes finding such insights and associated systematic solutions. For example, the closed-form eqs (0.1) tell us that although the elastokinematic effect represented by the '$0.0014U_Y^2$' term is inherent in any distributed compliance flexure mechanism, the kinematic effect represented by the '$0.03U_Y^2$' term is approximately eliminated by constraining the 'Δ_{YS}' displacement of the secondary stage to be exactly half that of the motion stage. An example of such a design can be found in reference [31] where the 'Δ_{YS}' displacement of the secondary stage

is constrained by additional topological features. The resulting modified double parallelogram flexure module obtained the superior stiffness characteristics of the parallelogram flexure module while retaining the superior straight line motion characteristics of the double parallelogram flexure module.

Given the clarity in understanding the operation of parallelogram and double parallelogram flexure mechanism that is brought by their individual closed form model, we set ourselves the goal of closed-form modeling of flexure elements in this dissertation so that we can generate closed-form models of other flexure mechanisms as well. It should be noted that throughout this dissertation only end loading of flexure elements is considered. Distributed loading in flexure elements that may occur, for example, due to its own weight is ignored. This is a good approximation in most flexure mechanisms as the mass of the rigid stages are generally much higher than the flexure elements. Other types of distributed beam loading, such as inertial forces due to dynamics, are also not considered here since we are focusing on quasi-static design and performance.

1.2.2 Accuracy versus complexity of the model

The second critical aspect of any analysis technique is its accuracy. In order to ensure accuracy, the nonlinear relations between displacements of flexure elements and the applied loads need to be captured. The significance of the nonlinearity can be easily gauged in the example of the double parallelogram flexure, in section 1.2.1, in which the DoC stiffness is shown to drop by more than 90% with increasing DoF displacements. However, due to nonlinearity, obtaining a closed-form model that perfectly describes the deformation of flexure elements is generally non-feasible. By restricting the amount of deformation as well as considering certain specific beam geometries (listed previously), simplifying assumptions may be made in order to model these flexure elements in the simplest way.

An Euler beam formulation [29] is a classic example of the use of pertinent assumptions that lead to useful models of beam-like flexure elements applicable under planar loading conditions[4]. Euler beam formulation is a good approximation when the in-plane thickness is

[4] Planar loading refers to one bending moment normal to the plane of bending and two mutually perpendicular forces in the plane of bending.

small with respect to the length of the beam and the out-of-plane width of the beam is either small (comparable to the in-plane thickness) or very large with respect to the length of the beam. The first case, when out-of-plane width of the beam is small, is an example of plane stress. On the other hand the case, when out-of-plane width of the beam is large, is an example of plane strain. Both the cases can be well-handled via a 2-D planar model derived from the general 3D model by ignoring variations in stress or strain, whichever is applicable, along the width of the beam. Under these conditions only bending effects are significant while shearing effects are negligible. A Timoshenko beam [32], on the other hand, takes shear effects into account also and is therefore applicable to short stubby beams with planar loading. More details on these beam formulations will be given in section 1.4.

In order to obtain the best tradeoff between closed form representation and accuracy in an optimal model for beam flexures, it is important to understand the physical significance of various nonlinearities in determining the constraint characteristics of flexure mechanism. The geometric nonlinearities of beam deformation are discussed in following four sub-sections.

1.2.2.1 Nonlinearity due to arc length conservation, equivalent to applying load-equilibrium in deformed configuration

The popular Euler beam formulation is capable of capturing nonlinearities due to arc-length conservation and curvature for planar loading cases. First, let us understand the nonlinearities incurred due to arc-length conservation. Figure 1.4(a) shows that the displacement U_{YL} resulting from beam bending also causes the beam end-point to move closer to ground in the X direction in order to ensure that the arc-length of the beam is equal to its original length plus the small extension due to axial load $\boldsymbol{F_{XL}}$. In terms of constraint characteristics, this means there is an unintended and generally undesired X motion at the end of the beam (a parasitic error motion) when it is actuated only in the Y direction. Furthermore, the end loads also move along the end of the beam causing additional bending moment from $\boldsymbol{F_{XL}}$. This causes a change in the stiffness values dF_{YL}/dU_{YL} and dF_{XL}/dU_{XL} in the Y and X directions respectively from their nominal values[5]. Since variation of dF_{YL}/dU_{YL} occurs due to the inclusion of F_X in calculating load equilibrium, it is called a load-stiffening effect [30, 33]. Since this stiffening affect arises

[5] The nominal value of dF_{YL}/dU_{YL} and dF_{XL}/dU_{XL} of a flexure beam with one fixed end and one free end is $EI/3L^3$ and EA/L, respectively, where all symbols have their usual meaning.

due to the geometrically finite displacements in the Y direction, it is also sometimes referred to geometric stiffening [34].

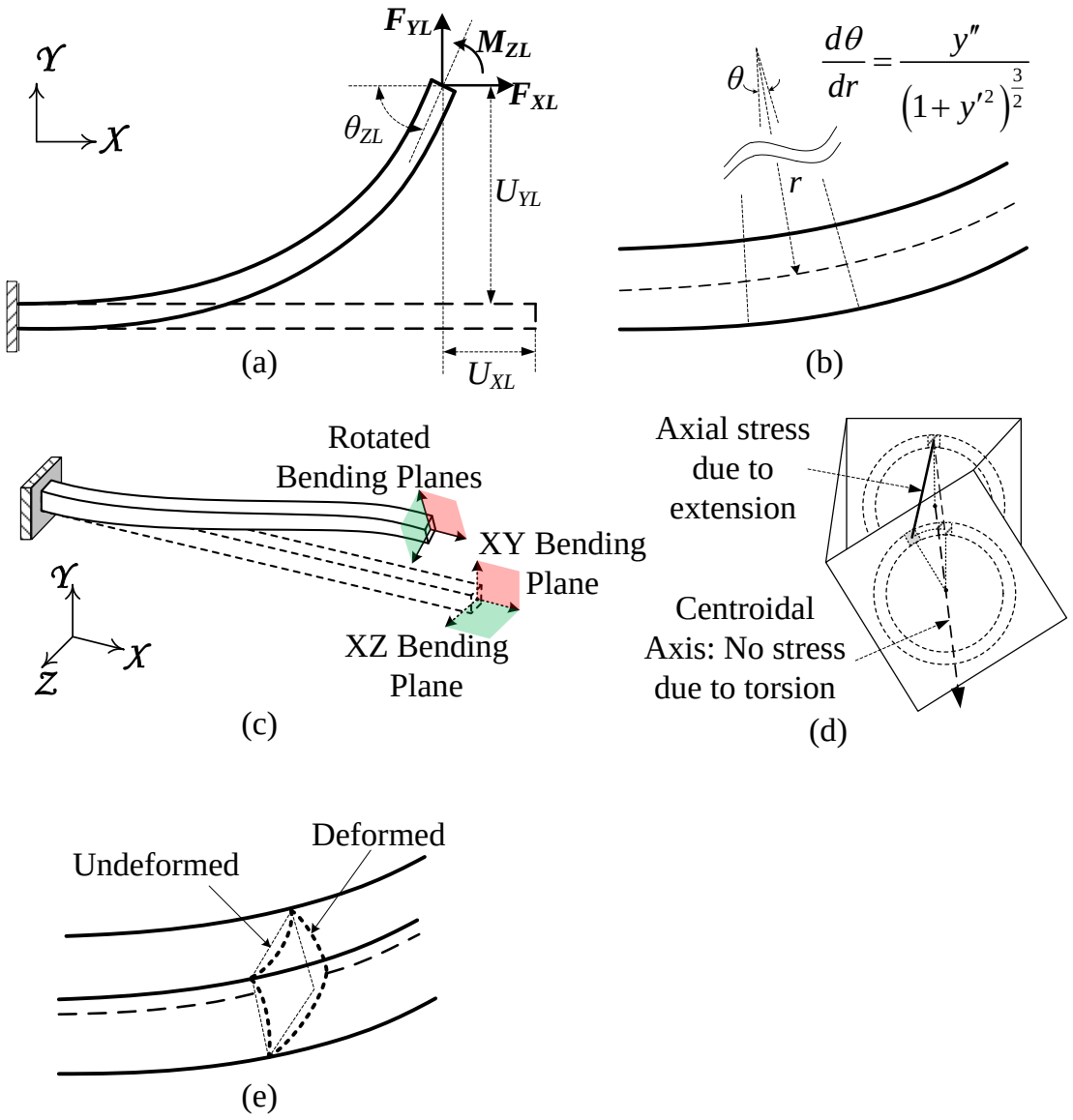

Figure 1.4: (a) Bending of beam causes nonlinear kinematic coupling between U_X and U_Y (b) Nonlinear curvature of a beam undergoing bending (c) Rotation of bending planes due to torsion (d) Trapeze effect due to torsion (e) Deformation of cross-section of a beam undergoing bending

It should be noted that the stiffness $dM_{ZL}/d\theta_{ZL}$ is also affected by the load stiffening effect in a fashion similar to dF_Y/dU_Y. On the other hand, a reduction in the dF_{XL}/dU_{XL} stiffness occurs due to the change in shape of the beam, which is caused by the additional bending moment produced by $\boldsymbol{F_X}$ and in turn the effect of this change on arc-length conservation.

This effect is known as the elasto-kinematic effect. A more detailed explanation was given earlier in section 1.2.1 using the comparison of the X-stiffness of parallelogram and double parallelogram flexure module.

1.2.2.2 Nonlinearity due to curvature

The curvature, the formula for which is given in Figure 1.4(b), is nonlinear when the deformation is expressed in terms of the co-ordinates of the deformed beam (X, Y). This nonlinearity affects the stiffness values in the X and Y directions as well as error motions in the X direction due to Y displacement. If, however, the curvature expressed in terms of the undeformed beam co-ordinates, a slightly different formula for the curvature is derived [35]. This formula of beam curvature will be discussed in Chapter 2. However in both representations of curvature, nonlinearity is present. In order to estimate the effect of this nonlinearity we compare U_{YL} for a given $\boldsymbol{F_{YL}}$, from two Euler beam formulations, one using the accurate formula for curvature and the other using a linearized formula of curvature (i.e. approximating the denominator of the curvature formula to 1). We find that the discrepancy increases cubically with increasing U_{YL}. A discrepancy of 3% occurs in estimating U_{YL} for a given $\boldsymbol{F_{YL}}$, when U_{YL} of approximately 0.1 times the length of the beam flexure, and 5% when U_{YL} is 0.2 times the length of the beam flexure (see Figure 1.5). Similar trend is found for θ_{ZL}. In contrast, end-displacement in the X-displacement is related in a quadratic manner to U_{YL} due to arc-length conservation. Therefore error in U_{XL} is approximately twice the error in U_{YL}. Although preserving curvature nonlinearity helps improve the accuracy in estimating the nominal stiffness values in transverse bending direction and associated error motions, it does not result in any new physical effects.

1.2.2.3 Nonlinearity due to torsion

When spatial loading (i.e. all six general forces and moments) of beams is considered, in addition to the effect of nonlinearities due to arc-length conservation and curvature, there is also nonlinearity due to torsional moment $\boldsymbol{M_{XL}}$. As shown in Figure 1.4(c), the bending of beams can be viewed as bending in two planes. In the absence of torsion these bending planes are the XY plane and XZ plane. However when torsion is present, these bending planes rotate about the centroidal axis[6]. Additionally, the amount of rotation, rather than being constant with X, is

[6] Centroidal axis of a beam is the locus of the centroids of all the cross-sectional areas of the beam

actually dependent on the applied twisting moment $\boldsymbol{M_{XL}}$ and varies with X. As a result, a portion of the displacements in the XY plane, i.e. U_Y and θ_Z, is contributed by the bending loads of the XZ plane, i.e. $\boldsymbol{F_{ZL}}$ and $\boldsymbol{M_{YL}}$, and vice versa. This is a form of cross-axis coupling error motion because displacements occur in DoF directions that are not along the actuating load. Additionally, the magnitude of error motion is proportional to the twisting moment $\boldsymbol{M_{XL}}$. This nonlinearity, pertinent only to spatial loading conditions, will be discussed in more detail in Chapter 4 and 5.

1.2.2.4 Nonlinearity due to trapeze effect

A small nonlinear effect that results in shortening of the beam due to torsion, called the trapeze effect, is also present in spatial beam deformation. As shown in Figure 1.4(d), when a beam twists, applying arc length conservation to the fibers parallel to the centroidal axis shows that the fibers away from the centroidal axis contract more than the ones nearer to it, thus producing a tension on the outside fibers and contraction on the centroidal fibers. This results in an overall or net compressive axial stress in the beam which results in a slight shortening of the beam arc-length. As a corollary effect, it is also seen that a beam in tension has a higher torsional stiffness. This complementary relation is further explained in Chapter 4 Section 4.3. Although the trapeze effect results in small error motions and small stiffness variations under normal circumstances, it may be significant in the presence of large axial loads and/or absence of any bending loads.

1.2.2.5 Nonlinearity due to cross-sectional warping

Finally, nonlinear relations between loads and displacements may result from initially plane cross-sections that do not remain plane after deformation (Figure 1.4 (e)). The cross-section may dilate in-plane (increase or decrease in area) due to Poisson's effect, and distort in-plane (a rectangle becoming a parallelogram) or warp out-of-plane (bulge along the centroidal axis) due to shear effects. Cross-sectional deformation gives rise to several complex effects such as variations in cross-sectional moment of area and variation in extension stress as well as shear stress. However, for slender beams, it has been found that cross-sectional distortion and warp does not significantly affect beam bending which may still be analyzed with Euler beam assumptions of plane cross-sections remaining plane and perpendicular after deformation. For

torsion calculations, cross-sectional deformations need to be considered [36]. However, in practice, the torsional analysis incorporating the cross-sectional deformation can be done separate from the beam bending analysis and the total effect of warping on beam deformation can be captured by using in an effective torsional constant instead of the traditional torsional moment of area. This torsion constant is specific to a chosen cross-section and its standard formulas for various cross-sections are readily found in several books [25].

Since, inclusion of all nonlinearities renders the possibility of a closed form model extremely challenging if not inconceivable, only some of nonlinearities can be considered while others are approximated or assumed to be negligible. From an analysis stand-point, it is challenging to determine which ones to retain and which ones to drop. In the proceeding section on literature survey of existing beam modeling approaches we will see that the nonlinearity due to arc-length conservation and torsion is given most importance while other sources of nonlinearity are generally approximated or ignored. In addition, in Chapters 2 through 5, nonlinearities that are relevant to each respective flexure element will be revisited and all simplifying assumptions taken to capture them in a closed-form manner will be discussed.

1.2.3 Energy Formulation and Manufacturing Variations

Other than the fundamental requirement of balancing representation and accuracy, there are two other features that are required to make an analytical model of beam flexure elements practically useable. Firstly, the model should be such that it enables the study of flexure mechanisms that comprise multiple flexure elements. Rather than using free body diagrams and load equilibrium for each individual flexure element of a flexure mechanism, it is often easier to use an energy based approach such as the principle of virtual work [37] (PVW) given by Eq.(0.2) , which states that at equilibrium the virtual work done by external forces over a set of geometrically compatible but otherwise arbitrary ‘virtual’ displacements is equal to the change in the strain energy due to these ‘virtual’ displacements.

$$\delta W = \delta V \tag{0.2}$$

Mathematical complexity is less for energy methods because the number of unknown variables that need to be determined are reduced by eliminating internal forces from consideration. Furthermore since the formulation is based on simple mathematical operations

like addition of strain energies and variations, it is easy to handle a large number of flexure elements. Therefore, in order to facilitate this approach, a model of a beam flexure should also include its total strain energy expressed in terms of its end-displacements.

Secondly, the analytical model should be able to take into account small dimensional variations due to inevitable manufacturing defects. The manufacturing defects could be of various types, for example: a) Non-straight undeformed configuration of a beam due to initial curvature and orientation which can become an important factor in intentionally over-constrained designs [38], and b) Small variations in cross-sectional area resulting in a varying moment of area along the beam length.

Formulating a nonlinear closed form models for beam-like flexure elements that satisfies all the above mentioned criteria will be helpful in not only improving design methods for flexure mechanisms but also in developing optimization tools and understanding their nonlinear dynamics. With this goal, we move forward to studying previous analytical models of flexure elements.

1.3 Literature Survey on Analytical Models for Slender Beams

Formulating a closed-form analytical model that satisfies all the requirements given in the previous section is challenging primarily due to the presence of nonlinearities associated with the deformation of the flexure strip and spatial beam flexure. Instead of finding a perfect solution to the problem, we aim to find the best possible tradeoff between retaining accuracy and obtaining closed-form representation.

Research on analysis of deformation of solid continua is said to have started with Galilei [39] in the 17^{th} Century, when Galilei tried to find the resistance of a beam from breaking due to its own weight when one of its end is fixed to a wall. Since then, there has been much work done in order to understand and develop analytical tools to help engineers analyze and design mechanisms and structures. In order to get a perspective of where this doctoral dissertation fits in the entire body of work of solid mechanics, a brief literature survey is presented next.

The first step to answer Galilei's question was taken by Hooke when he presented the proportionality between stress and strain in 1678 [40]. This finding was experimentally verified by Marriotte in his works published in 1680 [41]. James Bernoulli in 1705 conducted the

investigation of the existence of compression and extension of fibers in a bent beam under its own weight [42]. In his equations, Bernoulli showed that the stress at a cross-section generates a couple proportional to the curvature. This was the key assumption taken by Euler and Daniell Bernoulli in 1744 in deriving the equation of vibration of beams [43, 44]. Later in 1776, Coulomb determined the equation of equilibrium at a cross-section and defined the neutral line, which was also known as the axis of equilibrium. Coulomb was also the first one to look at a beam's resistance to torsion and a beam's ability to shear without rupturing [45]. In parallel to Coulomb's work, Young found the elastic modulus of solid continua [46]. Young was also the first one to consider shear as a type of strain. By the end of the 18th century, one might say that the basics of solid mechanics were established.

In the 19th century the focus shifted on finding a generalized theory of stress-strain relations. One of the notable works in this area was presented by Cauchy in 1827 [47-49]. In his work, Cauchy described the stress and strain at a point in terms of six independent quantities and derived the properties of stress-strain relations. He also found the principle stress and strains. Similar results were also independently found by Lamé in 1833 [50]. The finite strain measure, which may be used to derive Cauchy's stress, was presented by Green in 1837 [51]. St. Venant, a contemporary mathematician, showed the effects of different but statically equivalent loads become indistinguishable at sufficient large distances from the load in 1855 [52, 53]. Additionally St. Venant was also first to mathematically derive the exact solution for pure torsion of prismatic bars.

The development of generalized theory of stress-strain relations was aided throughout the rest of the 19th century by several scientists. Among them, names worth mentioning are those of Navier, Stokes, Poisson, Kirchhoff, Thompson and Maxwell. However, giving details of each of these seminal scientists is beyond the scope of this dissertation. It suffices to say that by the end of the 19th century, a vigorously verified generalized theory of deformation of solids was available. Books by Love [27] and Truesdell [54] give a comprehensive historical account of the work done on deformations of solids.

Based on the generalized theory of stress and strain, several analytical models of relevant solids can be derived. The simplest beam model is formulated using a linearized application of Euler-Bernoulli beam theory [29]. In this model, the bending and torsional moments are calculated assuming that the applied loads do not move with displacement. Additionally

curvature is also approximated as a linear function of displacement. Furthermore, X displacement of the beam end (Figure 1.4(a)) due to arc length conservation is ignored. These assumptions and approximations imply that all geometric nonlinearities are dropped and a simple model is obtained, as given in Eq.(0.3). This model predicts a linear relation between the loads and displacement and hence will be referred to as the linear model henceforth. It should be noted that while shear effects, which are also linear, can be easily added to the linear model as per Timoshenko Beam Theory, it is not included here as the beam is assumed to be long with respected to its width and thickness.

$$\begin{Bmatrix} \frac{\boldsymbol{F}_{YL}L^2}{EI_{ZZ}} \\ \frac{\boldsymbol{M}_{ZL}L}{EI_{ZZ}} \\ \frac{\boldsymbol{F}_{ZL}L^2}{EI_{YY}} \\ \frac{\boldsymbol{M}_{YL}L}{EI_{YY}} \\ \frac{\boldsymbol{F}_{XL}}{EA} \\ \frac{\boldsymbol{M}_{XL}L}{GJ} \end{Bmatrix} = \begin{bmatrix} 12 & -6 & 0 & 0 & 0 & 0 \\ -6 & 4 & 0 & 0 & 0 & 0 \\ 0 & 0 & 12 & 6 & 0 & 0 \\ 0 & 0 & 6 & 4 & 0 & 0 \\ 0 & 0 & 0 & 0 & 1 & 0 \\ 0 & 0 & 0 & 0 & 0 & 1 \end{bmatrix} \begin{Bmatrix} \frac{U_{YL}}{L} \\ \theta_{ZL} \\ \frac{U_{ZL}}{L} \\ \theta_{YL} \\ \frac{U_{XL}}{L} \\ \theta_{XL} \end{Bmatrix} \tag{0.3}$$

The assumptions and approximations upon which the linear model is based become increasingly inaccurate with increasing displacements. To verify this, a case study is shown in Figure 1.5 where the beam shown in Figure 1.4(a) is subjected to an end-load $\boldsymbol{F}_{YL}$ and the end-displacement U_{YL} is studied. The accuracy of the linear model is verified against an exact solution of Euler beam theory for this particular loading using elliptic integral that can be found in reference [55]. In addition to the prediction of the linear model and the exact model, the predictions of a finely meshed Finite Element Model (FEM) with solid elements (ANSYS Element # SOLID186), beam column theory and Planar Beam Constraint Model (PBCM) is also included in Figure 1.5 for comparison. The beam length, width, thickness, elastic modulus, Poisson's ratio and $\boldsymbol{F}_{XL}$ were 0.1m, 0.005m, 0.0025m, 210GPa, 0.3 and 200N, respectively.

As can be seen in Figure 1.5, only when deformations are very small (of the order of the in-plane thickness of the beam) the linear model captures the displacements at any point on the

beam within acceptable errors which is empirically taken as 5% of the actual displacement. The error increases significantly when load $\boldsymbol{F_{XL}}$ is also present in addition to $\boldsymbol{F_{YL}}$. This is expected because, for finite displacements, $\boldsymbol{F_{XL}}$ produces additional bending moment which needs to be taken into account. Additionally, when end-displacement, U_{YL}, is more that 10% of the length of the beam, linearization of curvature is no longer a good approximation.

It should also be observed that FEM predictions are in good agreement with the exact beam solution for the entire range of displacements. This is expected because FEM in ANSYS can 'turn on' the effect of geometric nonlinearities using the NLGEOM command. By doing so, FEM is capable of taking into account bending moments from all loads as well as the nonlinearities associated with curvature. Although not shown here, FEM was found to be accurate for beams with various other loading conditions as well. This is because FEM beam and plate elements (BEAM188, SHELL181) include the fundamental deformations such as extensional strain, shear strain and cross-sectional warping. Therefore physical effects that arise due to these deformation are accurately captured. Since the behavior of flexure elements that we are trying to capture align with the capability of FEM, for the rest of this dissertation, we will use FEM as reference for exact displacement predictions to given loading conditions.

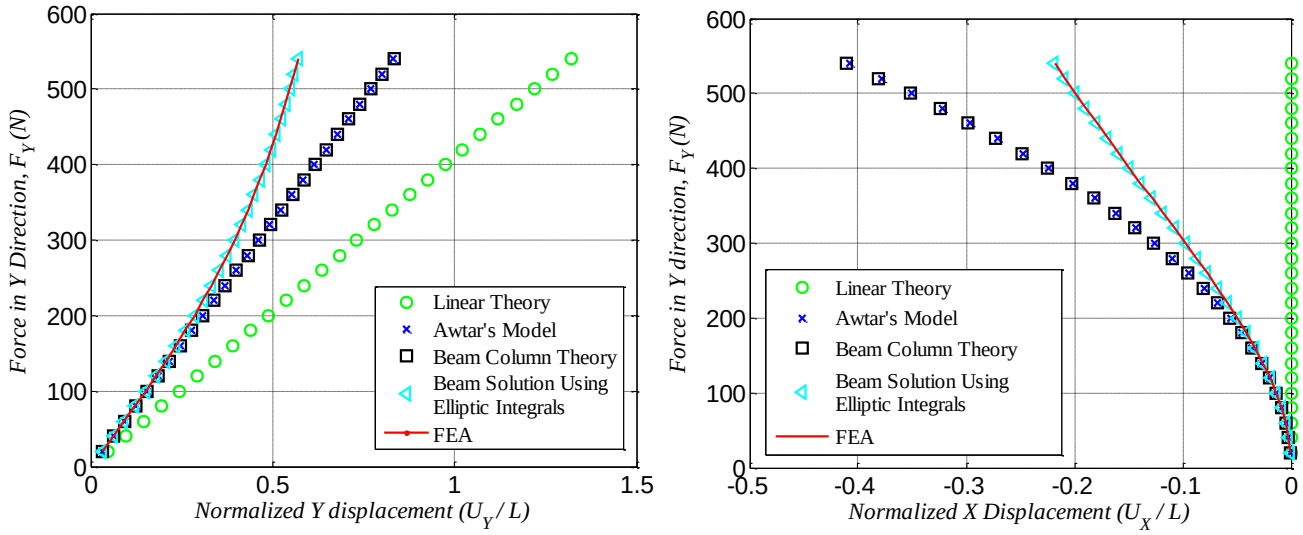

Figure 1.5: (a) Comparison of Y end-displacement for various planar beam formulations (b) Comparison of X displacement for various planar beam formulations

Although the exact beam solution using elliptic integrals is of limited use in design due to its non-closed-form nature, it may be used to derive a different model that is more suitable for

design. One such model is the Pseudo-Rigid body model (PRBM) that represents planar flexure beams as equivalent rigid link mechanisms in order to capture some of their constraint characteristics. PRBM was initiated by 1995 by Midha and Howell [56] by identifying that the end of a planar beam moves approximately in a circular path when subjected to a force at the end of the beam, perpendicular to the tangent of the neutral axis at the same point (Figure 1.6(a)). This hypothesis may be shown to be true using the exact beam solution [55]. Using regression techniques an optimal choice of rigid link, centered at the proper location with an appropriate torsional spring may to chosen to track the displacement of the beam end within a few percentage of error as shown in Figure 1.6(b). The length of the rigid link, the center of rotation and the torsional spring stiffness about the center of rotation is found to be dependent on the length of the planar flexure element as well as the load applied. In effect, this model converts distributed compliance of a planar beam flexure into lumped compliance of the torsional spring. The model, even though computationally derived, is parametric and therefore helps in subsequent analysis of more complex mechanisms. The key advantage of using the equivalent rigid body model is that existing analysis and synthesis techniques for rigid body mechanisms can be used in flexure mechanism design.

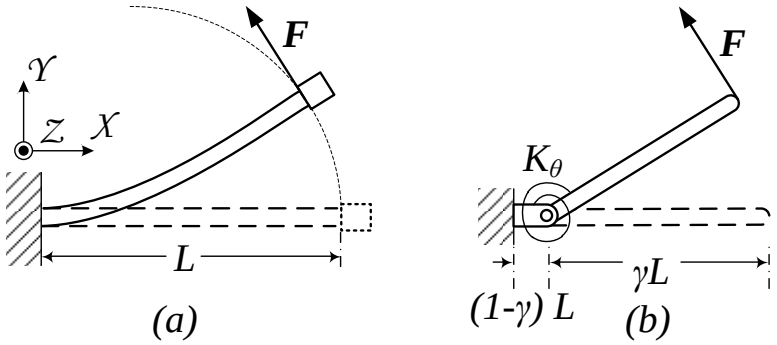

Figure 1.6: (a) Deformation of cantilever beam subjected to a force perpendicular to the neutral axis at the end of the beam (b) An equivalent Pseudo Rigid Body Model

One of the drawbacks of PRBM is that the model derivation is specific to a given loading condition. Therefore if the loading condition is changed, such as an addition of another moment $\boldsymbol{M_{ZL}}$, a new pseudo rigid body model would need to be reformulated by going through the optimization process again. Another key drawback of PRBM is that it doesn't give an accurate

estimate of the slope of the beam at the end the represents θ_{ZL}, a DoF displacement. Thirdly, due to the lumped parameter approximation, characteristics that are present due to distributed compliance alone, such as the elastic and elasto-kinematic effects in the axial direction, are not captured. Fourthly, variations due to the change of the cross-sectional shape of the beam and the orientation of its neutral axis are not studied. As discussed earlier, such a formulation will be important in gauging the effect of manufacturing defects. Finally, extending PRBM to spatial flexure beam is non-trivial because the mechanics of spatial beams leads to a more complicated relation between loads and displacement which is difficult to capture with just a rigid link and a hinge [57].

Returning to Figure 1.6, we now change our focus to another model technique, the beam column theory [58]. This model is based on a more careful application of Euler beam theory. Therefore the displacement predictions of the beam column theory are accurate for a larger range of displacement than the range for which the linear model is accurate. The reason why beam column theory is more accurate that the linear beam model is that it considers loads to move as the beam deforms and hence is able to include bending moments from $\boldsymbol{F_{XL}}$ in addition to $\boldsymbol{F_{YL}}$. This enables the beam column theory to be able to accurately predict beam displacements for end-displacement U_{YL} limited to 10% of length L. However beam column theory does not use the accurate nonlinear expression for curvature. This is why, for large displacements, its predictions are much larger than that predicted by the exact beam solution.

In the case of flexure mechanisms, it turns out that the maximum displacement range specifications are limited to 10-15% of the length of the flexure element due to material failure criteria. In this range, a model based on the beam column theory should sufficiently capture all constraint characteristics. Such a model is Planar Beam Constraint Model (PBCM), proposed by Awtar in 2004 [30] that may be used to analyze slender planar beams. Awtar observed that, for intermediate end displacement limited to 10% the length of the beam, the transcendental functions generated by the solution of beam column theory can be reduced to simple analytical expressions, given in Eq.(0.4) without incurring more than 5% error. The symbols below are in accordance to Figure 1.4(a). This model is known as the planar beam constraint model (PBCM) as it is applicable to beams with planar loading only.

$$\begin{bmatrix} \dfrac{\boldsymbol{F_{YL}}L^2}{EI} \\ \dfrac{\boldsymbol{M_{ZL}}L}{EI} \end{bmatrix} = \begin{bmatrix} 12 & -6 \\ -6 & 4 \end{bmatrix} \begin{bmatrix} \dfrac{U_{YL}}{L} \\ \theta_{ZL} \end{bmatrix} + \dfrac{\boldsymbol{F_{XL}}L^2}{EI_{ZZ}} \begin{bmatrix} 6/5 & -1/10 \\ -1/10 & 2/15 \end{bmatrix} \begin{bmatrix} \dfrac{U_{YL}}{L} \\ \theta_{ZL} \end{bmatrix} \quad (i) \tag{0.4}$$

$$\frac{U_{XL}}{L} = \frac{\boldsymbol{F_{XL}}}{AE} + \begin{bmatrix} \dfrac{U_{YL}}{L} & \theta_{ZL} \end{bmatrix} \begin{bmatrix} -3/5 & 1/20 \\ 1/20 & -1/15 \end{bmatrix} \begin{bmatrix} \dfrac{U_{YL}}{L} \\ \theta_{ZL} \end{bmatrix} + \frac{\boldsymbol{F_{XL}}L^2}{EI_{ZZ}} \begin{bmatrix} \dfrac{U_{YL}}{L} & \theta_{ZL} \end{bmatrix} \begin{bmatrix} 1/700 & 11/6300 \\ 11/6300 & -1/1400 \end{bmatrix} \begin{bmatrix} \dfrac{U_{YL}}{L} \\ \theta_{ZL} \end{bmatrix} \quad (ii)$$

Using this model, estimates of the load stiffening effect (second term on the right hand side of Eq.(0.4)(i)), elasto-kinematic effect (third term on the right hand side of Eq.(0.4)(ii)), both of which contribute to parasitic error motions in the axial direction, can be accurately found within this intermediate displacement range. It should be noted that, since PBCM is intended for slender planar beams (see footnote 3, page 18), shear effects in the YZ plane are not significant and hence not considered. Using PBCM, the constraint characteristics of common flexure modules such as parallelogram flexure module and double parallelogram flexure module can be studied more accurately and thoroughly than PRBM [33]. A brief derivation of PBCM is given in Chapter 2.

In spite of its advantages, PBCM also suffers from inadequacies. Firstly, it is nontrivial to extend the curvature linearization assumption to spatial beams, where all six independent displacements (translations and rotations about X, Y and Z axis) are important. This is because while complete linearization of curvature fails to predict the coupling between the two bending planes, consideration of the entire curvature nonlinearity leads to complex nonlinear differential equations which are very difficult to solve in closed form. Other small effects that are also present in spatial beam analysis are the anticlastic effect [29], warping effect [25], and trapeze effect [59]. In the case of flexure strips with width comparable to length, shearing effects in the XZ plane also need to be considered.

Secondly, PBCM is limited to beam geometries: planar beams with width of the order of thickness (plane stress formulation in the XY plane) and planar beams with width larger than the length of the beam (plane strain formulation in the XY plane). In the first case, the beam is assumed to be stress free in both the transverse directions Y and Z, while in the second case the beam is stress free in Y direction and strain free in Z direction. In spatial loading[7] and/or for

[7] Spatial loading refers to fully generalized end loading with 3 mutually perpendicular forces and moments.

intermediate beam width, stress and strains are more complex and need to be considered more carefully.

Finally, the PBCM proposed by Awtar did not account for manufacturing defects such as curvatures in undeformed beam and variations in rigidity modulus along the length of the beam.

In summary, PBCM illustrates the tradeoffs associated with capturing curvature nonlinearity in order to increase the range of applicability versus ignoring curvature nonlinearity for the sake of simplicity. Identifying that the typical displacement for most metallic high precision motion guidance stages is within 10% of the flexure length, limited by material failure criteria, PBCM's approach is found more suitable for the scope of this thesis and will be used as a starting point for this dissertation. An ad hoc extension of the PBCM to spatial beams may be found in Hao's work [60] on three-dimensional table - type flexure mechanisms. The limitation of this work lies in the inadequate generality of Hao's model, making it unsuitable for situations where beam torsion is present. More details on this will be provided in Chapter 5.

For spatial beams, where all six loads ($\boldsymbol{F_{XL}}$, $\boldsymbol{F_{YL}}$, $\boldsymbol{F_{ZL}}$ and $\boldsymbol{M_{XL}}$, $\boldsymbol{M_{YL}}$, $\boldsymbol{M_{ZL}}$) need to be considered, the mechanics is more involved since the displacements in the two bending planes cannot be simply superimposed. For moment loading only ($\boldsymbol{M_{XL}}$, $\boldsymbol{M_{YL}}$, $\boldsymbol{M_{ZL}}$) for a spatial beam an exact solution was provided by Frisch-Fay. However, the solution involves an infinite series summation of elliptic integration which makes it impractical for mechanism design.

Other models of spatial beams can be found in the work of Hodges [61] and DaSilva [36] which study helicopter blades. Starting from the basic stress-strain relations both Hodges and DaSilva derive the beam governing differential equations for bending, stretching and twisting, which turn out to be nonlinearly coupled. Although some simplification of the differential equations in either case was done through order of magnitude based approximations, the final differential equation was not solvable to find closed-form load-displacement relations that are required for flexure mechanism design.

Nonlinearities of spatial beam mechanics for large end-displacements have also been captured using the Cosserat rod theory, which is capable of capturing the geometric nonlinearities for generalized end-loading. Using this theory, the helical solution of spatial beams under certain torsional and bending loads was analyzed. Recent development has further generalized this theory by using non-linear constitutive relations as well as shear and extensional effects [23-25]. It should be noted that although Cosserat theory does not consider in-plane

distortion or out-of-plane warping of cross-sections, it is accurate for slender beams. However, given the mathematical complexity of the formulation, solutions based on Cosserat's theory also have to be obtained via numerical techniques.

1.4 Need for a New Approach for Modeling Beams with Spatial Loading

From the literature survey, while it is clear that the platform for finding analytical models of beams has been established using generalized stress-strain relations, a suitable model of flexure mechanism design that adequately capture nonlinearities with a simple representation does not exist. This is probably because requirements of flexure mechanism design are such that traditional approaches of approximating based on order of magnitude or ignoring selective nonlinearities either trivializes the beam model or doesn't make it simple enough.

To overcome this tradeoff, this dissertation recognizes that by choosing the beam shape to be such that either the two principle moments of area of the beam cross-section are equal or one is much greater than the other, closed-form load-displacement relations that capture all relevant nonlinearities can be assured even for generalized spatial loading. With this approach, spatial models of flexure strip and symmetric spatial beam will be formulated in Chapters 4 through 6. Chapter 2 and 3 generalize the existing PBCM for planar flexure strips by adding the effect of manufacturing defects such as a non-straight undeformed beam and varying cross-section or rigidity modulus with length. In particular, Chapter 2 derives the load-displacement relations for planar beam flexures while Chapter 3 derives the corresponding strain energy expression. It is observed that the analytical models for the planar as well the spatial beams have the same structure. Since planar analysis is easier to understand, it is placed before spatial analysis for the convenience of the reader. Using the relatively simpler concepts introduced in the planar analysis, understanding the spatial analysis will be easier.

1.5 Summary of Contributions

The goals and outcomes of this dissertation are listed below.

- Create analytical closed form models for flexure strip and spatial beam flexure subject to generalized end-loading that provide at least 95% accurate displacement and stiffness

estimates in a quasi-static equilibrium. A closed form model should express loads in terms of displacements or vice versa for six independent directions of the beam end point.

- Identify and quantify the trade-offs in the constraint characteristics of the flexure elements between three design criteria: 1. Make stiffness along DoF as low as possible 2. Make stiffness along DoC as high as possible 3. Reduce or eliminate all error motions.
- For each type of beam considered, formulate strain energy expressions in terms of end-displacements in closed-form that are compatible with the load-displacement relations for each flexure element. This compatible strain energy can be used to easily analyze flexure mechanism with multiple flexure elements in parallel using the principle of virtual work. Examples of its use with a parallel arrangement of planar beam and the spatial beam flexure element are shown.
- Effects of manufacturing defects in flexure strip and spatial beam flexure due to non-straight undeformed configuration and varying cross-section or rigidity modulus with beam length are quantified and discussed.

By quantifying the constraint properties of flexure elements, this work lays an enabling foundation for constraint-based synthesis [62] and optimization of flexure mechanisms in the future. Furthermore, using the stiffness estimates, preliminary analysis of the resonant frequencies associated with the first few modes of a given flexure mechanism can also be carried out. However, understanding all the dynamic modes and frequency response of flexure mechanism will require a more careful study and is beyond the scope of this dissertation.

Chapter 2

Planar Beam Constraint Model for Slender Beams with Planar Loading

2.1 Introduction

In several flexure mechanisms only translations and rotations in one plane are desired. Several examples of such mechanisms can be found in MEMS devices. In these mechanisms generally all flexure elements are arranged in one plane. Such mechanisms are referred to as planar mechanisms and the planar motion at a point or rigid body within the mechanism can be uniquely described by three mutually independent displacements. Let us choose the motion plane as the XY plane and the in-plane displacement co-ordinates as translation U_{XL} along X, translation U_{YL} along Y and rotation θ_{ZL} about Z as shown in Figure 2.1.

Flexure strips, which are often used as a building block for designing planar flexure mechanisms, have DoFs along planar displacements U_{YL} and θ_{ZL} and DoC along planar displacement U_{XL} when oriented with its centroidal axis along X, thickness measured along Y (shown in Figure 2.1) and width measured along Z. Although flexure strips also have a rotational DoF about the X axis (twisting), by using two or several flexure strips in parallel, the mechanism can be designed such that the out-of-plane motion resulting from this DoF is adequately constrained. Additionally if a large width to thickness ratio (or aspect ratio) is chosen, out-of-plane displacements U_{ZL} and θ_{YL} are relatively small. Thus, a nonlinear planar analysis of the in-plane displacements U_{XL}, U_{YL} and θ_{ZL} may be done ignoring the out-of-plane loads and displacements entirely. Furthermore, it will be shown in Chapter 4 and Chapter 5, that when torsional displacements are zero, out-of-plane loads and displacements have no significant effect on in-plane displacements. This is another case where a nonlinear planar analysis of the in-plane

displacements U_{XL}, U_{YL} and θ_{ZL} may be done ignoring the out-of-plane loads and displacements entirely. This is true even for beams when the width of the beam is comparable to the thickness of the beam. It should be noted that in either case, if there exists out-of-plane displacements, they can be estimate independent of the in-plane loads and displacement using standard theories like Euler beam theory or Timoshenko beam theory whichever is applicable.

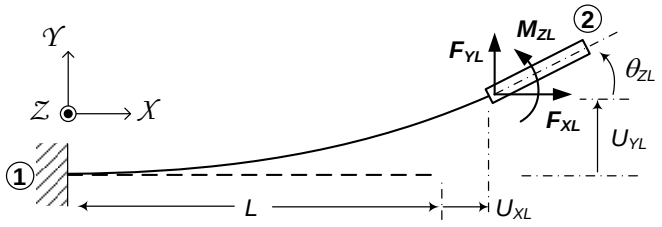

Figure 2.1: Planar Beam Flexure

A widely accepted approach of analyzing in-plane displacements of slender rectangular beams is the Euler beam theory [43]. In this approach, cross-sections initially plane and perpendicular to the centroidal axis[8] are assumed to stay plane and perpendicular to the deformed centroidal axis after loads are applied to the beam. For pure moment loading, this deformation assumption may be shown using symmetry arguments for cross-sections of a slender[9] beam away from the ends of the beam [29]. In the presence of bending forces, this deformation assumption is only approximate. However, it may be shown that the out-of-plane displacements of the points on the cross-section, prior to deformation, are proportional to the square of thickness to length ratio [25]. Hence, using Euler's assumption to analyze slender beams loaded with bending forces, leads to fairly accurate deformation prediction.

Further simplification can be done by linearizing strain, defined as rate of change of length of a fiber after deformation, in order to obtain compact closed form load-displacement relations. However as discussed in Chapter 1, such linearization leads to errors when displacements are finite. A second approach to formulate reasonably accurate as well as closed form load-displacement relations is to use second order approximations[10] in an appropriate manner. Typically, for planar analysis, the curvature nonlinearity is dropped, but arc-length conservation nonlinearity is retained to the second order. Beam column theory [58] uses this

[8] Centroidal axis is the locus of the centroids of all beam cross-sections
[9] A slender beam is one where the thickness is less than $1/20^{th}$ of the length [24].
[10] By second order approximations, it is meant that terms that contribute less that 1% is an analytical formula are dropped

approach to capture pertinent geometric nonlinearities in a closed form manner. Although in this approach, the relations between loads and displacements are transcendental in nature, they are closed-form nonetheless. A simpler closed-form model that is still 95% accurate with respect to the original solution can be extracted from the latter by using Taylor series expansion, as shown by Awtar [24]. This model is known as the planar beam constraint model (PBCM) as it captures the constraint properties of a planar beam. A detailed background of PBCM is given in Section 2.2. The contribution of this dissertation in the modeling of PRBM lies in the generalization of the PBCM by accounting for initial slope, curvature and shape variation of the beam. The generalizations are discussed in Sections 2.3, 2.4 and 2.5.

2.2 Background: The Planar Beam Constraint Model (PBCM)

An overview of the PBCM for a slender beam with planar loading, also known as a simple beam flexure (uniform thickness and initially straight) or a cantilever beam, is provided below for a better understanding of PBCM for a generalized beam flexure that will be presented in the subsequent sections. For a more detailed mathematical derivation the reader is referred to the prior literature [24].

2.2.1 Approach of PRBM

Figure 2.1 illustrates a simple beam (length: L, thickness: T_Y, depth: T_Z), interconnecting rigid bodies 1 and 2, subjected to generalized end-loads $\boldsymbol{F_{XL}}$, $\boldsymbol{F_{YL}}$, and $\boldsymbol{M_{ZL}}$, resulting in end-displacements U_{XL} (DoC), U_{YL} (DoF), and θ_{ZL} (DoF), with respect to the coordinate frame XYZ. I_{ZZ} denotes the second moment of area about the bending axis Y, E denotes the Young's modulus for a state of plane-stress in XY, and plate modulus for a state of plane-strain in XY. A 'mechanics of solids' approach is taken, which is to find the strain based on certain valid deformation assumptions, followed by finding the corresponding stress to obtain a force equilibrium condition, rather than 'theory of elasticity' approach which is solving out the strain with a continuum approach assuming a certain stress distribution and using compatibility relations. Employing **A.** the Euler-Bernoulli assumptions for long and slender beams i.e. plane sections remain plane and perpendicular to the neutral axis, **B.** curvature linearization for small displacements as given in Chapter 1 Section 3, and **C.** load equilibrium applied in the beam's

deformed configuration, leads to the following beam governing equation applicable at any given cross-section location X along the beam length:

$$EI_{ZZ}U_Y''(X) = \boldsymbol{M_{ZL}} + \boldsymbol{F_{YL}}(1+U_{XL}-X) - \boldsymbol{F_{XL}}(U_{YL}-U_Y(X)) \tag{2.1}$$

It should be noted here that the neutral axis, which is the locus of the point of minimum extensional strain of all the cross-sectional areas and is assumed to be the centroidal axis[11] and also assumed to not change with beam deformation. For intermediate deformations corresponding to $-0.1L < U_{YL} < 0.1L$ and $-0.1 < \theta_{ZL} < 0.1$ radians, this assumption is quite accurate. This is because for the above displacement ranges the maximum value of strains is of order 10^{-3}. This implies that by using the undeformed cross-section to calculate the centroid the error in position is less than 0.1%. The above equation may be solved in closed-form by differentiating twice with respect to X.

$$U_Y^{iv}(X) = \frac{\boldsymbol{F_{XL}}}{EI_{ZZ}}U_Y''(X) \tag{2.2}$$

and applying the following four boundary conditions:

$$U_Y(0)=0,\ \ U_Y'(0)=0,\ \ U_Y''(L)=\frac{\boldsymbol{M_{ZL}}}{EI_{ZZ}},\ \ U_Y'''(L)=\frac{-\boldsymbol{F_{YL}}+\boldsymbol{F_{XL}}U_Y'(L)}{EI_{ZZ}}$$

The importance of applying load equilibrium in the deformed configuration of the beam is that contribution of the axial direction load $\boldsymbol{F_{XL}}$ to bending moment, which may be large when the flexure element is supporting a large load, is taken into account. However, the differential equation itself and associated boundary conditions remain linear in the transverse-direction loads ($\boldsymbol{F_{YL}}$ and $\boldsymbol{M_{ZL}}$) and displacements ($U_Y(X)$ and its derivatives). Consequently, solving this equation leads to linear relations between these end-loads and end-displacements (U_{YL} and $\theta_{ZL} = U'_{YL}$). The associated stiffness terms, however, are no longer merely elastic terms, but transcendental functions of the axial load $\boldsymbol{F_{XL}}$. These functions are expanded and truncated to the first order in $\boldsymbol{F_{XL}}$, with minimal error, to yield the following transverse end load-displacement relation:

$$\begin{bmatrix} \boldsymbol{F_{YL}}L^2/EI_{ZZ} \\ \boldsymbol{M_{ZL}}L/EI_{ZZ} \end{bmatrix} = \begin{bmatrix} k_{11}^{(0)} & k_{12}^{(0)} \\ k_{12}^{(0)} & k_{22}^{(0)} \end{bmatrix} \begin{bmatrix} \frac{U_{YL}}{L} \\ \theta_{ZL} \end{bmatrix} + \frac{\boldsymbol{F_{XL}}L^2}{EI_{ZZ}} \begin{bmatrix} k_{11}^{(1)} & k_{12}^{(1)} \\ k_{12}^{(1)} & k_{22}^{(1)} \end{bmatrix} \begin{bmatrix} \frac{U_{YL}}{L} \\ \theta_{ZL} \end{bmatrix} + \left(\frac{\boldsymbol{F_{XL}}L^2}{EI_{ZZ}}\right)^2 \begin{bmatrix} k_{11}^{(2)} & k_{12}^{(2)} \\ k_{12}^{(2)} & k_{22}^{(2)} \end{bmatrix} \begin{bmatrix} \frac{U_{YL}}{L} \\ \theta_{ZL} \end{bmatrix} \tag{2.3}$$

[11] Centroidal axis of a beam is the locus of the centroid of all cross-sections of the beam.

The truncation of the infinite Taylor series of the transcendental expressions are done at the second power of $\boldsymbol{F_{XL}}$ for consistency with the geometric constraint and the strain energy relations which are truncated at the first and second power of $\boldsymbol{F_{XL}}$, respectively, as shown in the subsequent paragraph. If this consistency required is not kept in mind, the derivation of Eq. (2.1) and (2.2) using principle of virtual work, which will be shown later in Chapter 3, will yield inaccurate force-displacement relations. Next, the kinematic constraint imposed by the beam arc length may be captured via the following integral, to determine the dependence of the axial displacement U_{XL} on the transverse displacements:

$$L+\frac{(T/L)^2}{12}\frac{\boldsymbol{F_{XL}}L^3}{EI_{ZZ}}=\int_0^{L+U_{XL}}\left\{1+\frac{1}{2}\left(U_Y'(X)\right)^2\right\}dX \tag{2.4}$$

The left hand side is the original beam length plus its axial elastic stretching or compression due to the axial force $\boldsymbol{F_{XL}}$, while the right hand side is a continuous integral of the deformed arc of the beam. Both should represent the total beam arc length after the deflection and hence should be equal. In this case, it is important to include the second-order term in $U'_Y(X)$ on the RHS to capture the kinematics associated the beam deflection geometry. Dropping this terms makes U_{XL} simply equal to the elastic stretch/extension. Not only is this inadequate for constraint characterization, it also proves to be inconsistent with the transverse direction relations (2.2)-(2.3), as will be shown via an energy formulation later in Chapter 3.

Using the $U_Y(X)$ solution for Eq.(2.2), Eq.(2.4) may also be solved in closed form to reveal a quadratic dependence of a portion of U_{XL} on U_{YL} and θ_{ZL}. As might be expected, the coefficients in this quadratic relation are also transcendental functions of the axial load $\boldsymbol{F_{XL}}$. A series expansion and truncation to the first order in $\boldsymbol{F_{XL}}$ yields:

$$\frac{U_{XL}}{L}=\frac{(T/L)^2}{12}\frac{\boldsymbol{F_{XL}}L^2}{EI_{ZZ}}+\begin{bmatrix}\frac{U_{YL}}{L} & \theta_{ZL}\end{bmatrix}\begin{bmatrix}g_{11}^{(0)} & g_{12}^{(0)}\\ g_{12}^{(0)} & g_{22}^{(0)}\end{bmatrix}\begin{bmatrix}\frac{U_{YL}}{L}\\ \theta_{ZL}\end{bmatrix}+\frac{\boldsymbol{F_{XL}}L^2}{EI_{ZZ}}\begin{bmatrix}\frac{U_{YL}}{L} & \theta_{ZL}\end{bmatrix}\begin{bmatrix}g_{11}^{(1)} & g_{12}^{(1)}\\ g_{12}^{(1)} & g_{22}^{(1)}\end{bmatrix}\begin{bmatrix}\frac{U_{YL}}{L}\\ \theta_{ZL}\end{bmatrix} \tag{2.5}$$

For convenience of discussion, the three terms on the RHS above may be individually identified as $U_{XL}^{(e)}$, $U_{XL}^{(k)}$, and $U_{XL}^{(e-k)}$, respectively, and will be further described shortly. Equations (2.3) and (2.5), which constitute the PBCM, provide accurate, compact, closed-form, and parametric relations between the end-loads and end-displacements of a simple beam. Further, in this format, all loads, displacements, and stiffness terms are naturally normalized with respect to

the beam parameters: displacements and lengths are normalized by the beam length L, forces by EI_{ZZ}/L^2, and moments by EI_{ZZ}/L. Thus, one may define:

$$\frac{\boldsymbol{F}_{XL}L^2}{EI_{ZZ}} \triangleq \boldsymbol{f}_{x1} \quad ; \quad \frac{\boldsymbol{F}_{YL}L^2}{EI_{ZZ}} \triangleq \boldsymbol{f}_{y1} \quad ; \quad \frac{\boldsymbol{M}_{ZL}L}{EI_{ZZ}} \triangleq \boldsymbol{m}_{z1}$$

$$\frac{U_{XL}}{L} \triangleq u_{x1} \quad ; \quad \frac{U_{YL}}{L} \triangleq u_{y1} \quad ; \quad \theta_{ZL} \triangleq \theta_{z1} \quad ; \quad \frac{T}{L} \triangleq t \quad ; \quad \frac{X}{L} \triangleq x$$

The convention of representing non-normalized terms and the corresponding normalized terms by upper case and lower case letter, respectively, is followed throughout this thesis.

It will be shown in Section 2.4 that the coefficients k's and g's, in general, are non-dimensional 'beam characteristic coefficients' that are solely dependent on the beam shape and not its actual size [30]. These coefficients take the following numerical values for a simple beam.

$k_{11}^{(0)}$	12	$k_{11}^{(1)}$	6/5	$k_{11}^{(2)}$	-1/700	$g_{11}^{(0)}$	–3/5	$g_{11}^{(1)}$	1/700
$k_{12}^{(0)}$	–6	$k_{12}^{(1)}$	–1/10	$k_{12}^{(2)}$	1/1400	$g_{12}^{(0)}$	1/20	$g_{12}^{(1)}$	–1/1400
$k_{22}^{(0)}$	4	$k_{22}^{(1)}$	2/15	$k_{22}^{(2)}$	-11/6300	$g_{22}^{(0)}$	–1/15	$g_{22}^{(1)}$	11/6300

Table 2.1. Characteristic Coefficients for a Simple Beam

The PBCM helps characterize the constraint behavior of a simple beam flexure in terms of its stiffness and error motions. The first matrix term on the RHS of Eq.(2.3) provides the linear elastic stiffness in the DoF directions, while the second matrix captures load-stiffening, which results in a change in the effective stiffness in the DoF directions due to a DoC load. Both these matrix terms also capture the cross-axis coupling between the two DoF. Eq.(2.5) shows that the DoC direction displacement, which is a parasitic error motion, is comprised of three terms: $U_{XL}^{(e)}$ is a purely elastic component resulting from the stretching of the beam neutral axis in the X direction; $U_{XL}^{(k)}$ represents a purely kinematic component dependent on the two DoF displacements, and arises from the constant beam arc-length constraint; and $U_{XL}^{(e-k)}$ represents an elastokinematic component, called so because of its elastic dependence on the DoC force $\boldsymbol{F}_{XL}$ and its kinematic dependence on the two DoF displacements. The elastokinematic component is also a consequence of the beam arc-length constraint, and arises due to a change in the beam deformation when $\boldsymbol{F}_{XL}$ is applied, even as U_{YL} and θ_{ZL} are held fixed. The kinematic component

$U_{XL}^{(k)}$ dominates the DoC error motion and increases quadratically with increasing DoF displacements. The elastokinematic component of the DoC displacement, while small with respect to the purely kinematic component, is comparable to the purely elastic component and causes the DoC direction stiffness to drop quadratically from its nominal linear elastic value with increasing DoF displacements.

Thus, the PBCM not only highlights the non-ideal constraint behavior of a beam flexure, it also reveals interdependence and fundamental tradeoffs between the DoF quality (large range, low stiffness) and DoC quality (high stiffness, low parasitic error). The beam characteristic coefficients, *k*'s and *g*'s, serve as convenient performance metrics in a design.

2.2.2 Validation of PRBM

For validation, we provide a comparison between the PBCM for a simple beam and the corresponding non-linear FEA predications. An overview of the FEA procedure and settings used in this paper is provided in Appendix 2.A attached to the end of this chapter. Figure 2.2 plots the elastic stiffness coefficients ($k_{11}^{(0)}, k_{12}^{(0)}$, and $k_{22}^{(0)}$) and load-stiffening coefficients ($k_{11}^{(1)}$, $k_{12}^{(1)}$, and $k_{22}^{(1)}$) versus the normalized DoF displacement u_{y1} or θ_{z1}. Similarly, Figure 2.3 plots the kinematic ($g_{11}^{(0)}, g_{12}^{(0)}$, and $g_{22}^{(0)}$) and elastokinematic ($g_{11}^{(1)}, g_{12}^{(1)}$, and $g_{22}^{(1)}$) coefficients. The PBCM predictions are found to be within 6% of the FEA results for the DoF end-displacements (u_{y1} and θ_{z1}) in the range ±0.1 and the DoC end-load ($\boldsymbol{f_{x1}}$) in the range ±10. Any discrepancy can be entirely accounted for by: **A.** the non-linearity associated with the beam curvature [19], which is not incorporated in the PBCM, and **B.** the truncation of higher-order terms of $\boldsymbol{f_{x1}}$ in Eqs. (2.3) and (2.5). In general, this displacement and load range covers most practical flexure mechanism applications. The maximum error of 6% incurred over this range is a fair price for a greatly simplified and insightful closed-form parametric constraint model.

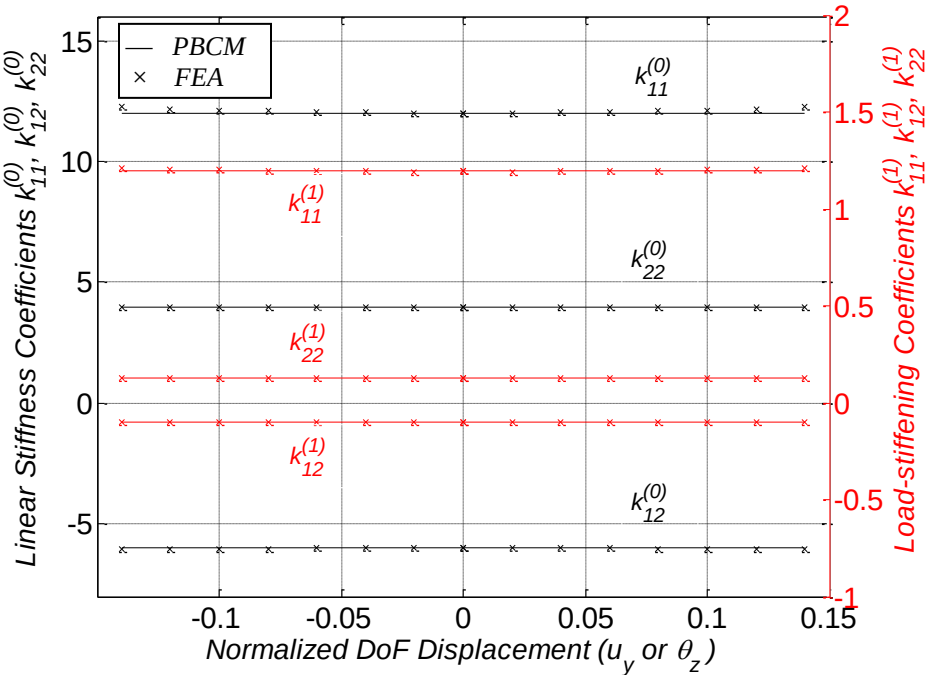

Figure 2.2: Elastic Stiffness Coefficients and Load-Stiffening Coefficients for a Simple Beam: PBCM vs. FEA

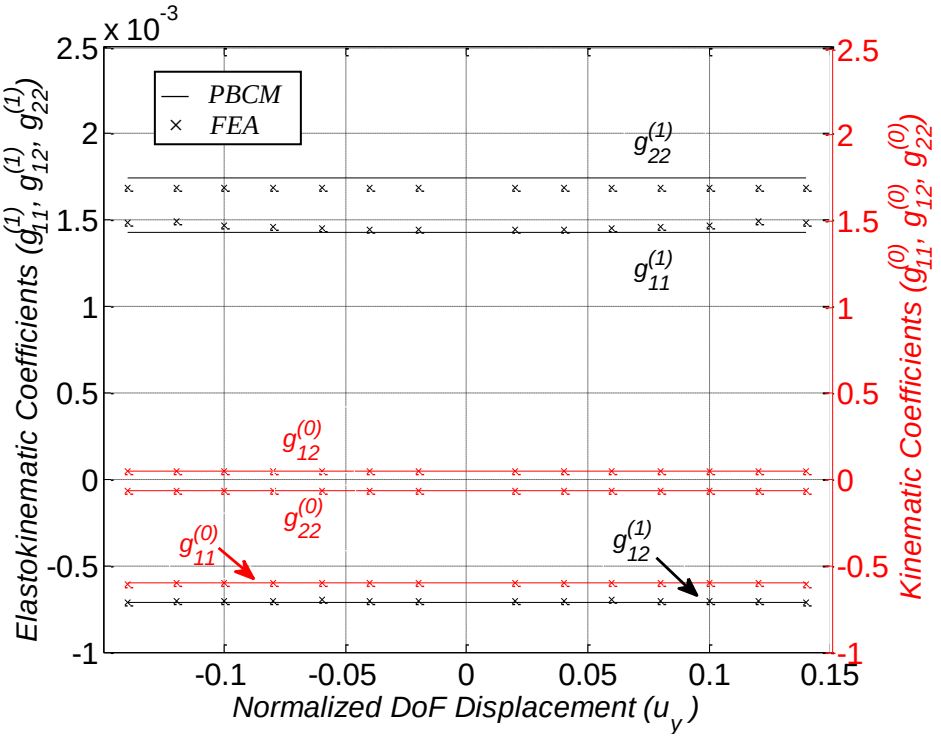

Figure 2.3: Kinematic and Elastokinematic Coefficients for a Simple Beam: PBCM vs. FEA

2.2.3 Comparison of PBCM with Linear Model and PRBM

In order to gauge the advantages of PBCM over other closed-form modeling techniques for planar analysis, we now proceed to compare the three modeling techniques Linear Model, PRBM and PBCM from the point of view of analyzing a flexure mechanism. As a case study we will use a parallelogram flexure (Figure 2.4), comprised of two identical simple beams, (Length, L = 250mm, Thickness, T = 5mm, Depth along Z, D = 50mm, Width, W = 75mm, Elastic modulus, E = 210000Nmm2) which is commonly used to generate approximate straight line motion.

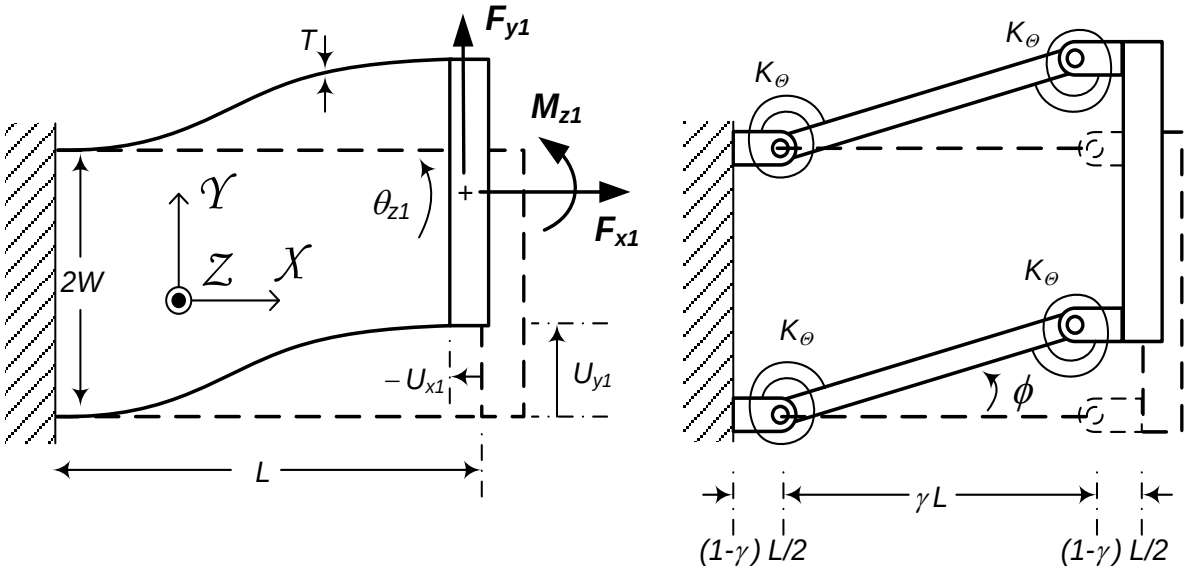

Figure 2.4: Parallelogram Flexure and its Pseudo Rigid Body Model

Using the normalization convention introduced earlier, the linear model for this flexure module may be shown to be [63]:

$$\boldsymbol{f}_{y1} = 24u_{y1} \quad ; \quad u_{x1} = 0 \quad ; \quad \theta_{z1} = \frac{t^2}{24w^2}\left[\boldsymbol{m}_{z1} + \frac{\boldsymbol{f}_{y1}}{2}\right] \tag{2.6}$$

The non-linear load-displacement results for this flexure module have been derived using the PBCM in the past [30]:

$$\boldsymbol{f}_{y1} = \left(24 + 1.2\,\boldsymbol{f}_{x1}\right)u_{y1} \quad ; \quad u_{x1} \approx \frac{t^2}{24}\,\boldsymbol{f}_{x1} - \frac{3}{5}u_{y1}^2 + \frac{1}{1400}u_{y1}^2\,\boldsymbol{f}_{x1}$$

$$\theta_{z1} = \frac{1}{2w^2}\left(\frac{t^2}{12} + \frac{u_{y1}^2}{700}\right)\left[\boldsymbol{m_{z1}} + \boldsymbol{f_{y1}}\frac{(12 + 0.1\boldsymbol{f_{x1}})}{(24 + 1.2\boldsymbol{f_{x1}})}\right] \tag{2.7}$$

A PRBM is also illustrated alongside the parallelogram flexure module in Fig.5. Assuming $\boldsymbol{m_{z1}}$ and $\boldsymbol{f_{x1}}$ to be zero, the model parameters are given by γ = 0.8517 and normalized torsional spring stiffness $k_\theta = K_\Theta L^3/(EI) = 2.65$, and the load-displacement results are given by [56]:

$$\boldsymbol{f_{y1}}\cos\phi - \boldsymbol{f_{x1}}\sin\phi = 8k_\Theta\phi \;\; ; \;\; u_{y1} = \gamma\sin\phi \;\; ; \;\; u_{x1} = \gamma(\cos\phi - 1) \tag{2.8}$$

Key constraint behavior predictions made by the above three models along with results from a non-linear FEA are plotted in Figure 2.5-7 over a u_{y1} range of ± 0.15. Figure 2.5 plots the non-linear dependence of u_{x1} (X DoC parasitic error motion) on u_{y1} (Y DoF displacement) and illustrates that both the PRBM and PBCM capture the kinematic effect in beams due to arc length conservation very accurately. However the linear model does not capture this effect at all. Figure 2.6 plots the variation in the X direction (DoC) stiffness with u_{y1} (Y DoF displacement). While the PRBM does not recognize any compliance in this DoC direction whatsoever, the linear model only captures the purely elastic stiffness component. The PBCM is the only model that accurately predicts the elastokinematic effects, as verified by the FEA. Figure 2.6 plots θ_{z1} (rotational DoC parasitic error motion) with increasing $\boldsymbol{f_{y1}}$ (Y DoF force). The PRBM predicts zero yaw rotation of the rigid stage, while the linear model is valid only for small forces and displacements. However, the PBCM accurately captures this parasitic error motion, also dominated by the elastokinematic effect, even for large values of the DoF force and displacement.

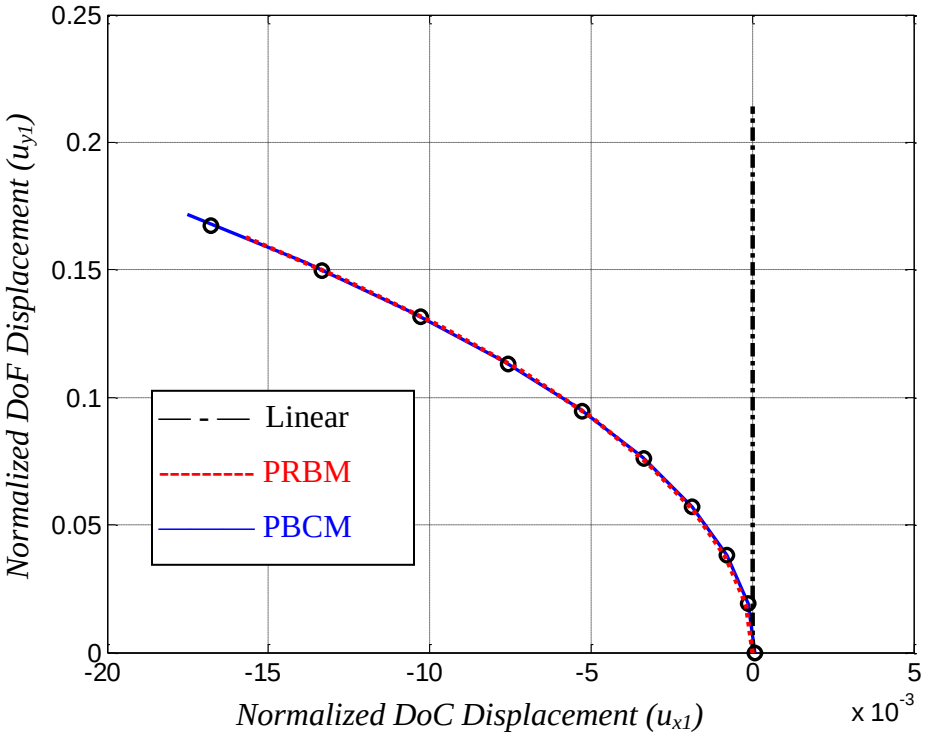

Figure 2.5: Dependence of u_{x1} (DoC) on u_{y1} (DoF)

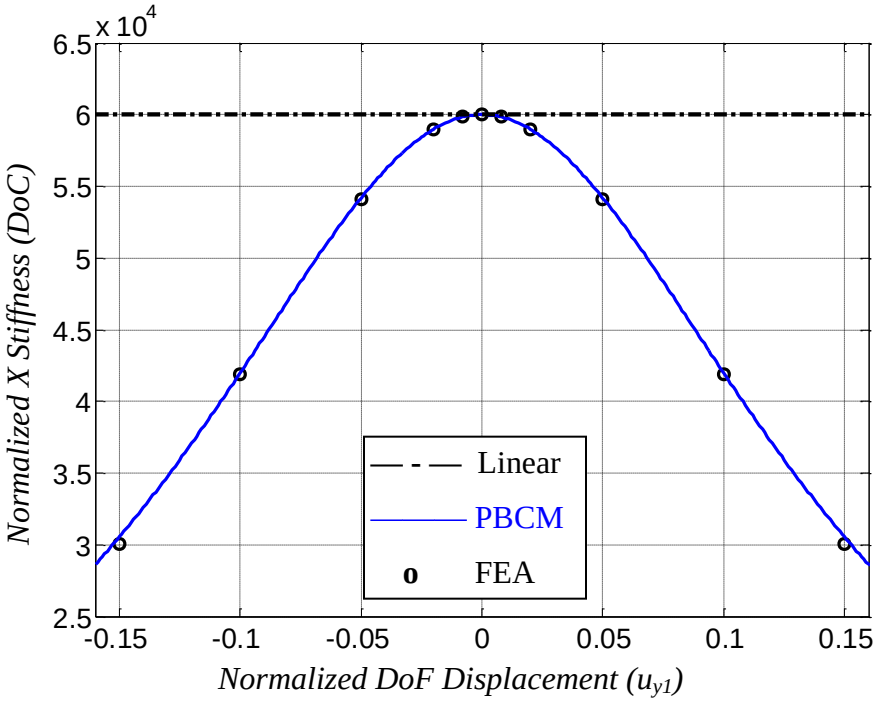

Figure 2.6: Dependence of X direction (DoC) Stiffness on u_{y1} (DoF)

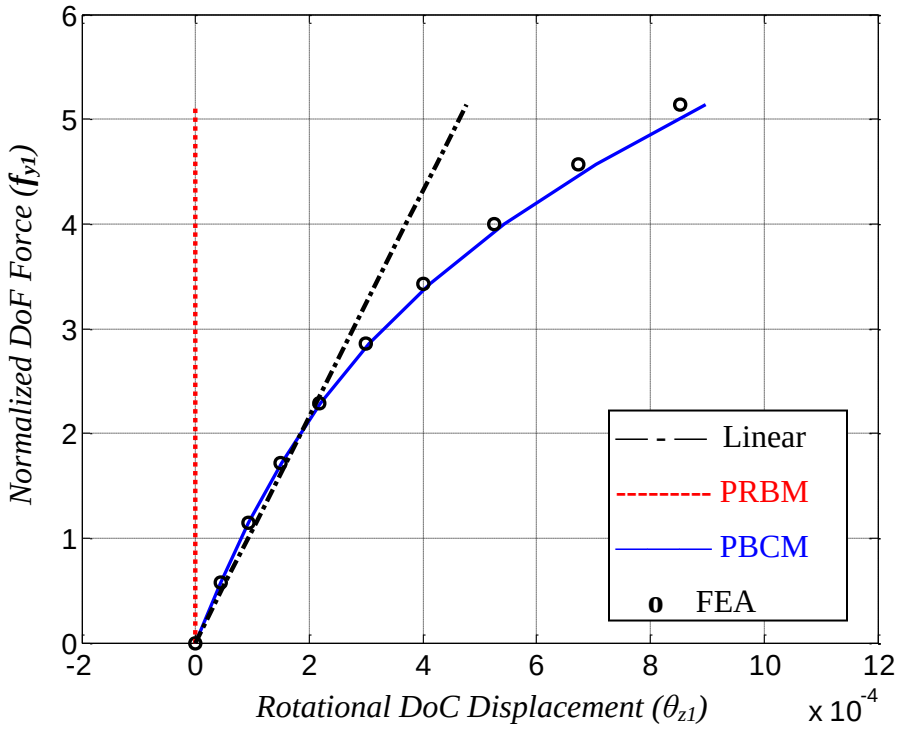

Figure 2.7: Dependence of θ_{z1} (rotational DoC) on f_{y1} (DoF)

Thus, for planar analysis, the PBCM is the only closed-form model that truly characterizes the constraint behavior of flexures in terms of stiffness variation and error motions. This demonstrates the importance of PBCM in planar flexure mechanism design.

2.3 Uniform Thickness Slender Beam with Generalized Boundary Conditions and Initial Curvature

Having done the FEA verification on previously presented PBCM for a simple beam flexure module, we next find the PBCM of more general beam flexure module by considering a uniform thickness beam with an arbitrary initial slope and an arbitrary but constant initial curvature. Note that choosing an arbitrary initial position simply shifts the coordinate frame of the beam by a constant value, and therefore is trivial. The objective is to capture these initial and boundary condition generalizations within the PBCM, which so far has only dealt with a simple beam. The motivation for doing so is two-fold: 1. Analytically capture the consequence of manufacturing variations, e.g. in MEMS devices micro-fabricated beams can often assume an initially bent/curved shape to relieve material stresses, and 2. Use initial slope and curvature as additional design and optimization variables to achieve desired constraint characteristics.

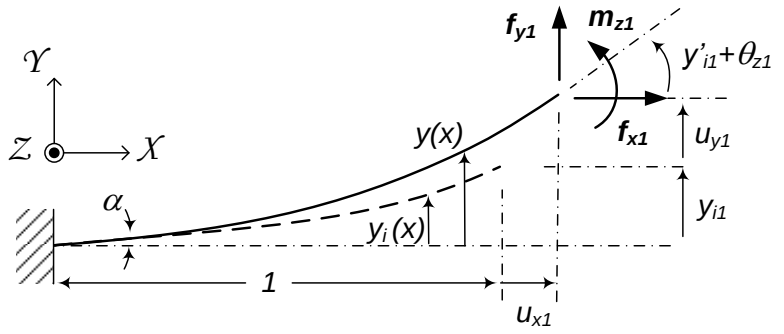

Figure 2.8: ***Initially Slanted and Curved Beam***

Figure 2.8 illustrates an initially slanted and curved beam with three generalized end-loads $\boldsymbol{f_{x1}}$, $\boldsymbol{f_{y1}}$, and $\boldsymbol{m_{z1}}$, and three end-displacements u_{x1}, u_{y1}, and θ_{z1}, along the coordinate frame XYZ. All lower-case quantities are normalized with respect to beam parameters, as described earlier. The beam is assumed to have an initial slope α and an initial curvature of κ. For small initial slope and curvature (~ *0.1*), the Y and Θ_Z directions still serve as DoF, and the X direction is a DoC. The initial (unloaded and undeformed) beam configuration is denoted by $y_i(x)$, final (loaded and deformed) beam configuration is given by $y(x)$, and the beam deformation in the Y direction is given by $u_y(x)$, where

$$y_i(x) = \alpha x + \frac{\kappa}{2}x^2, \text{ and } y(x) = y_i(x) + u_y(x) \tag{2.9}$$

The derivation of the load-displacement relations for this beam flexure is carried out along the same lines as in the previous case. Euler-Bernoulli and small curvature assumptions are made. The latter implies that the displacement, slope, and curvature of the beam in its deformed configuration remain of the order of *0.1*, so that the non-linearity associated with the beam curvature may be dropped here as well. The normalized bending moment, $\boldsymbol{m_z}(x)$, at a given cross section is computed by applying load equilibrium in the beam's deformed configuration:

$$\boldsymbol{m_z}(x) = \boldsymbol{m_{z1}} + \boldsymbol{f_{y1}}\left(1 + u_{x1} - x\right) - \boldsymbol{f_{x1}}\left(y_1 - y(x)\right) \tag{2.10}$$

The leads to the following normalized beam governing equation:

$$\begin{aligned} &y''(x) = \boldsymbol{m_{z1}} + \boldsymbol{f_{y1}}\left(1 + u_{x1} - x\right) - \boldsymbol{f_{x1}}\left(y_1 - y(x)\right) \\ &\Rightarrow y^{iv}(x) = \boldsymbol{f_{x1}}y''(x) \quad \{\text{Upon Double Differentiation}\} \end{aligned} \tag{2.11}$$

For positive values of $\boldsymbol{f_{x1}}$, the general solution to this fourth-order linear differential equation is given by:

$$y(x) = c_1 + c_2 x + c_3 \sinh(\boldsymbol{r}x) + c_4 \cosh(\boldsymbol{r}x), \text{ where } \boldsymbol{r}^2 \triangleq \boldsymbol{f}_{x1} \tag{2.12}$$

An analogous solution in terms of trigonometric functions, instead of hyperbolic functions, exists for negative values of $\boldsymbol{f}_{x1}$. The beam deflection, $u_y(x)$, then becomes:

$$u_y(x) = y(x) - y_i(x) = c_1 + (c_2 - \alpha x) - \frac{\kappa}{2} x^2 + c_3 \sinh(\boldsymbol{r}x) + c_4 \cosh(\boldsymbol{r}x) \tag{2.13}$$

Displacement boundary conditions at the two beam ends are given by:

$$u_y(0) = 0 \text{ , } u_y'(0) = 0 \text{ , } u_y(1) = u_{y1} \text{ , } u_y'(1) = \theta_{z1} \tag{2.14}$$

Using Eqs. (2.9) and (2.10), the load boundary conditions at $x=1$ can be shown to be:

$$u_y'''(1) = -\boldsymbol{f}_{y1} + \boldsymbol{f}_{x1}(\theta_{z1} + \alpha + \kappa) \text{ , } u_y''(1) = \boldsymbol{m}_{z1} \tag{2.15}$$

The above displacement and load boundary conditions are then used to determine the coefficients c_1, c_2, c_3, and c_4, which ultimately lead to the following relations between the DoF direction end-loads and end-displacements.

$$\begin{bmatrix} \boldsymbol{f}_{y1} \\ \boldsymbol{m}_{z1} \end{bmatrix} = \begin{bmatrix} \dfrac{\boldsymbol{r}^3 \sinh(\boldsymbol{r})}{\boldsymbol{r}\sinh(\boldsymbol{r}) - 2\cosh(\boldsymbol{r}) + 2} & \dfrac{\boldsymbol{r}^2 \{1 - \cosh(\boldsymbol{r})\}}{\boldsymbol{r}\sinh(\boldsymbol{r}) - 2\cosh(\boldsymbol{r}) + 2} \\ \dfrac{\boldsymbol{r}^2 \{1 - \cosh(\boldsymbol{r})\}}{\boldsymbol{r}\sinh(\boldsymbol{r}) - 2\cosh(\boldsymbol{r}) + 2} & \dfrac{\boldsymbol{r}^2 \cosh(\boldsymbol{r}) - \boldsymbol{r}\sinh(\boldsymbol{r})}{\boldsymbol{r}\sinh(\boldsymbol{r}) - 2\cosh(\boldsymbol{r}) + 2} \end{bmatrix} \begin{bmatrix} u_{y1} \\ \theta_{z1} \end{bmatrix} + \begin{bmatrix} \boldsymbol{r}^2 & -\dfrac{\boldsymbol{r}^2}{2} \\ 0 & \dfrac{4\{\cosh(\boldsymbol{r}) - \boldsymbol{r}\sinh(\boldsymbol{r}) - 1\} + \boldsymbol{r}^2\{1 + \cosh(\boldsymbol{r})\}}{2\{\boldsymbol{r}\sinh(\boldsymbol{r}) - 2\cosh(\boldsymbol{r}) + 2\}} \end{bmatrix} \begin{bmatrix} \alpha + \kappa \\ \kappa \end{bmatrix} \tag{2.16}$$

As is expected, setting $\alpha = \kappa = 0$, reduces the above expression to that for a simple beam, prior to series expansion and truncation. As earlier, expanding the transcendental functions in the above matrices, and truncating fourth-order or higher terms in $\boldsymbol{r}$ (or equivalently second-order or higher terms in $\boldsymbol{f}_{x1}$), provides a great degree of simplification at less than 3% error over a comfortably large $\boldsymbol{f}_{x1}$ range (±5). The simplified DoF direction force-displacement relations may thus be expressed as follows.

$$\begin{bmatrix} \boldsymbol{f}_{y1} \\ \boldsymbol{m}_{z1} \end{bmatrix} = \begin{bmatrix} 12 & -6 \\ -6 & 4 \end{bmatrix} \begin{bmatrix} u_{y1} \\ \theta_{z1} \end{bmatrix} + \boldsymbol{f}_{x1} \begin{bmatrix} 12 & -6 \\ -6 & 4 \end{bmatrix} \begin{bmatrix} u_{y1} \\ \theta_{z1} \end{bmatrix} + \boldsymbol{f}_{x1} \begin{bmatrix} 1 & -\dfrac{1}{2} \\ 0 & \dfrac{1}{12} \end{bmatrix} \begin{bmatrix} \alpha + \kappa \\ \kappa \end{bmatrix} \tag{2.17}$$

Clearly, the first two terms, in the above matrix equation, are identical to the elastic stiffness and load-stiffening terms in Eq.(2.3) for a simple beam. The last term is new and arises due to the initial slope and curvature. Even though this term might appear similar to the original load-stiffening term, it actually does not change the DoF stiffness values. The presence of α and κ simply shift the DoF load-displacement curves without affecting their slopes. This is corroborated to a high degree of accuracy by means of FEA for three different combinations of α and κ (Figure 2.9). The FEA is carried out over a relatively large u_{y1} range (± 0.1), with $\boldsymbol{f_{x1}}$ set to *5* and $\boldsymbol{m_{z1}}$ set to *0*. This constant shift for given beam geometry is a consequence of the fact that the DoC load $\boldsymbol{f_{x1}}$ produces additional bending moments along the beam length that are independent of the DoF displacements. The action of this load in the presence of DoF displacements indeed produces load-stiffing, but that is captured as usual by the second term in the above expression.

We next proceed to determine the DoC direction load-displacement expression for this flexure beam by imposing the following beam-arc length conservation relation:

$$\int_0^{1+u_{x1}^{(e)}} \left\{1+\frac{1}{2}\left(y_i'(x)\right)^2\right\} dx = \int_0^{1+u_{x1}} \left\{1+\frac{1}{2}\left(u_y'(x)+y_i'(x)\right)^2\right\} dx \tag{2.18}$$

The LHS is the total arc length, which is the initial length augmented by the elastic elongation of the beam, $u_{x1}^{(e)}$. The RHS computes the total arc length after deformation, and hence the upper limit of integration changes to *(1+u_{x1})*. This DoC direction constraint equation may be solved using the solution for $u_y(x)$ derived earlier in Eq.(2.13), to yield the following relation between end-displacements and DoC end-load:

$$u_{x1} = \boldsymbol{f_{x1}}\frac{t^2}{12} + \begin{bmatrix} u_{y1} & \theta_{z1} \end{bmatrix}\begin{bmatrix} g_{11} & g_{12} \\ g_{21} & g_{22} \end{bmatrix}\begin{bmatrix} u_{y1} \\ \theta_{z1} \end{bmatrix} - \left(\alpha+\frac{\kappa}{2}\right)u_{y1} + g_{33}\left(\frac{\kappa}{2}\right)\theta_{z1} + g_{44}\left(\frac{\kappa}{2}\right)^2 \tag{2.19}$$

where,

$$g_{11} = -\frac{\boldsymbol{r}^2\left\{\cosh^2(\boldsymbol{r})+\cosh(\boldsymbol{r})-2\right\} - 3\boldsymbol{r}\sinh(\boldsymbol{r})\left\{\cosh(\boldsymbol{r})-1\right\}}{2\left\{\boldsymbol{r}\sinh(\boldsymbol{r})-2\cosh(\boldsymbol{r})+2\right\}^2} \qquad \text{, where } \boldsymbol{r}^2 \triangleq \boldsymbol{f_{x1}}$$

$$g_{12} = g_{21} = \frac{\boldsymbol{r}^2\left\{\cosh(\boldsymbol{r})-1\right\} + \boldsymbol{r}\sinh(\boldsymbol{r})\left\{\cosh(\boldsymbol{r})-1\right\} - 4\left\{\cosh(\boldsymbol{r})-1\right\}^2}{4\left\{\boldsymbol{r}\sinh(\boldsymbol{r})-2\cosh(\boldsymbol{r})+2\right\}^2}$$

$$g_{22}=\frac{\boldsymbol{r}^3-\boldsymbol{r}^2\sinh(\boldsymbol{r})\{\cosh(\boldsymbol{r})+2\}+2\boldsymbol{r}\{2\cosh^2(\boldsymbol{r})-\cosh(\boldsymbol{r})-1\}-2\sinh(\boldsymbol{r})\{\cosh(\boldsymbol{r})-1\}}{4\boldsymbol{r}\{\boldsymbol{r}\sinh(\boldsymbol{r})-2\cosh(\boldsymbol{r})+2\}^2}$$

$$g_{33}=\frac{\boldsymbol{r}^3\{1+\cosh(\boldsymbol{r})\}-\boldsymbol{r}^2\sinh(\boldsymbol{r})\{5+\cosh(\boldsymbol{r})\}+4\boldsymbol{r}\{\cosh^2(\boldsymbol{r})+\cosh(\boldsymbol{r})-2\}-4\sinh(\boldsymbol{r})\{\cosh(\boldsymbol{r})-1\}}{2\boldsymbol{r}\{\boldsymbol{r}\sinh(\boldsymbol{r})-2\cosh(\boldsymbol{r})+2\}^2}$$

$$g_{44}=\frac{\boldsymbol{r}^3\{\cosh^2(\boldsymbol{r})+3\cosh(\boldsymbol{r})+2\}-\boldsymbol{r}^2\sinh(\boldsymbol{r})\{7\cosh(\boldsymbol{r})+11\}+4\boldsymbol{r}\{4\cosh^2(\boldsymbol{r})+\cosh(\boldsymbol{r})-5\}}{6\boldsymbol{r}\{\boldsymbol{r}\sinh(\boldsymbol{r})-2\cosh(\boldsymbol{r})+2\}^2}$$

$$-\frac{12\sinh(\boldsymbol{r})\{\cosh(\boldsymbol{r})-1\}}{6\boldsymbol{r}\{\boldsymbol{r}\sinh(\boldsymbol{r})-2\cosh(\boldsymbol{r})+2\}^2}$$

Upon setting α and κ to zero, the above DoC direction relation reduces to the one obtained for a simple beam, before series expansion and truncation. Next, as done for the DoF matrix equation, expanding the transcendental functions (g's) and dropping higher-order terms in f_{x1}, provides a considerably more simple and insightful relation, at less than 3% error over f_{x1} in the range of ±5.

$$u_{x1}=\boldsymbol{f}_{x1}\frac{t^2}{12}+\begin{bmatrix}u_{y1} & \theta_{z1}\end{bmatrix}\begin{bmatrix}-\frac{3}{5} & \frac{1}{20}\\ \frac{1}{20} & -\frac{1}{15}\end{bmatrix}\begin{bmatrix}u_{y1}\\ \theta_{z1}\end{bmatrix}+\boldsymbol{f}_{x1}\begin{bmatrix}u_{y1} & \theta_{z1}\end{bmatrix}\begin{bmatrix}\frac{1}{700} & -\frac{1}{1400}\\ -\frac{1}{1400} & \frac{11}{6300}\end{bmatrix}\begin{bmatrix}u_{y1}\\ \theta_{z1}\end{bmatrix}$$
$$-\left(\alpha+\frac{\kappa}{2}\right)u_{y1}-\frac{\kappa}{12}\theta_{z1}+\boldsymbol{f}_{x1}\frac{\kappa}{360}\theta_{z1}+\boldsymbol{f}_{x1}\frac{\kappa^2}{720} \qquad (2.20)$$

The first (purely elastic), second (purely kinematic) and third (elastokinematic) terms in the above expression are identical to those obtained for the simple beam (Eq.(2.5)). The effects of α and κ in the DoC direction are expressed via the last four terms. The fourth and fifth terms contribute to an extra purely kinematic component. Even though these terms do not exhibit a quadratic dependence on the DoF displacement like the previous kinematic terms, they are independent of the DoC load. The sixth term, which only depends on the initial curvature and not the slant, contributes to an extra elastokinematic effect, which again is not quadratic in the DoF displacement. However, this term produces a change in the DoC stiffness with increasing θ_{z1} displacement. The seventh and final term in the above expression is a new purely elastic term. Both the sixth and seventh terms arise due to 'uncurling' of the initial beam curvature in the

presence of a DoC load $\boldsymbol{f_{x1}}$. In case of an initially slanted beam with no initial curvature ($\kappa = 0$), since this uncurling does not exist, there are no elastic or elastokinematic components when DoF displacements are zero.

These mathematical and physical observations are further verified via FEA for three different combinations of α and κ (Figure 2.9, Figure 2.10 and Figure 2.11). Figure 2.9 plots the normalized DoF force $\boldsymbol{f_{y1}}$ vs normalized DoF displacement u_{y1} in the presence of normalized DoC load $\boldsymbol{f_{x1}}$ set to 5. This figure shows a constant shift in the force displacement curve without the change is stiffness (since the slope is the same). Obviously this is because for an initially slanted or curved beam $\boldsymbol{f_{x1}}$ produces a displacement even in the absence of $\boldsymbol{f_{y1}}$. Figure 2.10 plots the parasitic error motion along the X DoC, u_{x1}, against the Y DoF displacement, u_{y1}. The corresponding FEA is carried out with $\boldsymbol{f_{x1}}$ set to 5 and $\boldsymbol{m_{z1}}$ set to 0. Figure 2.11 plots the X DoC stiffness against the Y DoF displacement, u_{y1}, and the FEA is carried out with $\boldsymbol{f_{x1}}$ set to 5 and θ_{z1} set to 0. The FEA results are all found to be in good match with the generalized BCM developed in this section.

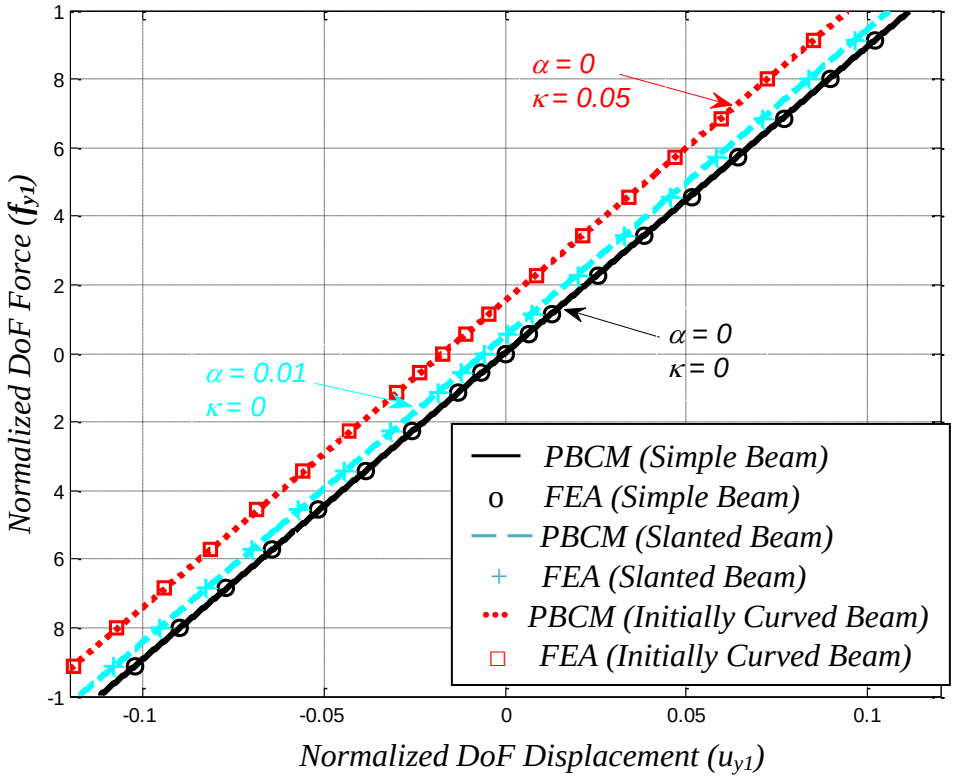

Figure 2.9: DoF force (f_{y1}) vs. DoF displacement (u_{y1}) for initially slanted or curved beams

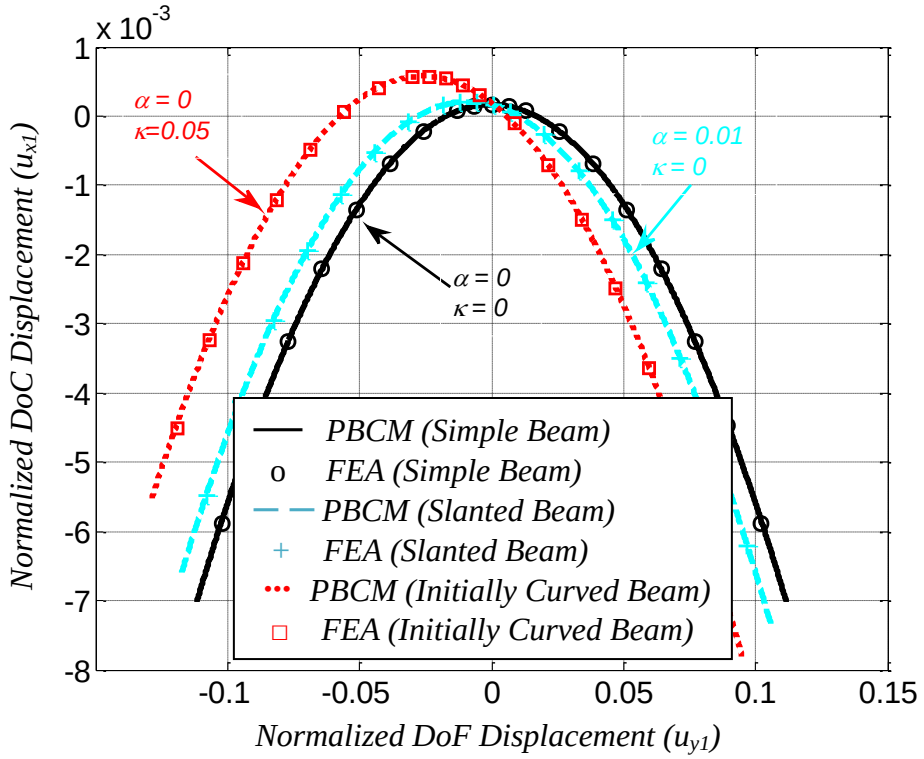

Figure 2.10: DoC Displacement(u_{x1}) vs. DoF displacement (u_{y1}) for initially slanted or curved beams

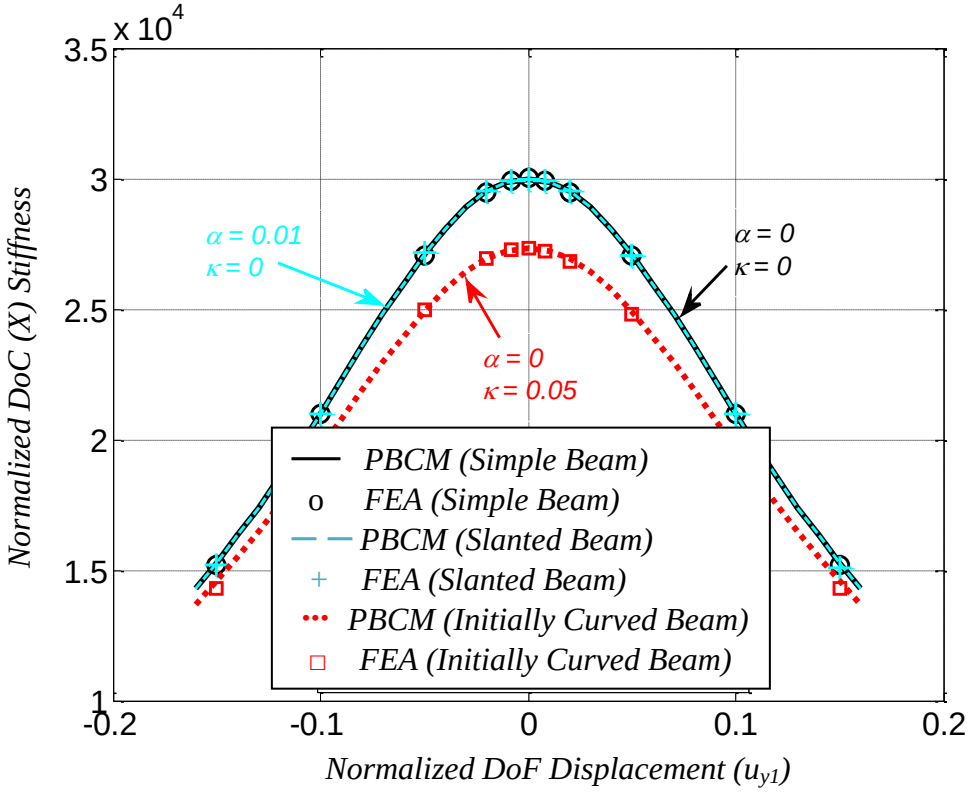

Figure 2.11: DoC Stiffness vs. DoF displacement (u_{y1}) for initially slanted or curved beams

Thus, overall, a uniform thickness beam flexure with initial slant and curvature continues to behave like a single DoC constraint element. The constraint characteristics along the DoF direction do not change considerably, but the DoC error motion as well stiffness is influenced by the presence of additional linear, kinematic, and elastokinematic terms.

2.4 Beam Shape Generalization

While in the previous two sections we have considered uniform thickness beams that may be initially straight, initially slanted, and/or initially curved, in this section we attempt a systematic process for developing the PBCM for an initially straight beam with any generalized beam cross-section variation along its length. Such beam shape variation allows a non-uniform distribution of compliance along the beam length, and if the consequence of distributed compliance is analytically understood in terms of the beam constraint characteristics, one can carry out beam shape optimization.

Figure 2.12 illustrates an initially straight beam with varying cross-section in its undeformed configuration subject to three generalized end-loads $\boldsymbol{f_{x1}}$, $\boldsymbol{f_{y1}}$, and $\boldsymbol{m_{z1}}$ along the coordinate frame XYZ. The resulting three end-displacements u_{x1}, u_{y1}, and θ_{z1}, are not shown but are also along the same coordinate frame. As earlier, all lower-case quantities are normalized with respect to beam parameters. It is reasonable to assume that the undeformed neutral axis lies along the X axis. It is also obvious that the Y and Θ_z directions still serve as the Degrees of Freedom, while the X direction is a Degree of Constraint.

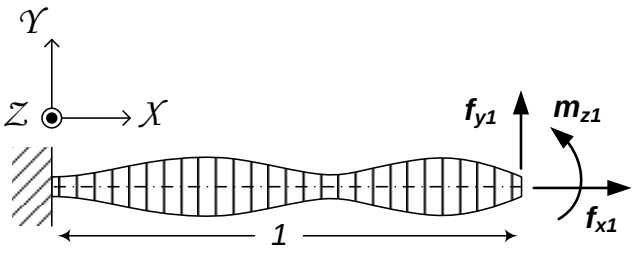

Figure 2.12: ***Straight Beam with Varying Cross-Section***

The modeling assumptions remain the same as earlier, except for the fact that I_{zz} is no longer constant and, instead, may be stated as $I_{ZZ}(x) = I_{ZZ0}\xi(x)$. I_{ZZ0}, a constant, is the nominal

second moment of area and is therefore used in the normalization scheme described earlier. Consequently, the beam governing equation (2.1) becomes:

$$\xi(x)u_y''(x) = \boldsymbol{m_{z1}} + \boldsymbol{f_{y1}}(1-x) - \boldsymbol{f_{x1}}\left(u_{y1} - u_y(x)\right) \tag{2.21}$$

Furthermore, assuming that the thickness change as the $T_Z(X) = T_{Z0}\zeta(X)$, the constraint equation for the x-displacement for a beam with variable cross-section is

$$u_{x1} = \frac{f_{x1}}{k_{33}} - \frac{1}{2}\int_0^1 u_y'^2 \, dX$$
$$\text{Where } k_{33} = \frac{(T_{Z0}/L)^2}{12}\int_0^1 \frac{dX}{\zeta(X)} \tag{2.22}$$

Given the arbitrariness of the function *ξ(x)* and *ζ(x)* a solution to this ordinary differential equation varying coefficients is no longer as easy as the case of a simple beam flexure. Nevertheless, Eq.(2.21) and the boundary conditions still remain linear in the transverse loads (***f*****y1** and ***m*****z1**) and displacements ($u_y(x)$ and it derivatives). This implies that the resulting relation between the transverse end-loads and displacement has to be linear, of the form:

$$\begin{Bmatrix} \boldsymbol{f_{y1}} \\ \boldsymbol{m_{z1}} \end{Bmatrix} = \begin{bmatrix} k_{11}(\boldsymbol{f_{x1}};\xi(x)) & k_{12}(\boldsymbol{f_{x1}};\xi(x)) \\ k_{21}(\boldsymbol{f_{x1}};\xi(x)) & k_{22}(\boldsymbol{f_{x1}};\xi(x)) \end{bmatrix} \begin{Bmatrix} u_{y1} \\ \theta_{z1} \end{Bmatrix} \tag{2.23}$$

In a similar fashion, since the x-displacement in Eq.(2.22) is quadratic in $u_y'(x)$ the constraint equation is expected to be of the form

$$u_{x1} = \frac{\boldsymbol{f_{x1}}}{k_{33}}\frac{t^2}{12} + \begin{Bmatrix} u_{y1} \\ \theta_{z1} \end{Bmatrix}^T \begin{bmatrix} g_{11}(\boldsymbol{f_{x1}};\xi(x)) & g_{12}(\boldsymbol{f_{x1}};\xi(x)) \\ g_{21}(\boldsymbol{f_{x1}};\xi(x)) & g_{22}(\boldsymbol{f_{x1}};\xi(x)) \end{bmatrix} \begin{Bmatrix} u_{y1} \\ \theta_{z1} \end{Bmatrix} \tag{2.24}$$

For both equations (2.23) and (2.24), each term in the matrices can be expanded in a taylor series of axial load ***f*****x1**. This would lead us to get models similar to PBCM for a simple beam flexure as given in Eq. (2.3) and (2.5). However as will be shown in Chapter 3, there exist inherent relations between the '*k*' matrices and the '*g*' matrices as shown below.

$$g_{\beta\lambda}^{(n)} = -\frac{n+1}{2}k_{\beta\lambda}^{(n+1)}, \quad \forall n = 0,...,\infty \qquad \text{where } \beta = 1 \text{ or } 2, \quad \lambda = 1 \text{ or } 2 \tag{2.25}$$

In this case we only need to solve for Eq. (2.23) and from that equation the constraint equation can be easily derived.

There are two approaches that we take to carry out the above strategy in solving Eq.(2.21) – analytical and numerical in order to determine Eq. (2.23). These two approaches are described below along with their merits and limitations.

2.4.1 Analytical Approach

This analytical approach is based on a series solution. Without any loss in generality, the beam shape may be expressed as:

$$\xi(x) = \left(b_0 + b_1 x + b_2 x^2 + ... + b_n x^n + ...\right) \qquad \text{where } b_o \triangleq 1 \tag{2.26}$$

Next, Eq. (2.21) is reduced to the following simplified homogenous form by choosing a new independent displacement variable $w(x) = \left\{\boldsymbol{m}_{z1} + \boldsymbol{f}_{y1}(1-x) - \boldsymbol{f}_{x1}\left(u_{y1} - u_y(x)\right)\right\}$,

$$\left(1 + \sum_{i=1}^{\infty} b_i x^i\right) w''(x) = \boldsymbol{f}_{x1} w(x) \tag{2.27}$$

Since the variable coefficient in this second order differential equation is an analytic function of x over the range of interest $\{0 \text{ to } 1\}$, it may be solved using the power series solution method [24]. The variable coefficient of *w''(x)* is never zero because that would mean the second moment of area is zero. That is possible only if the beam cross-section vanishes at that particular location, which is physically impractical. Since this coefficient is a polynomial, the solution to the above equation can be assumed to be an infinite polynomial series as follows:

$$w(x) = a_0 + a_1 x + a_2 x^2 + ... + a_n x^n + ... = \sum_{n=0}^{\infty} a_n x^n \tag{2.28}$$

The *a*'s in this expression will be referred to as the *solution coefficients*. Substituting this assumed solution in the homogenized beam governing equation (Eq.(2.27)) yields

$$\left(1 + \sum_{i=1}^{\infty} b_i x^i\right)\left(\sum_{n=0}^{\infty} \frac{(n+2)!}{n!} a_{n+2} x^n\right) = \sum_{m=0}^{\infty} a_m x^m \tag{2.29}$$

The above equation is true for all values of x and hence the coefficients of similar powers of x on the RHS and LHS can be equated. To equate the coefficients of the r^{th} power of x on both sides, Eq. (2.29) is differentiated r times and x is set to zero.

$$\left(\sum_{l=0}^{r}\left[{}^{r}c_l \left\{\frac{d^l}{dx^l}\left(\sum_{n=0}^{\infty} b_n x^n\right)\right\}\left\{\frac{d^{r-l}}{dx^{r-l}}\left(\sum_{m=0}^{\infty}\frac{(m+2)!}{m!} a_{m+2} x^m\right)\right\}\right]\right)_{x=0} = \left(\boldsymbol{f}_{x1}\frac{d^r}{dx^r}\left(\sum_{p=0}^{\infty} a_p x^p\right)\right)_{x=0}$$

$$\Rightarrow \sum_{l=0}^{r}\left[{}^{r}c_{l}\left\{ l!(r-l+2)!\right\} b_l a_{r-l+2}\right] = \boldsymbol{f}_{x1} a_r r!$$

$$\Rightarrow a_{r+2} = \frac{\boldsymbol{f}_{x1} a_r}{(r+1)(r+2)} - \sum_{i=0}^{r-1}\left\{ \frac{(r-i)(r-i+1)}{(r+1)(r+2)} a_{r-i+1} b_{i+1}\right\} \tag{2.30}$$

This equation relates the coefficient a_{r+2} with all its preceding coefficients, a_0 through a_{r+1}. The variables *l, m, p,* and *i* are dummy indices used for summation only. Using Eq.(2.30), the first four coefficients can be calculated to show

$$a_0 = 1 \,.\, a_0 + 0 \,.\, a_1 \quad , \quad a_1 = 0 \,.\, a_0 + 1 \,.\, a_1$$
$$a_2 = \frac{1}{2!}\boldsymbol{f}_{x1} a_0 + 0 \,.\, a_1 \quad , \quad a_3 = -\frac{b_1}{3!}\boldsymbol{f}_{x1} a_0 + \frac{1!}{3!}\boldsymbol{f}_{x1} a_1 \tag{2.31}$$

From Eq.(2.31), it may be observed that the initial four coefficients can be all expressed in term of a_0 and a_1. By the method of induction, it is next shown that all *a*'s can be similarly expressed as a linear combination of a_0 and a_1. Let us assume that for some *j*, each of the coefficients a_2 through a_j is represented in terms of a_0 and a_1:

$$a_n = h_{n,0} a_0 + h_{n,1} a_1 \qquad \forall\ 2 \le n \le j \tag{2.32}$$

Substituting Eq. (2.32) into Eq.(2.30), with $r+2 = j+1$, one may observe that a_{j+1} also turns out in terms of a_0 and a_1.

$$a_{j+1} = \frac{\boldsymbol{f}_{x1}\left(h_{j-1,0} a_0 + h_{j-1,1} a_1\right)}{(r+1)(r+2)} - \sum_{i=0}^{j-2}\left\{ \frac{(j-i)(j-i-1)}{j(j+1)} h_{j-i,0} b_{i+1}\right\} a_0$$
$$- \sum_{i=0}^{j-2}\left\{ \frac{(j-i)(j-i-1)}{j(j+1)} h_{j-i,1} b_{i+1}\right\} a_1 \tag{2.33}$$

Eq.(2.33) confirms that a_{j+1} can also be expressed in the form of Eq. (2.32). Thus, by the principle of induction, it is proven that all subsequent *a*'s are of the form of Eq. (2.32), where $h_{n,0}$ represents the coefficient of a_0 in a_n and $h_{n,1}$ represents the coefficient of a_1 in a_n. Using Eq.(2.30), the following recursion formula for $h_{n,0}$ and $h_{n,1}$ may be obtained for $n>2$.

$$h_{n,0} = \frac{\boldsymbol{f}_{x1} h_{n-2,0}}{n(n-1)} - \sum_{i=0}^{n-3}\left\{ \frac{(n-i-2)(n-i-1)}{n(n-1)} h_{n-i-1,0} b_{i+1}\right\}$$
$$h_{n,1} = \frac{\boldsymbol{f}_{x1} h_{n-2,1}}{n(n-1)} - \sum_{k=0}^{n-3}\left\{ \frac{(n-k-2)(n-k-1)}{n(n-1)} h_{n-k-1,1} b_{k+1}\right\} \tag{2.34}$$

In the above expressions, *i* and *k* are dummy variables used simply for summation. Also, it becomes evident that the coefficients $h_{n,0}$ and $h_{n,1}$ are functions of the beam shape parameters *b*'s and the DoC load $\boldsymbol{f}_{x1}$. Thus, using Eqs. (2.28), (2.32), and (2.34), the solution for *w(x)* and $u_y(x)$ may be stated as follows:

$$
\begin{aligned}
& w(x) = a_0\left(1 + h_{2,0}x^2 + .. + h_{n,0}x^n + ..\right) + a_1\left(x + h_{2,1}x^2 + .. + h_{n,1}x^n + ..\right) \\
& \Rightarrow u_y(x) = -\frac{1}{\boldsymbol{f}_{x1}}\left\{\boldsymbol{m}_{z1} + \boldsymbol{f}_{y1}(1-x)\right\} + u_{y1} + \frac{1}{\boldsymbol{f}_{x1}}\left\{a_0 s_0(x) + a_1 s_1(x)\right\} \\
& \text{where, } s_0(x) \triangleq \left(1 + h_{2,0}x^2 + .. + h_{n,0}x^n + ..\right) \\
& \qquad\quad s_1(x) \triangleq \left(x + h_{2,1}x^2 + .. + h_{n,1}x^n + ..\right)
\end{aligned}
\tag{2.35}
$$

The series-solution, given by Eq.(2.35), is meaningful only when the series is convergent. If the beam shape $\xi(x)$ in Eq.(2.26) is a q^{th} order polynomial, it can be shown that this series-solution is convergent at *x=1*, provided the following convergence criterion is met. The reader is referred to Appendix 2.B at the end of this chapter for the derivation of this criterion.

$$
\left\| \mathit{roots}\left(\rho^q + b_1\rho^{q-1} + ... + b_{q-1}\rho^1 + b_q = 0\right) \right\| < 1 \tag{2.36}
$$

The displacement solution given by Eq.(2.35) has two arbitrary constants a_0 and a_1. This is expected since the beam governing equation, Eq.(2.27), is second order. The two arbitrary constants are determined by applying the boundary conditions at the fixed end of the beam.

$$
\begin{aligned}
& u_y(0) = 0,\ u_y'(0) = 0 \\
& \Rightarrow a_0 = \boldsymbol{m}_{z1} + \boldsymbol{f}_{y1} - \boldsymbol{f}_{x1}u_{y1},\ a_1 = -\boldsymbol{f}_{y1}
\end{aligned}
\tag{2.37}
$$

Finally, the DoF direction end-load end-displacement relations are obtained by setting *x=1* in the Eq.(2.35).

$$
\begin{aligned}
& u_{y1} = u_y(1), \text{ and } \theta_{z1} = u_y'(1) \ \Rightarrow \\
& u_{y1}\left\{\boldsymbol{f}_{x1}s_0(1)\right\} = \boldsymbol{f}_{y1}\left(s_0(1) - s_1(1)\right) + \boldsymbol{m}_{z1}\left(s_0(1) - 1\right), \text{ and} \\
& \boldsymbol{f}_{x1}\theta_{z1} + \boldsymbol{f}_{x1}s_0'(1)u_{y1} = \boldsymbol{f}_{y1}\left(1 + s_0'(1) - s_1'(1)\right) + \boldsymbol{m}_{z1}s_0'(1)
\end{aligned}
\tag{2.38}
$$

This can be further converted to a matrix format as shown below:

$$
\boldsymbol{f}_{x1}\begin{bmatrix} s_0(1) & 0 \\ s_0'(1) & 1 \end{bmatrix}\begin{Bmatrix} u_{y1} \\ \theta_{z1} \end{Bmatrix} = \begin{bmatrix} s_0(1) - s_1(1) & s_0(1) - 1 \\ 1 + s_0'(1) - s_1'(1) & s_0'(1) \end{bmatrix}\begin{Bmatrix} \boldsymbol{f}_{y1} \\ \boldsymbol{m}_{z1} \end{Bmatrix} \tag{2.39}
$$

The above equation is solved to obtain the end-loads in terms of the end-displacements and functions $s_o(x)$ and $s_1(x)$.

$$\begin{Bmatrix} \boldsymbol{f}_{y1} \\ \boldsymbol{m}_{z1} \end{Bmatrix} = \begin{bmatrix} k_{11} & k_{12} \\ k_{21} & k_{22} \end{bmatrix} \begin{Bmatrix} u_{y1} \\ \theta_{z1} \end{Bmatrix}, \text{ where } \quad k_{11} = \frac{\boldsymbol{f}_{x1} s_0'(1)}{\left\{ s_0'(1) - s_1'(1) - s_0(1) + 2 \right\}},$$
$$k_{12} = k_{21} = \frac{\boldsymbol{f}_{x1} \left\{ 1 - s_0(1) \right\}}{\left\{ s_0'(1) - s_1'(1) - s_0(1) + 2 \right\}}, \quad k_{22} = \frac{\boldsymbol{f}_{x1} \left\{ s_0(1) - s_1(1) \right\}}{\left\{ s_0'(1) - s_1'(1) - s_0(1) + 2 \right\}} \tag{2.40}$$

Maxwell's reciprocity principle [25], which requires the stiffness matrix to be symmetric, has been employed in going from Eq.(2.39) to Eq.(2.40). This principle requires the following condition to hold true at all times, and may be used to check the convergence and validity of the solution, as explained later.

$$s_1(1) s_0'(1) - s_0(1) s_1'(1) = -1 \tag{2.41}$$

The above relation can be easily verified to be true for the simple case in which the variation in cross-section is taken to be zero, i.e., $\forall\, b$'s = 0. For this case, the expressions for $h_{n,0}$ and $h_{n,1}$, determined using Eq.(2.34), are:

$$h_{n,0} = \frac{\boldsymbol{f}_{x1} h_{n-2,0}}{n(n-1)}, \quad h_{j,1} = \frac{\boldsymbol{f}_{x1} h_{n-2,1}}{n(n-1)}$$
$$h_{0,0} = 1, \quad h_{1,0} = 0, \quad h_{0,1} = 0, \quad h_{1,1} = 1$$
$$h_{2,0} = \frac{\boldsymbol{f}_{x1}}{2!}, \quad h_{2,1} = 0$$
$$h_{3,0} = 0, \quad h_{3,1} = \frac{\boldsymbol{f}_{x1}}{3!} \tag{2.42}$$
$$h_{4,0} = \frac{\boldsymbol{f}_{x1}^{\,2}}{4!}, \quad h_{4,1} = 0$$
$$h_{5,0} = 0, \quad h_{5,1} = \frac{\boldsymbol{f}_{x1}^{\,2}}{5!}$$

Substituting these values of $h_{n,0}$ and $h_{n,1}$ in Eq.(2.35), it is observed that the functions $s_0(x)$ and $s_1(x)$ are simply hyperbolic sine and cosine functions as given below.

$$s_0(x) = \left(1 + \frac{\boldsymbol{f}_{x1}}{2!} x^2 + \frac{\boldsymbol{f}_{x1}^{\,2}}{4!} x^4 .. \right) = \cosh\left(\sqrt{\boldsymbol{f}_{x1}}\, x \right)$$
$$s_1(x) = \left(x + \frac{\boldsymbol{f}_{x1}}{2!} x^3 + \frac{\boldsymbol{f}_{x1}^{\,2}}{2!} x^5 .. \right) = \frac{1}{\sqrt{\boldsymbol{f}_{x1}}} \sinh\left(\sqrt{\boldsymbol{f}_{x1}}\, x \right) \tag{2.43}$$

These values of $s_0(x)$ and $s_1(x)$ satisfy Eq.(2.41), thus verifying Maxwell's reciprocity principle. One may also check that substituting these hyperbolic functions into the load-displacement relations of Eq.(2.40) results in the exact transcendental relations for a simple beam [30, 58].

Further, the reciprocity principle may be used to determine the number of solution coefficients, a's, to be used in Eq.(2.28). This is equivalent to choosing the highest power of x in $s_0(x)$ and $s_1(x)$ to be retained such that resulting $s_0(1)$ and $s_1(1)$ satisfy Eq.(2.41) within an acceptable margin of error.

As expected, Eq. (2.40) confirms the fact that even for a varying cross-section beam the DoF end-loads are linearly related to the DoF end-displacements by a stiffness matrix that is a function of only the DoC direction force $\boldsymbol{f_{x1}}$ and the beam shape coefficients b's. The final step now is to expand the stiffness coeffecients k's in Eq.(2.40) with respect to $\boldsymbol{f_{x1}}$: the first term (zeroth-order) will provide the elastic stiffness coefficients for the PBCM, the second term (first-order) provides the load-stiffening and kinematic coefficients for the PBCM, and the third term (second-order) provides the elastokinematic coefficients for the PBCM. As discussed earlier, an explicit solution to constraint equation (2.4) to determine the constraint matrix is not necessary.

Ultimately, it is seen above that the load-displacement relation format for the variable cross-section beam remains the same as that for the simple beam – only the beam characteristic coefficient change – thus validating the generality of the PBCM. The procedure is still closed-form because for a given beam shape, no iterative or numerical methods are required; furthermore, the beam shape coefficients show up as parameters in the resulting PBCM, thus preserving it parametric nature.

Recapping the analytical approach presented above: The beam shape is first quantified by expressing the second moment of area of the beam as a function of x coordinate and beam shape parameters b's as in Eq.(2.26). The beam shape parameters are then used to check the convergence criterion given by Eq.(2.36). Once the convergence criterion is satisfied, the beam shape parameters may be used to calculate the solution coefficients a's in terms of the variables $h_{n,0}$ and $h_{n,1}$ as per Eq. (2.34), followed by determination of $s_0(x)$ and $s_1(x)$ as per Eq. (2.35). The functions $s_0(x)$ and $s_1(x)$ are then truncated in powers of x such that Maxwell's reciprocity criterion, given in Eq.(2.41), is satisfied within a certain acceptable error (e.g. 1%) for the given range of problem parameters (DoC force $\boldsymbol{f_{x1}}$ and the beam shape parameters). These functions

then provide the stiffness matrix as per Eq.(2.40). Finally, the resulting stiffness coefficients are expanded in $\boldsymbol{f}_{x1}$ to provide the elastic, load-stiffening, kinematic and elasto-kinematic coefficients for the BCM.

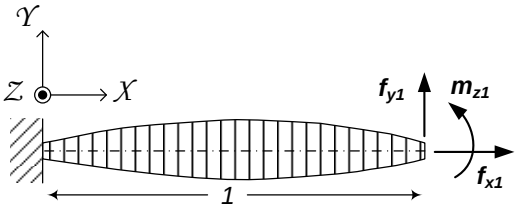

Figure 2.13: ***Straight Beam with a Sinusoidal Varying Moment of Area***

The above proposed analysis procedure is illustrated by an example. A variable cross-section beam (Figure 2.13) is described by Eq.(2.44). The resulting shape parameters *b*'s are given in Table 2.2. Without any loss in generality, the area moment of inertia, as opposed to the beam thickness, is taken to a sinusoidal function.

$$I(x) = I_{zz0}\left\{1 + \frac{\eta}{100}\sin(\pi x)\right\} \tag{2.44}$$

b_1	$\eta\pi/100$	b_5	$\eta\pi^5/(5!100)$	b_9	$\eta\pi^9/(9!100)$
b_2	0	b_6	0	b_{10}	0
b_3	$-\eta\pi^3/3!$	b_7	$-\eta\pi^7/(7!100)$	b_{11}	$-\eta\pi^{11}/(11!100)$
b_4	0	b_8	0	b_{12}	0

Table 2.2. Shape parameters for a sinusoidally varying beam cross-section

The variable η is the highest percentage increase in the area moment of inertia which occurs at the middle of the beam. Using the twelve beam shape parameters given above the second moment of inertia function can be estimated with 0.01% accuracy for all 0<x<1. Hence, the higher order *b*'s are neglected. It may be shown that the convergence criterion is satisfied by the shape parameters *b*'s for $\eta < 10$. Next the *h*'s and *s*'s functions are calculated as previously described in Eq. (2.34) and Eq. (2.35) but are not presented here for brevity. The expressions for the functions $s_0(x)$ and $s_1(x)$ are truncated after the tenth power of *x,* satisfying Maxwell's reciprocity principle, Eq.(2.41), with less than 1% error for $\eta < 10$ and $\boldsymbol{f}_{x1}$ in the range ±5. The resulting stiffness matrix may be further expanded in terms of $\boldsymbol{f}_{x1}$, as follows.

$$\begin{Bmatrix} \boldsymbol{f}_{y1} \\ \boldsymbol{m}_{z1} \end{Bmatrix} = \begin{bmatrix} k_{11}^{(0)}(\eta) & k_{12}^{(0)}(\eta) \\ k_{21}^{(0)}(\eta) & k_{22}^{(0)}(\eta) \end{bmatrix} \begin{Bmatrix} u_{y1} \\ \theta_{z1} \end{Bmatrix} + \boldsymbol{f}_{x1} \begin{bmatrix} k_{11}^{(1)}(\eta) & k_{12}^{(1)}(\eta) \\ k_{21}^{(1)}(\eta) & k_{22}^{(1)}(\eta) \end{bmatrix} \begin{Bmatrix} u_{y1} \\ \theta_{z1} \end{Bmatrix} + \boldsymbol{f}_{x1}^{\,2} \begin{bmatrix} k_{11}^{(2)}(\eta) & k_{12}^{(2)}(\eta) \\ k_{21}^{(2)}(\eta) & k_{22}^{(2)}(\eta) \end{bmatrix} \begin{Bmatrix} u_{y1} \\ \theta_{z1} \end{Bmatrix} + \ldots \tag{2.45}$$

where, $\Phi(\eta) \triangleq \left(1 - 0.01\eta - 0.0002\eta^2\right)$

$$k_{11}^{(0)}(\eta) = \frac{12 - 0.304\eta + 0.0311\eta^2}{\Phi(\eta)^3}$$

$$k_{12}^{(0)}(\eta) = k_{21}^{(0)}(\eta) = \frac{-6 + 0.1676\eta - 0.01453\eta^2}{\Phi(\eta)^3}$$

$$k_{22}^{(0)}(\eta) = \frac{4 - 0.101\eta + 0.009\eta^2}{\Phi(\eta)^3}$$

$$k_{11}^{(1)}(\eta) = \frac{1.201 - 0.048\eta - 0.0103\eta^2}{\Phi(\eta)^3}$$

$$k_{12}^{(1)}(\eta) = k_{21}^{(1)}(\eta) = \frac{-0.1 + 0.009\eta + 0.0052\eta^2}{\Phi(\eta)^3}$$

$$k_{22}^{(1)}(\eta) = \frac{0.131 - 0.0082\eta + 0.0034\eta^2}{\Phi(\eta)^3}$$

$$k_{11}^{(2)}(\eta) = \frac{-0.00136 - 0.00094\eta + 0.0030\eta^2}{\Phi(\eta)^3}$$

$$k_{12}^{(2)}(\eta) = k_{21}^{(2)}(\eta) = \frac{0.00068 - 0.00098\eta - 0.00014\eta^2}{\Phi(\eta)^3}$$

$$k_{22}^{(2)}(\eta) = \frac{-0.00152 + 0.00072\eta + 0.00094\eta^2}{\Phi(\eta)^3}$$

Eq. (2.45) shows that the stiffness coefficients are function of the beam shape and DoC force $\boldsymbol{f}_{x1}$ only. The relation can be verified to match exactly with that of a simple beam if η is set to zero. The first matrix in Eq.(2.45) is the elastic stiffness matrix while the second matrix represents the load-stiffening matrix. The stiffness matrix associated with $\boldsymbol{f}_{x1}^{\,2}$ and higher order terms may be neglected with respect to the load-stiffening matrix, at the expense of 1-2% error over an $\boldsymbol{f}_{x1}$ range of ±5.

The constraint relation obtained for this particular case after similarly truncating matrices with second order and higher powers of $\boldsymbol{f}_{x1}$ is given below. It is interesting to note that the

constraint relation has the same form as that for a simple beam, i.e., a summation of purely elastic term, a purely kinematic term, and an elastokinematic term.

$$u_{x1} = u_{x1}^{(e)} + \begin{Bmatrix} u_{y1} & \theta_{z1} \end{Bmatrix} \begin{bmatrix} g_{11}^{(0)}(\eta) & g_{12}^{(0)}(\eta) \\ g_{21}^{(0)}(\eta) & g_{22}^{(0)}(\eta) \end{bmatrix} \begin{Bmatrix} u_{y1} \\ \theta_{z1} \end{Bmatrix} + f_{x1} \begin{Bmatrix} u_{y1} & \theta_{z1} \end{Bmatrix} \begin{bmatrix} g_{11}^{(1)}(\eta) & g_{12}^{(1)}(\eta) \\ g_{21}^{(1)}(\eta) & g_{22}^{(1)}(\eta) \end{bmatrix} \begin{Bmatrix} u_{y1} \\ \theta_{z1} \end{Bmatrix} \tag{2.46}$$

where, $g_{11}^{(0)}(\eta) = -\dfrac{1.201 - 0.048\eta - 0.0103\eta^2}{2\Phi(\eta)^3}$

$$g_{12}^{(0)}(\eta) = g_{21}^{(0)}(\eta) = -\frac{-0.1 + 0.009\eta + 0.0052\eta^2}{2\Phi(\eta)^3}$$

$$g_{22}^{(0)}(\eta) = -\frac{0.131 - 0.0082\eta + 0.0034\eta^2}{2\Phi(\eta)^3}$$

$$g_{11}^{(1)}(\eta) = -\frac{-0.00136 - 0.00094\eta + 0.0030\eta^2}{\Phi(\eta)^3}$$

$$g_{12}^{(1)}(\eta) = g_{21}^{(1)}(\eta) = -\frac{0.00068 - 0.00098\eta - 0.00014\eta^2}{\Phi(\eta)^3}$$

$$g_{22}^{(1)}(\eta) = -\frac{-0.00152 + 0.00072\eta + 0.00094\eta^2}{\Phi(\eta)^3}$$

The above example shows that the form of the load-displacement and constraint relations remains invariant in the PBCM even for varying beam cross-sections. Thus, it may be concluded that PBCM is valid for any generalized beam whose shape parameters are known. The beam characteristic coefficients in the PBCM may be determined from the beam shape parameters using the above-described procedure. This generalization of the PBCM also provides a useful tool for beam shape optimization. Furthermore, the solution obtained for the specific family of variable cross-section beam is closed-form in nature. Any change of parameters such end-loads, end-displacement, or beam shape (η) does not require a reformulation of the entire model. However, it is found that the series solution approach outlined above provides convergence for small values of η (< 0.1). Lack of solution convergence for larger variations, relevant for the purpose of design and optimization, proves to be a serious limitation of this approach. A potential research task, not addressed further in this thesis, is to develop more robust ways for

determining and achieving solution convergence. To overcome this problem, we next propose a numerical approach which is more effective and powerful, in determining the beam characteristic co-efficients for any beam shape. Although, for a single beam of a particular shape, this approach is not closed-form, the resulting model can be used in the closed form analysis of flexure mechanisms that use one or several of such beam.

2.4.2. Numerical Approach

Given the limitations recognized above, a numerical procedure is developed to determine the elastic, load-stiffening, kinematic, and elastokinematic terms from Eq.(2.23) by numerically solving Eq.(2.21). Since this equation contains the end displacement u_{y1}, which is initially unknown, the numerical solution requires an iterative process such that u_{y1} is updated and incrementally corrected at each step.

The algorithm uses numerical values of the beam shape $I_{ZZ}(x)$ and the end-loads ($\boldsymbol{f}_{x1}$, $\boldsymbol{f}_{y1}$, and $\boldsymbol{m}_{z1}$), along with an initial guess for u_{y1} (= *0*). For a given end-displacement value $u_{y1}(i)^{in}$ at iteration *i*, Eq. (2.21) is solved numerically in MATLAB using ODE45 to output a new value of end-displacement $u_{y1}(i)^{out}$. This new value is then used to update the end-displacement in the next iteration step using a pre-specified parameter λ: $u_{y1}(i+1)^{in} = u_{y1}(i)^{in} + \lambda\left\{u_{y1}(i)^{out} - u_{y1}(i)^{in}\right\}$. This cycle is repeated until an acceptable convergence is achieved in the u_{y1} value, i.e. the error $u_{y1}(i)^{out}$ - $u_{y1}(i)^{in}$ becomes less than a pre-specified parameter ε. At this point, the final values of u_{y1} and u'_{y1} (or θ_{z1}) constitute the desired solution. Parameter λ is chosen optimally so that the algorithm converges quickly. Parameter ε simply dictates the accuracy of the resulting numerical solution, with a small value leading to greater accuracy but also greater convergence time. In our case, λ = *0.1* and ε = *0.00001*.

Next, in order to solve for the various stiffness coefficients (*k*'s) in Eq.(2.23), we first determine the analogous compliance coefficients, which are easier to solve for using the above algorithm.

$$\begin{Bmatrix} u_{y1} \\ \theta_{z1} \end{Bmatrix} = \begin{bmatrix} c_{11}\left(\boldsymbol{f}_{x1};\xi(x)\right) & c_{12}\left(\boldsymbol{f}_{x1};\xi(x)\right) \\ c_{21}\left(\boldsymbol{f}_{x1};\xi(x)\right) & c_{22}\left(\boldsymbol{f}_{x1};\xi(x)\right) \end{bmatrix} \begin{Bmatrix} \boldsymbol{f}_{y1} \\ \boldsymbol{m}_{z1} \end{Bmatrix} \tag{2.47}$$

The following steps are carried out for several discrete numerical values of the DoC force $\boldsymbol{f_{x1}}$, varied between -5 and +5. By setting $\boldsymbol{m_{z1}}$ to zero and $\boldsymbol{f_{y1}}$ to one, end displacement u_{y1} and θ_{z1} provide the numerical values for compliance terms, c_{11} and c_{21}, respectively, for a given value of $\boldsymbol{f_{x1}}$. Similarly by setting $\boldsymbol{m_{z1}}$ to one and $\boldsymbol{f_{y1}}$ to zero, end displacement u_{y1} and θ_{z1} give the compliance terms c_{12} and c_{22}, for the same given value of $\boldsymbol{f_{x1}}$. Numerical values of the stiffness coefficients for this given value $\boldsymbol{f_{x1}}$ is then simply found by matrix inversion:

$$\begin{bmatrix} k_{11} & k_{12} \\ k_{21} & k_{22} \end{bmatrix} = \frac{1}{c_{11}c_{22} - c_{12}c_{21}} \begin{bmatrix} c_{22} & -c_{12} \\ -c_{21} & c_{11} \end{bmatrix} \tag{2.48}$$

Having carried out the above step for several discrete values of $\boldsymbol{f_{x1}}$, each of the stiffness coefficients k_{11}, k_{12}= k_{21}, and k_{22}, is expressed as a 7th order polynomial function of $\boldsymbol{f_{x1}}$, using curve fitting techniques as shown in the equation below:

$$\begin{bmatrix} k_{11}(\boldsymbol{f_{x1}}) & k_{12}(\boldsymbol{f_{x1}}) \\ k_{21}(\boldsymbol{f_{x1}}) & k_{22}(\boldsymbol{f_{x1}}) \end{bmatrix} = \begin{bmatrix} k_{11}^{(0)} & k_{12}^{(0)} \\ k_{12}^{(0)} & k_{22}^{(0)} \end{bmatrix} \begin{Bmatrix} u_{y1} \\ \theta_{z1} \end{Bmatrix} + \boldsymbol{f_{x1}} \begin{bmatrix} k_{11}^{(1)} & k_{12}^{(1)} \\ k_{12}^{(1)} & k_{22}^{(1)} \end{bmatrix} \begin{Bmatrix} u_{y1} \\ \theta_{z1} \end{Bmatrix} + \boldsymbol{f_{x1}^2} \begin{bmatrix} k_{11}^{(2)} & k_{12}^{(2)} \\ k_{12}^{(2)} & k_{22}^{(2)} \end{bmatrix} \begin{Bmatrix} u_{y1} \\ \theta_{z1} \end{Bmatrix} + .. \tag{2.49}$$

As per the strategy described in the beginning of this section, only the first three terms in the above polynomial are needed for completing the PBCM. The first term (zeroth-order term in $\boldsymbol{f_{x1}}$) provides the elastic stiffness coefficients, the second term provides load-stiffening and kinematic coefficients, and third term provides the elastokinematic coefficients. The constraint relation can be found using the inherent relations between the '*k*' coefficients of the load displacement relation in Eq.(2.23) and 'g' co-efficients in Eq.(2.25).

Thus, using this numerical procedure, which has been completely automated, the BCM for a beam with any type of varying cross-section can be found. The approach is not limited by convergence issues and is applicable to considerably large shape variations, as long as Eq.(2.21) and its underlying assumptions remain valid. Next, we illustrate the application of this method to a specific case of beam shape generalization, shown in Figure 2.14. In this case, the beam shape is completely determined by parameter a_o: a_o*=1/2* represents the simple beam with uniformly distributed compliance, while $a_o \rightarrow 0$ corresponds to a lumped-compliance topology. Given the relative simplicity of this shape, closed-form parametric BCM can be derived for this beam and has been reported previously [30]. These closed-form results are used here to verify the effectiveness and accuracy of the proposed numerical approach.

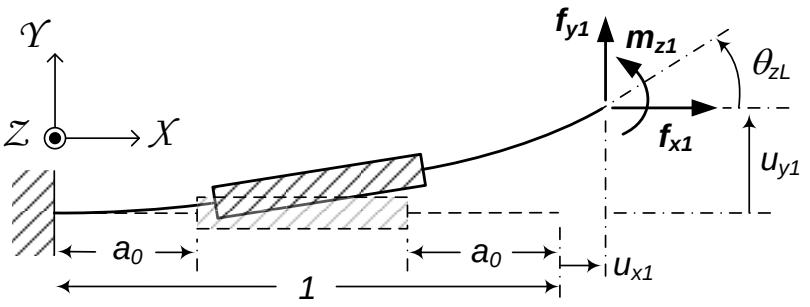

Figure 2.14: ***Variable cross-section beam***

A comparison of the load-displacement relations based on the closed-form PBCM, numerically derived PBCM, and non-linear FEA is illustrated in Fig.2.11 (elastic stiffness coefficients), Fig.2.12 (load-stiffening stiffness), and Fig.2.13 (elastokinematic coefficients). These figures show that the numerically derived BCM lies within a 1% deviation from the FEA as well as closed-form PBCM. The numerical PBCM derivation and FEA can be carried out only for discrete values of the beam shape parameter a_0, which was varied from *0.1* to *0.4* in increments of *0.05* in this study.

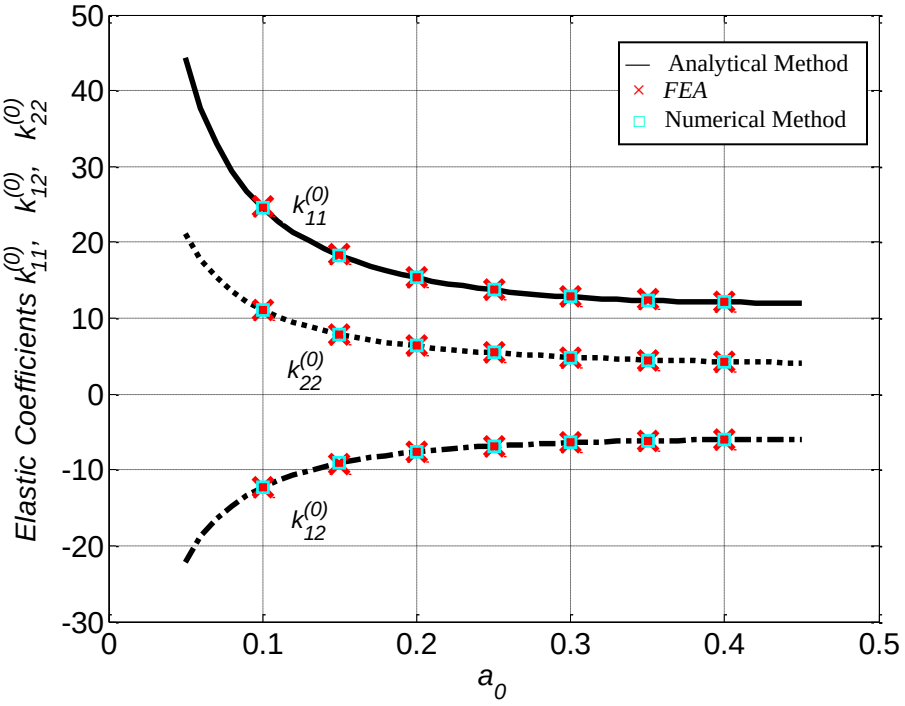

Figure 2.15: ***Elastic stiffness coefficients comparison***

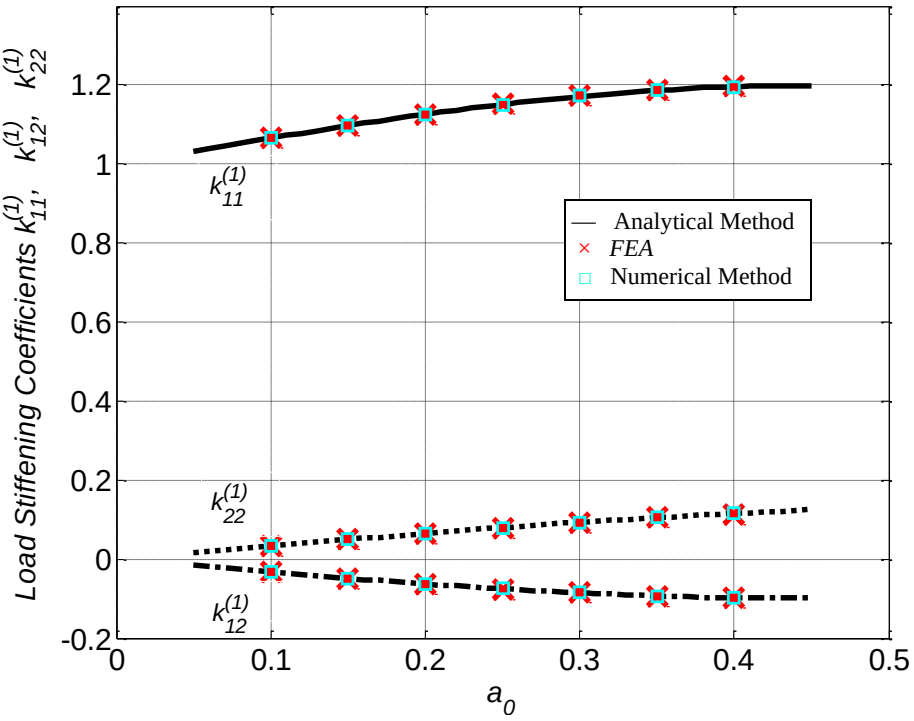

Figure 2.16: ***Load stiffening coefficients comparison***

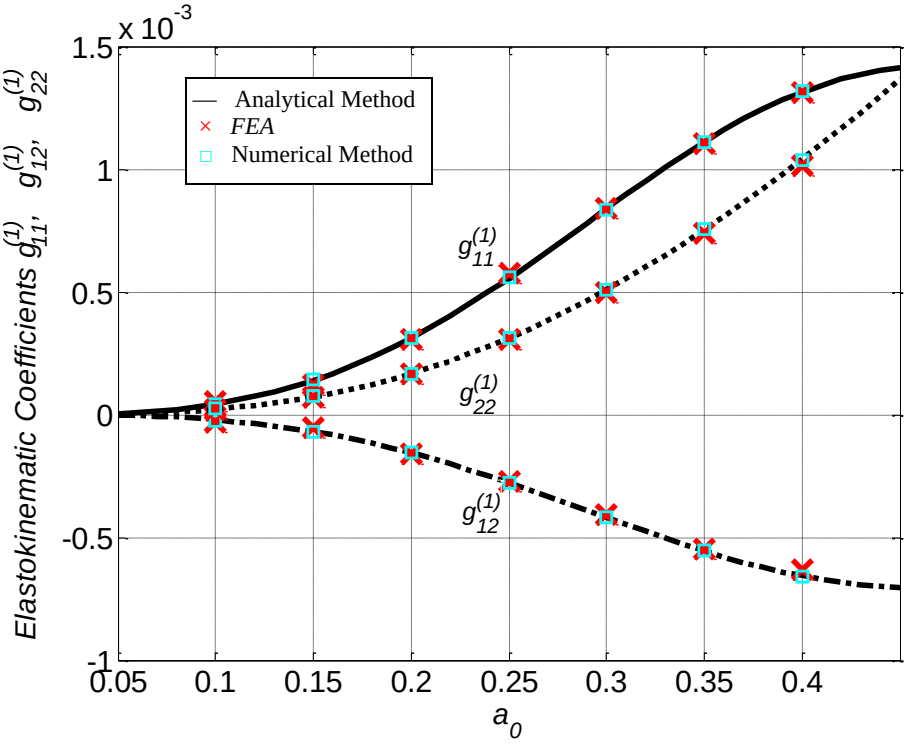

Figure 2.17: Geometric constraint coefficient (elastokinematic) comparison

The proposed numerical approach was also applied to other more complicated beam shapes including $I_{zz}(x) = I_{zzo}(1+\eta\sin(\pi x))$ and $I_{zz}(x) = I_{zzo}(1+\eta\sin^2(\pi x))$, with η as large as *2*. In each case, the resulting numerical PBCM was found to agree with non-linear FEA, within less 2% error. These detailed results are not included here for the sake of brevity.

Ultimately, the above analysis and examples show that the form of the load-displacement and constraint relations remains invariant in the PBCM, even for beams with varying cross-sections. This highlights the generality of the PBCM and therefore its strength in flexure mechanism design and optimization.

2.5 Discussion

In the chapter, the general framework of PBCM was shown. Although as we will analyze spatial loading of flexure strips the equations will get more complicated, the basic methodology will remain similar to key steps discussed here. The key understanding that is obtained in this chapter is the importance of performing load equilibrium in the deformed configurations especially in the presence on non-negligible axial force $\boldsymbol{f_{x1}}$. In flexure mechanisms, such axial forces are often present. This is because one of the primary functions of flexure mechanisms is load bearing which is nothing but resisting loads along its DoCs. Furthermore, when the beam flexure is not perfectly straight or aligned, the kinematic and elastokinematic characteristic of the flexure varies. A initially slant beam or a curved beam may be present due to these common manufacturing defects or by intentional design. Using the generalized model presented in section 2.3 one has the ability to work with loads and displacements in the global co-ordinate frame without performing unnecessary co-ordinate frame changes that would be required if the model for an initially straight beam is used. An example, when using the generalized model of a simple beam is advantageous, is a tilted parallelogram flexure which will be analyzed in Chapter 3 using this model.

Another key contribution of this Chapter is the model for simple beam flexure with varying cross-section. Two approaches were taken to generate an equivalent PBCM for this problem. The first approach employed a series based solution, in which PBCM was be derived analytically in a closed-form such that the beam shape parameter(s) show up in the model, without the need for any iterative or numerical procedures. However, this approach poses

convergence problems for large beam shape variations. An alternate numerical approach that is capable of handling any possible beam shape as well as large variations, without any convergence issues was also discuss. Although in this case determining the beam characteristic coefficients in the PBCM required numerical as well as iterative procedures, the fundamental relations between different beam characteristic coefficients, allowed the formulation of the complete PBCM of various beam shapes through the numerical solution of one differential equation. The utility of this approach does not lie in the model of one beam shape but in making more flexure elements available for closed-form design and analysis of flexure mechanisms. With more flexure elements available, optimization of flexure mechanism by changing flexure elements is easily possible.

One case that was not explicitly discussed was the case when the beam is initially slant, curved and also has a varying cross-section. However, an appropriate model can be easily formulated from our basic understanding of the slant and curved beam in section 2.3 as well as the model for straight beam with varying cross-section in section 2.4. We first note that the kinematic effect of the initial slant and curvature would remain unchanged because of geometric nature. Furthermore we also note that the beam characteristic coefficients are not affected by the initial slant and curvature. These coefficients will be solely determined by the beam's cross-section along its neutral axis. Finally, we note that the elasto-kinematic terms due to curvature, that depend on elastic behavior, kinematic behavior and the curvature of the beam, needs to be calculated by considering the initial slant, initial curvature and varying cross-sectional of the beam simultaneously. However, it can be shown that the powers of the force, displacements and curvature remain the same for these terms and the constant coefficient can be determined using a numerical procedure similar to section 2.4.2. There the analytical expressions for a beam that is initially slant, curved and also has a varying cross-section will be as follows.

$$\begin{bmatrix} \boldsymbol{f}_{y1} \\ \boldsymbol{m}_{z1} \end{bmatrix} = \begin{bmatrix} k_{11}^{(0)} & k_{12}^{(0)} \\ k_{12}^{(0)} & k_{22}^{(0)} \end{bmatrix} \begin{bmatrix} u_{y1} \\ \theta_{z1} \end{bmatrix} + \boldsymbol{f}_{x1} \begin{bmatrix} k_{11}^{(1)} & k_{12}^{(1)} \\ k_{12}^{(1)} & k_{22}^{(1)} \end{bmatrix} \begin{bmatrix} u_{y1} \\ \theta_{z1} \end{bmatrix} + \boldsymbol{f}_{x1} \begin{bmatrix} 1 & -\frac{1}{2} \\ 0 & \frac{1}{12} \end{bmatrix} \begin{bmatrix} \alpha + \kappa \\ \kappa \end{bmatrix} \tag{2.50}$$

$$u_{x1} = \boldsymbol{f}_{x1}\frac{t^2}{12} + \begin{bmatrix} u_{y1} & \theta_{z1} \end{bmatrix} \begin{bmatrix} g_{11}^{(0)} & g_{12}^{(0)} \\ g_{12}^{(0)} & g_{22}^{(0)} \end{bmatrix} \begin{bmatrix} u_{y1} \\ \theta_{z1} \end{bmatrix} + \boldsymbol{f}_{x1} \begin{bmatrix} u_{y1} & \theta_{z1} \end{bmatrix} \begin{bmatrix} g_{11}^{(1)} & g_{12}^{(1)} \\ g_{12}^{(1)} & g_{22}^{(1)} \end{bmatrix} \begin{bmatrix} u_{y1} \\ \theta_{z1} \end{bmatrix} \\ -\left(\alpha + \frac{\kappa}{2}\right) u_{y1} - \frac{\kappa}{12}\theta_{z1} + \boldsymbol{f}_{x1}\frac{\kappa}{360}\theta_{z1} + \boldsymbol{f}_{x1}\frac{\kappa^2}{720} \tag{2.51}$$

Appendix 2.A: Summary of FEA Procedure

The closed-form analytical expressions for the simple beam, parallelogram flexure module, initially slanted/curved beam, and the variable cross-section beams are validated by means of non-linear Finite Element Analysis performed in ANSYS. The non-linear formulation used in ANSYS is based on reference [64]. BEAM4 elements are used with consistent matrix and large displacement options turned on and shear coefficients set to zero. The material assumed is Stainless Steel, and typical values for Young's Modulus (210,000 $N.mm^{-2}$) and Poisson's Ratio (0.3) are used. Beam length (L) = 250mm, thickness (T) = 5mm, and height (W) = 50mm, are chosen for the FEA models. The undeformed neutral axis from the simple beam is taken along the x-axis. For all the beams, meshing is done at 300 elements per 250mm. The convergence criterion for all FEA experiments is set to tolerance limits = 0.001 on the L2 norm. The values of DoF force typically used for Figure 2.2-3 and Figure 2.9-7 is 0 and 1kN while for Figure 2.15-13 the DoC force vary between 0 and 5kN. Normalized beam characteristic coefficients $k_{11}^{(0)}$ and $k_{22}^{(0)}$ in Figure 2.2 and Figure 2.3 are measured one at time by setting u_{y1} and θ_{z1} alternately to 0 at zero DoC force. The corresponding load stiffness coefficients are measure by applying a DoC force but keeping the DoF displacements constants. By subtracting the two results, $k_{11}^{(1)}$ and $k_{22}^{(1)}$ is determined. The coupling coefficient $k_{12}^{(0)}$ of u_{y1} and θ_{z1} are determined but proper algebraic sum of the displacement measurements from three cases, 1) $u_{y1}=0$ and θ_{z1}=known value A, 2) u_{y1}=known value B and $\theta_{z1}=0$, 3) u_{y1}=known value 2 and θ_{z1}=known value 1. The load-stiffening coupling coefficients are similarly calculated by comparing the three sets of displacement at zero and non-zero DoC force values. The geometric constraint coefficients are calculated using a similar approach. The elastic stiffness is captured by setting u_{y1} and θ_{z1} to zero and applying a known DoC force. The kinematic geometric constraints coefficients are captured by the setting DoC force to zero. Finally the elastokinematic geometric constraint coefficients are calculated by setting DoF end displacements set to the same values as the case when purely kinematic displacement is measured. Using proper algebraic summation with purely kinematic and purely elastic case, the elastokinematic effect is isolated.

For the initially slanted beam in Figure 2.9-7 the base inclination angle is taken as 0.1radian from the X-axis in the YZ plane. For the initial curved beam in Figure 2.9-7, the base inclination angle is 0, while the radius of curvature is in 5mm. The center of curvature is located

vertically 5mm from the base of the beam at XY co-ordinates (0, 5). For measuring DoC stiffness for Figure 2.11 and Figure 2.17, the DoC force is varied between 1.5kN to 2kN keeping DoF end displacements u_{y1} and θ_{z1} fixed and measuring the DoC displacement u_{x1}.

To model variable cross-section beam Ansys beam element Beam4 is used with different cross-sectional area and moment of area on the two sides of the element. Macros is used to define each element individually. After the elements are designed they are meshed as one beam upto the force-displacement analysis is done.

Appendix 2.B: Convergence Criterion used in Section 2.4.1

For the power series solution given below to be a valid series, it has to be tested for convergence.

$$w(x) = a_0 + a_1 x + a_2 x^2 + \ldots + a_n x^n + \ldots \tag{2.52}$$

At *x=1*, the solution *w(1)* simply becomes a summation of all the coefficients. Thus, for the solution to exist at *x=1*, the magnitude of the coefficients should be decreasing. Let us consider the recursion relation for the coefficients, restated here for the convenience of the reader.

$$\begin{aligned} a_{r+2} &= \frac{\boldsymbol{f}_{x1} a_r}{(r+1)(r+2)} - \sum_{i=0}^{r-1}\left\{\frac{(r-i)(r-i+1)}{(r+1)(r+2)} a_{r-i+1} b_{i+1}\right\} \\ \Rightarrow \frac{a_{r+2}}{a_r} &= \frac{\boldsymbol{f}_{x1}}{(r+1)(r+2)} - \sum_{i=0}^{r-1}\left\{\frac{(r-i)(r-i+1)}{(r+1)(r+2)} \frac{a_{r-i+1}}{a_r} b_{i+1}\right\} \end{aligned} \tag{2.53}$$

As *r* tends to infinity *1/r* tends to zero. In this limiting situation one can derive Eq.(2.54). Also assuming that there are *q* shape parameters, i.e., $b_i = 0 \ \forall\, i > q$, the summation takes place from *0* to *q-1* as given below.

$$\frac{a_{r+2}}{a_r} + \sum_{i=0}^{q-1}\left\{\frac{a_{r-i+1}}{a_r} b_{i+1}\right\} = 0 \tag{2.54}$$

Let the ratio between two consecutive solution coefficients be *ρ(r).* The ratio should be less than 1 as *r* tends to infinity for the series to be convergent. Furthermore, this ratio may either be decreasing or constant. If constant, it must be less than 1 for the series to converge. If the ratio is less than 1 and decreasing then the series will converge fast. However, if the ratio is less than 1 but constant then the rate of convergence will be slower. Therefore, if a series is proven to be convergent with a constant ratio assumption, this would imply that the series will only converge faster if the ratio was decreasing. Hence, a constant ratio assumption represents a worst case scenario and is adopted here.

$$\begin{aligned} &\frac{a_{r+2}}{a_{r+1}} \frac{a_{r+1}}{a_r} + \sum_{i=0}^{q-1}\left\{\frac{a_{r-i+1}}{a_{r-i+2}} \frac{a_{r-i+2}}{a_{r-i+3}} .. \frac{a_{r-1}}{a_r} b_{i+1}\right\} = 0 \\ &\Rightarrow \rho^2 + \sum_{i=0}^{q-1}\left\{\frac{b_{i+1}}{\rho^{i-2}}\right\} = 0, \ \textit{where } \rho \triangleq \frac{a_{r+2}}{a_{r+1}}, \forall \text{ r as r} \to \infty \end{aligned} \tag{2.55}$$

The roots of equation are the possible ratios $\rho(r)$ as r tends to infinity. Only in the case when magnitudes of all the roots are less than one, can the series be considered convergent at $x=1$. This criterion can be mathematically stated as below.

$$\left\| roots\left(\rho^q + b_1\rho^{q-1} + ... + b_{q-1}\rho^1 + b_q = 0\right) \right\| < 1 \tag{2.56}$$

For practical purposes, it is found that if the highest magnitude of the roots is less than 0.5, the series converges fast enough to truncate the series solution after 7-10 terms.

Chapter 3

Energy Model for PBCM of Slender Beams with Planar Loading

3.1 Introduction

A model for the strain energy is required for using the Principle of Virtual Work (PVW) [37] as explained in Chapter 1. Since Chapter 2 described the modeling of the force-displacement and geometric constraint relation (Eq.(2.3), (2.5)) of a slender beam with planar loading, it makes sense to derive a compatible energy expression to complete the PBCM. With this strain energy model designers can use PVW to determine equilibrium conditions without working through an explicit Newtonian analytical framework of differential equations which tends to get complicated when the problem has a large number of beam components. PVW avoids using internal loads which make the procedure for formulation of the force displacement relation free from variable elimination which can be non-trivial for non-linear equations. The key ingredients required for using the above energy method are accurate geometric constraints and strain energy models.

Typical geometric constraints are expressed purely in terms of displacements. However, as illustrated by Chapter 2, the constraint equation predicted by PBCM for a simple beam, given by Eq.(3.1), is integrally dependent on the DoC force $\boldsymbol{F_{XL}}$. This is because of the presence of the elastokinematic term (third term in Eq.(3.1)) which prevents a complete separation of the elastic and kinematic effects. The effect of the elastokinematic motion is expected to fundamentally change the strain energy of the beam flexure. This is why using energy methods for flexure analysis is non-trivial.

$$\frac{U_{XL}}{L}=\frac{(T/L)^2}{12}\frac{\boldsymbol{F_{XL}}L^2}{EI_{ZZ}}+\begin{bmatrix}\frac{U_{YL}}{L} & \theta_{ZL}\end{bmatrix}\begin{bmatrix}-\frac{3}{5} & \frac{1}{20}\\ \frac{1}{20} & -\frac{1}{15}\end{bmatrix}\begin{bmatrix}\frac{U_{YL}}{L}\\ \theta_{ZL}\end{bmatrix}+\frac{\boldsymbol{F_{XL}}L^2}{EI_{ZZ}}\begin{bmatrix}\frac{U_{YL}}{L} & \theta_{ZL}\end{bmatrix}\begin{bmatrix}\frac{1}{700} & -\frac{1}{1400}\\ -\frac{1}{1400} & \frac{11}{6300}\end{bmatrix}\begin{bmatrix}\frac{U_{YL}}{L}\\ \theta_{ZL}\end{bmatrix} \tag{3.1}$$

The following section formulates in detail the strain energy of initially straight planar beam. Energy contributions from DoF displacements and the elastokinematic displacements are discussed thoroughly. Section 3.3 covers the effects of an initial angled or an initially curved beam flexure on strain energy. Section 3.4 illustrates the use of strain energy for a tilted parallelogram flexure module. Section 3.5 discusses the versatility of the use of constraint and strain energy relations through the analysis of an multi-beam parallelogram flexure.

3.2 Strain Energy of a Slender Beam with Planar Loading

The axial strain in a straight slender beam with planar loading in Figure 2.1, also known as a simple beam flexure, at location *X* with large deformation can be written in accordance to Euler-Bernoulli assumptions as follows [65]

$$\varepsilon_{XX}=\frac{\partial U_X}{\partial X}+\frac{1}{2}\left(\frac{\partial U_Y}{\partial X}\right)^2-\frac{U_Y}{\rho} \tag{3.2}$$

The variable U_X and U_Y are the DoC displacement along X-axis and DoF displacement along Y-axis while ρ is the curvature of the beam. The second term in the above equation corrects the first term for the kinematic X-displacement due to arc-length conservation to give the actual elastic axial strain on the neutral axis at coordinate location '*X*'. This can be simply derived from the definition of strain in Eq.(3.3) which is the ratio of the change of length of a differential element AB and its initial length. It is assumed here the position of B relative to A changes by U_X and U_Y along X and Y axes respectively due to deformation.

$$\varepsilon_{XX}(X,0)=\frac{\mathrm{A_fB_f}-\mathrm{A_iB_i}}{\mathrm{A_iB_i}}=\left[\left(1+U_X'\right)^2+U_Y'^2\right]^{1/2}-1\approx U_X'+\frac{U_Y'^2}{2} \tag{3.3}$$

The third term comes from Euler's plane cross-section theory and gives the axial strain at the point (*X*, *Y*) in the beam. The expression of strain energy in an Euler beam as in Fig.3.1 is obtained using a volume integral of half of the product of stress and strain. For consistency with Chapter 2 the curvature is approximated by $U_Y''(X)$.

$$V = \iiint_{Volume} \frac{E}{2} \varepsilon_{XX}^2 \, dA dX$$
$$= \frac{E}{2} \int_0^L \iint_A \left(\frac{\partial U_X}{\partial X} + \frac{1}{2} \left(\frac{\partial U_Y}{\partial X} \right)^2 - \frac{\partial^2 U_Y}{\partial X^2} Y \right)^2 dA dX \tag{3.4}$$

This can be simplified as follows.

$$V = \frac{E}{2} \int_0^L \left\{ \frac{\partial U_X}{\partial X} + \frac{1}{2} \left(\frac{\partial U_Y}{\partial X} \right)^2 \right\}^2 \left\{ \int_A dA \right\} dX$$
$$- E \int_0^L \left\{ \frac{\partial U_X}{\partial X} + \frac{1}{2} \left(\frac{\partial U_Y}{\partial X} \right)^2 \right\} \frac{\partial^2 U_Y}{\partial X^2} \left\{ \int_A Y dA \right\} dX \tag{3.5}$$
$$+ \frac{E}{2} \int_0^L \left(\frac{\partial^2 U_Y}{\partial X^2} \right)^2 \left\{ \int_A Y^2 dA \right\} dX$$

Both U_X and U_Y are functions of variable X alone and hence the area integral can be separated as shown above. The square term in the first integral in Eq.(3.5) is the actual elastic axial strain at the neutral axis equal to $\frac{\partial U_X^{(E)}}{\partial X}$. The second integral is zero by the definition of neutral axis. The third integral can be simplified by the definition of second moment of area. Using these simplifications the strain energy can be written as below.

$$V = \frac{E I_{ZZ}}{2} \int_L \left\{ U_Y'' \right\}^2 dX + \frac{E A U_{XL}^{(E)2}}{2L} \tag{3.6}$$

The virtual work δW is defined as

$$\delta W = \boldsymbol{F_{XL}} \delta U_{XL} + \boldsymbol{F_{YL}} \delta U_{YL} + \boldsymbol{M_{ZL}} \delta U'_{YL} \tag{3.7}$$

From Eq.(2.4) we can derive

$$\delta U_{XL} = \delta U_{XL}^E - \int_0^L \delta \left\{ \frac{1}{2} \left(U_Y' \right)^2 \right\} dX \qquad \text{where} \quad U_{XL}^E \triangleq \frac{(T/L)^2}{12} \frac{\boldsymbol{F_{XL}} L^3}{E I_{ZZ}} \tag{3.8}$$

The variable $U_{XL}^{(E)}$ is the elastic DoC displacement along X-axis at end of the beam. For equilibrium, the principle of virtual work in Eq.(0.2), Eq.(3.7) and Eq.(3.8) gives us the following.

$$\delta V = \delta W$$

$$\Rightarrow \frac{EI_{ZZ}}{2}\delta\int_0^L \left\{U_Y''\right\}^2 dX + \delta\left(\frac{EAU_{XL}^{(E)2}}{2L}\right) - \boldsymbol{F_{YL}}\delta U_{YL} - \boldsymbol{M_{ZL}}\delta U_{YL}' + \frac{\boldsymbol{F_{XL}}}{2}\int_0^L \delta\left\{\left(U_Y'\right)^2\right\} dx - \boldsymbol{F_{XL}}\delta U_{XL}^{(E)} = 0 \tag{3.9}$$

Solving the above equation the characteristic beam equation and the natural boundary conditions are obtained as below.

$$\begin{aligned} &U_Y{}^{iv}(X) = \frac{\boldsymbol{F_{XL}}}{EI_{ZZ}} U_Y''(X) \\ &B.C.: \quad U_Y''(L) = \frac{\boldsymbol{M_{ZL}}}{EI_{ZZ}}, \\ &\qquad \mathrm{U}_Y'''(X) = \frac{-\boldsymbol{F_{YL}} + \boldsymbol{F_{XL}} U_Y'(L)}{EI_{ZZ}} \\ &\qquad \boldsymbol{F_{XL}} = \frac{EAU_{XL}^{(E)}}{L} \end{aligned} \tag{3.10}$$

As expected the characteristic equation derived from energy methods are same as that derived from force equilibrium as the key approximations of the curvature and DoC x-end displacement are same in both cases. Due to the unusual involvement of DoC force $\boldsymbol{F_{XL}}$ in the load-displacement and constraint equation, it is obvious that the strain energy of the beam which is a function of the total deformation of the beam will be dependent on $\boldsymbol{F_{XL}}$. Since there isn't a standard or simple energy or constraint model for this situation, Eq.(3.10) has to be solved to determine the strain energy.

At this point all loads, displacements, energy and stiffness terms are normalized with respect to the beam parameters: displacements and lengths are normalized by the beam length *L*, forces by EI_{ZZ}/L^2, and moments by EI_{ZZ}/L and strain energy by EI_{ZZ}/L as in Chapter 2 and represented by corresponding lower case symbols. The new variable *t* is the normalized thickness of the beam flexure T_Y/L.

Using the normalized variable definitions the beam strain energy can be rewritten as below.

$$v = \frac{1}{2}\int_L \left\{u_y''(x)\right\}^2 dx + \frac{6u_{x1}^{(e)2}}{t^2} \tag{3.11}$$

The normalized DoF displacement $u_y(x)$ in terms of end displacements is solved from (3.10). It should be noted that this solution was presented in reference [24]. Furthermore, if θ_{z1} is used to represent u'_{y1} the solution of $u_y(x)$ can be writing as

$$
\begin{aligned}
&u_y(x) = c_1 e^{\boldsymbol{r}x} + c_2 e^{-\boldsymbol{r}x} + c_3 x + c_4 \\
&c_1 = \frac{\boldsymbol{r}(e^{-\boldsymbol{r}}-1)u_{y1} + (e^{-\boldsymbol{r}}+\boldsymbol{r}-1)\theta_{z1}}{\boldsymbol{r}\left[k(e^{\boldsymbol{r}}-e^{-\boldsymbol{r}}) - 2(e^{\boldsymbol{r}}+e^{-\boldsymbol{r}})+4\right]}, \qquad c_2 = \frac{\boldsymbol{r}(e^{\boldsymbol{r}}-1)u_{y1} - (e^{\boldsymbol{r}}-\boldsymbol{r}-1)\theta_{z1}}{\boldsymbol{r}\left[\boldsymbol{r}(e^{\boldsymbol{r}}-e^{-\boldsymbol{r}}) - 2(e^{\boldsymbol{r}}+e^{-\boldsymbol{r}})+4\right]} \\
&c_3 = \boldsymbol{r}(c_2 - c_1), \qquad c_4 = -c_1 - c_2 \\
&\text{where } \boldsymbol{r}^2 \triangleq \boldsymbol{f}_{y1}
\end{aligned}
\tag{3.12}
$$

Substituting the Eq. (3.12) into Eq.(3.11), the expression for the normalized strain energy can be easily derived in term for end displacements.

$$
\begin{aligned}
&v = \begin{Bmatrix} u_{y1} & \theta_{z1} \end{Bmatrix} \begin{bmatrix} v_{11} & v_{12} \\ v_{21} & v_{22} \end{bmatrix} \begin{Bmatrix} u_{y1} \\ \theta_{z1} \end{Bmatrix} + \frac{6u_{xe1}{}^2}{t^2} \\
&v_{11} = \frac{1}{2}\frac{\boldsymbol{r}^3\left\{\sinh(\boldsymbol{r})\cosh(\boldsymbol{r}) - \sinh(\boldsymbol{r}) + \boldsymbol{r} - \boldsymbol{r}\cosh(\boldsymbol{r})\right\}}{\left\{\boldsymbol{r}\sinh(\boldsymbol{r}) - 2\cosh(\boldsymbol{r}) + 2\right\}^2}, \\
&v_{12} = v_{21} = \frac{1}{4}\frac{\boldsymbol{r}^3\left\{\sinh(\boldsymbol{r}) - \sinh(\boldsymbol{r})\cosh(\boldsymbol{r}) - \boldsymbol{r} + \boldsymbol{r}\cosh(\boldsymbol{r})\right\}}{\left\{\boldsymbol{r}\sinh(\boldsymbol{r}) - 2\cosh(\boldsymbol{r}) + 2\right\}^2} \\
&v_{22} = \frac{1}{4}\frac{\boldsymbol{r}\left[\sinh(\boldsymbol{r})\left\{2\cosh(\boldsymbol{r}) - 2 + \boldsymbol{r}^2\cosh(\boldsymbol{r}) - 2\boldsymbol{r}^2\right\}\right]}{\left\{\boldsymbol{r}\sinh(\boldsymbol{r}) - 2\cosh(\boldsymbol{r}) + 2\right\}^2} + \frac{1}{4}\frac{\boldsymbol{r}\left[\boldsymbol{r}^3 + 2\boldsymbol{r}\cosh(\boldsymbol{r})\left\{1 - \cosh(\boldsymbol{r})\right\}\right]}{\left\{\boldsymbol{r}\sinh(\boldsymbol{r}) - 2\cosh(\boldsymbol{r}) + 2\right\}^2}
\end{aligned}
\tag{3.13}
$$

The strain energy above is expressed in term of hyperbolic sine and cosine functions for mathematical convenience. The series expansion of the transcendental expressions, given above, followed by a truncation after the second power of $\boldsymbol{f}_{x1}$ yields the following expression.

$$
v = \frac{1}{2}\begin{Bmatrix} u_{y1} & \theta_{z1} \end{Bmatrix} \begin{bmatrix} 12 + \frac{\boldsymbol{f}_{x1}{}^2}{700} & -6 - \frac{\boldsymbol{f}_{x1}{}^2}{1400} \\ -6 - \frac{\boldsymbol{f}_{x1}{}^2}{1400} & 4 + \frac{11\boldsymbol{f}_{x1}{}^2}{6300} \end{bmatrix} \begin{Bmatrix} u_{y1} \\ \theta_{z1} \end{Bmatrix} + \frac{6u_{x1}^{(e)2}}{t^2} \tag{3.14}
$$

It is interesting to see that there is no term associated with $\boldsymbol{f}_{x1}$ term. The coefficients free of $\boldsymbol{f}_{x1}$ are same as obtained from linear analysis. To understand better the significance of the absence of $\boldsymbol{f}_{x1}$ terms and the origin of $\boldsymbol{f}_{x1}{}^2$ terms, the PVW is carried out to obtain the force-displacement relation. The normalized constraint relation, derived in Chapter 2, is given below.

The coefficients free of $\boldsymbol{f_{x1}}$ represent the purely kinematic DoC displacement along x-axis while the coefficients of $\boldsymbol{f_{x1}}$ represent the elastokinematic DoC displacement along x-axis.

$$u_{x1}^{(k)} + u_{x1}^{(e-k)} = \frac{1}{2}\begin{Bmatrix} u_{y1} & \theta_{z1} \end{Bmatrix} \begin{bmatrix} -\frac{6}{5} + \frac{\boldsymbol{f_{x1}}}{350} & \frac{1}{10} - \frac{\boldsymbol{f_{x1}}}{700} \\ \frac{1}{10} - \frac{\boldsymbol{f_{x1}}}{700} & -\frac{2}{15} + \frac{11\boldsymbol{f_{x1}}}{3150} \end{bmatrix} \begin{Bmatrix} u_{y1} \\ \theta_{z1} \end{Bmatrix} \tag{3.15}$$

The relevant equation for PVW is given below. The DoC displacement along x-axis is broken up in three components, namely the elastic, kinematic and elastokinematic components.

$$\delta v = \boldsymbol{f_{y1}}\delta u_{y1} + \boldsymbol{f_{x1}}\left(\delta u_{x1}^{(e)} + \delta u_{x1}^{(k)} + \delta u_{x1}^{(e-k)}\right) + \boldsymbol{m_{z1}}\delta\theta_{z1} \tag{3.16}$$

Using the strain energy from Eq.(3.14) and the constraint relation from Eq.(3.15) in PVW Eq.(3.16) an equation involving the variations of three independent variables, u_{y1}, θ_{z1} and $u_{x1}^{(e)}$.

$$\begin{aligned} \begin{Bmatrix} \delta u_{y1} & \delta\theta_{z1} \end{Bmatrix} \begin{bmatrix} 12 + \frac{\boldsymbol{f_{x1}}^2}{700} & -6 - \frac{\boldsymbol{f_{x1}}^2}{1400} \\ -6 - \frac{\boldsymbol{f_{x1}}^2}{1400} & 4 + \frac{11\boldsymbol{f_{x1}}^2}{6300} \end{bmatrix} \begin{Bmatrix} u_{y1} \\ \theta_{z1} \end{Bmatrix} + \frac{12u_{x1}^{(e)}\delta u_{x1}^{(e)}}{t^2} &= \boldsymbol{f_{y1}}\delta u_{y1} + \boldsymbol{m_z}\delta\theta_z + \boldsymbol{f_{x1}}\delta u_{x1}^{(e)} \\ + \boldsymbol{f_{x1}}\begin{Bmatrix} \delta u_{y1} & \delta\theta_{z1} \end{Bmatrix} \begin{bmatrix} -\frac{6}{5} + \frac{\boldsymbol{f_{x1}}}{350} & \frac{1}{10} - \frac{\boldsymbol{f_{x1}}}{700} \\ \frac{1}{10} - \frac{\boldsymbol{f_{x1}}}{700} & -\frac{2}{15} + \frac{11\boldsymbol{f_{x1}}}{3150} \end{bmatrix} \begin{Bmatrix} u_{y1} \\ \theta_{z1} \end{Bmatrix} & \end{aligned} \tag{3.17}$$

Since the variations in these variables are arbitrary, their coefficients on LHS and RHS should be identical. Equating the respective coefficients, the force displacement relations are obtained.

$$\begin{Bmatrix} \boldsymbol{f_{y1}} \\ \boldsymbol{m_{z1}} \end{Bmatrix} = \begin{bmatrix} 12 + \frac{6}{5}\boldsymbol{f_{x1}} - \frac{\boldsymbol{f_{x1}}^2}{700} & -6 - \frac{1}{10}\boldsymbol{f_{x1}} + \frac{\boldsymbol{f_{x1}}^2}{1400} \\ -6 - \frac{1}{10}\boldsymbol{f_{x1}} + \frac{\boldsymbol{f_{x1}}^2}{1400} & 4 + \frac{2}{15}\boldsymbol{f_{x1}} - \frac{11\boldsymbol{f_{x1}}^2}{6300} \end{bmatrix} \begin{Bmatrix} u_{y1} \\ \theta_{z1} \end{Bmatrix} \tag{3.18}$$

$$\boldsymbol{f_{x1}} = \frac{12u_{x1}^{(e)}}{t^2}$$

As expected the force-displacement relations are same as that derived by explicit analysis in Chapter 2. In fact the force displacement relations match even while working with the transcendental functions thus proving the validity of the strain energy expression in Eq.(3.13)

and Eq.(3.14). The f_{x1}^2 terms in Eq.(3.18) can be dropped as their coefficient is very low but is retained for consistency with the strain energy approximation in Eq.(3.14).

When Eq.(3.18) is observed more closely, it is realized that the coefficients associated with f_{x1} in the stiffness matrix is derived entirely from the kinematic DoC displacement while the coefficients of f_{x1}^2 are a combination of the elastokinematic DoC displacement terms and the non-linear strain energy terms. This means that the load stiffening term has no energy associated with it and hence is unaffected by the strain energy expression. This is quite expected because load stiffening is cause by geometric constraint and not by a force, and hence logically it should be derived from the constraint equation. This also explains the absence of the f_{x1} terms in the strain energy expression in Eq.(3.14). The f_{x1} in the strain energy term can come from two sources, either from the f_{x1} term in the force displacement relation or the f_{x1} free term from the DoC constraint relation. Since both of these are a result of purely geometric constraints, the coefficient of f_{x1} in the strain energy term is zero.

3.3 Fundamental Relations between Beam Characteristic Coefficients for a Slender Beam with Planar Loading

It has been shown in Chapter 2, Section 2.4, that the form of PBCM remains invariant even for a straight beam with variable cross-section. Therefore a general expression for the strain energy, constraint relations and load-displacement relations may be assumed as below where the variables *v*'s and *g*'s are functions of the shape of the beam.

$$v = \frac{1}{2}k_{33}u_{x1}^{(e)2} + \frac{1}{2}\sum_{n=0}^{\infty} f_{x1}^{n} \begin{Bmatrix} u_{y1} & \theta_{z1} \end{Bmatrix} \begin{bmatrix} v_{11}^{(n)} & v_{12}^{(n)} \\ v_{21}^{(n)} & v_{22}^{(n)} \end{bmatrix} \begin{Bmatrix} u_{y1} \\ \theta_{z1} \end{Bmatrix} \tag{3.19}$$

$$u_{x1} = \frac{f_{x1}}{k_{33}} + \sum_{n=0}^{\infty} f_{x1}^{n} \begin{Bmatrix} u_{y1} & \theta_{z1} \end{Bmatrix} \begin{bmatrix} g_{11}^{(n)} & g_{12}^{(n)} \\ g_{21}^{(n)} & g_{22}^{(n)} \end{bmatrix} \begin{Bmatrix} u_{y1} \\ \theta_{z1} \end{Bmatrix} \tag{3.20}$$

$$\begin{Bmatrix} f_{y1} \\ m_{z1} \end{Bmatrix} = \sum_{n=0}^{\infty} f_{x1}^{n} \begin{bmatrix} k_{11}^{(n)} & k_{12}^{(n)} \\ k_{21}^{(n)} & k_{22}^{(n)} \end{bmatrix} \begin{Bmatrix} u_{y1} \\ \theta_{z1} \end{Bmatrix} \tag{3.21}$$

Using PVW on Eqs. (3.19) and (3.20) and doing similar operations as done in Eqs.(3.16) and (3.17) the force displacement relation can be shown as below.

$$\begin{bmatrix} \boldsymbol{f}_{y1} \\ \boldsymbol{m}_{z1} \end{bmatrix} = \begin{bmatrix} v_{11}^{(0)} & v_{12}^{(0)} \\ v_{21}^{(0)} & v_{22}^{(0)} \end{bmatrix} \begin{Bmatrix} u_{y1} \\ \theta_{z1} \end{Bmatrix} + \sum_{n=0}^{\infty} \boldsymbol{f}_{x1}^{\boldsymbol{n}} \begin{bmatrix} v_{11}^{(n)} - 2g_{11}^{(n-1)} & v_{12}^{(n)} - 2g_{12}^{(n-1)} \\ v_{21}^{(n)} - 2g_{21}^{(n-1)} & v_{22}^{(n)} - 2g_{22}^{(n-1)} \end{bmatrix} \begin{Bmatrix} u_{y1} \\ \theta_{z1} \end{Bmatrix} \tag{3.22}$$

Equation (3.22) is an expected result and provides no new information. However, a comparison between Eqs.(3.21) and (3.22), both of which should be identical, given the above-mentioned consistency in the energy formulation, reveals a fundamental relation between the stiffness, constraint, and energy coefficients,

$$\begin{aligned} k_{\beta\lambda}^{(0)} &= v_{\beta\lambda}^{(0)} \\ k_{\beta\lambda}^{(n)} &= v_{\beta\lambda}^{(n)} - 2g_{\beta\lambda}^{(n-1)} \qquad \forall n = 1,...,\infty, \quad \beta = 1 \text{ or } 2, \quad \lambda = 1 \text{ or } 2 \end{aligned} \tag{3.23}$$

The above relations may be readily verified for the case of a simple beam using the known results Eqs.(3.14), (3.15) and (3.18); however, it should be noted that these are valid for any general beam shape, as proven above.

A second argument based on the conservation of energy provides yet another fundamental relation between the beam characteristic coefficients. Since a given set of end loads $\boldsymbol{f}_{x1}$, $\boldsymbol{f}_{y1}$, and $\boldsymbol{m}_{z1}$ produces a unique set of end displacements u_{x1}, u_{y1}, and θ_{z1}, the resulting strain energy stored in the deformed beam is also unique, as given by Eq.(3.19). This strain energy remains the same irrespective of the order in which the loading is carried out. We consider the case when loading in done in two steps (1) $\boldsymbol{f}_{yl}$ and $\boldsymbol{m}_{z1}$ are applied on the beam to obtain end displacements u_{y1} and θ_{z1} and (2) $\boldsymbol{f}_{xl}$ is applied while holding u_{y1} and θ_{z1} fixed. The strain energy stored in the system due to step 1 is obtained by setting $\boldsymbol{f}_{x1}$ to zero in Eq.(3.19) and is given below.

$$v_1 = \frac{1}{2} k_{33} u_{x1}^{(e)2} + \frac{1}{2} \begin{Bmatrix} u_{y1} & \theta_{z1} \end{Bmatrix} \begin{bmatrix} v_{11}^{(0)} & v_{12}^{(0)} \\ v_{21}^{(0)} & v_{22}^{(0)} \end{bmatrix} \begin{Bmatrix} u_{y1} \\ \theta_{z1} \end{Bmatrix} \tag{3.24}$$

The DoC force $\boldsymbol{f}_{x1}$ is now applied keeping u_{y1} and θ_{z1} fixed. This implies that during the process of application of $\boldsymbol{f}_{x1}$ the loads $\boldsymbol{f}_{yl}$ and $\boldsymbol{m}_{z1}$ adjust themselves to keep a constant u_{y1} and θ_{z1}. However, since u_{y1} and θ_{z1} are constant, $\boldsymbol{f}_{yl}$ and $\boldsymbol{m}_{z1}$ do not perform any additional work on the system. Next, assuming a conservative system, the work done in step 2 is $\boldsymbol{f}_{x1}\left(\bar{u}_{x1} - u_{x1}\right)$ where $\bar{u}_{x1}$ and u_{x1} are the x-displacement after steps 1 and 2 respectively. Displacement $\bar{u}_{x1}$ can be found by setting $\boldsymbol{f}_{x1}$ to zero in Eq.(3.20).

$$\bar{u}_{x1} = \frac{1}{2}\begin{Bmatrix} u_{y1} & \theta_{z1} \end{Bmatrix}\begin{bmatrix} g_{11}^{(0)} & g_{12}^{(0)} \\ g_{21}^{(0)} & g_{22}^{(0)} \end{bmatrix}\begin{Bmatrix} u_{y1} \\ \theta_{z1} \end{Bmatrix} \tag{3.25}$$

An integral needs to be carried out to calculate the total work done on the beam in this step, since the relation between $\boldsymbol{f_{x1}}$ and u_{x1} is nonlinear. However, since inverting Eq.(3.20) which provides displacement in terms of force, is not trivial, determining the work done in this fashion is difficult if not impossible. Therefore, instead we choose to determine the complementary work, which can be readily derived from Eq. (3.20)

$$v_2^* = \boldsymbol{f_{x1}}\left(u_{x1} - \bar{u}_{x1}\right) - \int_0^{\boldsymbol{f_{x1}}} \left(u_{x1} - \bar{u}_{x1}\right) d\boldsymbol{f_{x1}} \tag{3.26}$$

This result is then used to calculate the strain energy stored in the beam due step 2 as follows:

$$\begin{aligned} v_2 &= \frac{\boldsymbol{f_{x1}}^2}{k_{33}} + \sum_{n=0}^{\infty} \boldsymbol{f_{x1}}^{\boldsymbol{n+1}} \begin{Bmatrix} u_{y1} & \theta_{z1} \end{Bmatrix}\begin{bmatrix} g_{11}^{(n)} & g_{12}^{(n)} \\ g_{21}^{(n)} & g_{22}^{(n)} \end{bmatrix}\begin{Bmatrix} u_{y1} \\ \theta_{z1} \end{Bmatrix} - \frac{\boldsymbol{f_{x1}}^2}{2k_{33}} \\ &\quad - \sum_{n=0}^{\infty} \frac{\boldsymbol{f_{x1}}^{\boldsymbol{n+1}}}{n+1} \begin{Bmatrix} u_{y1} & \theta_{z1} \end{Bmatrix}\begin{bmatrix} g_{11}^{(n)} & g_{12}^{(n)} \\ g_{21}^{(n)} & g_{22}^{(n)} \end{bmatrix}\begin{Bmatrix} u_{y1} \\ \theta_{z1} \end{Bmatrix} \\ &= \frac{\boldsymbol{f_{x1}}^2}{2k_{33}} + \sum_{n=0}^{\infty} \frac{(n-1)\,\boldsymbol{f_{x1}}^{\boldsymbol{n}}}{n} \begin{Bmatrix} u_{y1} & \theta_{z1} \end{Bmatrix}\begin{bmatrix} g_{11}^{(n-1)} & g_{12}^{(n-1)} \\ g_{21}^{(n-1)} & g_{22}^{(n-1)} \end{bmatrix}\begin{Bmatrix} u_{y1} \\ \theta_{z1} \end{Bmatrix} \end{aligned} \tag{3.27}$$

The strain energy given by v_1+v_2 is identical by definition to the strain energy in Eq.(3.19). By comparing the coefficients of the respective terms we get the following relations.

$$v_{\beta\lambda}^{(n)} = 2\left(\frac{n-1}{n}\right) g_{\beta\lambda}^{(n-1)}, \quad \forall n = 1,...,\infty, \quad \beta = 1 \text{ or } 2, \quad \lambda = 1 \text{ or } 2 \tag{3.28}$$

Equation (3.23) and (3.28) can be manipulated to express all v's and g's in the strain energy and constrain relation.

$$\begin{aligned} g_{\beta\lambda}^{(n)} &= -\frac{n+1}{2} k_{\beta\lambda}^{(n+1)}, \quad \forall n = 0,...,\infty, \\ v_{\beta\lambda}^{(0)} &= k_{\beta\lambda}^{(0)}, \\ v_{\beta\lambda}^{(n)} &= -(n-1) k_{\beta\lambda}^{(n)}, \quad \forall n = 1,...,\infty, \\ &\text{where } \beta = 1 \text{ or } 2, \quad \lambda = 1 \text{ or } 2 \end{aligned} \tag{3.29}$$

Together, Eqs. (3.28) and (3.29) present the far-reaching conclusion that the stiffness, constraint, and energy expressions are all interrelated; any one can be expressed in terms of any of the other two. These relations may be readily verified for the known case of a simple beam via

Eqs. (3.14), (3.15), and (3.18) but are true for any general beam shape, as proven above. Moreover, these relations offer considerable insight into the nature of the nonlinear results for variable cross-section beam flexures. Some specific observations are noted below:

1. Equation (3.29) indicates that no matter what the beam shape is, $v_{\beta\lambda}^{(1)}$ is always zero. This simply implies that while all other stiffness coefficients contribute to the strain energy, the stiffness coefficient associated with the first power of $\boldsymbol{f_{x1}}$, which represents a load stiffening, does not.
2. Equation (3.29) also shows that $g_{\beta\lambda}^{(0)} = -\frac{1}{2}k_{\beta\lambda}^{(1)}$, irrespective of the beam shape. This indicates that the load-stiffening effect seen in the transverse-direction load-displacement relation and the kinematic component seen in the axial-direction geometric constraint relation are inherently related. In hindsight, this is physically reasonable because both these effects arise from the consideration of the beam in a deformed configuration.
3. The above relations also highlight the fact that the transverse load-displacement expression(3.18), the axial geometric constraint expression (3.15), and the strain energy expression (3.14) for a generalized beam are not entirely independent. The geometric constraint expression captures all the beam characteristic coefficients, except for the elastic stiffness $k_{\beta\lambda}^{(0)}$. The strain energy, on the other hand, captures all the beam characteristic coefficients except for load stiffening and kinematic ones. However, the transverse-direction load-displacement relation is the most complete of the three in that it captures all the beam characteristic coefficients. This is reasonable because as per the PVW, both the strain energy and geometric constraint relations are used in deriving the transverse load-displacement relation.

This last observation leads to an important practical advantage. It implies that in the derivation of the nonlinear transverse stiffness, constraint, and energy relations for a beam, which ultimately lead to the BCM, it is no longer necessary to determine all three individually. In fact, solving for the constraint and energy relations individually is mathematically more tedious because of the integration steps and the quadratic terms in u_{y1} and θ_{z1} involved. Instead, one may simply derive the transverse load-displacement relation and determine the constraint and energy

relations indirectly using Eqs. (3.29). This finding has been employed in deriving the BCM for generalized beam shapes discussed in Chapter 2.

3.4 Strain Energy for Slender Beam with Planar Loading and Generalized Boundary Conditions

We now consider strain energy for a uniform thickness flexure strip (see Figure 3.1) with an arbitrary initial angle and an arbitrary but constant curvature. The explicit derivation of this flexure module is given in Chapter 2 but for the benefit of the reader the diagram and initial beam equation is reiterated here.

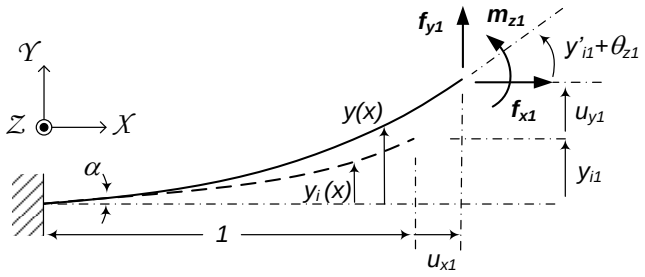

Figure 3.1: Initially Slanted and Curved Planar Flexure Strip

$$y_i(x) = \alpha x + \frac{\kappa}{2}x^2 \tag{3.30}$$

The DoF displacement along y-axis is also restated from Chapter 2.

$$u_y(x) = y(x) - y_i(x) = c_1 + (c_2 - \alpha x) - \frac{\kappa}{2}x^2 + c_3\sinh(\boldsymbol{r}x) + c_4\cosh(\boldsymbol{r}x) \tag{3.31}$$

$$c_1 = \frac{\{1-\cosh(\boldsymbol{r})\}u_{y1}}{\boldsymbol{r}\sinh(\boldsymbol{r})-2\cosh(\boldsymbol{r})+2} + \frac{\{\sinh(\boldsymbol{r})-\boldsymbol{r}\}\theta_{z1}}{\boldsymbol{r}\{\boldsymbol{r}\sinh(\boldsymbol{r})-2\cosh(\boldsymbol{r})+2\}} + \frac{\left[\boldsymbol{r}\{\cosh(\boldsymbol{r})+1\}-2\sinh(\boldsymbol{r})\right]}{\boldsymbol{r}\{\boldsymbol{r}\sinh(\boldsymbol{r})-2\cosh(\boldsymbol{r})+2\}}\kappa$$

$$c_2 = \frac{\boldsymbol{r}\sinh(\boldsymbol{r})u_{y1}}{\boldsymbol{r}\sinh(\boldsymbol{r})-2\cosh(\boldsymbol{r})+2} + \frac{\{1-\cosh(\boldsymbol{r})\}\theta_{z1}}{\boldsymbol{r}\sinh(\boldsymbol{r})-2\cosh(\boldsymbol{r})+2} + \kappa + \alpha$$

$$c_3 = -\frac{1}{\boldsymbol{r}}(c_2 - \alpha)$$

$$c_4 = -c_1$$

Substituting the constants into Eq.(3.31), an accurate expression of DoF displacement u_{y1} is obtained which is used in Eq.(3.11) to obtain the expression for the strain energy.

$$v = \frac{6u_{xe1}{}^2}{t^2} + \begin{Bmatrix} u_{y1} & \theta_{z1} \end{Bmatrix} \begin{bmatrix} v_{11} & v_{12} \\ v_{21} & v_{22} \end{bmatrix} \begin{Bmatrix} u_{y1} \\ \theta_{z1} \end{Bmatrix} + v_{33}\left(\theta_{z1} + \kappa\right)\kappa$$

$$v_{11} = \frac{1}{2}\frac{\boldsymbol{r}^3\left\{\sinh\left(\boldsymbol{r}\right)\cosh\left(\boldsymbol{r}\right) - \sinh\left(\boldsymbol{r}\right) + \boldsymbol{r} - \boldsymbol{r}\cosh\left(\boldsymbol{r}\right)\right\}}{\left\{\boldsymbol{r}\sinh\left(\boldsymbol{r}\right) - 2\cosh\left(\boldsymbol{r}\right) + 2\right\}^2}$$

$$v_{12} = v_{21} = \frac{1}{4}\frac{\boldsymbol{r}^3\left\{\sinh\left(\boldsymbol{r}\right) - \sinh\left(\boldsymbol{r}\right)\cosh\left(\boldsymbol{r}\right) - \boldsymbol{r} + \boldsymbol{r}\cosh\left(\boldsymbol{r}\right)\right\}}{\left\{\boldsymbol{r}\sinh\left(\boldsymbol{r}\right) - 2\cosh\left(\boldsymbol{r}\right) + 2\right\}^2}$$

$$v_{22} = \frac{1}{4}\frac{\boldsymbol{r}\left[\sinh\left(\boldsymbol{r}\right)\left\{2\cosh\left(\boldsymbol{r}\right) - 2 + \boldsymbol{r}^2\cosh\left(\boldsymbol{r}\right) - 2\boldsymbol{r}^2\right\}\right]}{\left\{\boldsymbol{r}\sinh\left(\boldsymbol{r}\right) - 2\cosh\left(\boldsymbol{r}\right) + 2\right\}^2} + \frac{1}{4}\frac{\boldsymbol{r}\left[\boldsymbol{r}^3 + 2\boldsymbol{r}\cosh\left(\boldsymbol{r}\right)\left\{1 - \cosh\left(\boldsymbol{r}\right)\right\}\right]}{\left\{\boldsymbol{r}\sinh\left(\boldsymbol{r}\right) - 2\cosh\left(\boldsymbol{r}\right) + 2\right\}^2}$$

$$v_{33} = \frac{\left[\boldsymbol{r}^4\left\{1 + \cosh\left(\boldsymbol{r}\right)\right\} + \boldsymbol{r}^3\sinh\left(\boldsymbol{r}\right)\left\{\cosh\left(\boldsymbol{r}\right) - 3\right\}\right]}{\left\{\boldsymbol{r}\sinh\left(\boldsymbol{r}\right) - 2\cosh\left(\boldsymbol{r}\right) + 2\right\}^2} + \frac{\left\{1 - \cosh\left(\boldsymbol{r}\right)\right\}\left[\left(8\boldsymbol{r}^2 + 16\right)\cosh\left(\boldsymbol{r}\right) - 20\boldsymbol{r}\sinh\left(\boldsymbol{r}\right) + 4\boldsymbol{r}^2 - 16\right]}{\left\{\boldsymbol{r}\sinh\left(\boldsymbol{r}\right) - 2\cosh\left(\boldsymbol{r}\right) + 2\right\}^2} \tag{3.32}$$

The Taylor series expansion of the transcendental functions is given below.

$$v = \frac{6u_{x1}^{(e)2}}{t^2} + \frac{1}{2}\begin{Bmatrix} u_{y1} & \theta_{z1} \end{Bmatrix} \begin{bmatrix} 12 + \dfrac{\boldsymbol{f}_{x1}{}^2}{700} & -6 - \dfrac{\boldsymbol{f}_{x1}{}^2}{1400} \\ -6 - \dfrac{\boldsymbol{f}_{x1}{}^2}{1400} & 4 + \dfrac{11\boldsymbol{f}_{x1}{}^2}{6300} \end{bmatrix} \begin{Bmatrix} u_{y1} \\ \theta_{z1} \end{Bmatrix} + \boldsymbol{f}_{x1}{}^2\frac{\kappa\theta_{z1}}{720} + \boldsymbol{f}_{x1}{}^2\frac{\kappa^2}{1440} \tag{3.33}$$

The strain energy expression in Eq.(3.33) shows two new energy terms in addition to those that were already present for the simple beam in Eq.(3.14). It is also interesting to notice the absence of initial angle α in the strain energy expression in Eq.(3.33). To understand these terms better it is important to look at the constraint equation for this model derived in Chapter 2.

$$u_{x1} = \boldsymbol{f}_{x1}\frac{t^2}{12} + \begin{Bmatrix} u_{y1} & \theta_{z1} \end{Bmatrix} \begin{bmatrix} -\dfrac{3}{5} & \dfrac{1}{20} \\ \dfrac{1}{20} & -\dfrac{1}{15} \end{bmatrix} \begin{Bmatrix} u_{y1} \\ \theta_{z1} \end{Bmatrix} + \boldsymbol{f}_{x1}\begin{Bmatrix} u_{y1} & \theta_{z1} \end{Bmatrix} \begin{bmatrix} \dfrac{1}{700} & -\dfrac{1}{1400} \\ -\dfrac{1}{1400} & \dfrac{11}{6300} \end{bmatrix} \begin{Bmatrix} u_{y1} \\ \theta_{z1} \end{Bmatrix} - \left(\alpha + \frac{\kappa}{2}\right)u_{y1} - \frac{\kappa}{12}\theta_{z1} + \boldsymbol{f}_{x1}\frac{\kappa}{360}\theta_{z1} + \boldsymbol{f}_{x1}\frac{\kappa^2}{720} \tag{3.34}$$

Since α has no coefficient of $\boldsymbol{f}_{x1}$, it is a purely kinematic term. Hence it does not show up in the strain energy relation, but rather shows up in the force displacement relation as a load stiffening term. In addition to the α term there are two other pure kinematic terms associated with κ that do not contribute to strain energy but show up as loading stiffening terms.

The two new terms associated with κ in the strain energy expression turns out to be associated with the elastokinematic terms in the constraint equation. The first of these two term is associated with DoF displacement θ_{z1}, and comes into the picture due to coupling between curvature and angle of rotation. The second term is associated with the 'unwinding' of the curved beam due to the DoC force $\boldsymbol{f_{x1}}$ like a torsional spring. This energy is similar to the elastic energy stored in the beam due to stretching.

3.5 Application of energy methods

The strain energy expressions derived for PBCM of a planar slender beam enables the use of energy methods for the analysis of flexure mechanisms. Two examples in which energy methods provides a distinct advantage in term of reduced mathematical complexity are given below.

3.5.1 Tilted Beam Parallelogram Flexure Solved by Energy Methods

The utility of having a model for a slanted simple beam flexure can be realized in the analysis of tilted beam parallelogram flexure using energy methods. Tilted beam parallelogram flexure has a similar arrangement of simple beam flexures as a parallelogram flexure except that the simple beam flexures attached to a stage are actually not perfectly parallel. In this mechanism, as shown in Figure 3.2, both the beams are at an angle α to the x-axis. With only a model for a simple beam, the end displacement of each beam would need to be expressed in their local co-ordinate axis which would be rotated by an angle α to the global X-Y-Z co-ordinate frame. Furthermore, while summing the individual strain energies, the displacement variables will have to be reconverted to the global co-ordinate frame. The additional complexity of transformation of co-ordinate frame is avoided using the model for a slanted simple beam flexure in which all end-load and end-displacements are expressed in the global co-ordinate frame.

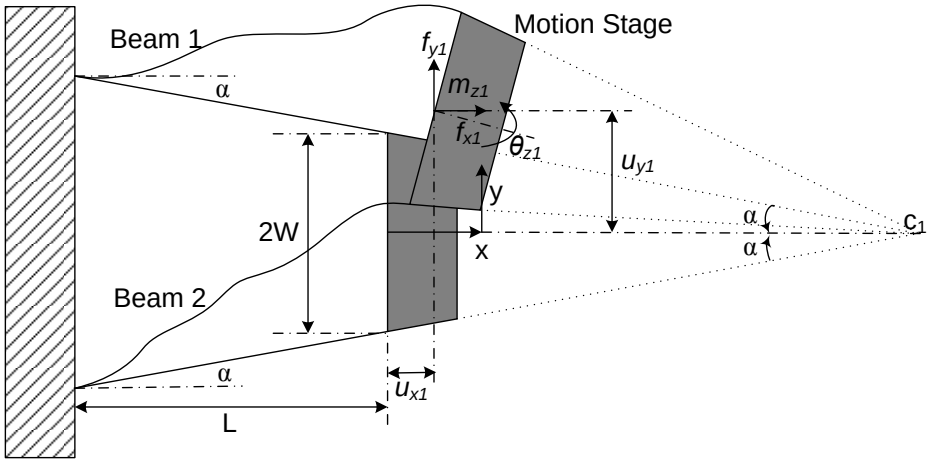

Figure 3.2: ***Tilted Parallelogram flexure***

Previously reported explicit analysis [30] shows that the stage DoF displacements, u_{y1} and the θ_{z1} are kinematically strongly related for $\alpha \sim 0.1$. This results in a one DoF system. Such a system can result from improper alignment that often occurs due to manufacturing defects. It may also be an intentional design as the tilted parallelogram flexure may rotate the stage by small angles about a predefined remote center of rotation c_1 as shown in Figure 3.2. This section reformulates the load-displacement results using energy methods and compares its computational complexity with explicit analysis.

Using geometric considerations the end displacements can be related to the stage displacements as below. The displacements in each beam are denoted by a superscript (b1) or (b2) for beam 1 and beam 2 respectively. The stage rotation θ_{z1} is found experimentally to be of the order of 10^{-2} for $-5 < \boldsymbol{f_{y1}} < +5$ and $-5 < \boldsymbol{f_{x1}} < +5$ and hence sine and cosine term of θ_{z1} can be linearized as θ_{z1} and *1* respectively.

$$
\begin{aligned}
u_{x1}^{(b1)} &= u_{x1} - w\sin\left(\theta_{z1}\right) \approx u_{x1} - w\theta_{z1} \\
u_{x1}^{(b2)} &= u_{x1} + w\sin\left(\theta_{z1}\right) \approx u_{x1} + w\theta_{z1} \\
u_{y1}^{(b1)} &= u_{y1} - w\cos\left(\theta_{z1}\right) \approx u_{y1} \\
u_{y1}^{(b2)} &= u_{y1} + w\cos\left(\theta_{z1}\right) \approx u_{y1} \\
\theta_{z1}^{(b1)} &= \theta_{z1}^{(b2)} = \theta_{z1}
\end{aligned}
\tag{3.35}
$$

The two beams in this case have initial angles of $+\alpha$ or $-\alpha$ and radius of curvature of *0*. The total strain energy stored in the flexure module is the algebraic sum of the strain energy stored in either of the beams. Eq.(3.33) is used to find the individual strain energies and

Eq.(3.35) is used to obtain the total strain energy of the system in terms of stage end displacement variables u_{y1}, θ_{z1} and u_{x1}.

$$v = \frac{6\left[u_{x1}^{(b1)(e)2} + u_{x1}^{(b2)(e)2}\right]}{t^2} + \frac{1}{2}\begin{Bmatrix} u_{y1} & \theta_{z1} \end{Bmatrix}\begin{bmatrix} 12+\frac{\boldsymbol{f}_{x1}^{(b1)2}}{700} & -6-\frac{\boldsymbol{f}_{x1}^{(b1)2}}{1400} \\ -6-\frac{\boldsymbol{f}_{x1}^{(b1)2}}{1400} & 4+\frac{11\boldsymbol{f}_{x1}^{(b1)2}}{6300} \end{bmatrix}\begin{Bmatrix} u_{y1} \\ \theta_{z1} \end{Bmatrix}$$
$$+\frac{1}{2}\begin{Bmatrix} u_{y1} & \theta_{z1} \end{Bmatrix}\begin{bmatrix} 12+\frac{\boldsymbol{f}_{x1}^{(b2)2}}{700} & -6-\frac{\boldsymbol{f}_{x1}^{(b2)2}}{1400} \\ -6-\frac{\boldsymbol{f}_{x1}^{(b2)2}}{1400} & 4+\frac{11\boldsymbol{f}_{x1}^{(b2)2}}{6300} \end{bmatrix}\begin{Bmatrix} u_{y1} \\ \theta_{z1} \end{Bmatrix} \tag{3.36}$$

In Eq.(3.36) the strain energy expression has the DoC forces and the elastic DoC end displacements of both the beams. The axial DoC forces in the two beams can be expressed in terms of their respective axial DoC elastic displacements as below.

$$\boldsymbol{f}_{\boldsymbol{x1}}^{\boldsymbol{(b1)}} = k_{33}u_{x1}^{(b1)(e)}, \qquad \boldsymbol{f}_{\boldsymbol{x1}}^{\boldsymbol{(b2)}} = k_{33}u_{x1}^{(b2)(e)}$$
$$\text{where } k_{33} \triangleq \frac{12}{t^2} \tag{3.37}$$

Using the above equation the DoC force variables of the individual beams in the strain energy expression in Eq.(3.36) is eliminated and the strain energy in terms of displacements only is formulated as below.

$$v = \left\{12u_{y1}{}^2 - 12u_{y1}\theta_{z1} + 4\theta_{z1}{}^2\right\} + \frac{1}{2}k_{33}\left(u_{x1}^{(b1)(e)}\right)^2\left\{1+k_{33}\left(\frac{u_{y1}{}^2}{700} - \frac{u_{y1}\theta_{z1}}{700} + \frac{11\theta_{z1}{}^2}{6300}\right)\right\}$$
$$+\frac{1}{2}k_{33}\left(u_{x1}^{(b2)(e)}\right)^2\left\{1+k_{33}\left(\frac{u_{y1}{}^2}{700} - \frac{u_{y1}\theta_{z1}}{700} + \frac{11\theta_{z1}{}^2}{6300}\right)\right\} \tag{3.38}$$

The constraint equations for the two beams can be formulated using Eq.(3.34) and by simple manipulation $u_{x1}^{(b1)(e)}$ and $u_{x1}^{(b2)(e)}$ can be expressed in terms of stage DoC end displacement u_{x1}.

$$u_{x1}^{(b1)(e)} = \frac{u_{x1} - w\theta_{z1} + \frac{3}{5}u_{y1}{}^2 - \frac{1}{10}u_{y1}\theta_{z1} + \frac{1}{15}\theta_{z1}{}^2 - \alpha u_{y1}}{1+k_{33}\left\{\frac{1}{700}u_{y1}{}^2 - \frac{1}{700}u_{y1}\theta_{z1} + \frac{11}{6300}\theta_{z1}{}^2\right\}}$$
$$u_{x1}^{(b2)(e)} = \frac{u_{x1} + w\theta_{z1} + \frac{3}{5}u_{y1}{}^2 - \frac{1}{10}u_{y1}\theta_{z1} + \frac{1}{15}\theta_{z1}{}^2 + \alpha u_{y1}}{1+k_{33}\left\{\frac{1}{700}u_{y1}{}^2 - \frac{1}{700}u_{y1}\theta_{z1} + \frac{11}{6300}\theta_{z1}{}^2\right\}} \tag{3.39}$$

The expressions in the equation above are substituted in Eq.(3.38) to eliminate the individual elastic DoC displacements and obtain the strain energy in terms of stage displacement variables only.

$$v = \left\{12u_{y1}{}^2 - 12u_{y1}\theta_{z1} + 4\theta_{z1}{}^2\right\} + \frac{1}{2}k_{33}\frac{\left(u_{x1} - w\theta_{z1} + \frac{3}{5}u_{y1}{}^2 - \frac{1}{10}u_{y1}\theta_{z1} + \frac{1}{15}\theta_{z1}{}^2 - \alpha u_{y1}\right)^2}{\left\{1 + k_{33}\left(\frac{u_{y1}{}^2}{700} - \frac{u_{y1}\theta_{z1}}{700} + \frac{11\theta_{z1}{}^2}{6300}\right)\right\}} + \frac{1}{2}k_{33}\frac{\left(u_{x1} + w\theta_{z1} + \frac{3}{5}u_{y1}{}^2 - \frac{1}{10}u_{y1}\theta_{z1} + \frac{1}{15}\theta_{z1}{}^2 + \alpha u_{y1}\right)^2}{\left\{1 + k_{33}\left(\frac{u_{y1}{}^2}{700} - \frac{u_{y1}\theta_{z1}}{700} + \frac{11\theta_{z1}{}^2}{6300}\right)\right\}} \tag{3.40}$$

The PVW for the present problem is stated below in terms of stage displacement variables.

$$\delta v = \boldsymbol{f_{y1}}\delta u_{y1} + \boldsymbol{f_{x1}}\delta u_{x1} + \boldsymbol{m_{z1}}\delta\theta_{z1} \tag{3.41}$$

Substituting the strain energy expression, given in Eq.(3.40), in the above equation, and equating the coefficients of independent variation quantities δu_{x1}, δu_{y1} and $\delta\theta_{z1}$ on L.H.S. and R.H.S. the following relations are obtained.

$$\boldsymbol{f_{y1}} = \left\{24u_{y1} - 12\theta_{z1}\right\} + \boldsymbol{f_{x1}}\left\{\frac{6}{5}u_{y1} - \frac{1}{10}\theta_{z1}\right\} - \boldsymbol{f_{x1}}{}^2\left\{\frac{1}{700}u_{y1} - \frac{1}{1400}\theta_{z1}\right\} + 2k_{33}\alpha\frac{\left(w\theta_{z1} + \alpha u_{y1}\right)}{\left\{1 + k_{33}\left(\frac{u_{y1}{}^2}{700} - \frac{u_{y1}\theta_{z1}}{700} + \frac{11\theta_{z1}{}^2}{6300}\right)\right\}} \tag{i}$$

$$\boldsymbol{m_{z1}} = \left\{-12u_{y1} + 8\theta_{z1}\right\} + \boldsymbol{f_{x1}}\left\{-\frac{1}{10}u_{y1} + \frac{2}{15}\theta_{z1}\right\} - \boldsymbol{f_{x1}}{}^2\left\{-\frac{1}{1400}u_{y1} + \frac{11}{6300}\theta_{z1}\right\} + 2k_{33}w\frac{\left(w\theta_{z1} + \alpha u_{y1}\right)}{\left\{1 + k_{33}\left(\frac{u_{y1}{}^2}{700} - \frac{u_{y1}\theta_{z1}}{700} + \frac{11\theta_{z1}{}^2}{6300}\right)\right\}} \tag{ii}$$

$$\boldsymbol{f_{x1}} = 2k_{33}\frac{\left(u_{x1} + \frac{3}{5}u_{y1}{}^2 - \frac{1}{10}u_{y1}\theta_{z1} + \frac{1}{15}\theta_{z1}{}^2\right)}{\left\{1 + k_{33}\left(\frac{u_{y1}{}^2}{700} - \frac{u_{y1}\theta_{z1}}{700} + \frac{11\theta_{z1}{}^2}{6300}\right)\right\}} \tag{iii}$$

(3.42)

The tilted parallelogram flexure for small deflections rotated the stage about the center located at c_1 as shown in Fig.3. This implies that u_{y1} and θ_{z1} are related by a geometric relation. In order to find this relation let us assume that only $\boldsymbol{f_{y1}}$ is applied and $\boldsymbol{m_{z1}}$ and $\boldsymbol{f_{x1}}$ are zero. Furthermore, let us consider the case when both u_{y1} and θ_{z1} are small, that is of the order of -2. Under these conditions Eq.(3.42)(ii) can be rearranged to obtain the approximate relation given below.

$$\frac{\left\{12u_{y1}-8\theta_{z1}\right\}}{2k_{33}w}\left\{1+k_{33}\left(\frac{{u_{y1}}^2}{700}-\frac{u_{y1}\theta_{z1}}{700}+\frac{11{\theta_{z1}}^2}{6300}\right)\right\}=w\theta_{z1}+\alpha u_{y1}$$

$$\because u_{y1},\theta_{z1} \text{ are of the order of } -2, \text{ and } k_{33} \text{ is of the order of } 4 \quad \therefore \text{L.H.S.} \approx 0 \tag{3.43}$$

$$\Rightarrow \theta_{z1} \approx -\frac{\alpha u_{y1}}{w}$$

It is observed that the coefficients of the $\boldsymbol{f_{x1}}^2$ terms in Eq.(3.42) are small w.r.t. other term and hence are dropped. Using the approximation for θ_{z1}, given in Eq.(3.43), in the moment equation in Eq.(3.42), the following expression for θ_{z1} is obtained. The expression for u_{y1} and u_{x1} is obtained from the DoF force equation and DoC force equation respectively in Eq.(3.42) using similar approximations.

$$\theta_{z1}=-\frac{\alpha u_{y1}}{w}+\frac{1}{2w^2}\left[m_{z1}+\left\{\left(12+8\frac{\alpha}{w}\right)-\boldsymbol{f_{x1}}\left(\frac{1}{10}+\frac{2\alpha}{15w}\right)\right\}u_{y1}\right]\left\{\frac{1}{k_{33}}+{u_{y1}}^2\left(\frac{1}{700}+\frac{\alpha}{700w}+\frac{11\alpha^2}{6300w^2}\right)\right\}$$

$$u_{y1}=\frac{\boldsymbol{f_{y1}}-\frac{\alpha}{w}\boldsymbol{m_{z1}}}{24+24\frac{\alpha}{w}+8\frac{\alpha^2}{w^2}+\boldsymbol{f_{x1}}\left(\frac{6}{5}+\frac{2\alpha}{10w}+\frac{2\alpha^2}{15w^2}\right)} \tag{3.44}$$

$$u_{x1}=\frac{\boldsymbol{f_{x1}}}{2k_{33}}-{u_{y1}}^2\left\{\left(\frac{3}{5}+\frac{\alpha}{10w}+\frac{\alpha^2}{15w^2}\right)+\frac{\boldsymbol{f_{x1}}}{2}\left(\frac{1}{700}+\frac{\alpha}{700w}+\frac{11\alpha^2}{6300w^2}\right)\right\}$$

The end-displacement expressions given by Eq.(3.44) are same as previously derived using explicit analysis in reference [30]. However, the mathematical complexity in this case is significantly lower because the entire formulation was done using linear operations. It should be noted using linear operation is simply a mathematical step and does not imply dropping geometric nonlinearities.

3.5.2 Multiple-Beam Parallelogram Flexure

Parallelogram mechanisms are widely used because of its ability to produce approximately straight-line motion in a direction perpendicular to the orientation of the beams, while providing a high degree of constraint towards rotation and translation parallel to the beams.

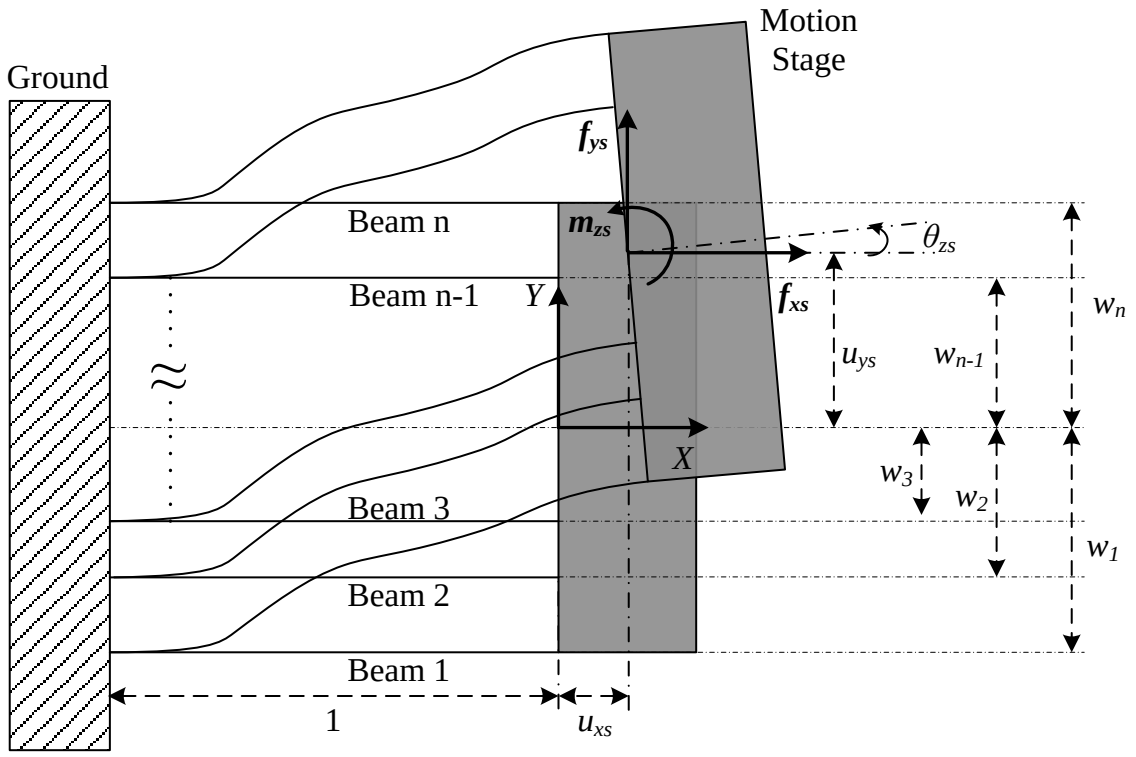

Figure 3.3: ***Multi-Beam Parallelogram flexure***

A multi-beam parallelogram flexure mechanism is shown in Figure 3.3. The motion stage is connected to ground via parallel and identical beams, not necessarily uniform in thickness, numbered *1* through *n*. External loads $\boldsymbol{f_{xs}}$, $\boldsymbol{f_{ys}}$, and $\boldsymbol{m_{zs}}$, normalized as per the previously described scheme, act at point O on the motion stage. A reference line, passing through O and parallel to the undeformed beams, is used to specify the location of the i^{th} beam via the geometric parameter w_i measured along the positive Y axis. The spacing between the beams is arbitrary. The normalized displacements of point O, under the given loads, are denoted by u_{xs}, u_{ys}, and θ_{zs}. It is

physically obvious that the Y direction represents a DoF, while the axial direction X and transverse rotational direction Θ_Z represent DoC given their high stiffness.

The multi-beam parallelogram flexure module allows the use of thinner beams that leads to a low DoF stiffness without compromising DoC stiffness. This ensures a larger DoF motion range along with good DoC load bearing capacity [38, 66]. Consequently, one would like to study the effect of the number of beams and their spacing on stiffness and error motion behavior. This necessitates the determination of the stage displacements in terms of the three externally applied loads. A direct analysis of this system would require the creation of Free Body Diagrams for each beam, explicitly identifying its end-loads. The end load-displacement relations for each beam provide *3n* constitutive relations, while another *3* equations are obtained from the load equilibrium of the stage in its displaced configuration. These *3(n+1)* equations have to be solved simultaneously for the *3n* unknown internal end-loads and the three displacements of the motion stage (u_{xs}, u_{ys}, and θ_{zs}). Even though the *3n* internal end-loads are of no interest, they have to be determined in this direct analysis. Obviously, the complexity associated with solving *3(n+1)* equations grows with increasing number of beams.

Instead, an energy based approach for determining the load-displacement relations for the multi-beam parallelogram flexure turns out to be far more efficient. We first identify the geometric compatibility conditions in this case by expressing the end displacements of each beam in terms of the stage displacements. Since a physical understanding of the system as well as previous analytical results show that the stage angle θ_{zs} is very small (~10^{-3}), the small angle approximations $\cos\theta_{zs} = 1$ and $\sin\theta_{zs} = \theta_{zs}$ are well-justified. Thus, the end displacements for the i^{th} beam are given by:

$$\begin{aligned} u_{x1(i)} &\approx u_{xs} - w_{(i)}\theta_{zs} \\ u_{y1(i)} &\approx u_{ys} \\ \theta_{z1(i)} &\approx \theta_{zs} \end{aligned} \tag{3.45}$$

Next, using Eq.(3.14), the strain energy for the i^{th} beam is given by:

$$v_{(i)} = \frac{1}{2}k_{33}\frac{\left(u_{xs} - w_{(i)}\theta_{zs} + \frac{1}{2}\begin{Bmatrix} u_{ys} & \theta_{zs} \end{Bmatrix}\begin{bmatrix} k_{11}^{(1)} & k_{12}^{(1)} \\ k_{12}^{(1)} & k_{22}^{(1)} \end{bmatrix}\begin{Bmatrix} u_{ys} \\ \theta_{zs} \end{Bmatrix}\right)^2}{\left(1 - k_{33}\begin{Bmatrix} u_{ys} & \theta_{zs} \end{Bmatrix}\begin{bmatrix} k_{11}^{(2)} & k_{12}^{(2)} \\ k_{12}^{(2)} & k_{22}^{(2)} \end{bmatrix}\begin{Bmatrix} u_{ys} \\ \theta_{zs} \end{Bmatrix}\right)} + \frac{1}{2}\begin{Bmatrix} u_{ys} & \theta_{zs} \end{Bmatrix}\begin{bmatrix} k_{11}^{(0)} & k_{12}^{(0)} \\ k_{12}^{(0)} & k_{22}^{(0)} \end{bmatrix}\begin{Bmatrix} u_{ys} \\ \theta_{zs} \end{Bmatrix} \tag{3.46}$$

Instead of numerical values, the beam characteristic coefficients in the above equation are left as symbols so that this analysis is valid for simple beam flexures with varying cross-section. The total strain energy of the system is simply the sum of the strain energies of all the beams:

$$v = \frac{1}{2}k_{33}\frac{\sum_{i=1}^{n}\left(u_{xs} - w_{(i)}\theta_{zs} + \frac{1}{2}\left\{k_{11}^{(1)}u_{ys}^2 + 2k_{12}^{(1)}u_{ys}\theta_{zs} + k_{22}^{(1)}\theta_{zs}^2\right\}\right)^2}{\left(1 - k_{33}\left\{k_{11}^{(2)}u_{ys}^2 + 2k_{12}^{(2)}u_{ys}\theta_{zs} + k_{22}^{(2)}\theta_{zs}^2\right\}\right)} + \frac{1}{2}n\left\{k_{11}^{(0)}u_{ys}^2 + 2k_{12}^{(0)}u_{ys}\theta_z + k_{22}^{(0)}\theta_{zs}^2\right\} \quad (3.47)$$

Applying the PVW, the variation of strain energy in response to virtual displacements δu_{xs}, δu_{ys}, and $\delta\theta_{zs}$ may be equated to the virtual work done by external forces. In the resulting equation, the coefficients of each of these mutually independent virtual displacements may be identically set to zero. This results in the following three relations, where the first one is used to simplify the subsequent two:

$$\boldsymbol{f_{xs}} = nk_{33}\frac{\left(u_{xs} + \frac{1}{2}\left\{k_{11}^{(1)}u_{ys}^2 + 2k_{12}^{(1)}u_{ys}\theta_{zs} + k_{22}^{(1)}\theta_{zs}^2\right\}\right) - \left(\frac{1}{n}\sum_{i=1}^{n}w_{(i)}\right)\theta_{zs}}{\left(1 - k_{33}\left\{k_{11}^{(2)}u_{ys}^2 + 2k_{12}^{(2)}u_{ys}\theta_{zs} + k_{22}^{(2)}\theta_{zs}^2\right\}\right)} \quad (3.48)$$

$$\begin{aligned}\boldsymbol{f_{ys}} = {} & k_{33}\sum_{i=1}^{n}\left\{\frac{\boldsymbol{f_{xs}}}{nk_{33}} + \frac{\left(\frac{1}{n}\sum_{i=1}^{n}w_{(i)} - w_{(i)}\right)\theta_{zs}}{\left(1 - k_{33}\left\{k_{11}^{(2)}u_{ys}^2 + 2k_{12}^{(2)}u_{ys}\theta_{zs} + k_{22}^{(2)}\theta_{zs}^2\right\}\right)}\right\}\left(k_{11}^{(1)}u_{ys} + k_{12}^{(1)}\theta_{zs}\right) \\ & + k_{33}^2\sum_{i=1}^{n}\left\{\frac{\boldsymbol{f_{xs}}}{nk_{33}} + \frac{\left(\frac{1}{n}\sum_{i=1}^{n}w_{(i)} - w_{(i)}\right)\theta_{zs}}{\left(1 - k_{33}\left\{k_{11}^{(2)}u_{ys}^2 + 2k_{12}^{(2)}u_{ys}\theta_{zs} + k_{22}^{(2)}\theta_{zs}^2\right\}\right)}\right\}^2\left(k_{11}^{(2)}u_{ys} + k_{12}^{(2)}\theta_{zs}\right) \\ & + n\left(k_{11}^{(0)}u_{ys} + k_{12}^{(0)}\theta_{zs}\right)\end{aligned} \quad (3.49)$$

$$\boldsymbol{m}_{zs} = k_{33}\sum_{i=1}^{n}\left[\left\{\frac{\boldsymbol{f}_{xs}}{nk_{33}}+\frac{\left(\frac{1}{n}\sum_{i=1}^{n}w_{(i)}-w_{(i)}\right)\theta_{zs}}{\left(1-k_{33}\left\{k_{11}^{(2)}u_{ys}^{2}+2k_{12}^{(2)}u_{ys}\theta_{zs}+k_{22}^{(2)}\theta_{zs}^{2}\right\}\right)}\right\}\left(-w_{(i)}+k_{12}^{(1)}u_{ys}+k_{22}^{(1)}\theta_{zs}\right)\right]$$

$$+k_{33}^{2}\sum_{i=1}^{n}\left\{\frac{\boldsymbol{f}_{xs}}{nk_{33}}+\frac{\left(\frac{1}{n}\sum_{i=1}^{n}w_{(i)}-w_{(i)}\right)\theta_{zs}}{\left(1-k_{33}\left\{k_{11}^{(2)}u_{ys}^{2}+2k_{12}^{(2)}u_{ys}\theta_{zs}+k_{22}^{(2)}\theta_{zs}^{2}\right\}\right)}\right\}^{2}\left(k_{12}^{(2)}u_{ys}+k_{22}^{(2)}\theta_{zs}\right) \tag{3.50}$$

$$+n\left(k_{12}^{(0)}u_{ys}+k_{22}^{(0)}\theta_{zs}\right)$$

For a DoF motion range $u_{ys} \sim 0.1$, Eq.(3.48) may be simplified by recognizing that $\theta_{zs} << u_{ys}$ to yield the axial direction displacement:

$$u_{xs} = \frac{\boldsymbol{f}_{xs}}{nk_{33}} \quad -\frac{1}{2}k_{11}^{(1)}u_{ys}^{2} \quad -\frac{\boldsymbol{f}_{xs}}{n}k_{11}^{(2)}u_{ys}^{2} \tag{3.51}$$

Clearly, the first term above is a purely elastic term arising from an axial stretching of the beams. The second term is a kinematic term, which is independent of the number of beams. The final term is an elastokinematic term. Similarly, Eq.(3.49) may be simplified to the following form:

$$\boldsymbol{f}_{ys} = \left(nk_{11}^{(0)} + \boldsymbol{f}_{xs}\,k_{11}^{(1)} + \frac{1}{n}\boldsymbol{f}_{xs}^{2}k_{11}^{(2)}\right)u_{ys} \tag{3.52}$$

Here, the first term may be identified to be the elastic stiffness term and the second term is a load-stiffening term, which is seen to be independent of the number of beams. The consistency of the energy formulation, described above, dictates that if the elastokinematic term is captured in Eq.(3.51), the third term (second power in $\boldsymbol{f}_{xs}$) will appear in Eq.(3.52). At this final stage, one may choose to drop this second power term because its contribution is practically negligible for typical beam shapes and load ranges of interest.

Similarly, Eq.(3.50) may be simplified as follows:

$$\theta_{zs} = \frac{\left[\boldsymbol{m}_{zs}+\frac{\boldsymbol{f}_{xs}}{n}\left(\sum_{i=1}^{n}w_{(i)}\right)-\left(nk_{12}^{(0)}+\boldsymbol{f}_{xs}k_{12}^{(1)}+\frac{\boldsymbol{f}_{xs}^{2}}{n}k_{12}^{(2)}\right)u_{y}\right]\left(\frac{1}{k_{33}}-k_{11}^{(2)}u_{ys}^{2}\right)}{\left[\sum_{i=1}^{n}w_{(i)}^{2}-\frac{1}{n}\left\{\left(\sum_{i=1}^{n}w_{(i)}\right)^{2}\right\}+\left(\frac{1}{k_{33}}-k_{11}^{(2)}u_{ys}^{2}\right)\left(nk_{22}^{(0)}+k_{22}^{(1)}\boldsymbol{f}_{xs}+\frac{k_{22}^{(2)}\boldsymbol{f}_{xs}^{2}}{n}\right)\right]}$$

Furthermore, recognizing that k_{33} is several orders of magnitude larger than all the other stiffness coefficients and that the second power terms in $\boldsymbol{f}_{xs}$ may be neglected, the above relation reduces to:

$$\theta_{zs} \approx \frac{\left[\boldsymbol{m}_{zs} + \frac{\boldsymbol{f}_{xs}}{n}\left(\sum_{i=1}^{n} w_{(i)}\right) - \left(nk_{12}^{(0)} + \boldsymbol{f}_{xs}k_{12}^{(1)}\right)u_{ys}\right]\left(\frac{1}{k_{33}} - k_{11}^{(2)}u_{ys}^{2}\right)}{\left[\sum_{i=1}^{n} w_{(i)}^{2} - \frac{1}{n}\left\{\left(\sum_{i=1}^{n} w_{(i)}\right)^{2}\right\}\right]} \tag{3.53}$$

Next, the accuracy of the above closed-form parametric analytical results is corroborated via non-linear FEA carried out in ANSYS. A 7-beam parallelogram flexure is selected for this FEA study, with the beam locations w_i arbitrarily chosen with respect to a reference X axis that passes through the center of the stage. Each simple beam (initially straight and uniform in thickness) is *5mm* in thickness, *50mm* in height, and *250mm* in the length; the latter serves to normalize all other displacements and length dimensions. The normalized values of the w_i's selected are: *– 0.6*, *– 0.45*, *– 0.25*, *– 0.1*, *0.2*, *0.35* and *0.6*. BEAM4 elements are used for meshing, and the consistent matrix and large displacement (NLGEOM) options are turned on to capture all non-linearities in the problem. A Young's modulus of *210,000 N/mm*^{2} and Poisson's ratio of *0.3* are used assuming the material to be Steel. The normalized DoF displacement u_y is varied from *– 0.12* to *0.12*. The parasitic axial displacement of the stage u_x (Figure 3.4) is determined while keeping $\boldsymbol{f}_{xs} = \boldsymbol{m}_{xs} = 0$. The parasitic rotation of the stage θ_z (Figure 3.5) and the X direction stiffness (Figure 3.6) are determined while setting the normalized axial force $\boldsymbol{f}_{xs}$ to *1* and $\boldsymbol{m}_{xs}$ and to *0*.

These FEA results for the 7-beam parallelogram are in agreement with the BCM predictions (Eqs. (3.51), (3.52), and (3.53)), within 5% error. In general, this flexure module exhibits constraint characteristics very similar to the 2-beam parallelogram flexure module. Its key advantage is a 3.5 times greater X DoC stiffness (and therefore load bearing capacity) without compromising the motion Y DoF motion range and adversely affecting the X and Θ_Z DoC parasitic errors.

This example shows that once a consistent BCM energy formulation has been derived, the use of energy methods considerably reduces the mathematical complexity in the analysis of increasingly sophisticated flexure mechanisms. The above procedure is relatively independent of

the number of beams chosen or the shapes of the individual beams, as long as the strain energy associated with each beam is accounted for correctly.

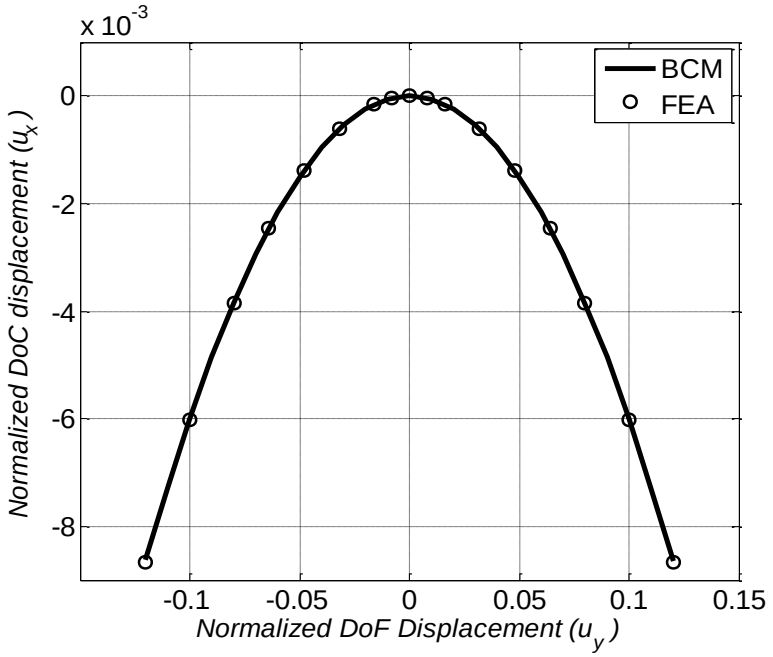

Figure 3.4: Parasitic axial displacement u_x (DoC) vs. transverse displacement u_y (DoF)

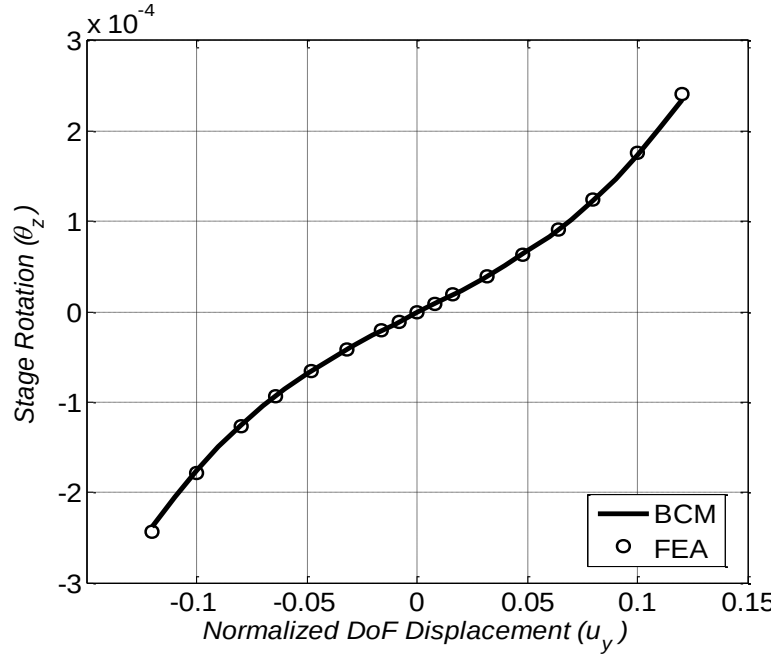

Figure 3.5: Parasitic stage rotation θ_z (DoC) vs. transverse displacement u_y (DoF)

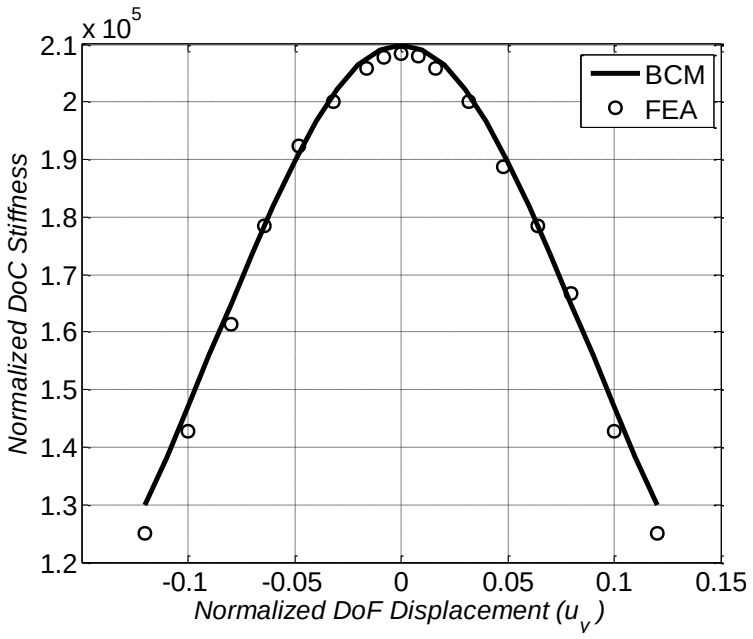

Figure 3.6: ***Axial stiffness (DoC) vs. transverse displacement u_y (DoF)***

Equations (3.51), (3.52) and (3.53) are the load-displacement relations for the multi-beam parallelogram flexure. Using energy methods the relations are not only derived quickly but the complexity of the analysis is independent of the number of beams in the mechanism or their relative spacing. Therefore the model for the n-beam parallelogram can be used for optimizing the number of flexure beams, the beam cross-section as well as the spacing between the beams.

It should be noted that the above derivation can be easily extended to cases where the beams are not perfectly parallel. Since the strain energy of tilted flexure beams are available to us in the global co-ordinate system, one may simple use it in place of the strain energy for simple (non-tilted) beam flexure and obtain an accurate model for the mechanism.

3.6 Discussion

The strain energy and constraint equation of a planar beam flexure are unusual as they are dependent not only on displacement but also on forces. This nonlinear behavior is difficult to capture and are not present in traditional linear analysis or Pseudo-Rigid Body Model. However, this chapter models the strain energy and constraint equation energy methods for a generalized planar beam flexure more accurately and points out additional contribution of axial force $\boldsymbol{f_{x1}}$ in both strain energy and the constraint equation. Through the example of the tilted beam

parallelogram beam flexure and multi-beam parallelogram flexure module, the accuracy of the analysis performed using the new strain energy are demonstrated.

Misalignments due to manufacturing defects are often seen in flexure mechanisms. Analyzing these situations using the PBCM for straight flexure strip can be complicated due to the local co-ordinate systems of the flexure elements being different from the global co-ordinate system. However, by using the PBCM for slanted flexure strip, these situations can be analyzed as easily as working with straight beams. This was demonstrated in the tilted beam parallelogram flexure example.

Additionally, this chapter also showed the existence of fundamental relations between beam characteristic coefficients which paves a simple way of extracting the strain energy and constraint relations from the DoF load-displacement relations. Using these relations in conjunction with the approaches discussed in Chapter 2, Section 4 to find the DoF load-displacement relations a simple beam flexure with varying cross-section, PBCM for other flexure beams with various varying cross-sections can be generated and added to a library of flexure elements. These new flexure elements can then be used to design various flexure mechanisms.

Chapter 4

Spatial Beam Constraint Model for Flexure Strip with Generalized Loading

4.1 Introduction

The Planar Beam Constraint Model (PBCM), developed in Chapter 2 and Chapter 3, cannot be adequately used for modeling, analysis, and constraint based design [62] of flexure mechanisms where the pertinent loads as well as displacements do not lie in one plane. This is the case whenever the flexure mechanism is such that fully generalized loads are required to be considered. Such loading can be divided into three mutually perpendicular forces and three mutually perpendicular moments as shown in Figure 4.1 and will be referred to as spatial loading. In these cases several additional nonlinear effects become significant, particularly in the presence of axial torsion. These nonlinearities will be captured in a spatial beam constraint model (SBCM), presented in this and subsequent chapters.

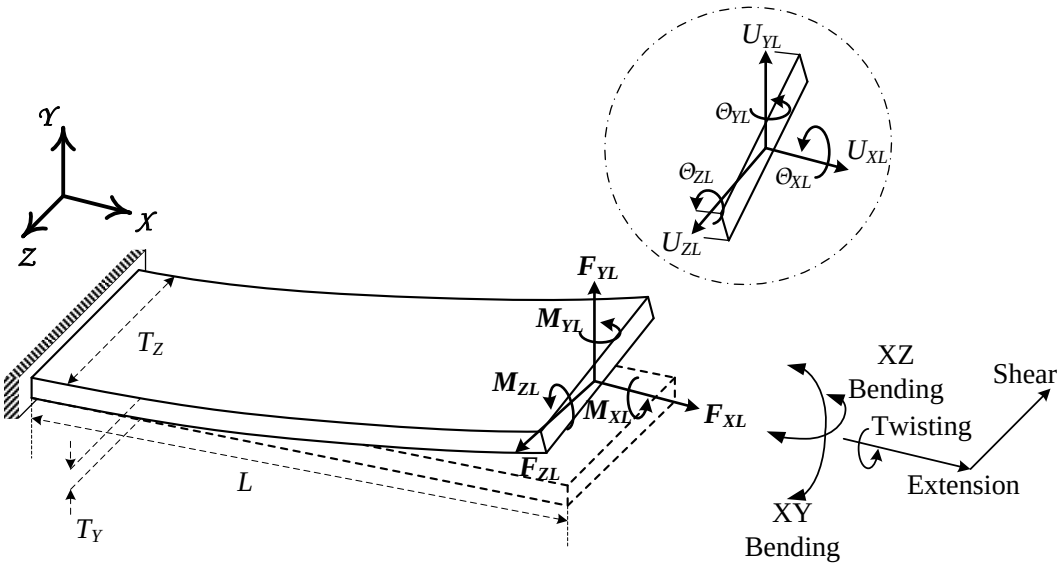

Figure 4.1: A flexure strip with spatial loads and displacements

In addition to capturing nonlinearities, the SBCM also aims to capture the effect of ε_{ZZ} strain that originates from the Poisson Effect and results in the anticlastic curvature [29] of a beam while bending. This effect, at times known as the anticlastic effect, results in Z displacements even in the absence of loads in the Z direction. Instead of Z loads, ε_{ZZ} arises due to the stress along X through the Poisson's ratio, v as stated in the constitutive relations. During bending, this strain in Z direction leads to expansion of the width (T_Z) where there is compressive stress along X while contraction of the width where there is tension along X These deformations physically imply that the beam assumes a curvature in the XZ plane as shown in Figure 4.2. This curvature is known as the anticlastic curvature. The magnitude of the anticlastic curvature is at its maximum at the edges and close to zero away from the edges. This is because, except at the edges, everywhere else the material tries to resist this deformation. Since strain along X and Z are related through constitutive relations, this implies an increase in the resistance to bending as well. When the width, T_Z, is infinite, the additional resistance to bending due to anticlastic curvature can be easily captured by replacing elastic modulus, E, by $E^* = E / (1-\nu^2)$, in the linear beam model as well as in PBCM. On the other hand when the beam width, T_Z, is of the order of beam thickness, T_Y, then additional resistance to bending due to anticlastic curvature is very small and can be neglected. If only planar loading is considered, then for this case as well the PBCM can be used to estimate displacements. However for any intermediate width, the effect of the anticlastic curvature is non-trivial.

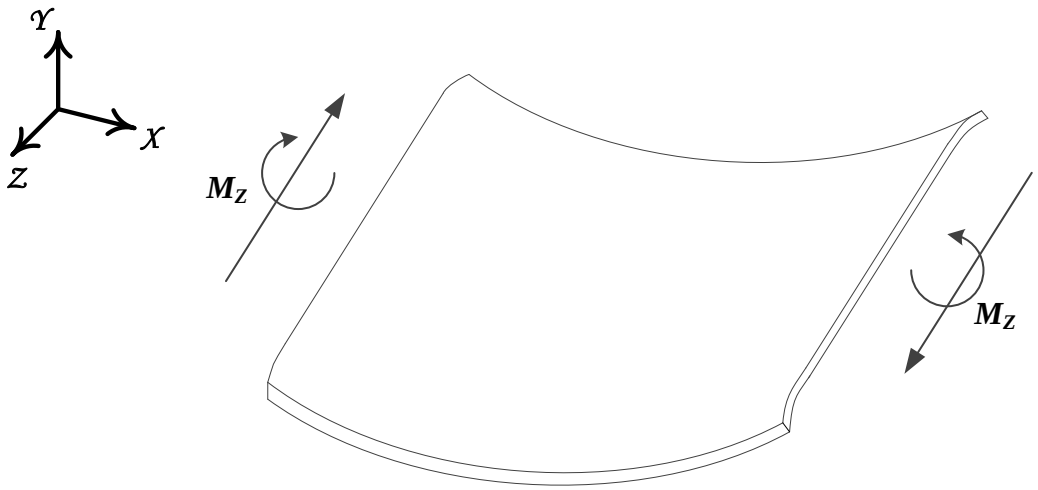

Figure 4.2: Anticlastic curving of plates

It should be noted here one common approach of modeling flexure strips is to assume that the flexure strip is relatively much stiffer in the XZ plane and hence all displacements in the XZ plane are very small compared to displacements in the XY plane. Therefore displacements in the XZ plane may be estimated independent of displacements in the XY plane using Timoshenko's linear beam theory. Furthermore, PBCM may be used to estimate the displacements in the XY while ignoring loads and displacements in the XZ planes. The validity and utility of this approach depends on the particular flexure mechanism. For example, in MEMS devices where parallelogram flexure modules are used as a building block, the out-of-plane stiffness is relatively high and the out-of-plane loads are relatively low. This is a suitable scenario where PBCM can accurately estimate the performance of the flexure mechanism. However from a generalized point of view where out-of-plane loads are present and out-of-plane displacement are not constrained, this approach is not appropriate.

4.2 Motivation for a Spatial Beam Constraint Model (SBCM) of a flexure strips

There are several flexure mechanisms where consideration of spatial loading is necessary for estimating the relevant constraint characteristics. One such flexure mechanism is shown in Figure 4.3(a). In this mechanism, the four component flexure strips are arranged in an 'cross' formation in the YZ plane [67] with their centroidal axis parallel to X axis. The only degree of freedom of the motion stage supported by this mechanism is a rotation about an axis parallel to the X axis passing through the point of intersection of the flexure strips as seen in the YZ plane.

Since all other displacements of the motion stage are constrained, this flexure mechanism is appropriate for mounting rotary actuators such as limit-stroke DC motors which require rotary bearing for supporting its rotor. Another use of this flexure mechanism could be building a flexural universal joint by attaching three of these mechanisms such that the rotational axis of each individual mechanism is perpendicular to the other two. Such a mechanism will be useful in designing micro/nano-manipulators. In either application the component flexure strips experience torsion in addition to bending during rotation of the motion stage about X. As a result, PBCM cannot be used to analyze this flexure mechanism.

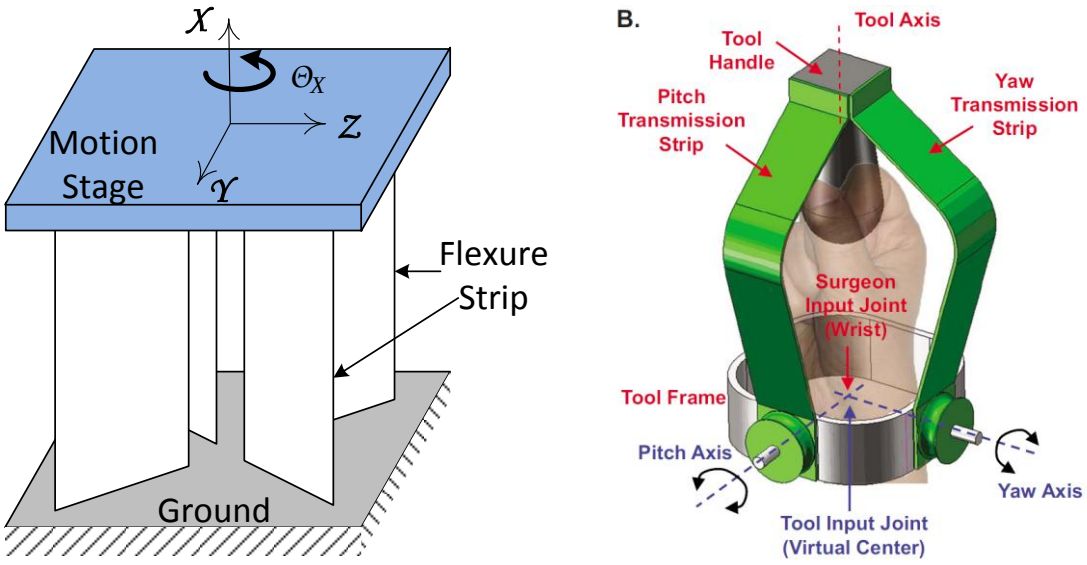

Figure 4.3: (a) 1 rotational DoF flexure mechanism, (b) Flexure Strips used for transmission

Rather than allowing torsional rotation, flexure strips can also be arranged in order to transmit rotation. An example of such a mechanism, shown in Figure 4.3(b), is used in a medical device design [68]. In this mechanism, the rotation of the hand about the wrist is required to be transmitted to an end effector. This is accomplished by two flexure strips which transmit the rotary motion of the hand about the wrist to a wire hub while absorbing all other motions of the hand. Through the wire hub, the motion is transmitted to the end effector. In order to function properly, the torsion stiffness of the flexure strips should be maximized while the bending stiffness in the primary bending direction should be minimized. Here too we find of the need to analyze the effect of spatial loads rather than planar loads.

In several other mechanisms [69, 70], actuator forces or the weight of the motion stages can produce significant moments on the flexure elements when the point of application in general is not at the center of torsional stiffness ($d\boldsymbol{M_{XL}}/d\theta_{XL}$) or XZ bending stiffness ($d\boldsymbol{M_{YL}}/d\theta_{YL}$ and $d\boldsymbol{F_{ZL}}/dU_{ZL}$). In order to reduce the dependence on the point of application of loads, the torsional stiffness and the XZ bending stiffness of the flexure elements are generally designed to be high. However, even a small angular displacement can be significant if it is connected to the motion/output stage by a long lever arm since the resulting displacement at the motion/output stage is amplified by the length of the lever arm. Additionally, as will be shown at the end of this chapter, the torsional stiffness and the XZ bending stiffness of a flexure strip drops in a quadratic manner as it is bent in the XY plane. Therefore, for a better analysis of both these situations, a generalized model of a flexure strip that considers all possible end-loads is required.

4.3 Additional Nonlinearities captured in the SBCM

When generalized loading of a flexure strip is considered, several new nonlinear effects arise in addition to those discussed for PBCM in Chapter 2. Let us first identify the nonlinearities associated with torsion. By considering load equilibrium being applied in the deformed state, we can easily see that the torsional displacement may be caused by a nonlinear combination of XY and XZ bending loads in addition to torsional load $\boldsymbol{M_{XL}}$. This effect can be visualized in Figure 4.1, by first applying a positive $\boldsymbol{F_{YL}}$ to displace the beam end in the Y direction by U_{YL} followed by applying positive $\boldsymbol{F_{ZL}}$. The torsional moment at any point is equal to the Y displacement at that point multiplied by $\boldsymbol{F_{ZL}}$. The maximum torsional moment on the flexure strip is at its base and is equal to $\boldsymbol{F_{ZL}}\times U_{YL}$. It should be noted that a torsional moment in an opposite sense will also be generated by a positive $\boldsymbol{F_{YL}}$ due to positive U_Z displacement of the flexure strip. However as U_Z displacements are much smaller than U_Y displacements, torsional moment due to $\boldsymbol{F_{YL}}$ may be ignored in comparison to torsional moment due to $\boldsymbol{F_{ZL}}$. Using the beam characteristic differential equations we will see that this nonlinearity not only results in torsional displacement but also results in a reduction of torsional stiffness, $d\boldsymbol{M_{XL}}/d\theta_{XL}$.

Another source of nonlinearity is the fact that initially planar cross-sections do not nominally remain planar after deformation. This warping of the cross-section takes place during bending as well as torsion. When bending is only consider this deformation may be ignored as it does not result in significant variation of stresses. However, when torsion is present, the variation

in stresses due by warping is significant and needs to be considered. For getting a better understanding the reader is encouraged to review Figure 4.4 which shows a fiber at distance R away from the centroid of the cross-section needing to be stretched if the cross-section is to remain a plane. This creates an extensional force in the fiber. If, no external axial force along X is applied then, in order to establish force equilibrium for the entire cross-section, some fibers (closer to the centroid) will also develop a compressive stress. However, due to the constitutive relations, the stress translates into strain which is nothing but the warping of the cross-section.

When a beam is slender in thickness and width and subjected to moderately spatial loads, only the torsional displacement is affected by the warping of cross-sections, which displacement due to bending and extension is relatively unaffected. One may easily capture this effect by using torsional constant instead of the polar are moment of inertia. For beams that are still slender but subjected to humungous axial tensile loads, an additional nonlinear coupling between the axial extension direction and torsional direction becomes important. The nonlinear coupling results in the stiffening of the torsional direction due to axial tensile force. It is also known as the trapeze effect [59]. Next, when the beams become wider (more like flexure strips), then the torsional stiffness increases even more than what is predicted by the trapeze effect or by using torsion constant in place of polar area moment of inertia. Depending on the width of the beam relative to its length and thickness, the torsional stiffness increase linearly or in a quadratic manner. This additional stiffening of the torsional direction is called the Wagner's effect [71].

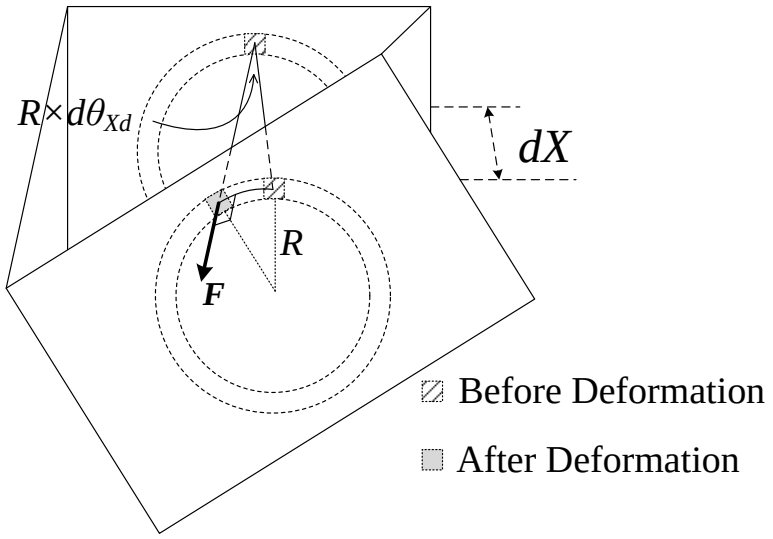

Figure 4.4: Development of extensional and compressive force in axial fibers due to torsion

A nonlinear effect that is seen while estimating bending displacements due to torsional angle is the kinematic coupling between the displacements in the XY and XZ planes. As shown in Figure 4.5, when the beam is twisted, the bending plane changes from the XY and XZ plane to deformed planes, the X_dY_d and X_dZ_d plane. Here the $\mathcal{X}_d$ axis is defined along the tangent to the deformed centroidal axis at location P′ and the axes $\mathcal{Y}_d$ and $\mathcal{Z}_d$ complete the deformed coordinate frame. The orientation of $\mathcal{Y}_d$ and $\mathcal{Z}_d$ with respected to the deformed cross-section is determined to be the same as the position that $\mathcal{Y}$ and $\mathcal{Z}$ would have reached if it was fixed to the undeformed cross-section and the beam deformed such that the warping of the cross-sections was zero. As the displacements of the beam need to be expressed in the X-Y-Z co-ordinate frame, the bending displacements in the $\mathcal{X}_d$-$\mathcal{Y}_d$-$\mathcal{Z}_d$ coordinate frame are vectorially added and split into displacement components in the XY and XZ planes. Due to this transformation, the total value of bending displacement of the XZ plane (U_{ZL} and θ_{YL}) is kinematically dependent on the bending displacement of the XY plane (U_{YL} and θ_{ZL}) in the presence of torsion. It should be noted that since bending stiffness values in XZ plane is relatively high, bending displacements of the XY plane is relatively less affected by the bending displacements of the XZ plane. However, as bending stiffness values in XY plane is relatively low, bending displacements of the XZ plane is relatively more affected by the bending displacements of the XY plane.

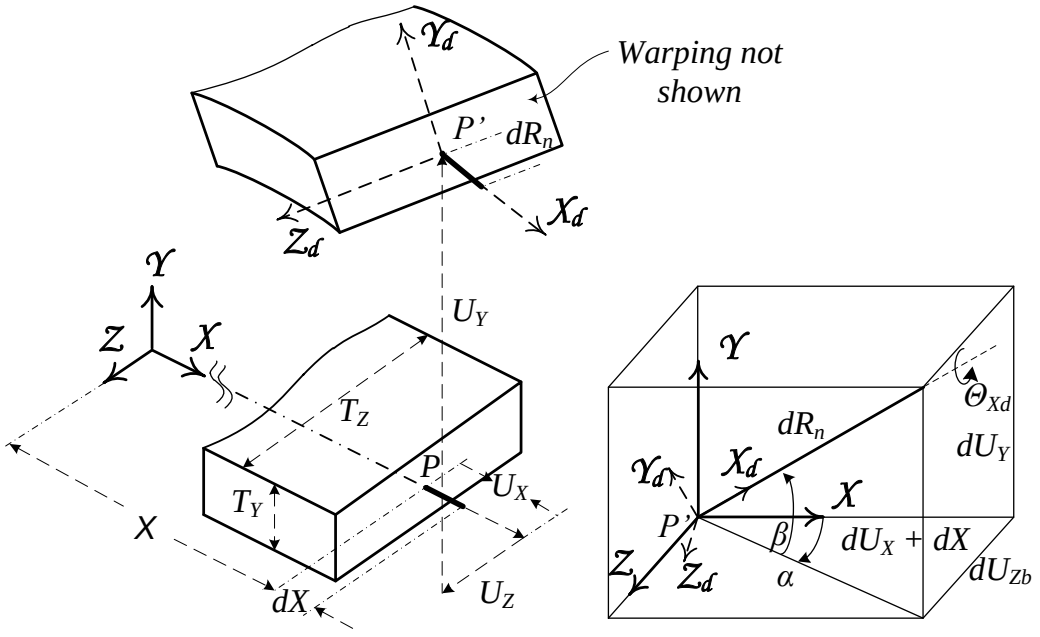

Figure 4.5: Spatial deformation of flexure strip prior to shear

There are also linear and nonlinear effects associated with the presence of the anticlastic curvature as discussed earlier in section 4.1. Capturing the nonlinear effects of the anticlastic effects requires the use of nonlinear plate theory which does not easily lead to closed-form solutions. Instead we attempt to capture the linear effect of anticlastic curvature using beam theory by finding an equivalent elastic modulus, $\bar{E}$, that results in the accurate estimation of the constraint characteristics of the flexure strip.

4.4 Prior Art and Approach

In spite of our extensive literature survey, a closed-form model for a flexure strip with arbitrary width could not be found. However, several scholarly articles that derived nonlinear differential equation of similar problems were studied. Using nonlinear plate theory, Reissner derived differential equations for finite twisting and bending of thin rectangular plates in 1957 [72]. The loading considered was a bending and a torsional couple applied simultaneous on opposite sides of the plate. Since, loading due to axial force is not considered; nonlinear effects such as load stiffening effect and elasto-kinematic effect are not captured. Additionally, the Wagner's effect is also not considered. Even though these nonlinearities were not considered, the resulting differential equations were partial differential equations with two independent variables that still needed to be numerically solved. As partial differential equations are unavoidable in plate mechanics, we turn our attention to beam based solutions of flexure strip with the hope of finding analysis that result ordinary differential equations which are generally more easily solvable.

For width comparable to thickness, beam governing equations that capture most of the nonlinearities in Section 4.3 as well as the nonlinearities discussed in Chapter 2 was derived by Hodges [61] and Da Silva [36]. The only nonlinearity that was not required to be considered was the effect of anticlastic curvature. However, in either formulation, the final four beam characteristic differential equations (for XY bending, XZ bending, twisting and stretching) are highly nonlinear even when second order approximations based on the assumption that the maximum values of translational and rotational displacements are of the order of $0.1L$ and 0.1 radians were taken. As a result, a closed form model could not be formulated from these equations.

More recent work that derives closed form model of parallelogram flexure module built using two flexure strips is based on regression curve fitting of FEA simulations [73]. Although, through FEA, this approach has the potential of capturing all nonlinearities discussed, it is susceptible to numerical errors in the FEA itself. Additionally, since this approach finds models using displacement solution only, the effects that are significant only when calculating stiffness rather than displacement can potentially be completely missed in this process. Furthermore, because of the numerical nature of this approach, a physical understanding of the origin of each term of the model is not always evident.

Instead of the above approaches, an alternate approach is taken in this dissertation where a specific range of beam geometry is chosen such that additional approximations become applicable, making the nonlinear beam characteristic differential equations solvable for generalized loading and generalized displacements. We consider flexure strips in which the indices of aspect ratio defined by $T_Z^2/(T_Y L)$, T_Y/T_Z and T_Y/L are less than 15, 0.1 and 0.05 respectively. By restricting $T_Z^2/(T_Y L)$ to less than 15, the nonlinear Wagner's effect becomes negligible for torsional angle Θ_{Xd} within -0.1 and 0.1 radians as will be shown in Section 4.7. Additionally by restricting T_Y/T_Z to less than 0.1 we ensure that loading stiffening effect in the XZ bending plane is negligible. Finally as flexure strips are typically slender, T_Y/L is assumed to be less than 0.05.

For the chosen beam geometry, we observe the presence of significant anticlastic curving of the flexure strips which imply that neither ε_{ZZ} nor σ_{ZZ} are close to being zero (plane strain and plane stress conditions respectively). This is because $T_Z^2/(T_Y \times L)$ has to be of the order of 100 or more, in order to ensure that the magnitude of the anticlastic curvature is insignificant everywhere other than near the lateral edges [29, 74]. Even though the flexure strip is assumed to be rigidly clamped at both the ends as in flexure mechanisms, which generally helps in reducing the magnitude of anticlastic curvature, significant anticlastic curvature was still found for $T_Z^2/(T_Y L) = 15$. Therefore we assume the stress σ_{ZZ} to be somewhere in between 0 and $\nu \times \sigma_{XX}$ which are the plane stress and plane strain conditions respectively and empirically propose that σ_{ZZ} is equal to $p \times \nu \times \sigma_{XX}$ where p is a function of T_Y, T_Z, L and ν (i.e. geometric, material properties and boundary conditions) but independent of displacement or load variables. Clearly as p varies from 0 to 1, the equivalent $\bar{E}$ that is used in the governing differential equations varies from elastic modulus, E (plane stress condition) to plate modulus, $E/(1-\nu^2)$ (Plane strain

condition). We will estimate $\bar{E}$ in Section 4.7 by using regression curve fitting of infinitesimal displacements of beams of various dimensions and material properties subjected to a simple bending moment about direction. By verifying that the estimation of all beam displacements (bending displacements in XY and XZ plane, axial displacement and torsional displacement) over a finite range for generalized loads can be accurately done by only changing the elastic modulus to $\bar{E}$, that is estimated using a single loading condition, we will show the validity of the assumption of σ_{ZZ} taken here.

Using the above beam geometry we next formulate the beam deformation and resulting strain in Section 4.5. The strain will then be used to derive the strain energy in the beam in Section 4.6. The strain energy is used to derive the beam characteristic differential equations using principle of virtual work for generalized loads in the same section. The validity of the beam characteristic differential equations is shown in Section 4.7 by comparing it with FEA. Finally a discussion of the contribution of this model is given in Section 4.8.

4.5 Beam Deformation and Strain

In order to determine the non-linear strain in a slender spatial beam with any general cross-section and general end-loading, the first step is to mathematically characterize its spatial deformation. The beam deformation may be completely defined in terms of five deformation components associated with each cross-sectional plane of the beam that is perpendicular to the beam centroidal axis prior to deformation: **(i)** Translation and rotation of this cross-section to remain plane and perpendicular to deformed centroidal axis, **(ii)** In-plane distortion of the cross-section, **(iii)** in-plane shape dilation of the cross-section while preserving the angles at the vertices, **(iv)** Out-of-plane warping of the cross-section, and **(v)** Translation along $\mathcal{Y}_d$ and $\mathcal{Z}_d$ axis of the deformed cross-sections from the previous state while preserving the orientation of the cross-section.

Deformation **(i)** corresponds to the Euler's assumption of plane section initially perpendicular to the neutral axis remain plane and perpendicular to the deformed neutral axis and is central to beam bending. The in-plane distortion **(ii)** is associated with torsion of the beam. St. Venant formulated the exact solution for slender beams with any general cross-section in pure torsion and demonstrated that the in-plane distortion is exactly zero for a compatible torsional load distribution at the end surface [25]. For slender prismatic beams under combined end-loads,

this deformation can be non-zero but is still negligible [36]. Therefore, contribution of this deformation to displacements is dropped where appropriate. In the absence of any loads on the lateral surfaces of the beam, the change of shape of the cross-section **(iii)** arises solely due to Poisson's effect in the $\mathcal{Y}$ and $\mathcal{Z}$ directions. Although the dilation or contraction of the sides of the cross-section is negligible, the cross-section can be curved in the $\mathcal{Y}_d\mathcal{Z}_d$ plane due to the anticlastic effect. This deformation is included in the analysis and is captured via an equivalent elastic modulus that has a value in between the actual elastic modulus and plate modulus. The out-of-plane cross-sectional warping **(iv)** is exactly zero for a circular cross-section beam under pure torsion as will be proved by symmetry arguments in Chapter 5. However it does exist in a general cross-section beam and affects the torsional constant, and is therefore included in this analysis. Deformation **(v)** is associated with shear deformation in the plane of bending and was captured by Timoshenko [25] in his exact solution of cantilever beams subjected to a transverse end force. The translation of the cross-section along the $\mathcal{Y}_d$ and $\mathcal{Z}_d$ axis is due to shear and is shown to be of the order of $(T_Y/L)^2$ and $(T_Z/L)^2$ times the displacement of the centroid of the cross-section along $\mathcal{Y}$ and $\mathcal{Z}$. Since $(T_Y/L)^2$ is of the order of 10^{-3} or smaller for the considered flexure strips, the translation along $\mathcal{Y}_d$ of deformation is negligible and ignored while the translation along $\mathcal{Z}_d$ is considered in this analysis.

An analytical expression of the deformation of a point P (X,0,0) on the neutral axis is shown, in terms of translational displacements U_X, U_Y, U_{Zb} and orientation given by the Euler angles α, β and Θ_{Xd}. The order of rotation is illustrated in Figure 4.5. It should be noted that displacement U_{Zb} along $\mathcal{Z}$ axis occurs due to bending alone and is recorded prior to shear deformation. Since shear deformation cannot change the orientation of the cross-section, it is sufficient to use U_{Zb} rather than the Z-displacement due to shear, $U_{Z\text{-}Shear}$, to express the rotations α and β in terms of the displacement variables U_X, U_Y, U_{Zb}. The deformed element, dR_n, corresponding to the undeformed fiber dX, is along X_d which is tangential to the deformed centroidal axis of the beam prior to shearing. It should be noted here that the centroid of a cross-section practically does not change relative to the cross-section after deformation. This is because in-plane distortion, dilation/contraction for the flexure strips is negligible while the curving of the beam cross-section in the $\mathcal{Y}_d\mathcal{Z}_d$ plane due to anticlastic effect is localized to a relatively small area near the lateral edges of the beam.

A coordinate transformation matrix [T] is determined by considering the differential beam element, originally along the neutral axis at P (X,0,0), in its undeformed (dX) and deformed (dR_n) configurations. A mathematical expression of [T] that relates the unit vectors $\hat{i}_d$, $\hat{j}_d$ and $\hat{k}_d$ along the deformed coordinate frame $\mathcal{X}_d$–$\mathcal{Y}_d$–$\mathcal{Z}_d$ to the unit vectors $\hat{i}$, $\hat{j}$ and $\hat{k}$ along the undeformed coordinate frame $\mathcal{X}$–$\mathcal{Y}$–$\mathcal{Z}$, is calculated in terms of the displacements U_X, U_Y, U_{Zb} and θ_{xd} below.

$$\begin{Bmatrix} \hat{i}_d \\ \hat{j}_d \\ \hat{k}_d \end{Bmatrix} = [T] \begin{Bmatrix} \hat{i} \\ \hat{j} \\ \hat{k} \end{Bmatrix} \tag{4.1}$$

$$[T] = \begin{bmatrix} \Delta_{YZ} & U_Y^+ & U_{Zb}^+ \\ -\dfrac{\mathrm{c}(\Theta_{xd})U_Y^+\Delta_{YZ}}{\Delta_Y} - \dfrac{\mathrm{s}(\Theta_{xd})U_{Zb}^+}{\Delta_Y} & \mathrm{c}(\Theta_{xd})\Delta_Y & -\dfrac{\mathrm{c}(\Theta_{xd})U_Y^+U_{Zb}^+}{\Delta_Y} + \dfrac{\mathrm{s}(\Theta_{xd})\Delta_{YZ}}{\Delta_Y} \\ \dfrac{\mathrm{s}(\Theta_{xd})U_Y^+\Delta_{YZ}}{\Delta_Y} - \dfrac{\mathrm{c}(\Theta_{xd})U_{Zb}^+}{\Delta_Y} & -\mathrm{s}(\Theta_{xd})\Delta_Y & \dfrac{\mathrm{s}(\Theta_{xd})U_Y^+U_{Zb}^+}{\Delta_Y} + \dfrac{\mathrm{c}(\Theta_{xd})\Delta_{YZ}}{\Delta_Y} \end{bmatrix}$$

where, the superscript $^+$ refers to derivative with respect to R_n,

$$\Delta_{YZ} \triangleq \sqrt{1-\left(\frac{dU_Y}{dR_n}\right)^2-\left(\frac{dU_{Zb}}{dR_n}\right)^2} \quad , \quad \Delta_Y \triangleq \sqrt{1-\left(\frac{dU_Y}{dR_n}\right)^2} \quad ,$$

and $dR_n = \sqrt{(dX + dU_X)^2 + dU_Y{}^2 + dU_{Zb}{}^2}$, $\mathrm{c}(\Theta_{xd}) \triangleq \cos(\Theta_{xd})$; $\mathrm{s}(\Theta_{xd}) \triangleq \sin(\Theta_{xd})$

Using physical insight from St. Venant solution of prismatic beams with any cross-section as well other studies of beam [36], the function $\lambda(Y,Z)\times\kappa_{Xd}$ will be used to represent the out-of-plane warping causing displacement parallel to the deformed neutral axis [75]. Here $\lambda(Y,Z)$ is a small warping function independent of coordinate X that is, in general, different from what was derived by St. Venant as there is stretching and bending in addition to torsion in this case. It should be noted that since warping would disappear if the beam was reduced to a line therefore we can say $\lambda(0,0)=0$. κ_{Xd} is the rate of torsion and is calculated by taking the derivative of the transformation matrix.

$$\frac{d[T]}{dR_n} = \begin{bmatrix} 0 & \kappa_{zd} & -\kappa_{yd} \\ -\kappa_{zd} & 0 & \kappa_{xd} \\ \kappa_{yd} & -\kappa_{xd} & 0 \end{bmatrix} [T] = [\kappa][T] \tag{4.2}$$

where,

$$\kappa_{Xd} = \frac{\Theta_{xd}^{+} \Delta_{YZ} \Delta_Y - U_{Zb}^{++} U_Y^{+} \Delta_Y - U_Y^{++} U_{Zb}^{+} \left(U_Y^{+}\right)^2}{\Delta_{YZ} \Delta_Y^{\,2}}, \quad \kappa_{Yd} = \frac{\sin\left(\Theta_{xd}\right) U_Y^{++} \Delta_{YZ} - \cos\left(\Theta_{xd}\right) U_Z^{++} - \cos\left(\Theta_{xd}\right) U_Y^{+} U_{Zb}^{+} U_Y^{++}}{\Delta_{YZ} \Delta_Y^{\,2}}$$

$$+ \frac{\cos\left(\Theta_{xd}\right) U_{Zb}^{++} \left(U_Y^{+}\right)^2}{\Delta_{YZ} \Delta_Y^{\,2}}$$

$$\kappa_{Zd} = \frac{\cos\left(\Theta_{xd}\right) U_Y^{++} \Delta_{YZ} + \sin\left(\Theta_{xd}\right) U_{Zb}^{++} + \sin\left(\Theta_{xd}\right) U_Y^{+} U_{Zb}^{+} U_Y^{++}}{\Delta_{YZ} \Delta_Y}$$

$$- \frac{\sin\left(\Theta_{xd}\right) U_{Zb}^{++} \left(U_Y^{+}\right)^2}{\Delta_{YZ} \Delta_Y}$$

It may be noted that the skew-symmetric matrix [κ] is analogous to the angular velocity matrix [ω] associated with the rigid-body rotation transformation. Upon further simplification, shown later in this section, it will become obvious that κ_{Yd} and κ_{Zd} are related to the beam curvature in the X_dY_d and X_dZ_d planes while κ_{Xd} is rate of torsion.

With the deformation field thus defined, we can now define the strains using the Green's strain measure given in (5.7).

$$d\vec{R}_d \bullet d\vec{R}_d - d\vec{R}_0 \bullet d\vec{R}_0 = 2\{dX \quad dY \quad dZ\} \begin{bmatrix} \varepsilon_{XX} & \varepsilon_{XY} & \varepsilon_{XZ} \\ \varepsilon_{YX} & \varepsilon_{YY} & \varepsilon_{YZ} \\ \varepsilon_{ZX} & \varepsilon_{ZY} & \varepsilon_{ZZ} \end{bmatrix} \begin{Bmatrix} dX \\ dY \\ dZ \end{Bmatrix} \tag{4.3}$$

The above is also sometimes referred to as finite strain or large rotation strain. Here $\vec{R}_0$ and $\vec{R}_d$ is the position vector of a general point before and after deformation. In order to relate the Green's strain measure to infinitesimal strain, let us consider the co-ordinates of the general point to be (X, Y, Z) and ($X+U$, $Y+V$, $Z+W$) before and after deformations, respectively. Here U, V and W represent displacement along the three co-ordinate axis X,Y and Z and, in general, are dependent on the all of X, Y and Z co-ordinates. Starting with a differential fiber starting at (X, Y, Z) and ending at ($X+dX$, $Y+dY$, $Z+dZ$) we find $d\vec{R}_0$ as follows.

$$d\vec{R}_0 = \begin{Bmatrix} dX \\ dY \\ dZ \end{Bmatrix} \tag{4.4}$$

After deformation, assuming the line is still straight (since it is an infinitesimal differential element), its two end points will be ($X+U$, $Y+V$, $Z+W$) and ($X + dX + U + \frac{\partial U}{\partial X} dX + \frac{\partial U}{\partial Y} dY + \frac{\partial U}{\partial Z} dZ$, $Y + dY + V + \frac{\partial V}{\partial X} dX + \frac{\partial V}{\partial Y} dY + \frac{\partial V}{\partial Z} dZ$, $Z + dZ + W + \frac{\partial W}{\partial X} dX + \frac{\partial W}{\partial Y} dY + \frac{\partial W}{\partial Z} dZ$). Using these coordinates $d\vec{R}_d$ can be written as follows.

$$d\vec{R}_d = \begin{Bmatrix} dX + \frac{\partial u}{\partial X} dX + \frac{\partial u}{\partial Y} dY + \frac{\partial u}{\partial Z} dZ \\ dY + \frac{\partial v}{\partial X} dX + \frac{\partial v}{\partial Y} dY + \frac{\partial v}{\partial Z} dZ \\ dZ + \frac{\partial w}{\partial X} dX + \frac{\partial w}{\partial Y} dY + \frac{\partial w}{\partial Z} dZ \end{Bmatrix} \tag{4.5}$$

Using Eq.(4.3), (4.4) and (4.5) the six strains can be calculated as below.

$$\varepsilon_{xx} = \frac{\left(dX + \frac{\partial U}{\partial X} dX \right)^2 + \left(\frac{\partial V}{\partial X} dX \right)^2 + \left(\frac{\partial W}{\partial X} dX \right)^2 - dX^2}{2dX^2} = \frac{\partial U}{\partial X} + \frac{1}{2}\left(\frac{\partial U}{\partial X} \right)^2 + \frac{1}{2}\left(\frac{\partial V}{\partial X} \right)^2 + \frac{1}{2}\left(\frac{\partial W}{\partial X} \right)^2$$

$$\varepsilon_{yy} = \frac{\partial V}{\partial Y} + \frac{1}{2}\left(\frac{\partial U}{\partial Y} \right)^2 + \frac{1}{2}\left(\frac{\partial V}{\partial Y} \right)^2 + \frac{1}{2}\left(\frac{\partial W}{\partial Y} \right)^2$$

$$\varepsilon_{zz} = \frac{\partial W}{\partial Z} + \frac{1}{2}\left(\frac{\partial U}{\partial Z} \right)^2 + \frac{1}{2}\left(\frac{\partial V}{\partial Z} \right)^2 + \frac{1}{2}\left(\frac{\partial W}{\partial Z} \right)^2$$

$$\varepsilon_{xy} = \varepsilon_{yx} = \frac{dX\left(1 + \frac{\partial u}{\partial X} \right)\frac{\partial u}{\partial Y} dY + dX\left(1 + \frac{\partial v}{\partial Y} \right)\frac{\partial v}{\partial X} dY + dX \frac{\partial w}{\partial X}\frac{\partial w}{\partial Y} dY}{2dXdY}$$

$$= \frac{1}{2}\left(\frac{\partial U}{\partial Y} + \frac{\partial V}{\partial X} + \frac{\partial U}{\partial X}\frac{\partial U}{\partial Y} + \frac{\partial V}{\partial X}\frac{\partial V}{\partial Y} + \frac{\partial W}{\partial X}\frac{\partial W}{\partial Y} \right)$$

$$\varepsilon_{yz} = \varepsilon_{zy} = \frac{1}{2}\left(\frac{\partial V}{\partial Z} + \frac{\partial W}{\partial Y} + \frac{\partial U}{\partial Z}\frac{\partial U}{\partial Y} + \frac{\partial V}{\partial Z}\frac{\partial V}{\partial Y} + \frac{\partial W}{\partial Z}\frac{\partial W}{\partial Y} \right)$$

$$\varepsilon_{zx} = \varepsilon_{xz} = \frac{1}{2}\left(\frac{\partial W}{\partial X} + \frac{\partial U}{\partial Z} + \frac{\partial U}{\partial X}\frac{\partial U}{\partial Z} + \frac{\partial V}{\partial X}\frac{\partial V}{\partial Z} + \frac{\partial W}{\partial X}\frac{\partial W}{\partial Z} \right) \tag{4.6}$$

It is easy to see that dropping the nonlinear terms in the strain expressions gives the well-known definition of infinitesimal strains. By retaining the nonlinear terms in the strain expression we can capture all geometric nonlinearities other than the error due to truncation in Eq.(4.5).

Direct use of the strain expressions of Eq.(4.6) is inconvenient and hence, we will use Eq. (4.3) and re-derive the expression for $d\vec{R}_d$ using the transformation matrix in (4.1). First we may write $\vec{R}_d$ as

$$\vec{R}_d = \begin{Bmatrix} \hat{i} & \hat{j} & \hat{k} \end{Bmatrix} \left[\begin{Bmatrix} X + U_X \\ U_Y \\ U_Z \end{Bmatrix} dR_n + [T]^T \begin{Bmatrix} \kappa_{xd}\lambda \\ Y_d \\ Z_d + U_{Z-Shear} \end{Bmatrix} \right] \tag{4.7}$$

It should be noted that $U_{Z\text{-}Shear}$ is assumed to be a variable of dR_n alone and is directed along $\hat{k}_d$. Also Y_d and Z_d are the dilated co-ordinates in the $\mathcal{Y}_d\mathcal{Z}_d$ plane of the point initially at (X, Y, Z) before deformation. This dilation is due to the Poisson effect. Using the expression in Eq.(4.7) $d\vec{R}_d$ can be simplified as shown in the following steps.

$$d\vec{R}_d = \begin{Bmatrix} \hat{i} & \hat{j} & \hat{k} \end{Bmatrix} \left[\begin{Bmatrix} X^+ + U_X^+ \\ U_Y^+ \\ U_{Zb}^+ \end{Bmatrix} dR_n + [T]^{T+} \begin{Bmatrix} \kappa_{xd}\lambda \\ Y_d \\ Z_d + U_{Z-Shear} \end{Bmatrix} dR_n \right.$$
$$\left. + [T]^T \begin{Bmatrix} \lambda \dfrac{d\kappa_{xd}}{dR_n} dR_n + \kappa_{xd} \dfrac{d\lambda}{dY_d} dY_d + \kappa_{xd} \dfrac{d\lambda}{dZ_d} dZ_d \\ dY_d \\ dZ_d + \dfrac{dU_{Z-Shear}}{dR_n} dR_n \end{Bmatrix} \right]$$

$$= \begin{Bmatrix} \hat{i}_d & \hat{j}_d & \hat{k}_d \end{Bmatrix} \left[[T] \begin{Bmatrix} X^+ + U_X^+ \\ U_Y^+ \\ U_{Zb}^+ \end{Bmatrix} dR_n + [T][T]^{T+} \begin{Bmatrix} \kappa_{xd}\lambda \\ Y_d \\ Z_d + U_{Z-Shear} \end{Bmatrix} dR_n \right.$$
$$\left. + [T][T]^T \begin{Bmatrix} \lambda \dfrac{d\kappa_{xd}}{dR_n} dR_n + \kappa_{xd} \dfrac{d\lambda}{dY_d} dY_d + \kappa_{xd} \dfrac{d\lambda}{dZ_d} dZ_d \\ dY_d \\ dZ_d + \dfrac{dU_{Z-Shear}}{dR_n} dR_n \end{Bmatrix} \right]$$

$$\because \quad [T][T]^T = \begin{bmatrix} 1 & 0 & 0 \\ 0 & 1 & 0 \\ 0 & 0 & 1 \end{bmatrix} \Rightarrow \left([T][T]^T\right)^+ = 0$$

$$\Rightarrow \quad [T][T]^{T+} = -\left([T]\right)^+ [T]^T = \begin{bmatrix} 0 & -\kappa_{zd} & \kappa_{yd} \\ \kappa_{zd} & 0 & -\kappa_{xd} \\ -\kappa_{yd} & \kappa_{xd} & 0 \end{bmatrix} [T]^T$$

$$\Rightarrow d\vec{R}_d = \begin{Bmatrix} \hat{i}_d & \hat{j}_d & \hat{k}_d \end{Bmatrix} \begin{bmatrix} [T] \begin{Bmatrix} X^+ + U_X^+ \\ U_Y^+ \\ U_{Zb}^+ \end{Bmatrix} dR_n + \begin{bmatrix} 0 & -\kappa_{zd} & \kappa_{yd} \\ \kappa_{zd} & 0 & -\kappa_{xd} \\ -\kappa_{yd} & \kappa_{xd} & 0 \end{bmatrix} \begin{Bmatrix} \kappa_{xd}\lambda \\ Y_d \\ Z_d + U_{Z-Shear} \end{Bmatrix} dR_n \\ + \begin{Bmatrix} \lambda \dfrac{d\kappa_{xd}}{dR_n} dR_n + \kappa_{xd} \dfrac{d\lambda}{dY_d} dY_d + \kappa_{xd} \dfrac{d\lambda}{dZ_d} dZ_d \\ dY_d \\ dZ_d + \dfrac{dU_{Z-Shear}}{dR_n} dR_n \end{Bmatrix} \end{bmatrix} \tag{4.8}$$

From the above equation, we note that $\left.\dfrac{d\vec{r}_d}{dR_n}\right|_{Y=Z=\lambda=0} = \begin{Bmatrix} \hat{i}_d & \hat{j}_d & \hat{k}_d \end{Bmatrix} [T] \begin{Bmatrix} X^+ + U_X^+ \\ U_Y^+ \\ U_{Zb}^+ \end{Bmatrix}$

However, the LHS above is also the definition of $\hat{i}_d$. This knowledge may be used to simplify Eq.(4.8), as follows:

$$\Rightarrow d\vec{R}_d = \begin{Bmatrix} \hat{i}_d & \hat{j}_d & \hat{k}_d \end{Bmatrix} \begin{bmatrix} \begin{Bmatrix} 1 \\ 0 \\ 0 \end{Bmatrix} dR_n + \begin{bmatrix} 0 & -\kappa_{zd} & \kappa_{yd} \\ \kappa_{zd} & 0 & -\kappa_{xd} \\ -\kappa_{yd} & \kappa_{xd} & 0 \end{bmatrix} \begin{Bmatrix} \kappa_{xd}\lambda \\ Y_d \\ Z_d + U_{Z-Shear} \end{Bmatrix} dR_n \\ + \begin{Bmatrix} \lambda \dfrac{d\kappa_{xd}}{dR_n} dR_n + \kappa_{xd} \dfrac{d\lambda}{dY_d} dY_d + \kappa_{xd} \dfrac{d\lambda}{dZ_d} dZ_d \\ dY_d \\ dZ_d + \dfrac{dU_{Z-Shear}}{dR_n} dR_n \end{Bmatrix} \end{bmatrix} \tag{4.9}$$

Now the definition of $d\vec{r}_d$ and $d\vec{r}_0$ from Eqs.(4.4) and (4.9) can be applied in Eq.(4.4) to obtain the strains.

$$\varepsilon_{XX} = \frac{1}{2}\left[\begin{array}{l}\left(1-Y_d\kappa_{Zd}+\left(Z_d+U_{Z-Shear}\right)\kappa_{Yd}+\lambda\dfrac{d\kappa_{Xd}}{dR_n}\right)^2+\left(\lambda\kappa_{Zd}-Z_d-U_{Z-Shear}\right)^2\kappa_{Xd}^2 \\ +\left\{\dfrac{dU_{Z-Shear}}{dR_n}+\left(-\lambda\kappa_{Yd}+Y_d\right)\kappa_{Xd}\right\}^2\end{array}\right]\left(\frac{dR_n}{dX}\right)^2-\frac{1}{2}$$

$$\varepsilon_{YY} = \frac{1}{2}\left[\left(\frac{dY_d}{dY}\right)^2-1+\left(\kappa_{Xd}\frac{d\lambda}{dY}\right)^2\right], \varepsilon_{ZZ} = \frac{1}{2}\left[\left(\frac{dZ_d}{dZ}\right)^2-1+\left(\kappa_{Xd}\frac{d\lambda}{dZ}\right)^2\right], \qquad \gamma_{YZ} = 2\varepsilon_{YZ} = \kappa_{Xd}^2\frac{d\lambda}{dY}\frac{d\lambda}{dZ}$$

$$\gamma_{XY} = 2\varepsilon_{XY} = \left[\kappa_{Xd}\frac{d\lambda}{dY}\left(1-Y_d\kappa_{Zd}+Z_d\kappa_{Yd}+\lambda\frac{d\kappa_{Xd}}{dR_n}\right)+\left(\lambda\kappa_{Xd}\kappa_{Zd}-Z_d\kappa_{Xd}\right)\frac{dY_d}{dY}\right]\frac{dR_n}{dX}$$

$$\gamma_{XZ} = 2\varepsilon_{XZ} = \left[\kappa_{Xd}\frac{d\lambda}{dZ}\left(1-Y_d\kappa_{Zd}+Z_d\kappa_{Yd}+\lambda\frac{d\kappa_{Xd}}{dR_n}\right)+\left(-\lambda\kappa_{Xd}\kappa_{Yd}+Y_d\kappa_{Xd}+\frac{dU_{Z-Shear}}{dR_n}\right)\frac{dZ_d}{dZ}\right]\frac{dR_n}{dX}$$

$$\text{where} \quad \frac{dR_n}{dX} = \sqrt{\left\{\left(1+\frac{dU_X}{dX}\right)^2+\left(\frac{dU_Y}{dX}\right)^2+\left(\frac{dU_{Zb}}{dX}\right)^2\right\}}$$

(4.10)

At this point the strains for the assumed deformation field are exact. The axial strain ε_{XX} is a metric for estimating the change in length of a fiber initially along X. The first bracket in the expression of ε_{XX} is the square of the deformed length of a fiber along the centroidal axis. Clearly as one looks at fibers away from the centroidal axis, the deformed length is also affected by bending, captured by κ_{Yd} and κ_{Zd}, torsion, captured by κ_{Xd}, and warping captured by $\lambda(Y,Z)$. The strain expressions for ε_{YY} and ε_{ZZ} capture the contraction along Y and Z axis due to the Poisson effect. However, given that the typical strain in slender metallic beam are of the order of 10^{-3}, the net difference between Y_d and Y due to ε_{YY} and ε_{ZZ} is very small.

The strain expression can be approximated to the second order based on a magnitude analysis of the displacement variables. Firstly the geometry dictates that co-ordinates Y and Y_d are of the order of $0.01L$ while Z and Z_d are of the order of $0.1L$. Secondly, in the displacement range of interest U_Y is limited to the order of $0.1L$. This implies that U_X is of the order of $0.01L$. The shear displacement $U_{Z\text{-}Shear}$, which is calculated as $\boldsymbol{F_{ZL}}L/GA$, is of the order of $10^{-4}L$ for the current beam geometry. This was calculated assuming the force $\boldsymbol{F_{ZL}}$, which is a DoC force to be one order higher that $\boldsymbol{F_{YL}}$ which is of the order of EI_{ZZ}/L^2. For the same magnitude of $\boldsymbol{F_{ZL}}$, the order of bending displacement along Z direction, U_{Zb}, which is equal to $\boldsymbol{F_{ZL}}L^3/3EI_{YY}$ in the absence of any other load, is determined to be of the order of $10^{-4}L$. Curvatures κ_{Xd} and κ_{Zd} are of

the order on 0.1/L while κ_{Yd} is of the order of 0.0001/L. The warping function λ is of the order of $T_Y T_Z$ which is of the order of $10^{-3}L^2$. The differential dY_d/dY-1 is due to the Poisson effect mainly and therefore is of the order of $v\times\varepsilon_{XX}$ which is of the order of 10^{-4}. Therefore, dR_n, dY_d and dZ_d may be equated to dX, dY and dZ, respectively, within this second order approximation.

Using the above order of magnitude analysis, the strains approximated to the second order can be written as

$$\varepsilon_{XX} \approx \frac{dU_X}{dX} + \frac{1}{2}\left(\frac{dU_Y}{dX}\right)^2 + \frac{1}{2}\left(\frac{dU_{Zb}}{dX}\right)^2 + \lambda\frac{d\kappa_{Xd}}{dX} - Y\kappa_{Zd} + Z\kappa_{Yd} + \frac{1}{2}\kappa_{Xd}^2\left(Y^2+Z^2\right)$$

$$\varepsilon_{YY} = \frac{1}{2}\left[\left(\frac{dY_d}{dY}\right)^2 - 1 + \left(\kappa_{Xd}\frac{d\lambda}{dY}\right)^2\right], \quad \varepsilon_{ZZ} = \frac{1}{2}\left[\left(\frac{dZ_d}{dZ}\right)^2 - 1 + \left(\kappa_{Xd}\frac{d\lambda}{dZ}\right)^2\right], \tag{4.11}$$

$$\gamma_{YZ} = 2\varepsilon_{YZ} = \kappa_{Xd}^2\frac{d\lambda}{dY}\frac{d\lambda}{dZ}, \quad \gamma_{XY} \approx \kappa_{Xd}\frac{d\lambda}{dY} - Z\kappa_{Xd}, \quad \gamma_{XZ} \approx \kappa_{Xd}\frac{d\lambda}{dZ} + Y\kappa_{Xd} + \frac{dU_{Z-Shear}}{dX}$$

The first three terms in the axial strain, given by Eq.(4.11), collectively represent the elastic extension in the axial direction, corrected for the kinematic effect of rotation due to bending. This captures the non-linearity associated with beam arc-length conservation. The remaining terms depend on κ_{Xd}, κ_{Yd}, κ_{Zd}, and warping function λ which arise from the combined effect of bending and torsion. The first term represents the additional axial strain due to warping of the cross-section. In Section 4.6 we find that this term finally leads to an additional torsional moment other the torsional moment due to shears γ_{XY} and γ_{XZ} that oppose the external applied twisting moment. The next two terms capture the axial strain in X due to bending in the XY and XZ planes. These effects are commonly seen in Euler beam formulations. Finally the last term captures the Wagner's effect or the trapeze effect of elastic coupling between the axial and torsional directions. The shear strain, γ_{XY}, depends only on the torsion rate κ_{Xd} and warping function λ, while shear strain, γ_{XZ} has an additional term due to shearing force $\boldsymbol{F_{ZL}}$ represented as d$U_{Z\text{-}Shear}$/dX. It should be noted that the simplified non-linear strain expressions given by Eq.(4.11) is in agreement with Hodges [61] and DaSilva [36].

The curvatures can also be approximated to the second order as

$$\begin{aligned}
\kappa_{Xd} &\approx \Theta'_{Xd} - U'_Y U''_{Zb} \approx \Theta'_{Xd} \\
\kappa_{Yd} &\approx \sin\left(\Theta_{Xd}\right)U''_Y - \cos\left(\Theta_{Xd}\right)U''_{Zb} \\
\kappa_{Zd} &\approx \cos\left(\Theta_{Xd}\right)U''_Y + \sin\left(\Theta_{Xd}\right)U''_{Zb}
\end{aligned} \tag{4.12}$$

The first equation in Eq.(4.12) shows the presence of a kinematic component of rate of torsion κ_{Xd} that depends on the bending displacements U_Y and U_{Zb}. However, as this kinematic term is of the order of 10^{-3} or 10^{-4}, it is dropped at this point. Since U_Y'' and U_Z'' are the linearized curvature of the beam in the $\mathcal{X}\mathcal{Y}$ and $\mathcal{X}\mathcal{Z}$ planes, respectively, the latter two relations in Eq.(4.12) imply that, κ_{Yd} and κ_{Zd} are representative of curvatures of the beam in the $\mathcal{X}_d\mathcal{Y}_d$ and $\mathcal{X}_d\mathcal{Z}_d$ planes, respectively, which agrees with the physical understanding of the deformed geometry. The significance of Eq.(4.12) is that while it partially linearizes the three curvature expressions, which is critical to reducing mathematical complexity and ultimately enabling closed-form results, it still captures the coupling between the torsional and bending directions. Full linearization of curvatures at this stage would lead to complete decoupling between the torsional and two bending directions, which is an over-simplification as discussed earlier.

Thus, a careful choice of deformation components, use of Green's strain measure, partial linearization of curvatures, and the second order approximation in the strain components, all help capture the relevant physical effects and non-linearities in a slender beam over an intermediate displacement range, while limiting the mathematical complexity of the strain formulation.

4.6 Non-linear Strain Energy and Beam Governing Differential Equations

In order to find the beam governing differential equations of a flexure strip, the strain energy is first determined as

$$V = \int_{vol} \left\{ \int_0^{\varepsilon_{XX}} \sigma_{XX} d\varepsilon_{XX} + \int_0^{\varepsilon_{YY}} \sigma_{YY} d\varepsilon_{YY} + \int_0^{\varepsilon_{ZZ}} \sigma_{ZZ} d\varepsilon_{ZZ} + \int_0^{\gamma_{XY}} \tau_{XY} d\gamma_{XY} + \int_0^{\gamma_{YZ}} \tau_{YZ} d\gamma_{YZ} + \int_0^{\gamma_{ZX}} \tau_{ZX} d\gamma_{ZX} \right\} d(vol) \quad (4.13)$$

Since the flexure strip is thin in the Y direction and also free from loads on the lateral surfaces, it can be reasonably assumed that $\sigma_{YY} = 0$. Additionally since the order of γ_{YZ} is 10^{-6} as compared to other strains that are of the order of 10^{-3}, τ_{YZ} is assumed to be zero as well. Finally, by the assumption made is Section 4.4 σ_{ZZ} is assumed to be $p\nu\sigma_{XX}$. Under these conditions the constitutive relations can be simplified as:

$$\varepsilon_{XX} = \frac{1 - p\nu^2}{E}\sigma_{XX}; \quad \varepsilon_{YY} = -\frac{\nu(1 + p\nu)}{E}\sigma_{XX}; \quad \varepsilon_{ZZ} = \frac{\nu(p-1)}{E}\sigma_{XX}$$
$$\varepsilon_{XY} = \frac{\tau_{XY}}{G}; \quad \varepsilon_{YZ} = 0; \quad \varepsilon_{ZX} = \frac{\tau_{ZX}}{G} \quad (4.14)$$

Using Eq.(4.14) the strain energy can be simplified to

$$V=\int_0^L\left\{\int_A\left\{\frac{\bar{E}}{2}\varepsilon_{XX}^2+\frac{G}{2}\left(\gamma_{XY}^2+\gamma_{ZX}^2\right)\right\}dA\right\}dX \quad \text{where} \quad \bar{E}=\frac{1-2p\nu^2+p^2\nu^2}{\left(1-p\nu^2\right)}E$$

Using the expressions of strain from Eq.(4.11), V can be written as

$$\begin{aligned}V=&\frac{\bar{E}}{2}\int_0^L\left\{\int_A\left\{\left(\frac{dU_X}{dX}+\frac{1}{2}\left(\frac{dU_Y}{dX}\right)^2+\frac{1}{2}\left(\frac{dU_{Zb}}{dX}\right)^2+\lambda\frac{d\kappa_{Xd}}{dR_n}-Y\kappa_{Zd}+Z\kappa_{Yd}+\frac{1}{2}\kappa_{Xd}{}^2\left(Y^2+Z^2\right)\right)^2\right\}dA\right\}dX\\&+\frac{G}{2}\int_0^L\left\{\int_A\kappa_{Xd}^2\left\{\left(Y-Y_W\right)^2+\left(Z-Z_W\right)^2\right\}dA\right\}dX+\frac{G}{2}\int_0^L\left\{\int_A 2\kappa_{Xd}\left[Y-Y_W\right]\frac{dU_{Z-Shear}}{dX}dA\right\}dX\\&+\frac{G}{2}\int_0^L\left\{\int_A\left(\frac{dU_{Z-Shear}}{dX}\right)^2dA\right\}dX\\=&I_1+I_2+I_3+I_4\end{aligned}$$

where $Y_W=-\frac{d\lambda}{dZ}$, $Z_W=\frac{d\lambda}{dY}$

The order of magnitude of I_3 is determined to be of the order of $10^{-10}L^2$ as calculated from Eq.(4.15) and is two orders smaller than I_1 and I_2.

$$o\left(I_3\right)=o\left(\int_0^L\left\{\int_A\kappa_{Xd}\left[Y+\frac{d\lambda}{dZ}\right]\frac{F_{ZL}}{A}dA\right\}\right)=o\left(\frac{1}{A}\int_0^L\kappa_{Xd}F_{ZL}\left(\int_A\frac{d\lambda}{dZ}dA\right)dX\right) \tag{4.15}$$

Although, I_3 is only one order smaller than I_4, for the sake of simplicity I_3 is dropped. By approximating I_3 equal to zero, we are physically assuming that bending or torsion has no effect on shear in the X_dZ_d plane. As a result, the displacement due to shear is approximated by the linear relation $\frac{dU_{Z-Shear}}{dX}=\frac{F_{Zd}}{kGA}$. The constant k determines how much of the area actually participates in shear and is $10\left(1+\nu\right)/\left(12+11\nu\right)$ for rectangular cross-section [25, 32].

Once the total strain energy for the spatial beam has been obtained, the Principle of Virtual Work (PVW) may be applied to generate the beam differential equations and boundary conditions. According to the PVW, the virtual work done by external forces over a set of geometrically compatible but otherwise arbitrary 'virtual' displacements is equal to the change in the strain energy due to these 'virtual' displacements:

$$\delta W=\delta V \tag{4.16}$$

The variation to the strain energy is found first as follows:

$$\delta V = \bar{E}\int_0^L \left\{ \int_A \left\{ \begin{array}{l} \left(\dfrac{dU_X}{dX} + \dfrac{1}{2}\left(\dfrac{dU_Y}{dX}\right)^2 + \dfrac{1}{2}\left(\dfrac{dU_{Zb}}{dX}\right)^2 - Y\kappa_{Zd} + Z\kappa_{Yd} + \lambda\dfrac{d\kappa_{Xd}}{dX} + \dfrac{1}{2}{\kappa_{Xd}}^2\left(Y^2+Z^2\right)\right)\times \\ \left(\dfrac{d\left(\delta U_X\right)}{dX} + \dfrac{dU_Y}{dX}\dfrac{d\left(\delta U_Y\right)}{dX} + \dfrac{dU_{Zb}}{dX}\dfrac{d\left(\delta U_{Zb}\right)}{dX} - Y\delta\kappa_{Zd} + Z\delta\kappa_{Yd} \right. \\ \left. +\lambda\delta\left(\dfrac{d\kappa_{Xd}}{dX}\right) + \left(Y^2+Z^2\right)\kappa_{Xd}\delta\kappa_{Xd} \right) \end{array} \right\} dA \right\} dX$$

$$+ G\int_0^L\int_A \left\{ \left(Y - Y_W\right)^2 + \left(Z - Z_W\right)^2 \right\} \kappa_{Xd}\delta\kappa_{Xd}\, dA dX + G\int_0^L\int_A \frac{dU_{Z-Shear}}{dX}\,\delta\left(\frac{dU_{Z-Shear}}{dX}\right) dA dX \tag{4.17}$$

The variation of strain energy can be simplified by expanding and using the symmetry of rectangular cross-section.

$$\begin{aligned} \delta V = {} & \bar{E}A\int_X \left(\frac{dU_X}{dX} + \frac{1}{2}\left(\frac{dU_Y}{dX}\right)^2 + \frac{1}{2}\left(\frac{dU_{Zb}}{dX}\right)^2 \right)\left(\frac{d\left(\delta U_X\right)}{dX} + \frac{dU_Y}{dX}\frac{d\left(\delta U_Y\right)}{dX} + \frac{dU_{Zb}}{dX}\frac{d\left(\delta U_{Zb}\right)}{dX} \right) dX \\ & + \frac{\bar{E}I_X}{2}\int_X {\kappa_{Xd}}^2 \left(\frac{d\left(\delta U_X\right)}{dX} + \frac{dU_Y}{dX}\frac{d\left(\delta U_Y\right)}{dX} + \frac{dU_{Zb}}{dX}\frac{d\left(\delta U_{Zb}\right)}{dX} \right) dX \\ & + \bar{E}I_X\int_X \left(\frac{dU_X}{dX} + \frac{1}{2}\left(\frac{dU_Y}{dX}\right)^2 + \frac{1}{2}\left(\frac{dU_{Zb}}{dX}\right)^2 \right)\kappa_{Xd}\delta\kappa_{Xd}\, dX \\ & + \bar{E}\int_X \left(I_{ZZ}\kappa_{Zd}\delta\kappa_{Zd} + I_{YY}\kappa_{Yd}\delta\kappa_{Yd} + \frac{1}{2}\kappa_{Xd}^3 I_{X^2}\delta\kappa_{Xd} + I_W\frac{d\kappa_{Xd}}{dX}\delta\left(\frac{d\kappa_{Xd}}{dX}\right) \right) dX \\ & + GJ\int_X \kappa_{Xd}\delta\kappa_{Xd}\, dX + GA\int_X \frac{dU_{Z-Shear}}{dX}\,\delta\left(\frac{dU_{Z-Shear}}{dX}\right) dX \end{aligned} \tag{4.18}$$

Due to cross-sectional symmetry (rectangular)

$$\int_A Y dA = \int_A Z dA = \int_A \lambda dA = \int_A \lambda Y dA = \int_A \lambda Z dA = \int_A YZ dA$$

$$= \int_A Y^2 Z dA = \int_A Y^3 dA = \int_A YZ^2 dA = \int_A Z^3 dA = \int_A \lambda Y^2 dA = \int_A \lambda Z^2 dA = 0,$$

also $\int_A Y^2 dA \triangleq I_{ZZ}$, $\int_A Z^2 dA \triangleq I_{YY}$, $\int_A \left(Y^2+Z^2\right) dA \triangleq I_X = I_{YY} + I_{ZZ}$,

$\int_A \left(Y^2+Z^2\right)^2 dA \triangleq I_{X^2}$, $\int_A \lambda^2 dA \triangleq I_W$

Substituting the values of curvatures from Eq.(4.12) and simplifying we get

$$\delta V = \bar{E}A\int_0^L \left\{ \begin{array}{l} \left\{ \left(\dfrac{dU_X}{dX} + \dfrac{1}{2}\left(\dfrac{dU_Y}{dX} \right)^2 + \dfrac{1}{2}\left(\dfrac{dU_{Zb}}{dX} \right)^2 \right) + \dfrac{\bar{E}I_X}{2}\Theta_{Xd}'^2 \right\} \times \\ \qquad \left(\dfrac{d\left(\delta U_X\right)}{dX} + \dfrac{dU_Y}{dX}\dfrac{d\left(\delta U_Y\right)}{dX} + \dfrac{dU_{Zb}}{dX}\dfrac{d\left(\delta U_{Zb}\right)}{dX} \right) \end{array} \right\} dX$$

$$+ \bar{E}I_X \int_0^L \int_X \left\{ \left(\frac{dU_X}{dX} + \frac{1}{2}\left(\frac{dU_Y}{dX} \right)^2 + \frac{1}{2}\left(\frac{dU_{Zb}}{dX} \right)^2 \right)\Theta_{Xd}' + \frac{1}{2}\bar{E}I_{X^2}\Theta_{Xd}'^3 + GJ\Theta_{Xd}' \right\} \delta\Theta_{Xd}' dX \qquad (4.19)$$

$$+ \bar{E}I_W \int_0^L \frac{d\kappa_{Xd}}{dX}\delta\left(\frac{d\kappa_{Xd}}{dX} \right) dX + GA\int_0^L \frac{dU_{Z-Shear}}{dX}\delta\left(\frac{dU_{Z-Shear}}{dX} \right) dX$$

$$+ \bar{E}\int_0^L \left(\begin{array}{l} \left(I_{ZZ}\kappa_{Zd}\cos\left(\Theta_{Xd}\right) + I_{YY}\kappa_{Yd}\sin\left(\Theta_{Xd}\right) \right)\left(\delta U_Y'' + U_{Zb}''\delta\Theta_{Xd} \right) \\ \qquad + \left(I_{ZZ}\kappa_{Zd}\sin\left(\Theta_{Xd}\right) - I_{YY}\kappa_{Yd}\cos\left(\Theta_{Xd}\right) \right)\left(\delta U_{Zb}'' - U_Y''\,\delta\Theta_{Xd} \right) \end{array} \right) dX$$

In order to express δV in terms of the variation of the displacements U_X, U_Y, U_Z and Θ_{Xd}, integration by part is carried out to generate the following expression.

$$\delta V = \left[V_X\delta U_X \,|_0^L + V_X U_Y'\delta U_Y \,|_0^L + V_X U_{Zb}'\delta U_{Zb} \,|_0^L \right] - \int_0^L V_X'\delta U_X dX - \int_0^L \left(V_X U_Y' \right)'\delta U_Y dX$$

$$- \int_0^L \left(V_X U_{Zb}' \right)'\delta U_{Zb} dX + T_X\delta\Theta_{Xd}\,|_0^L - \int_0^L T_X'\delta\Theta_{Xd} dX + P_X\delta\Theta_{Xd}'\,|_0^L - P_X'\delta\Theta_{Xd}\,|_0^L$$

$$+ \int_X P_X''\delta\Theta_{Xd} dX + \left(M_{Zd}\cos\left(\Theta_{Xd}\right) + M_{Yd}\sin\left(\Theta_{Xd}\right) \right)\delta U_Y'\,|_0^L$$

$$- \left(M_{Zd}\cos\left(\Theta_{Xd}\right) + M_{Yd}\sin\left(\Theta_{Xd}\right) \right)'\delta U_Y\,|_0^L + \left(M_{Zd}\sin\left(\Theta_{Xd}\right) - M_{Yd}\cos\left(\Theta_{Xd}\right) \right)\delta U_{Zb}'\,|_0^L$$

$$- \left(M_{Zd}\sin\left(\Theta_{Xd}\right) - M_{Yd}\cos\left(\Theta_{Xd}\right) \right)'\delta U_{Zb}\,|_0^L + \int_0^L \left(M_{Zd}\cos\left(\Theta_{Xd}\right) + M_{Yd}\sin\left(\Theta_{Xd}\right) \right)''\delta U_Y dX$$

$$+ \int_0^L \left(M_{Zd}\sin\left(\Theta_{Xd}\right) - M_{Yd}\cos\left(\Theta_{Xd}\right) \right)''\delta U_{Zb} dX + \int_0^L \left(M_{Zd}\cos\left(\Theta_{Xd}\right) + M_{Yd}\sin\left(\Theta_{Xd}\right) \right)U_{Zb}''\delta\Theta_{Xd} dX$$

$$- \int_0^L \left(M_{Zd}\sin\left(\Theta_{Xd}\right) - M_{Yd}\cos\left(\Theta_{Xd}\right) \right)U_Y''\delta\Theta_{Xd} dX + GA\frac{dU_{Z-Shear}}{dX}\delta U_{Z-Shear}\Big|_0^L$$

$$- \int_0^L \frac{d^2U_{Z-Shear}}{dX^2}\delta U_{Z-Shear} dX$$

Where

$$\begin{aligned}
&\bar{E}A\left(\frac{dU_X}{dX}+\frac{1}{2}\left(\frac{dU_Y}{dX}\right)^2+\frac{1}{2}\left(\frac{dU_{Zb}}{dX}\right)^2\right)+\frac{\bar{E}I_X\Theta'^2_{Xd}}{2}\triangleq V_X,\\
&\bar{E}I_X\left(\frac{dU_X}{dX}+\frac{1}{2}\left(\frac{dU_Y}{dX}\right)^2+\frac{1}{2}\left(\frac{dU_{Zb}}{dX}\right)^2\right)\Theta'_{Xd}+\frac{1}{2}\bar{E}I_{X^2}\Theta'^3_{Xd}+GJ\Theta'_{Xd}\triangleq T_X,\\
&\bar{E}I_W\Theta''_{Xd}\triangleq P_X\qquad \bar{E}I_{ZZ}\kappa_{Zd}\triangleq M_{Zd},\quad \bar{E}I_{YY}\kappa_{Yd}\triangleq M_{Yd}
\end{aligned}\tag{4.20}$$

We now proceed to express δW of Eq.(4.16) in terms of the six generalized displacement co-ordinates U_{XL}, U_{YL}, U_{ZbL}, $U_{Z-Shear-L}$, Θ_{XdL}, U'_{YL} and U'_{ZL}. Typically δW is expressed in terms of displacement that are along the direction of the loads as shown in Eq.(4.21).

$$\delta W=\boldsymbol{F_{XL}}\delta U_{XL}+\boldsymbol{F_{YL}}\delta U_{YL}+\boldsymbol{F_{ZL}}\delta U_{ZL}+\boldsymbol{M_{XL}}\delta\Theta_{XL}+\boldsymbol{M_{YL}}\delta\Theta_{YL}+\boldsymbol{M_{ZL}}\delta\Theta_{ZL}\tag{4.21}$$

In order to compare coefficients using the PVW equation, δU_{XL}, δU_{YL}, δU_{ZbL}, $\delta U_{Z-Shear-L}$, $\delta\Theta_{XdL}$, $\delta U'_{YL}$ and $\delta U'_{ZL}$ are required to be related to δU_{XL}, δU_{YL}, δU_{ZL}, $\delta\Theta_{XL}$, $\delta\Theta_{YL}$, $\delta\Theta_{ZL}$. The translational displacements of former displacement sets can be vectorially separated $\hat{i}$, $\hat{j}$ and $\hat{k}$ component to get the translational displacements of the latter displacement set.

$$\begin{aligned}
&U_{XL}\hat{i}+U_{YL}\hat{j}+U_{ZL}\hat{k}+U_{Z-Shear-L}\hat{k}_d\\
&=U_{XL}\hat{i}+U_{YL}\hat{j}+U_{ZL}\hat{k}+U_{Z-Shear-L}\left\{\begin{array}{l}\left(\dfrac{\mathrm{s}(\Theta_{XdL})U^+_{YL}\Delta_{YZ}}{\Delta_Y}-\dfrac{\mathrm{c}(\Theta_{Xd})U^+_{ZbL}}{\Delta_Y}\right)\hat{i}-\mathrm{s}(\Theta_{XdL})\Delta_Y\hat{j}\\ \qquad+\left(\dfrac{\mathrm{s}(\Theta_{XdL})U^+_{YL}U^+_{ZbL}}{\Delta_Y}+\dfrac{\mathrm{c}(\Theta_{XdL})\Delta_{YZ}}{\Delta_Y}\right)\hat{k}\end{array}\right\}\\
&\approx U_{XL}\hat{i}+U_{YL}\hat{j}+(U_{ZL}+U_{Z-Shear-L})\hat{k}
\end{aligned}\tag{4.22}$$

Relating the rotational displacements of the two displacement sets are more difficult because two of the three rotational displacements are finite rotations that cannot be represented by vectors. However the variation of the rotational displacements can be assumed to be infinitesimally small without any loss of generality. Specifically, we choose to express virtual rotations $\delta\Theta_{XL}$, $\delta\Theta_{YL}$ and $\delta\Theta_{ZL}$ as functions of δU_{XL}, δU_{YL}, δU_{ZL}, $\delta\Theta_{XdL}$, $\delta U'_{YL}$ and $\delta U'_{ZL}$. The virtual rotations at the beam end may be expressed as variations of the corresponding Euler angles (Figure 4.5):

$$\delta\Theta_{XL}\hat{i}+\delta\Theta_{YL}\hat{j}+\delta\Theta_{ZL}\hat{k} \;=\; -\delta\alpha\,\hat{j}\Big|_L+\left\{\cos(\alpha)\hat{k}-\sin(\alpha)\hat{i}\right\}\delta\beta\Big|_L + \left\{\frac{1+U'_X}{1+\bar{U}'_X}\hat{i}+\frac{U'_Y}{1+\bar{U}'_X}\hat{j}+\frac{U'_Z}{1+\bar{U}'_X}\hat{k}\right\}\delta\Theta_{Xd}\Big|_L \tag{4.23}$$

where $\delta\alpha=-\dfrac{\delta U'_Z}{1+U'_X}+\dfrac{U'_Z\delta U'_X}{\left(1+U'_X\right)^2}$ and $\delta\beta=\dfrac{\delta U'_Y}{1+U'_X+\frac{1}{2}U'^2_Z}-\dfrac{U'_Y\left(\delta U'_X+U'_Z\delta U'_Z\right)}{\left(1+U'_X+\frac{1}{2}U'^2_Z\right)^2}$

Using second order approximations, we get

$$\begin{aligned}
\delta\Theta_{XL} &\approx \delta\Theta_{XdL}-U'_{ZbL}\delta U'_{YL}+U'_{ZL}U'_{YL}\left(\delta U'_{XL}+U'_{ZbL}\delta U'_{ZbL}\right)\\
\delta\Theta_{YL} &\approx -\delta U'_{ZbL}+U'_{ZbL}\delta U'_{XL}+U'_{YL}\delta\Theta_{XdL}\\
\delta\Theta_{ZL} &\approx \delta U'_{YL}-U'_{YL}\left(\delta U'_{XL}+U'_{ZbL}\delta U'_{ZbL}\right)+U'_{ZbL}\delta\Theta_{XdL}
\end{aligned} \tag{4.24}$$

Using Eqs.(4.22) and (4.24), the left hand side of PVW in Eq. (4.16) can be expressed in terms of $\delta U_{XL},\delta U_{YL},\delta U_{ZL},\delta\Theta_{XdL},\delta U'_{XL},\delta U'_{YL}$ and $\delta U'_{ZL}$. The only remaining dependent displacement variable now is $\delta U'_{XL}$. Although its dependence on the other virtual displacements is not known at this stage, we know that it is mathematically independent of δU_{XL}. Therefore, the coefficients of δU_{XL} and δU_X on both sides of Eq. (4.16) can be respectively compared and equated.

$V_X=\boldsymbol{F_{XL}},\quad V'_X=0$

The two relations imply that

$$V_X=\bar{E}A\left(U'_X+\frac{1}{2}U'^2_Y+\frac{1}{2}U'^2_{Zb}\right)+\frac{\bar{E}I_X\Theta'^2_{Xd}}{2}=\boldsymbol{F_{XL}}\ \text{ for }\forall\ \text{X} \tag{4.25}$$

This relation may now be used to derive the geometric dependence of U'_{XL} on the other displacement variables.

$$\delta U'_{XL}+U'_{YL}\delta U'_{YL}+U'_{ZbL}\delta U'_{ZbL}=0 \tag{4.26}$$

Here, $\delta\Theta'_{XdL}$ is equal to zero since at X=L the flexure strip is connected to a rigid body. Therefore, using Eqs.(4.22), (4.24) and (4.26) δW can be expressed as

$$\delta W\approx\boldsymbol{F_{XL}}\delta U_{XL}+\boldsymbol{F_{YL}}\delta U_{YL}+\boldsymbol{F_{ZL}}\delta U_{ZbL}+\boldsymbol{F_{ZL}}\delta U_{Z-Shear-L}+\boldsymbol{M_{XdL}}\delta\Theta_{XdL}-\boldsymbol{M_{YL}}\delta U'_{ZbL}+\boldsymbol{M_{ZL}}\delta U'_{YL} \tag{4.27}$$

where $\boldsymbol{M_{XdL}}\triangleq\boldsymbol{M_{XL}}+U'_{YL}\boldsymbol{M_{YL}}+U'_{ZL}\boldsymbol{M_{ZL}}$

It should be noted that an additional moment component equal to $U'_{ZbL}\boldsymbol{M}_{\boldsymbol{XdL}}$ along the direction of $\boldsymbol{M}_{\boldsymbol{ZL}}$ is ignored because of the order of magnitude of U'_{ZbL} is 10^{-3} to 10^{-4}. This approximation is consistent with dropping the kinematic torsional rotation in Eq.(4.12).

We, next, move on to comparing the coefficients of δU_Y, δU_{Zb}, δU_{YL}, δU_{ZbL}, $\delta U'_{YL}$, and $\delta U'_{ZbL}$ terms from which we get two beam governing equations

$$\begin{aligned}
&\left(M_{Zd}\cos\left(\Theta_{Xd}\right)+M_{Yd}\sin\left(\Theta_{Xd}\right)\right)''-\left(\boldsymbol{F}_{\boldsymbol{XL}}U'_Y\right)'=0\\
&\left(M_{Zd}\sin\left(\Theta_{Xd}\right)-M_{Yd}\cos\left(\Theta_{Xd}\right)\right)''-\left(\boldsymbol{F}_{\boldsymbol{XL}}U'_{Zb}\right)'=0
\end{aligned} \tag{4.28}$$

and four natural boundary conditions.

$$\begin{aligned}
&-\left(M_{Zd}\cos\left(\Theta_{Xd}\right)+M_{Yd}\sin\left(\Theta_{Xd}\right)\right)'\Big|_{X=L}+\boldsymbol{F}_{\boldsymbol{XL}}U'_Y\big|_{X=L}=\boldsymbol{F}_{\boldsymbol{YL}}\\
&-\left(M_{Zd}\sin\left(\Theta_{Xd}\right)-M_{Yd}\cos\left(\Theta_{Xd}\right)\right)'\Big|_{X=L}+\boldsymbol{F}_{\boldsymbol{XL}}U'_{Zb}\big|_{X=L}=\boldsymbol{F}_{\boldsymbol{ZL}}\\
&\left(M_{Zd}\sin\left(\Theta_{Xd}\right)-M_{Yd}\cos\left(\Theta_{Xd}\right)\right)\Big|_{X=L}=-\boldsymbol{M}_{\boldsymbol{YL}}\\
&\left(M_{Zd}\cos\left(\Theta_{Xd}\right)+M_{Yd}\sin\left(\Theta_{Xd}\right)\right)\Big|_{X=L}=\boldsymbol{M}_{\boldsymbol{ZL}}
\end{aligned} \tag{4.29}$$

Using the values of M_{Yd} and M_{Zd} from Eq.(4.20) and recognizing the I_{YY} is at least two orders of magnitude higher than I_{ZZ}, the beam governing differential equations and natural boundary condition in Eqs.(4.28) and (4.29) can be simplified as below.

Beam governing differential equations are:

$$\begin{aligned}
&-\left(\bar{E}I_{ZZ}U''_Y+\bar{E}I_{YY}\left(\Theta_{Xd}U''_Y-U''_{Zb}\right)\Theta_{Xd}\right)''+\boldsymbol{F}_{\boldsymbol{XL}}U''_Y\approx 0\\
&\left(\bar{E}I_{YY}\left(\Theta_{Xd}U''_Y-U''_{Zb}\right)\right)''+\boldsymbol{F}_{\boldsymbol{XL}}U''_{Zb}\approx 0
\end{aligned} \tag{4.30}$$

Natural boundary conditions are:

$$\left\{-\left(\bar{E}I_{ZZ}U_Y'' + \bar{E}I_{YY}\left(\Theta_{Xd}U_Y'' - U_{Zb}''\right)\Theta_{Xd}\right)'\right\}\Big|_{X=L} + \boldsymbol{F_{XL}}U_{YL}' \approx \boldsymbol{F_{YL}}$$
$$\left\{\left(\bar{E}I_{YY}\left(\Theta_{Xd}U_Y'' - U_{Zb}''\right)\right)'\right\}\Big|_{X=L} + \boldsymbol{F_{XL}}U_{ZbL}' \approx \boldsymbol{F_{ZL}} \tag{4.31}$$
$$\left(\bar{E}I_{ZZ}U_{YL}'' + \bar{E}I_{YY}\left(\Theta_{XdL}U_{YL}'' - U_{ZbL}''\right)\Theta_{XdL}\right) \approx \boldsymbol{M_{ZL}}$$
$$\bar{E}I_{YY}\left(\Theta_{XdL}U_{YL}'' - U_{ZbL}''\right) \approx \boldsymbol{M_{YL}}$$

Finally for the torsion direction, comparing the coefficients of $\delta\Theta_{XdL}$ and $\delta\Theta_{Xd}$, we get

$$T_X - P_X'\big|_{X=L} = \boldsymbol{M_{XdL}},$$
$$T_X' - P_X'' - \left(M_{Zd}\cos\left(\Theta_{Xd}\right) + M_{Yd}\sin\left(\Theta_{Xd}\right)\right)U_{Zb}'' + \left(M_{Zd}\sin\left(\Theta_{Xd}\right) - M_{Yd}\cos\left(\Theta_{Xd}\right)\right)U_Y'' = 0 \tag{4.32}$$

In order to simplify the second relation in (4.32), the differential equations in Eq.(4.28) is integrated twice and its constants of integration are solved using boundary conditions in Eg.(4.29).

$$M_{Zd}\cos\left(\Theta_{Xd}\right) + M_{Yd}\sin\left(\Theta_{Xd}\right) = \boldsymbol{M_{ZL}} + \boldsymbol{F_{YL}}\left(L - X\right) - \boldsymbol{F_{XL}}\left(U_{YL} - U_Y\right) = \boldsymbol{M_Z}\left(X\right)$$
$$-\left(M_{Zd}\sin\left(\Theta_{Xd}\right) - M_{Yd}\cos\left(\Theta_{Xd}\right)\right) = \boldsymbol{M_{YL}} - \boldsymbol{F_{ZL}}\left(L - X\right) + \boldsymbol{F_{XL}}\left(U_{ZbL} - U_{Zb}\right) = \boldsymbol{M_Y}\left(X\right) \tag{4.33}$$

Therefore, physically $M_{Zd}\cos\left(\Theta_{Xd}\right) + M_{Yd}\sin\left(\Theta_{Xd}\right)$ and $\left(M_{Zd}\sin\left(\Theta_{Xd}\right) - M_{Yd}\cos\left(\Theta_{Xd}\right)\right)$ are nothing but the total bending moments $\boldsymbol{M_Z}(X)$ and $-\boldsymbol{M_Y}(X)$. Using the relations in Eqs.(4.20), (4.25) and (4.33), the natural boundary condition and beam governing differential equation in Eq.(4.32) can be simplified to

$$\frac{1}{2}\bar{E}\left(I_{X^2} - \frac{I_X^2}{A}\right)\Theta_{XdL}'^3 + \left(GJ + \frac{I_X}{A}\boldsymbol{F_{XL}}\right)\Theta_{XdL}' - \bar{E}I_W\Theta_{XdL}''' = \boldsymbol{M_{XdL}} \quad \ldots \quad (a)$$
$$\frac{1}{2}\bar{E}\left(I_{X^2} - \frac{I_X^2}{A}\right)\left(\Theta_{Xd}'^3\right)' + \left(GJ + \frac{I_X}{A}\boldsymbol{F_{XL}}\right)\Theta_{Xd}'' - \bar{E}I_W\Theta_{Xd}^{iv} - \boldsymbol{M_Z}\left(X\right)U_{Zb}'' - \boldsymbol{M_Y}\left(X\right)U_Y'' = 0 \quad ..(b) \tag{4.34}$$

In Eq.(4.34) (a), we notice the cubic term due to Wagner's effect, a nonlinear term that is non-zero in the presence of $\boldsymbol{F_{XL}}$ commonly referred to as the trapeze effect and a new linear term in addition to the linear term associated with shear. The new linear term is the additional internal torsional moment developed in the beam even for small twists and zero $\boldsymbol{F_{XL}}$. This term is consistent with literature on torsional-lateral buckling and was first identified by Saint Venant in his work on torsion of beams [76]. In Eq.(4.34) (b), torsional load due to bending loads appears

that couple the torsion angle to the bending displacements. As explained in Section 4.3, this term captures the torsional moment produced by bending loads in one bending plane (XY or XZ plane) in the presence of bending displacement present in the other bending plane.

Finally let us compare the co-efficients of $\delta U_{Z\text{-}Shear}$ and $\delta U_{Z\text{-}Shear\text{-}L}$.

$$GA\frac{dU_{Z-Shear}}{dX}\bigg|_{X=L} = \boldsymbol{F_{ZL}}, \qquad GA\frac{d^2U_{Z-Shear}}{dX^2} = 0 \tag{4.35}$$

Using Eq.(4.35) differential equation in the shear direction can be written as

$$GA\frac{dU_{Z-Shear}}{dX} = \boldsymbol{F_{ZL}} \quad \text{for } \forall \text{ X} \tag{4.36}$$

Equation (4.36) can be easily solve for $U_{Z\text{-}Shear\text{-}L}$ as below

$$U_{Z-Shear-L} = \frac{\boldsymbol{F_{ZL}}L}{kGA} \tag{4.37}$$

It should be noted the Timoshenko shear co-efficient k is included in Eq.(4.37) since the entire area does not take part in shearing.

The geometric boundary conditions for the flexure strip are summarized below.

$$\begin{aligned} &U_X = U_Y = U_{Zb} = U_{Z-Shear} = \Theta_{Xd} = U'_{Zb} = U'_Y = \Theta'_{Xd} = 0 \qquad \text{at} \quad X = 0 \\ &\Theta'_{Xd} = 0 \qquad \text{at} \quad X = L \end{aligned} \tag{4.38}$$

At this point in the analysis, all the loads and displacements are normalized per the following scheme to make the equations and results compact:

$$\boldsymbol{m_{z1}} \triangleq \frac{\boldsymbol{M_{ZL}}L}{\bar{E}I_{ZZ}}, \boldsymbol{m_{y1}} \triangleq \frac{\boldsymbol{M_{YL}}L}{\bar{E}I_{ZZ}}, \boldsymbol{m_{xd1}} \triangleq \frac{\boldsymbol{M_{XdL}}L}{\bar{E}I_{ZZ}}, \boldsymbol{f_{z1}} \triangleq \frac{\boldsymbol{F_{ZL}}L^2}{\bar{E}I_{ZZ}}, \boldsymbol{f_{y1}} \triangleq \frac{\boldsymbol{F_{YL}}L^2}{\bar{E}I_{ZZ}}, \boldsymbol{f_{x1}} \triangleq \frac{\boldsymbol{F_{XL}}L^2}{\bar{E}I_{ZZ}}, \boldsymbol{m_z}(x) \triangleq \frac{\boldsymbol{M_Z}(X)L}{\bar{E}I_{ZZ}}$$

$$\boldsymbol{m_y}(x) \triangleq \frac{\boldsymbol{M_Y}(X)L}{\bar{E}I_{ZZ}}, \nu \triangleq \frac{VL}{EI}, u_y \triangleq \frac{U_Y}{L}, u_z \triangleq \frac{U_Z}{L}, u_{y1} \triangleq \frac{U_{YL}}{L}, u_{z1} \triangleq \frac{U_{ZL}}{L}, x \triangleq \frac{X}{L}, \theta_{xd} \triangleq \Theta_{Xd}, \theta_{xd1} \triangleq \Theta_{XdL}$$

Using this normalization scheme, the beam governing differential equations can be restated as

$$d\left(u_x' + \frac{1}{2}u_y'^2 + \frac{1}{2}u_{zb}'^2\right) + \frac{(a+1)\theta_{xd}'^2}{2} = \boldsymbol{f_{x1}} \qquad (i)$$

$$\left(u_y'' + a\left(\theta_{Xd}u_y'' - u_{Zb}''\right)\theta_{Xd}\right)'' - \boldsymbol{f_{x1}}u_y'' \approx 0 \qquad (ii)$$

$$a\left(\theta_{Xd}u_y'' - u_{Zb}''\right)'' + \boldsymbol{f_{x1}}u_{zb}'' \approx 0 \qquad (iii) \qquad (4.39)$$

$$\frac{1}{2}c_1\left(\theta_{xd}'^3\right)' + \left(c_{21} + c_{22}\boldsymbol{f_{x1}}\right)\theta_{xd}'' - c_3\theta_{xd}^{iv} - \boldsymbol{m_z}(x)u_{zb}'' - \boldsymbol{m_y}(x)u_y'' = 0 \qquad (iv)$$

Where

$$d \triangleq \frac{AL^2}{I_{ZZ}},\ a \triangleq \frac{I_{YY}}{I_{ZZ}},\ c_1 \triangleq \left(\frac{I_{X^2}}{I_{ZZ}L^2} - \frac{I_X^2}{AI_{ZZ}L^2}\right),\ c_{21} \triangleq \frac{GJ}{\bar{E}I_{ZZ}},\ c_{22} \triangleq \frac{I_X}{AL^2},\ c_3 \triangleq \frac{I_W}{I_{ZZ}L^2}$$

Similarly the boundary condition can be restated as

$$-\left(u_y'' + a\left(\theta_{xd}u_y'' - u_{zb}''\right)\theta_{xd}\right)' + \boldsymbol{f_{x1}}u_y' = \boldsymbol{f_{y1}} \qquad (i)$$

$$\left(a\left(\theta_{xd}u_y'' - u_{zb}''\right)\right)' + \boldsymbol{f_{x1}}u_{zb}' = \boldsymbol{f_{z1}} \qquad (ii)$$

$$a\left(\theta_{xd1}u_{y1}'' - u_{zb1}''\right) = \boldsymbol{m_{y1}} \qquad (iii)$$

$$u_{y1}'' + a\left(\theta_{xd1}u_{y1}'' - u_{zb1}''\right)\theta_{xd1} = \boldsymbol{m_{z1}} \qquad (iv) \qquad (4.40)$$

$$-c_3\theta_{xd1}''' = \boldsymbol{m_{xd1}} \qquad (v)$$

At this point we observe that the beam governing differential equations are nonlinearly coupled and non-trivial to solve in a closed-form manner. Therefore, to facilitate a simple yet fairly accurate solution, we make some important observations. First for $T_Y/T_Z < 0.1$, we observe that the load-stiffening effect captured by the $\frac{\boldsymbol{f_{x1}}}{a}(u_{zb1} - u_{zb})$ term in Eq.(4.41) does not contribute significantly to displacement or stiffness estimation. Hence this term can be ignored. Using this approach, we next estimate u_{zb}'' by integrating Eq.(4.39)(iii) and using boundary conditions in Eqs.(4.40)(ii) and (iii) to determine the constants of integration.

$$u_{zb}'' = \theta_{xd}u_y'' - \frac{1}{a}\left\{\boldsymbol{m_{y1}} - \boldsymbol{f_{z1}}(1-x)\right\} \qquad (4.41)$$

Using the relation obtained from Eq.(4.41), the differential equation Eq.(4.39) (ii) can be decoupled from u_{zb} as shown below.

$$u_y'' + \boldsymbol{f_{x1}}\left(u_{y1} - u_y\right) = \boldsymbol{m_{z1}} + \boldsymbol{f_{y1}}\left(1-x\right) - \left(\boldsymbol{m_{y1}} - \boldsymbol{f_{z1}}\left(1-x\right)\right)\theta_{xd}$$
$$\Rightarrow u_y^{iv} - \boldsymbol{f_{x1}} u_y'' = -\left[\left\{\boldsymbol{m_{y1}} - \boldsymbol{f_{z1}}\left(1-x\right)\right\}\theta_{xd}\right]'' \tag{4.42}$$

In order to simplify the differential equation for torsion we restrict ourselves to flexure strips with $T_Z^2/T_Y L < 15$. In this case, the nonlinear term $\frac{1}{2}c_1\theta_{xd}'^3$ is at least two orders smaller than the linear terms for θ_{xd1} within -0.1 radians and 0.1 radians. Furthermore, since both $\boldsymbol{m_{z1}}$ and u_{z1} are one and two order smaller than $\boldsymbol{m_{y1}}$ and u_{y1} respectively, $\boldsymbol{m_z}(x)u_{zb}''$ may be dropped with respect to $\boldsymbol{m_y}(x)u_y''$ in Eq.(4.39)(iv). In order to decouple the torsion relation with displacements u_y and u_z, $\boldsymbol{m_y}(x)u_y''$ is estimated using Eq.(4.41) and (4.42) as

$$\left\{\boldsymbol{m_{y1}} - \boldsymbol{f_{z1}}\left(1-x\right)\right\}\left\{\boldsymbol{m_{z1}} + \boldsymbol{f_{y1}}\left(1-x\right) - \boldsymbol{f_{x1}}\left(u_{y1} - u_y\right) - \left(\boldsymbol{m_{y1}} - \boldsymbol{f_{z1}}\left(1-x\right)\right)\theta_{xd}\right\}$$

Therefore the torsion differential equation becomes

$$\left(c_{21} + c_{22}\boldsymbol{f_{x1}}\right)\theta_{xd}'' - c_3\theta_{xd}^{iv}$$
$$-\left\{\boldsymbol{m_{y1}} - \boldsymbol{f_{z1}}\left(1-x\right)\right\}\left\{\boldsymbol{m_{z1}} + \boldsymbol{f_{y1}}\left(1-x\right) - \boldsymbol{f_{x1}}\left(u_{y1} - u_y\right) - \left(\boldsymbol{m_{y1}} - \boldsymbol{f_{z1}}\left(1-x\right)\right)\theta_{xd}\right\} = 0 \tag{4.43}$$

Using the simplifications brought about by the geometry of the flexure strip, we now have two linearly coupled equations in (4.42) and (4.43). Using the solution of u_y and θ_{xd} equations (4.41) and (4.39)(i) can be solved.

Since the beam governing differential equations are linear equations with variable coefficients, we require more sophisticated mathematical techniques than simple linear algebra. One viable option is the use of perturbation methods in which a simple function that obeys the boundary conditions of the problem is used to find an asymptotic solution of the problem. Among various types of perturbation methods available in the literature, the homotopy perturbation method [77] was used to find an approximate solution. Unfortunately, this method led to transcendental solutions which resulted in extremely large expressions. Using Maple ™ 2011, we were unable to extract load-displacement or energy expressions from these. An alternate method is using neural networks [78] that can output approximate closed form solution of system of differential equation. However, this is a vast topic and out of scope of this thesis. Instead we proceed to validating the differential equations by comparing its numerical solution to FEA, thus proving that plates of certain geometry under certain loading condition can be

modeled accurately as beams by simply using an equivalent elastic modulus i.e. using only one independent variable rather than two.

4.7 Numerical Validation of Beam Governing Differential Equations

The entire analysis in Section 4.5 and 4.6 hinges on the assumption of the existance of a equivalent elastic modulus free of load or displacement variables as given in Section 4.4. This is because without this assumption we would be forced use two independent variable X and Y. In this section we will find and validate the appropriate equivalent elastic modulus. Finding this quantity from differential equations derived from plate theory is challenging. Therefore a simple numerical procedure was set up to estimate the equivalent elastic modulus. Using linear FEA, a small bending load was applied to a flexure strip model with plate/shell elements (SHELL181) and an identically shaped flexure strip model with beam elements (BEAM188). In the case of the flexure strip model with plate/shell elements, boundard conditions of the ends of the flexure strip being rigid and straight was taken into account. Starting with the same material properties and bending load $\boldsymbol{F_{YL}}$, the output displacement U_{YL} for either model was recorded. Next, the ratio of the output displacement of the flexure strip model with plate elements and the output displacement of flexure strip model with beam elements was recorded. This ratio was found to be constant as the applied loads was varied while keeping the beam shape the same. This means that if the product of this ratio and the elastic modulus was used in place of the actual elastic modulus in the BEAM188 FEA experiments we would the same result as the SHELL181 FEA experiments elements for all values of the $\boldsymbol{F_{YL}}$ loads. Therefore, this new elastic modulus is the equivalent elastic modulus that maybe used to simulate plate/shell like elements with beam analysis for simple bending for very small displacements. Next, by running the same experiment for various value of L, T_Y, T_Z and ν such that $T_Z^2/T_Y L < 15$ and $T_Y/T_Z < 0.1$ a regression curve fit of the second order was used to find the the equivalent elastic modulus in terms of the geometric and material properties. It should be noted that for the SHELL 181 FEA experiments, the edges on which load was applied was constrained to remain in a straight line as is the case in typical flexure mechanisms.

$$\bar{E} = \frac{E}{1-\nu^2}\left(1-\nu^2 e^{-0.454\frac{T_Z}{L}}\right) \tag{4.44}$$

In order to validity the applicability of the equivalent elastic modulus to generalized spatial loading over a finite range of displacements, we next compare the numerical solutions of the beam governing differential equations (Eqs. (4.39)(i), (4.41)-(4.43)) using the above equivalent elastic modulus and to nonlinear FEA for generalized loading in 6 mutually independent directions.

4.7.1 Linear Behavior of Spatial Flexure Strips

Since the equivalent elastic stiffness was calculated based on the comparison of U_{YL} displacement in response to $\boldsymbol{F_{YL}}$ loads using linear formulation which is very well captured in the this analysis, the displacement results of the beam governing equation is certain to match that of the finite element model of the flexure strip when $\boldsymbol{F_{YL}}$ is the only end-load present. Since, this does not guarantee the agreement of the beam governing differential equations when the flexure strip is under other bending, shearing, twisting and stretching loads, tests that can compare those loading conditions need to be carried out. In this section, we will be comparing the solution of the beam governing differential equations (Eqs. (4.39)(i), (4.41)-(4.43)) to the FEA plate model of the flexure strip due to pure bending, simple shearing and twisting separately. These effects, when studied individually, constitute the linear behavior of the flexure strip. For these tests, we have arbitrarily chosen three geometries of flexure strip that are of equal length and thickness but varying depth/width. The length and thickness are 0.1m and 0.001m, respectively, while the depth is either 0.01m or 0.025m or 0.4m. The nominal elastic modulus and Poisson's ratio are taken to be 210GPa and 0.3, respectively. It should be noted that although all the verification is done with these parameters, because of the normalized form of the differential equation, the verification is valid for all geometries when $T_Z^2/T_Y L < 15$ and $T_Y/T_Z < 0.1$. Shell 181 is used to model the flexure strip in ANSYS with element size of 0.0005m. Furthermore, geometrical nonlinearities are turned on in the FEA by using the command NLGEOM, 1. Rigid beam element MPC184 is used to prevent the ends of the flexure strips from deforming.

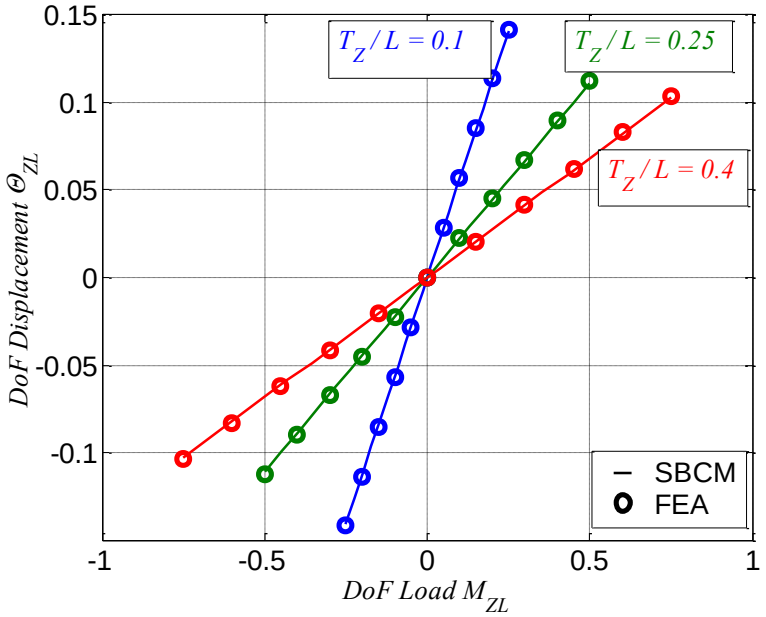

Figure 4.6: Pure Bending of Flexure Strip with varying depth

In Figure 4.6, variation of the primary bending angle Θ_{ZL} with bending moment $\boldsymbol{M_{ZL}}$ is verified. Since the bending action of $\boldsymbol{M_{ZL}}$ is very similar to $\boldsymbol{F_{YL}}$ this agreement between the differential equations and FEA is expected. However, it would be noted that while the equivalent elastic modulus was calculated for very small displacements (<L/100), the error is less that 3% of the measure quantity even for intermediate displacement of Θ_{ZL} well above 0.1 radians.

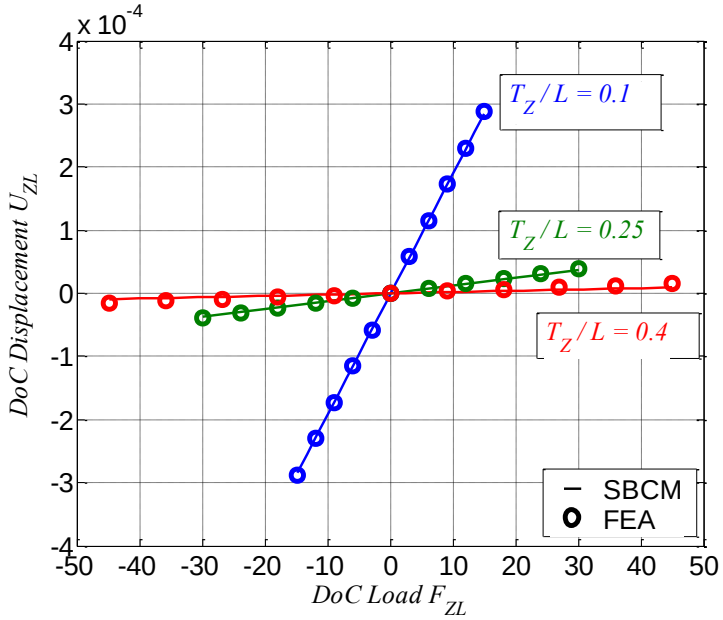

Figure 4.7: DoC displacement U_{ZL} due to shear and bending the XZ plane

While, there is excellent agreement between the differential equation and FEA in Figure 4.7 for flexure strip with T_Z/L equal to 0.1 and 0.25, the numerical solving errors affect the z-displacement of the flexure strip with T_Z/L equal to 0.4 and these errors are approximately 15%. Since the displacement of the flexure strip is very small, such errors originate from the numerical error of FEA.

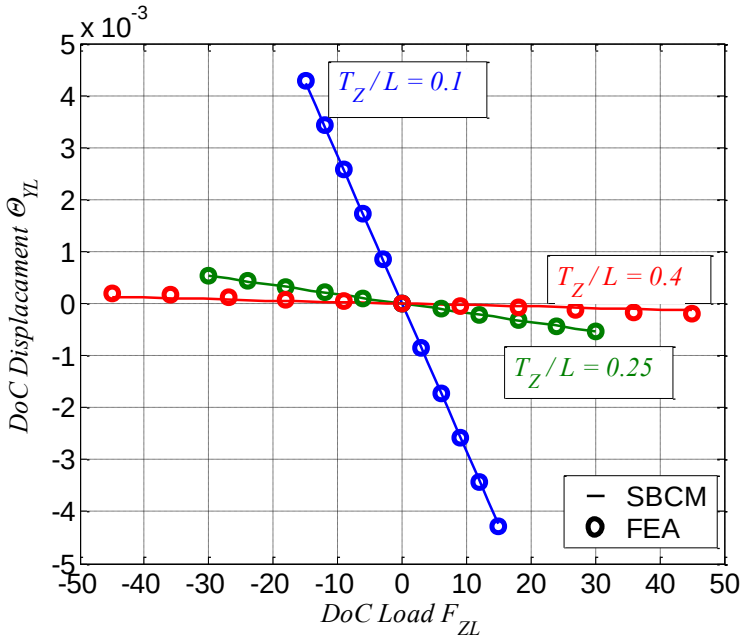

Figure 4.8: DoC Displacement Θ_{YL} due to DOC bending load F_{ZL}

Since shearing cannot create any rotations in the flexure strip, it is the bending action of the DoC load $\boldsymbol{F_{ZL}}$ give rise to the DoC displacement Θ_{YL}. Again in Figure 4.8 there is agreement within 4% between all the results from the differential equation and FEA.

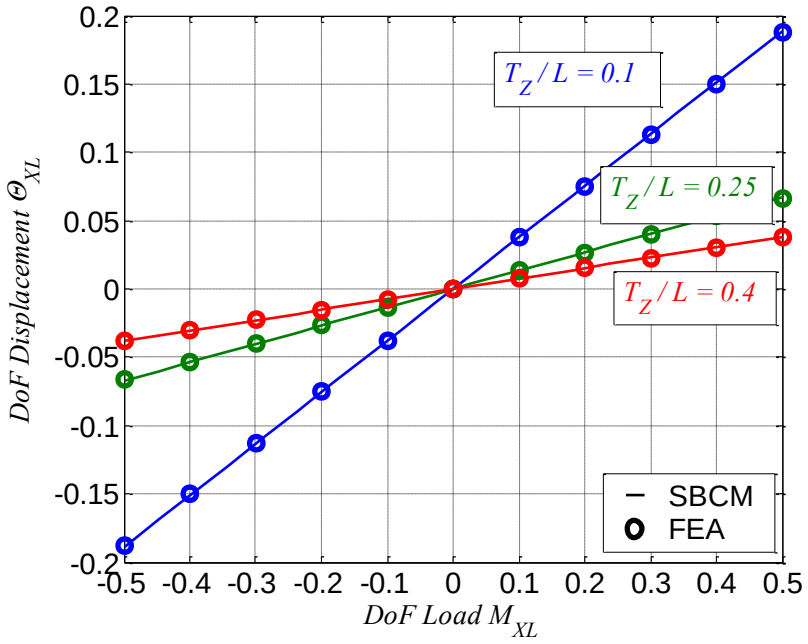

Figure 4.9: Pure twisting of the flexure strip

Finally the last of the linear deformations of the flexure strip is twisting which is verified in Figure 4.9. Although the twisting stiffness changes with width due to the variation of the torsion constant, the load-displacement in twist itself is linear for all the beam geometry. It should be note that for wider flexure strips, a cubic stiffening of the twisting direction occurs due to differential contraction of fiber close to and far away from the neutral axis. However as long as $T_Z^2/T_Y L < 15$, this nonlinearity is not significant. For flexure strip with T_Z/L = 0.4, the error is 2%.

4.7.2 Nonlinear Behavior of Spatial Flexure Strips

Several new nonlinear behaviors of spatial flexure strips are identified from the governing differential equation in addition to those that arise from $\boldsymbol{F_{XL}}$ and are seen for planar flexure strips. First of all, let us study the nonlinearities in the twisting direction. Firstly as discussed in Section 4.3, twisting can occur when loads in both XY and XZ bending planes are presented even if no twisting moment is applied. This is shown in Figure 4.10. It should be noted that the large values of the loads $\boldsymbol{F_{YL}}$ and $\boldsymbol{F_{ZL}}$ are chosen for which the displacements U_{YL} and U_{ZL} are of the order of 0.1L and 0.001L respectively.

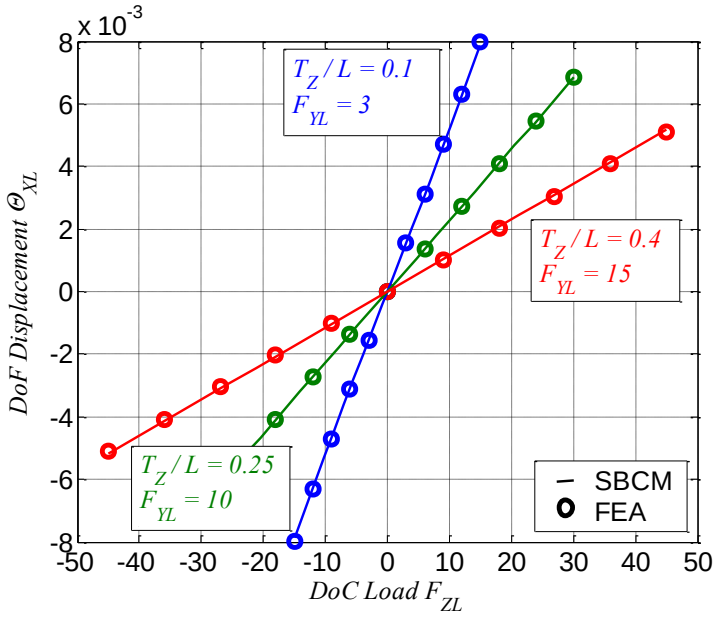

Figure 4.10: Twisting due the combination of XY and XZ plane's bending loads

The trapeze effect results in a change of twisting angle when an axial force $\boldsymbol{F_{XL}}$ is applied in the presence of a twisting moment $\boldsymbol{M_{XL}}$. As was mentioned earlier, the trapeze effect originates from fibers parallel to the centroidal axis being stretched or compressed due to torsion. Since after torsion these fibers are no longer perpendicular to the cross-sectional plane, the tensile or compressive force along these wires is not parallel to the X axis. Hence the combination of the tensile and compressive force from all the fibers produces a net resisting torque that resists the twisting moment. A more detailed explanation of the trapeze effect is given in Section 4.4. The net effect is an increase in torsional stiffness or decrease of twist at constant torsional load, either of which grows with increasing the width of the flexure strip or increasing axial force $\boldsymbol{F_{XL}}$. As shown in Figure 4.11, the twisting angle changes approximately by 5% for $T_Z/L = 0.25$.

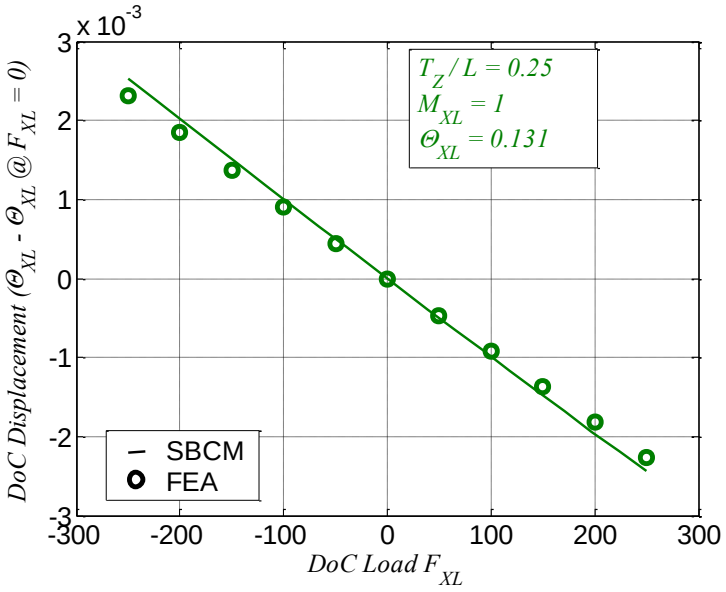

Figure 4.11: Change in twisting due to F_{XL} (Trapeze effect)

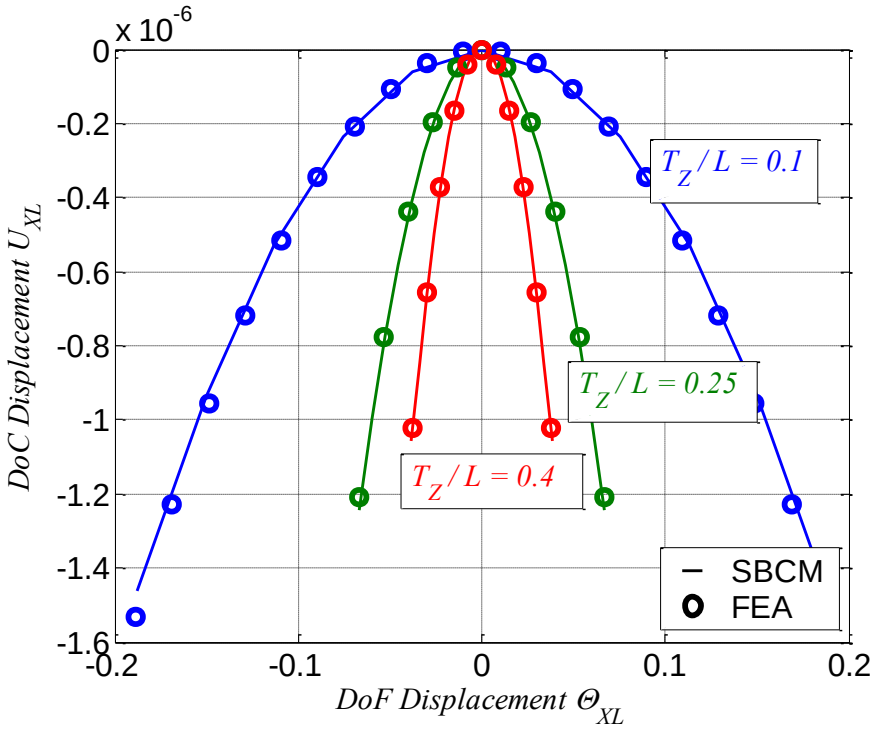

Figure 4.12: Kinematic coupling between twisting and axial extension

Twisting of the flexure strip also causes additional displacement along the axial direction. This is corollary of the trapeze effect. This is a kinematic coupling because it occurs due the arc length conservation of the individual fiber parallel to the centroidal axis. The quadratic nature of

the relationship between Θ_{XL} and U_{XL} denotes that only negative axial displacement is possible due to twisting. This is logical because as the undeformed flexure strip is straight, the arc-length conservation of the undeformed fibers along the x axis in the undeformed state can only shorten deformation.

We next move on to the effects on the XZ plane displacements due to DoF loads. In the presence of XZ bending load, if XY bending load $\boldsymbol{F_{YL}}$ is applied, then a net twist is obtained as shown in Figure 4.10. Due to this twist some of the Y- displacement is rotated towards the XZ plane. As a result additional U_{ZL} displacement is observed as shown in Figure 4.13.

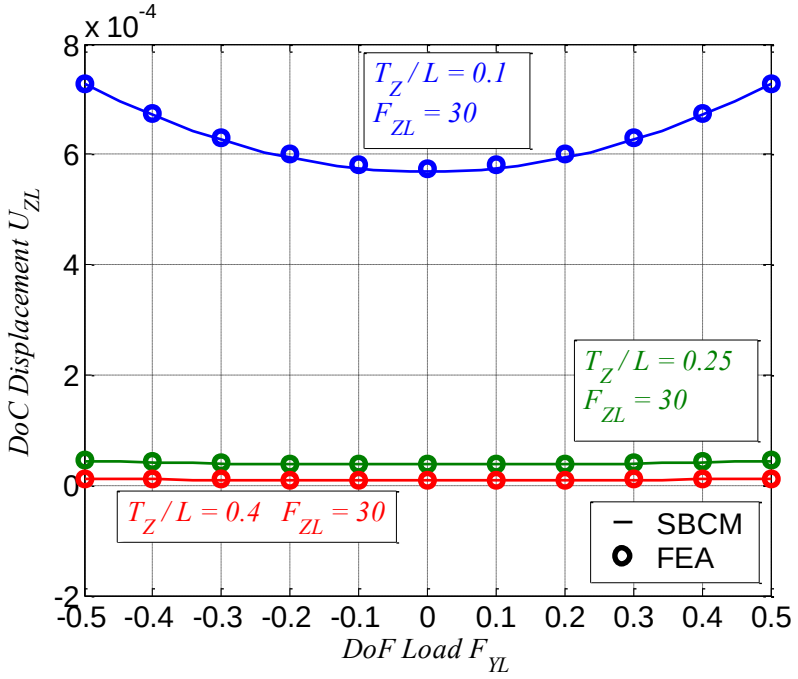

Figure 4.13: Displacement in XZ plane due to bending force in XY planes

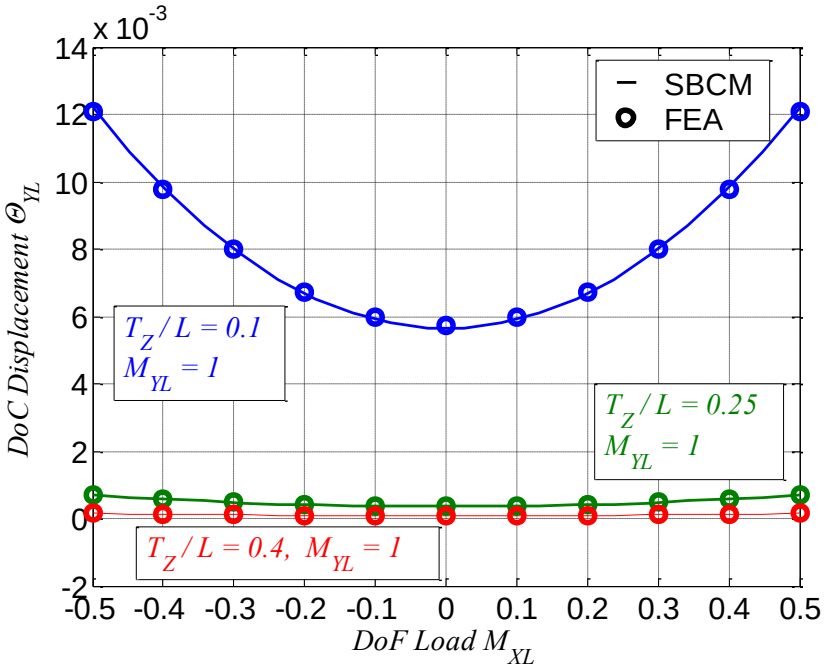

Figure 4.14: Displacement in XZ plane due to twisting moment

Instead of the twist being caused by the $\boldsymbol{F_{YL}}$, the twist can also be caused by a twisting moment $\boldsymbol{M_{XL}}$ itself. In both case, the relationship between XZ plane displacements U_{ZL} and Θ_{YL} is quadratic for T_Z/L = 0.1, 0.25 and 0.4 which implies the direction of the twisting is immaterial. In either case, the twist on the flexure strip reduces its stiffness in the XZ plane.

Although several other loading conditions including the simultaneous application of all six loads were validated again FEA results, they are not shown here since they do not represent a different type of nonlinearity. For most of the comparisons the discrepancy between the displacements predicted between SBCM and FEA was less that 3% for translational and rotational displacements of 0.1L and 0.1 radians respectively. In the case of estimating axial displacement U_{XL} the maximum discrepancy was 5% for $\boldsymbol{F_{XL}}$ five times the maximum allowed bending force $\boldsymbol{F_{YL}}$. The other DoC loads $\boldsymbol{F_{ZL}}$ and $\boldsymbol{M_{YL}}$ were also limited to five times their corresponding DoF loads. Overall, the comparison with numerical solution of the beam governing equations determines the validity of the beam equation with a certain level of confidence.

4.8 Discussion

Although a final closed form model for the spatial flexure strip could not be formulated, several important observations can be made. First of all, this chapter showed that a plate with generalized loading can be analyzed as a beam with the same generalized loading for the same displacement range as long as inequalities $T_Z^2/T_Y L < 15$ and $T_Y/T_Z < 0.1$ are satisfied. This understanding show that for a sufficiently large family of flexure strips, relatively simplified beam characteristic differential equations may be derived which preserve accuracy as well.

Secondly, the numerical solution of the derived beam characteristic differential equations brought forth several new nonlinearities due to spatial loading of a flexure strip. A more complete picture of the spatial flexure strip can be found via a closed form solution of the beam governing differential equations. Since traditional perturbation methods as well as homotopy perturbation method did not yield such a closed form solution, non-traditional approaches to solve the differential equations such as neural networks may be considered in future work.

Chapter 5

Spatial Beam Constraint Model for symmetric Spatial Beam Flexure with Generalized Loading

5.1 Introduction

A spatial beam flexure is another common flexure element used to design flexure mechanism. In the past, it has been used to make precision positioning systems [79], compliant assembly device [80], vibratory bowl feeder [81] and a minimally invasive surgical tool [68]. Additionally several MEMS devices such as micro-mirror applications [21], micro-grippers, displacement amplifier, micro-leverage systems are also known to use the spatial beam flexure. Furthermore it is extensively used in constraint based synthesis techniques based on screw theory [82] as the primary building block.

In order to study constraint properties, the spatial beam flexure is compared with a ball bearing in Figure 5.1. A ball bearing is in some sense an ideal constraint that it provides close to infinite stiffness for any vertical motion between bodies (1) and (2) and close to zero resistance, if there are no frictional losses, along the other five independent directions of motion between bodies (1) and (2). In comparison a spatial beam flexure behaves as a non-ideal constraint by providing high but not infinite stiffness in the vertical direction and low but not zero stiffness in the other five directions of relative motion between bodies (1) and (2). In spite of its non-ideal behavior, spatial beam flexures have been often modeled as constraint elements in the past [60].

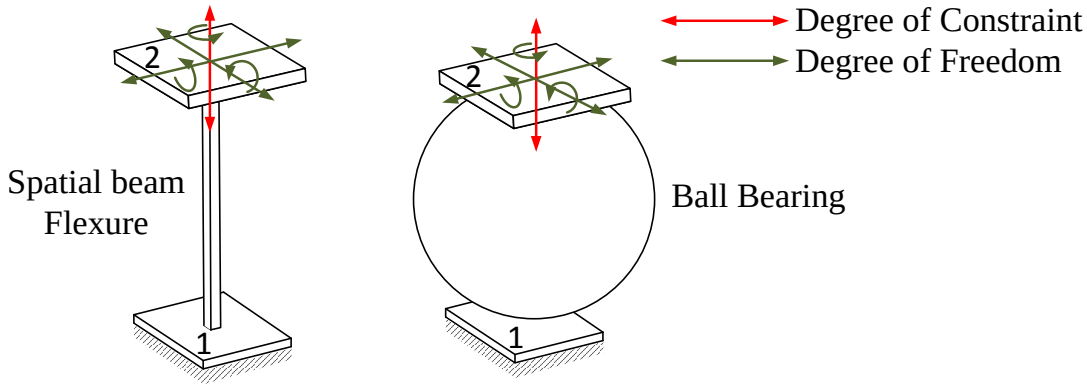

Figure 5.1: Comparison of the Degrees of Freedom and Degrees of Constraint of a Spatial Beam Flexure and a Ball Bearing

Most closed-form force displacements equations of the spatial beam flexure available in the literature are linear and valid over an infinitesimal displacement range. This is because when a finite range for translational and rotational displacements are considered, for example of $0.1L$ and 0.1 radians, respectively, four major nonlinear geometric effects become significant. These nonlinearities force the differential equations relating loads and displacements of the spatial beam in equilibrium to be nonlinear and hence are difficult to solve in closed-form. These nonlinear geometric effects are as follows:

1. The spatial beam flexure has finite stiffness values along each DoF directions that is not constant. They vary with the magnitude of an axial stretching or compressive force.
2. The relative motion of body (2) with respect to body (1) in Figure 5.1 along any of the DoF directions of spatial beam flexure is accompanied with an error motion along a DoC direction [24].
3. In the presence of a torsional moment, bending loads in any one plane, say the XY plane, causes displacements in the other bending plane, which in this case will be the XZ plane. This effect, called cross-axis coupling between the bending planes, is another type of error motion.
4. The relative motion of rigid body (2) with respect to body (1) along any of the DoF directions of spatial beam flexure also causes a drop in stiffness along the DoC direction.
5. Torsional rotation of rigid body (2) with respect to body (1) causes a small contraction in the length of the spatial beam flexure.

These effects, which collectively represent the non-ideal constraint behavior of a spatial beam flexure, in terms of stiffness values and error motion, need to be quantified in order to

understand performance limitations and tradeoffs as well as generate physical insight and enable design optimization on the elemental as well as on the mechanism level. In the absence of a convenient closed form model that is applicable of the mentioned finite displacement value, designers generally use numerical methods such FEA software to analyze flexure models that involve spatial beam flexures. Given the merits of closed form analysis, discussed in Chapter 1, we aim to formulate a closed form model in this chapter.

Previous analysis of slender prismatic spatial beam with arbitrary cross-section [61] show that beam governing bending equations for bending, stretching and torsion are in general nonlinear and coupled. However, in the special case when the beam cross-section is symmetric such that its two primary moment of area are equal, the bending equations become linear with respect to bending loads and displacements. Although, the twisting and stretching loads terms that are present in the bending differential equations, represent geometric nonlinearities, one may treat these two loads as constants in a mathematical sense while solving the bending differential equations. Using the displacement solution in the bending direction, the nonlinear twisting and stretching differential equations may be solved. A detailed derivation of the assumptions, beam governing differential equations, displacement solution and the constraint model is given in sections 5.2 to 5.5.

5.2 Spatial Beam Deformation

In order to determine the nonlinear strain as well as the end-displacements U_{XL}, U_{YL}, U_{ZL}, Θ_{XL}, Θ_{YL}, and Θ_{ZL}, the deformation at each point interior to the spatial beam, shown in Figure 5.2, needs to be mathematically characterized.

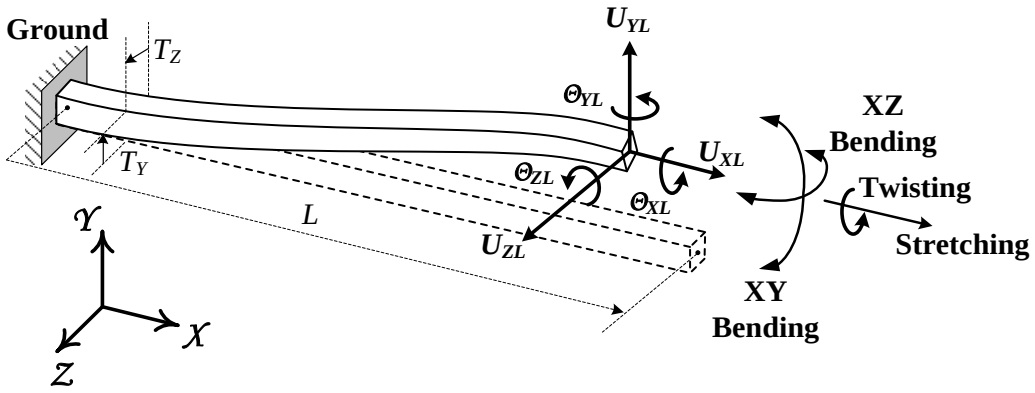

Figure 5.2: Spatial Beam Flexure: Undeformed and Deformed

When a long, slender[12], circular cross-section beam is subjected to pure torsion, symmetry implies that the Euler-Bernoulli assumptions hold true [29], i.e. plane sections remain plane and perpendicular to the neutral axis after deformation. For a physical argument, we study a slender circular beam in Figure 5.3 that is subjected to pure torsion. Given that the beam is slender, any cross-section away from either end should experience the same warping. Let us assume the warped cross-section to an arbitrary shape as shown in Figure 5.3. If the beam is rotated about the Y axis or the Z axis by 180^o the warped cross-section gets flipped about the Y or Z axis. However as the loading after the rotation remains identical, any cross-section away from the ends in a long beam should have the same warping along X before and after rotation. For this condition to be true, the out-of-plane component of warping along X has to symmetrical about the Y axis as well as the Z axis. The only possible solution of the out-of-plane warping along X that satisfies this condition is zero over the entire YZ plane. To eliminate in-plane cross-sectional distortion we consider any amount of rotation about X-axis and again find that the loading is same in each case and hence conclude that in plane cross-sectional distortion should also be zero as well. Furthermore this symmetry argument also implies in-plane dilation, due to non-zero Poisson's ratio, should be rotationally symmetric about the X-axis. Therefore, we can safely say that the neutral axis after deformation is the same as the centroidal axis. A similar argument based on symmetry considerations can be made for pure bending to show that plane section that are not near the ends of the beam, remain plane and perpendicular to the centroidal axis after deformation.

[12] Slender generally implies a length to thickness ratio greater than 20 [24, 35]

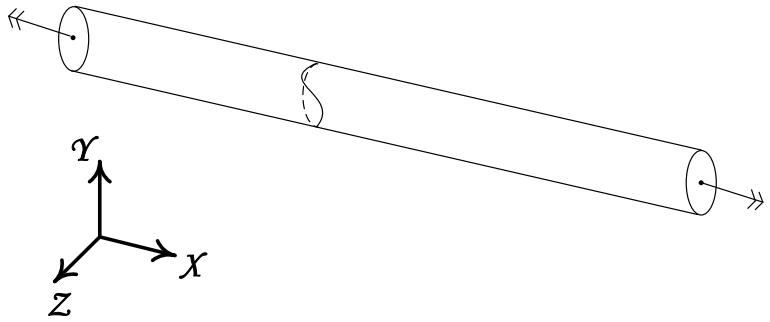

Figure 5.3: A beam under pure torsion

Using the deformation characteristics of any cross-sectional plane perpendicular to the centroidal axis, the shear at any point on a cross-section of a beam in the YZ plane under pure torsion can be calculated as follows.

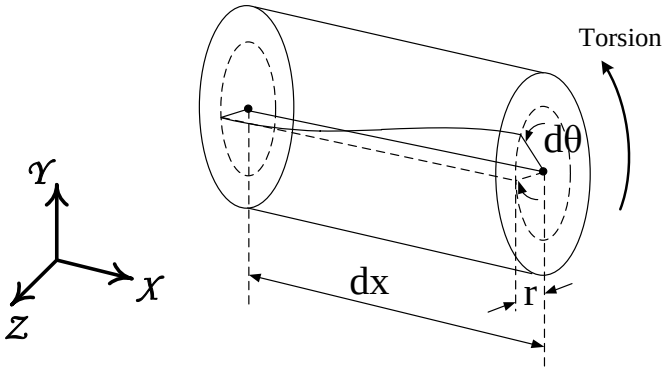

Figure 5.4: Shear due to torsion in beam with circular cross-section

Using Figure 5.4, the shear at a general point on a cross-section at an arbitrary location x is.

$$\gamma_{x\theta} = \tan^{-1}\left(r\frac{d\theta}{dx} \right) \approx r\frac{d\theta}{dx} \tag{5.1}$$

The approximation in Eq.(5.1) assumes deformation/strains to very small (at most of the order of 10^{-3}) with respect to unity. Using Hooke's constitutive relations the shear stress is calculated as:

$$\tau_{X\theta} = Gr\frac{d\theta}{dx} \tag{5.2}$$

Since there is no in-plane distortion the quantity $d\theta/dx$ should be constant throughout the cross-section. Therefore for moment balance the following equation should be satisfied.

$$T = \int_A Gr^2 \frac{d\theta}{dx} dA = G\frac{d\theta}{dx}\int_A r^2 dA = GI_X \frac{d\theta}{dx} \qquad \text{where } I_X = \text{ polar moment of area} \qquad (5.3)$$

Given that the torsional moment as well as the shear modulus is constant throughout the beam, the shear strain at any point can be restated as in Eq.(5.4) which says that under the assumption of isotropic material, plane sections remaining plane, undistorted and perpendicular to neutral axis and small strains, the shear component $\tau_{x\theta}$ can be derived to be proportional to the radial distance from the neutral axis.

$$\gamma_{X\theta} = r\frac{T}{GI_X} \qquad (5.4)$$

Eq.(5.4) further implies that shear stress $\tau_{X\theta}$ are maximum as the outer most boundary. Equilibrium of forces and moments on a differential element at the boundary dictates the presence of $\tau_{\theta X}$ as well. This is shown in Figure 5.5 (A). These shear stresses do not violate the boundary condition as the lateral (or exterior) surface remains free of any external stresses.

However, for pure torsion of long, slender rectangular cross-section beams, the maximum shear stress is not necessarily along the boundary as a similar argument cannot be made in this case. A physical reasoning can be understood from Figure 5.5 (B).

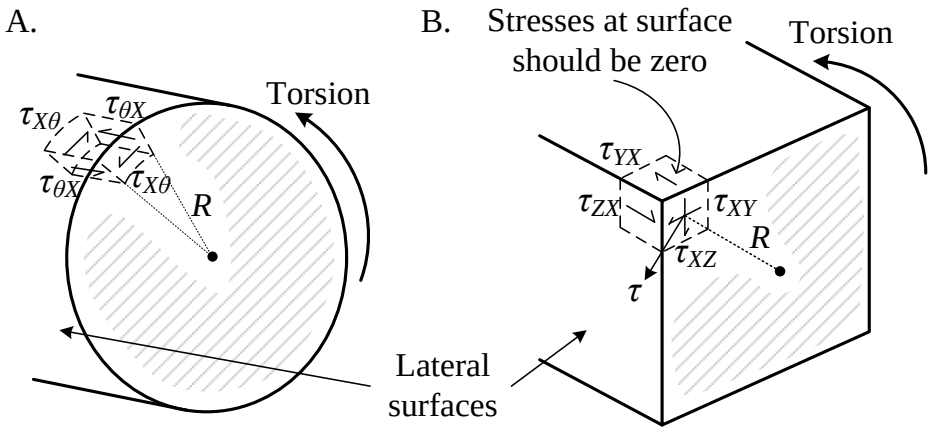

Figure 5.5: Spatial Beam with circular and rectangular cross-section under torsion

If the shear stress at any point on a cross-section was proportional to its distance from the neutral axis then a finite shear stress τ will exist at the differential boundary element of the beam perpendicular to the radial line from the neutral axis as shown in Figure 5.5. This shear strain τ can be resolved into its component τ_{XZ} and τ_{XZ}. This would mean, for equilibrium, non-zero τ_{YX} and τ_{ZX} will exist on lateral surfaces. This is in violation of the boundary condition that the lateral

surfaces are free of forces and therefore by contradiction we conclude that shear stresses are not proportional to their radial distance from the neutral axis. This, in turn, implies that plane sections do not remain plane after torsion for beams with rectangular cross-sections and non-circular cross-sections in general. This was shown experimentally by A. Duleau by 1820 [83] that small warping of cross-section does take place in order to satisfy boundary conditions for shearing stresses. The first exact solution of prismatic beam with any general cross-section under pure torsion was first formulated by St. Venant in 1850 [25]. He showed that the warping redistributes the shear stress such that the maximum shear stress is located at the middle of the lateral edges of the cross-section, while zero shear stress is present at the corners.

Given that all the above observations about deformation of a beam were made when the beam is undergoing bending or torsion separately, the same observations will not strictly hold when a beam undergoes bending, stretching and torsion simultaneously. In spite of this, for displacement (U_Y and U_Z) in the range of $0.1L$[13], where L is the length of the spatial beam, and rotations (Θ_X, Θ_Y, and Θ_Z) in the range of 0.1 radians[14], several previous articles [36, 61] use the above assumptions of zero in-plane distortion and constant warping along X, in order to study the static and dynamic behavior of slender prismatic beams. It should be noted that out-of-plane warping and in-plane dilation are not ignored as that would violate boundary conditions and geometric compatibility conditions respectively. This assumption is appropriate when length is at least an order of magnitude higher than thickness and width of the beam. This is because the difference between the slope of local tangent at any point on a cross-section and the average slope of the cross-section of the order of (thickness×width)/(length^2) for the given range of displacements. This estimation can be easily developed from the exact beam solutions given in references [25, 74].

By ignoring in-plane distortion, this approach implicitly implies that the displacements corresponding to extensional strains due to bending and warping effects arising from torsion are algebraically added when both are expressed in a non-physical co-ordinate frame X_d-Y_d-Z_d defined below (Figure 5.6). This is because displacements of any point on a cross-section due by bending and out-of-plane warping occur along the same direction X_d. Therefore one may algebraically add deformations due to bending and torsion alone to obtain the combined effect of

[13] ±10% of the length of the beams is used as intermediate range for translational end-displacement of the beam
[14] ±0.1 radians is used as intermediate range for rotational end-displacement of the beam

both in a beam. A proof of this method leading to the correct estimates of deformation would require rigorous experimentation. In spite of the unavailability of such experiments in literature the above assumption is quite common [4, 36, 61, 65, 84-86] and is known to lead to useful expressions for design and analysis of beams.

Now we process to explicitly derive the strain at any point based on the preceding discussion. First, a reference X-Y-Z co-ordinate frame is defined such that its X axis is along the centroidal axis (locus of the centroid of all cross-sections) of the undeformed prismatic beam, while its Y and Z axis represent the primary directions of cross-sectional moment of area. Using the ideal case of circular cross-section, very long beam, small strains, pure bending or torsion, plane sections remain plane and perpendicular to the centroidal axis even after deformation, we define the co-ordinate frame X_d-Y_d-Z_d as the transformed X-Y-Z co-ordinate frame resulting from rigid body translations and rotations (Euler angles) of a cross-section of the beam undergoing deformation with the X-Y-Z axis stuck to its centroid. It should be noted that the third rigid body rotation which will occur about the X_d axis is what we define as the angle of twist. This is not a unique definition of twist because for any change of orientation in space 24 different sets of Euler angles can be found to relation in the initial and final orientation.

As discussed earlier, although in finitely long beams undergoing finite bending and torsion, plane section doesn't exactly remain plane, undistorted and perpendicular to the centroidal axis, these variations from ideal behavior are small when the end-displacement is restricted to intermediate values.

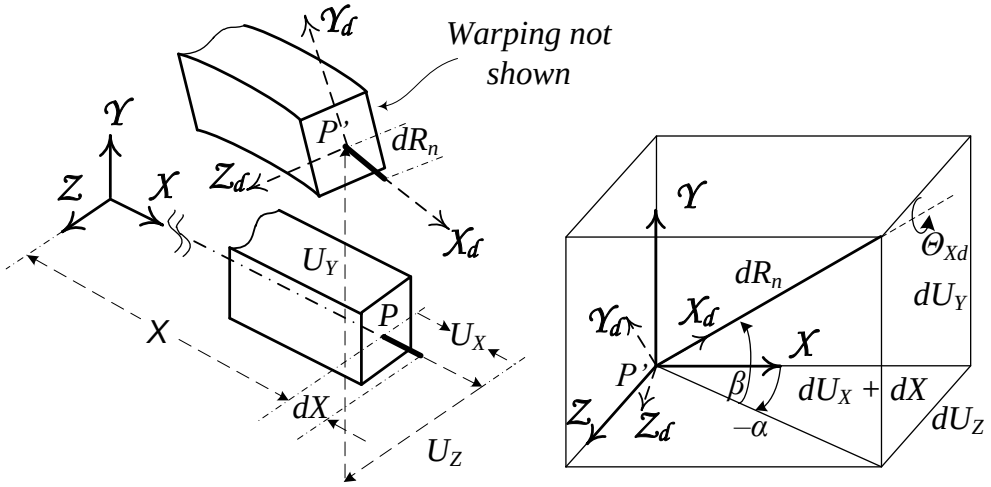

Figure 5.6: Spatial Kinematics of Beam Deformation

Similar to the analysis of the deformation of the flexure strip in Chapter 4, deformation of a differential fiber of a slender beam at point *P* (X,0,0) on the neutral axis is shown, in terms of translational displacements U_X, U_Y, U_Z and orientation given by the Euler angles α, β and Θ_{Xd}. The order of rotation is illustrated in Figure 5.6. However it should be noted that there is no significant shear effects in this case. The deformed element, dR_n, corresponding to the undeformed fiber dX, is along X_d which is tangential to the deformed centroidal axis of the beam. For small strains the deformed centroidal axis also turns out to be approximately the deformed neutral axis. This is because in plane distortion, dilation/contraction is negligible for slender beams.

Similar to Chapter 4, the coordinate transformation matrix [*T*] is determined by considering the differential beam element, originally along the neutral axis at P (*X*,*0*,*0*), in its undeformed (*dX*) and deformed (dR_n) configurations. A mathematical expression of [*T*] that relates the unit vectors $\hat{i}_d$, $\hat{j}_d$ and $\hat{k}_d$ along the deformed coordinate frame X_d–Y_d–Z_d to the unit vectors $\hat{i}$, $\hat{j}$ and $\hat{k}$ along the undeformed coordinate frame X–Y–Z, is calculated in terms of the three Euler angles -α, β and θ_{xd} below.

$$\begin{Bmatrix} \hat{i}_d \\ \hat{j}_d \\ \hat{k}_d \end{Bmatrix} = [T] \begin{Bmatrix} \hat{i} \\ \hat{j} \\ \hat{k} \end{Bmatrix} \tag{5.5}$$

$$[T]=\begin{bmatrix} \Delta_{YZ} & U_Y^+ & U_Z^+ \\ -\dfrac{c(\Theta_{xd})U_Y^+\Delta_{YZ}}{\Delta_Y}-\dfrac{s(\Theta_{xd})U_Z^+}{\Delta_Y} & c(\Theta_{xd})\Delta_Y & -\dfrac{c(\Theta_{xd})U_Y^+U_Z^+}{\Delta_Y}+\dfrac{s(\Theta_{xd})\Delta_{YZ}}{\Delta_Y} \\ \dfrac{s(\Theta_{xd})U_Y^+\Delta_{YZ}}{\Delta_Y}-\dfrac{c(\Theta_{xd})U_Z^+}{\Delta_Y} & -s(\Theta_{xd})\Delta_Y & \dfrac{s(\Theta_{xd})U_Y^+U_Z^+}{\Delta_Y}+\dfrac{c(\Theta_{xd})\Delta_{YZ}}{\Delta_Y} \end{bmatrix}$$

where, the superscript $^+$ refers to derivative with respect to R_n,

$\Delta_{YZ} \triangleq \sqrt{1-\left(\dfrac{dU_Y}{dR_n}\right)^2-\left(\dfrac{dU_Z}{dR_n}\right)^2}$, $\Delta_Y \triangleq \sqrt{1-\left(\dfrac{dU_Y}{dR_n}\right)^2}$,

and $dR_n = \sqrt{(dX + dU_X)^2 + dU_Y{}^2 + dU_Z{}^2}$, $c(\Theta_{xd}) \triangleq \cos(\Theta_{xd})$; $s(\Theta_{xd}) \triangleq \sin(\Theta_{xd})$

Since we would finally want to state the final load-displacement results for the spatial beam in the undeformed coordinate frame, it is desirable to express the [*T*] matrix in term of variables defined in the undeformed coordinate frame XYZ.

Similarly the beam curvatures in the X_dY_d and X_dZ_d planes, κ_{Yd} and κ_{Zd}, and the rate of torsion, κ_{Xd}, can be defined by studying the its rate of change of the transformation matrix [*T*] with R_n.

$$\frac{d[T]}{dR_n}=\begin{bmatrix} 0 & \kappa_{zd} & -\kappa_{yd} \\ -\kappa_{zd} & 0 & \kappa_{xd} \\ \kappa_{yd} & -\kappa_{xd} & 0 \end{bmatrix}[T]=[\kappa][T] \tag{5.6}$$

where,

$$\kappa_{Xd}=\frac{\Theta_{xd}^+\Delta_{YZ}\Delta_Y-U_Z^{++}U_Y^+\Delta_Y-U_Y^{++}U_Z^+\left(U_Y^+\right)^2}{\Delta_{YZ}\Delta_Y{}^2},\ \kappa_{Yd}=\frac{\sin(\Theta_{xd})U_Y^{++}\Delta_{YZ}-\cos(\Theta_{xd})U_Z^{++}-\cos(\Theta_{xd})U_Y^+U_Z^+U_Y^{++}}{\Delta_{YZ}\Delta_Y{}^2}$$
$$+\frac{\cos(\Theta_{xd})U_Z^{++}\left(U_Y^+\right)^2}{\Delta_{YZ}\Delta_Y{}^2}$$

$$\kappa_{Zd}=\frac{\cos(\Theta_{xd})U_Y^{++}\Delta_{YZ}+\sin(\Theta_{xd})U_Z^{++}+\sin(\Theta_{xd})U_Y^+U_Z^+U_Y^{++}}{\Delta_{YZ}\Delta_Y}$$
$$-\frac{\sin(\Theta_{xd})U_Z^{++}\left(U_Y^+\right)^2}{\Delta_{YZ}\Delta_Y}$$

Furthermore, using the physical insight from St. Venant solution of prismatic beams with any cross-section as well other studies of beam, the function $\lambda(Y,Z)\kappa_{Xd}$ will also be used to

represent the out-of-plane warping causing displacement parallel to the deformed neutral axis [75]. It should be noted that $\lambda(Y,Z)$ which is generally of the order of the cross-sectional area is small for slender beams compared to its value for flexure strips.

With the deformation field thus defined, we can now define the strains using the Green's Strain measure given in (5.7).

$$d\vec{r}_d \bullet d\vec{r}_d - d\vec{r}_0 \bullet d\vec{r}_0 = 2\{dX \quad dY \quad dZ\}\begin{bmatrix}\varepsilon_{XX} & \varepsilon_{XY} & \varepsilon_{XZ}\\ \varepsilon_{YX} & \varepsilon_{YY} & \varepsilon_{YZ}\\ \varepsilon_{ZX} & \varepsilon_{ZY} & \varepsilon_{ZZ}\end{bmatrix}\begin{Bmatrix}dX\\ dY\\ dZ\end{Bmatrix} \tag{5.7}$$

Using a similar analysis to Chapter 4, $d\vec{r}_d$ and $d\vec{r}_0$ can be calculated and applied in Eq.(5.7) to obtain the strains.

$$\varepsilon_{XX} = \frac{1}{2}\left\{\left(1+\frac{dU_X}{dX}\right)^2+\left(\frac{dU_Y}{dX}\right)^2+\left(\frac{dU_Z}{dX}\right)^2\right\}\left[\begin{array}{l}\left(1-Y_d\kappa_{Zd}+Z_d\kappa_{Yd}+\lambda\dfrac{d\kappa_{Xd}}{dR_n}\right)^2\\ +\left\{\left(\lambda\kappa_{Zd}-Z_d\right)^2+\left(-\lambda\kappa_{Yd}+Y_d\right)^2\right\}\kappa_{Xd}^2\end{array}\right]-\frac{1}{2}$$

$$\varepsilon_{YY} = \frac{1}{2}\left[\left(\frac{dY_d}{dY}\right)^2-1+\left(\kappa_{Xd}\frac{d\lambda}{dY}\right)^2\right], \varepsilon_{ZZ} = \frac{1}{2}\left[\left(\frac{dZ_d}{dZ}\right)^2-1+\left(\kappa_{Xd}\frac{d\lambda}{dZ}\right)^2\right], \quad \gamma_{YZ} = \kappa_{Xd}^2\frac{d\lambda}{dY}\frac{d\lambda}{dZ} \tag{5.8}$$

$$\gamma_{XY} = 2\varepsilon_{XY} = \kappa_{Xd}\frac{d\lambda}{dY}\left(1-Y_d\kappa_{Zd}+Z_d\kappa_{Yd}+\lambda\frac{d\kappa_{Xd}}{dR_n}\right)+\left(\lambda\kappa_{Xd}\kappa_{Zd}-Z_d\kappa_{Xd}\right)$$

$$\gamma_{XZ} = 2\varepsilon_{XZ} = \kappa_{Xd}\frac{d\lambda}{dZ}\left(1-Y_d\kappa_{Zd}+Z_d\kappa_{Yd}+\lambda\frac{d\kappa_{Xd}}{dR_n}\right)+\left(-\lambda\kappa_{Xd}\kappa_{Yd}+Y_d\kappa_{Xd}\right)$$

The only difference between the strain expressions given here, in Eq.(5.8) and the strain expressions given in Eq.(4.10), is the displacement in the Z_d direction. At this point the strains for the assumed deformation field are exact. For a qualitative understanding of the various terms in the strain expression the reader is referred to section 4.2 in Chapter 4.

For intermediate displacements, which means U_{XL}/L, U_{YL}/L, U_{ZL}/L, Θ_{XL}, Θ_{YL}, and Θ_{ZL} is limited to ±0.1, we can determine that the slopes and curvatures are limited to 0.1 and 0.1/L respectively. Under these assumptions, a simplified strain expression can be determined by approximated the strains in (5.8) to the second order. It is expected that the error due to this approximation will be less than 1% with the specified displacement range.

$$
\begin{aligned}
&\varepsilon_{XX} \approx U_X' + \frac{1}{2}U_Y'^2 + \frac{1}{2}U_Z'^2 - Y\kappa_{Zd} + Z\kappa_{Yd} + \frac{1}{2}\kappa_{Xd}{}^2\left(Y^2 + Z^2\right)\\
&\gamma_{XY} \approx \kappa_{Xd}\left[Y - Y_W\right] \qquad \text{where } Y_W \triangleq \frac{d\lambda}{dZ}\\
&\gamma_{XZ} \approx \kappa_{Xd}\left[Z - Z_W\right] \qquad \text{where } Z_W \triangleq \frac{d\lambda}{dY}\\
&\varepsilon_{YY} \approx -\nu\varepsilon_{XX}, \quad \varepsilon_{ZZ} \approx -\nu\varepsilon_{XX}, \quad \gamma_{YZ} \approx 0
\end{aligned}
\tag{5.9}
$$

It should be noted here that although finite end displacements are considered, the strains are still small because the beam is assumed to be slender. The first three terms in the axial strain, ε_{XX}, collectively represent the elastic stretching in the axial direction, while correcting for kinematic effects. The next three terms depend on the beam curvatures κ_{Xd}, κ_{Yd} and κ_{Zd}, which are defined in the deformed coordinate axis X_d–Y_d–Z_d. These terms arise from the combined effect of torsion and bending and depend only on X. Although the last of these three terms is significantly smaller than the other terms, it is retained because it becomes significant in the absence of axial stretching and bending loads. The approximate value of the three beam curvatures, accurate to the second order are given below.

$$
\begin{aligned}
&\kappa_{Xd} \approx \Theta_{Xd}' - U_Z'' U_Y'\\
&\kappa_{Yd} \approx \sin\left(\Theta_{Xd}\right)U_Y'' - \cos\left(\Theta_{Xd}\right)U_Z'\\
&\kappa_{Zd} \approx \cos\left(\Theta_{Xd}\right)U_Y'' + \sin\left(\Theta_{Xd}\right)U_Z''
\end{aligned}
\tag{5.10}
$$

The shear strains given in Eq.(5.9) depend on curvature κ_{Xd} and warping. However, since the warping is captured by $\lambda(Y,Z)\kappa_{Xd}$ where $\lambda(Y,Z)$ does not depend on loading, its effect can be represented using the correction terms Y_W and Z_W. Strains ε_{YY} and ε_{ZZ} caused due to Poisson's effect are small and are included in this discussion. However they do not affect strain energy as σ_{YY} and σ_{ZZ} are approximately zero and thus does not affect the calculation of the end-displacements. Other nonlinear terms in strain expressions reported in the previous literature [36, 61, 65] are at most of the order of 10^{-5} and contribute negligibly to the strains, which are generally of the order of 10^{-2} for the given maximum loading conditions. Therefore, these nonlinear terms have been dropped in Eq.(5.9). It should be noted here that infinitesimal strain theory does not capture the nonlinearities in the curvatures κ_{Xd}, κ_{Yd} and κ_{Xd} in Eq.(5.10), the kinematic correction terms $\frac{1}{2}U_Y'^2 + \frac{1}{2}U_Z'^2$, the $\kappa_{Xd}{}^2$ term in ε_{XX}, or warping effect in the shear strains γ_{XY} and γ_{XZ}. Since infinitesimal theory does not capture these multiple important physical

effects that are critical for constraint characterization of spatial beams, it proves to be inadequate in our modeling effort.

5.3 Non-linear Strain Energy and Beam Governing Differential Equations

As the first step in deriving the beam governing equation using energy methods, the strain energy for the spatial beam flexure is expressed below by assuming linear material properties.

$$V = \frac{E}{2}\int_{vol} \varepsilon_{xx}^2 dAdX + \frac{G}{2}\int_{vol} \left(\gamma_{xy}^2 + \gamma_{xz}^2\right) dAdX \tag{5.11}$$

Due to the slenderness of the beam, the variation of stresses σ_{YY} and σ_{ZZ} is close to zero. However, since there are no externally applied stresses on the lateral surfaces of the beam, σ_{YY} and σ_{ZZ} remain zero throughout the beam. Therefore, the ε_{YY} and ε_{ZZ} strain components do not contribute to the strain energy.

There are two components of the strain energy: the first integral above is the strain energy due to axial strain that arises from transverse bending and axial extension, and the second term represents the energy due to the shear strains that arise due to torsion. This strain energy expression may be expanded using the strain expressions from Eq.(5.9).

$$\begin{aligned} V = {} & \frac{E}{2}\int_{vol}\left(U_X' + \frac{1}{2}U_Y'^2 + \frac{1}{2}U_Z'^2\right)^2 dAdX + \frac{E}{2}\int_{vol} 2\left(U_X' + \frac{1}{2}U_Y'^2 + \frac{1}{2}U_Z'^2\right)\left(-Y\kappa_{Zd} + Z\kappa_{Yd}\right) dAdX \\ & + \frac{E}{2}\int_{vol}\left\{\kappa_{Xd}{}^2\left(Y^2 + Z^2\right)\right\}\left(-Y\kappa_{Zd} + Z\kappa_{Yd}\right) dAdX + \frac{E}{2}\int_{v}\left(-Y\kappa_{Zd} + Z\kappa_{Yd}\right)^2 dAdX \\ & + \frac{E}{2}\int_{vol}\left(U_X' + \frac{1}{2}U_Y'^2 + \frac{1}{2}U_Z'^2\right)\left[\kappa_{Xd}{}^2\left(Y^2 + Z^2\right)\right] dAdX + \frac{E}{8}\int_{vol}\left\{\kappa_{Xd}{}^2\left(Y^2 + Z^2\right)\right\}^2 dAdX \\ & + \frac{G}{2}\int_{vol}\kappa_{Xd}{}^2\left\{\left(Y - Y_W\right)^2 + \left(Z - Z_W\right)^2\right\} dAdX \\ \triangleq {} & I_1 + I_2 + I_3 + I_4 + I_5 + I_6 + I_7 \end{aligned} \tag{5.12}$$

The seven individual integrals in V are denoted by I_1 through I_7, in the order that they are listed. Of these, the integrals I_2 and I_3 are identically zero by the definition of the centroidal axis. For a slender beam with twisting angle Θ_{Xd} limited to ±0.1, it may be shown that integral I_6 is at least four orders of magnitude smaller than integral I_1, and is therefore dropped. Next, the strain energy expression is simplified by recognizing that the beam curvatures, given in Eq.(5.10), are

only dependent on the axial coordinate X. Thus, each volume integral can be decomposed into a double integral over the cross-section and a single integral over X.

$$V = \frac{EA}{2}\int_0^L \left(\bar{U}'_X\right)^2 dX \;+\; \frac{EI}{2}\int_0^L \left(U''^2_Y + U''^2_Z\right) dX \;+\; EI\int_0^L \left(\bar{U}'_X\right)\kappa^2_{Xd} dX \;+\; \frac{GJ}{2}\int_0^L \kappa^2_{Xd} dX$$
$$\text{where} \quad \bar{U}'_X \triangleq \left(U'_X + \frac{1}{2}U'^2_Y + \frac{1}{2}U'^2_Z\right) \tag{5.13}$$

The first integral I_1 above describes energy associated with axial extension. Through U_Y' and U_Z', it also captures the geometric coupling between the bending and axial directions. The second term, I_4, captures the strain energy associated with bending. The third term, I_5, captures the coupling between the torsion and axial extension directions. Finally, the last term I_7 captures the energy solely from torsion. In the last step of deriving Eq.(5.13), a symmetric beam cross-section is assumed, which implies that the two principal bending moments of area (I_{YY} and I_{ZZ}) are identical and equal to I. Due to this symmetry, the polar moment of area is equal to $2I$. The torsion constant J is, in general, different from the polar moment of area due to warping [25], as shown below.

$$\int_A Y^2 dA = \int_A Z^2 dA \triangleq I \quad ; \quad \int_A YZ dA = 0$$
$$\int_A \left(Y^2 + Z^2\right) dA = 2I \quad ; \quad \int_A \left\{\left(Y - Y_W\right)^2 + \left(Z - Z_W\right)^2\right\} dA \triangleq J \tag{5.14}$$

Once the total strain energy for the spatial beam has been obtained, the Principle of Virtual Work (PVW) [20] may be applied to generate the beam differential equations and boundary conditions. According to the PVW, the virtual work done by external forces over a set of geometrically compatible but otherwise arbitrary 'virtual' displacements is equal to the change in the strain energy due to these 'virtual' displacements:

$$\delta W = \delta V \tag{5.15}$$

U_X, U_Y, U_Z, Θ_{Xd}, U'_Y and U'_Z may be chosen as the six generalized coordinates which, along with their boundary conditions, completely define the deformation and strain energy of the beam. The variation of the beam strain energy expression (5.13) with respect to these generalized coordinates is given by:

$$\delta V = \delta I_1 + \delta I_4 + \delta I_5 + I_7 \tag{5.16}$$

where,

$$\delta I_1 = EA\left\{\bar{U}'_X\left(\delta U_X + U'_Y\,\delta U_Y + U'_Z\,\delta U_Z\right)\right\}\Big|_0^L - EA\int_0^L \bar{U}''_X\,\delta U_X\,dX - EA\int_0^L\left(\bar{U}'_X U'_Y\right)'\delta U_Y\,dX$$
$$- EA\int_0^L\left(\bar{U}'_X U'_Z\right)'\delta U_Z\,dX$$

$$\delta I_4 = EI\left(U''_Y\delta U'_Y + U''_Z\delta U'_Z - U'''_Y\delta U_Y - U'''_Z\delta U_Z\right)\Big|_0^L + EI\int_0^L\left(U^{iv}_Y\delta U_Y + U^{iv}_Z\delta U_Z\right)dX$$

$$\delta I_5 = EI\left\{\kappa^2_{Xd}\left(\delta U_X + U'_Y\,\delta U_Y + U'_Z\,\delta U_Z\right)\right\}\Big|_0^L - EI\int_0^L\left(\kappa^2_{Xd}\right)'\delta U_X\,dX - EI\int_0^L\left(\kappa^2_{Xd}U'_Y\right)'\delta U_Y\,dX$$
$$- EI\int_0^L\left(\kappa^2_{Xd}U'_Z\right)'\delta U_Z\,dX + 2EI\left[\bar{U}'_X\kappa_{Xd}\delta\Theta_{Xd} - \bar{U}'_X\kappa_{Xd}\left(U'_Y\,\delta U'_Z + U''_Z\,\delta U_Y\right) + \left(\bar{U}'_X\kappa_{Xd}U'_Y\right)'\delta U_Z\right]_0^L$$
$$- 2EI\left[\int_0^L\left\{\left(\bar{U}'_X\kappa_{Xd}U'_Y\right)''\delta U_Z - \left(\bar{U}'_X\kappa_{Xd}U''_Z\right)'\delta U_Y\right\}dX\right] - 2EI\int_0^L\left\{\kappa_{Xd}\bar{U}'_X\right\}'\delta\Theta_{Xd}\,dX$$

$$\delta I_7 = GJ\left[\left\{\kappa_{Xd}\delta\Theta_{Xd} - \kappa_{Xd}\left(U'_Y\,\delta U'_Z + U''_Z\,\delta U_Y\right) + \left(\kappa_{Xd}U'_Y\right)'\delta U_Z\right\}\right]_0^L$$
$$- GJ\left[\int_0^L\left\{\left(\kappa_{Xd}U'_Y\right)''\delta U_Z - \left(\kappa_{Xd}U''_Z\right)'\delta U_Y\right\}dX\right] - GJ\int_0^L\kappa'_{Xd}\delta\Theta_{Xd}\,dX$$

This variation of the strain energy is expressed in terms of the six generalized virtual displacements δU_X, δU_Y, δU_Z, $\delta\Theta_{Xd}$, $\delta U'_Y$ and $\delta U'_Z$, all variables in the X coordinate, and their boundary values at the fixed and free ends of the beam.

At the fixed end, i.e., X = *0*

$$\delta U_X = 0;\ \delta U_Y = 0;\ \delta U_Z = 0;\ \delta\Theta_{Xd} = 0;\ \delta\Theta_Y = 0;\ \delta\Theta_Z = 0 \tag{5.17}$$

At the free end i.e. X = *L*

$$\delta U_X = \delta U_{XL};\ \delta U_Y = \delta U_{YL};\ \delta U_Z = \delta U_{ZL};\ \ \delta\Theta_{Xd} = \delta\Theta_{XdL};\ \delta\Theta_Y = \delta\Theta_{YL};\ \delta\Theta_Z = \delta\Theta_{ZL} \tag{5.18}$$

Next, the virtual work done by external loads $\boldsymbol{F_{XL}}$, $\boldsymbol{F_{YL}}$, $\boldsymbol{F_{ZL}}$, $\boldsymbol{M_{XL}}$, $\boldsymbol{M_{YL}}$ and $\boldsymbol{M_{ZL}}$ may be expressed as:

$$\delta W = \boldsymbol{F_{XL}}\delta U_{XL} + \boldsymbol{F_{YL}}\delta U_{YL} + \boldsymbol{F_{ZL}}\delta U_{ZL} + \boldsymbol{M_{XL}}\delta\Theta_{XL} + \boldsymbol{M_{YL}}\delta\Theta_{YL} + \boldsymbol{M_{ZL}}\delta\Theta_{ZL} \tag{5.19}$$

where δU_{XL}, δU_{YL}, δU_{ZL}, $\delta\Theta_{XL}$, $\delta\Theta_{YL}$ and $\delta\Theta_{ZL}$ represent a slightly different set of six independent virtual displacements at the beam end in the respective directions of the six external loads. These six virtual end-displacements have to be expressed in terms of the previous set of

six virtual end-displacements that are used in the variation of the strain energy in Eq.(5.16) so that coefficients of the same virtual end-displacements on both sides of Eq. (5.15) may be equated. Specifically, this requires expressing virtual rotations $\delta\Theta_{XL}$, $\delta\Theta_{YL}$ and $\delta\Theta_{ZL}$ as functions of δU_{XL}, δU_{YL}, δU_{ZL}, $\delta\Theta_{XdL}$, $\delta U'_{YL}$ and $\delta U'_{ZL}$. Since virtual rotations can be chosen to be arbitrarily small, they can be represented as vectors. Therefore, the virtual rotations at the beam end may be expressed as variations of the corresponding Euler angles (Fig.2):

$$\begin{aligned}\delta\Theta_{XL}\hat{i}+\delta\Theta_{YL}\hat{j}+\delta\Theta_{ZL}\hat{k} \;=\; & -\delta\alpha\,\hat{j}\Big|_L+\left\{\cos(\alpha)\hat{k}-\sin(\alpha)\hat{i}\right\}\delta\beta\Big|_L \\ & +\left\{\frac{1+U'_X}{1+\bar{U}'_X}\hat{i}+\frac{U'_Y}{1+\bar{U}'_X}\hat{j}+\frac{U'_Z}{1+\bar{U}'_X}\hat{k}\right\}\delta\Theta_{Xd}\Big|_L\end{aligned} \tag{5.20}$$

where $\delta\alpha=-\dfrac{\delta U'_Z}{1+U'_X}+\dfrac{U'_Z\delta U'_X}{\left(1+U'_X\right)^2}$ and $\delta\beta=\dfrac{\delta U'_Y}{1+U'_X+\frac{1}{2}U'^2_Z}-\dfrac{U'_Y\left(\delta U'_X+U'_Z\delta U'_Z\right)}{\left(1+U'_X+\frac{1}{2}U'^2_Z\right)^2}$

For the range of end displacements considered, $\bar{U}'_{XL}$, U'_{XL}, U'_{YL}, and U'_{ZL} are of the order of 10^{-3}, 10^{-2}, 10^{-1} and 10^{-1}, respectively. Therefore, second order approximations are made to simplify Eq.(5.20) to yield:

$$\begin{aligned}\delta\Theta_{XL} &\approx \delta\Theta_{XdL}-U'_{ZL}\delta U'_{YL}+U'_{ZL}U'_{YL}\left(\delta U'_{XL}+U'_{ZL}\delta U'_{ZL}\right)\\ \delta\Theta_{YL} &\approx -\delta U'_{ZL}+U'_{ZL}\delta U'_{XL}+U'_{YL}\delta\Theta_{XdL}\\ \delta\Theta_{ZL} &\approx \delta U'_{YL}-U'_{YL}\left(\delta U'_{XL}+U'_{ZL}\delta U'_{ZL}\right)+U'_{ZL}\delta\Theta_{XdL}\end{aligned} \tag{5.21}$$

Using Eq.(5.21), the left hand side of PVW in Eq. (5.15) can be expressed in terms of $\delta U_{XL}, \delta U_{YL}, \delta U_{ZL}, \delta\Theta_{XdL}, \delta U'_{XL}, \delta U'_{YL}$ and $\delta U'_{ZL}$. The only remaining dependent displacement variable now is $\delta U'_{XL}$. Although its dependence on the other virtual displacements is not known at this stage, we know that it is mathematically independent of δU_{XL}. Therefore, the coefficients of δU_{XL} and δU_X on both sides of Eq. (5.15) can be respectively compared and equated.

$$\left(EA\bar{U}'_X+EI\kappa^2_{Xd}\right)\Big|_L=\boldsymbol{F_{XL}},\ \text{and}\ \ \left(EA\bar{U}'_X+EI\kappa^2_{Xd}\right)'=0$$

These two relations imply that

$$EA\bar{U}'_X+EI\kappa^2_{Xd}=\text{constant}=\boldsymbol{F_{XL}} \tag{5.22}$$

This relation may now be used to derive the geometric dependence of U'_{XL} on the other displacement variables. Since $\frac{\partial \sigma_{YY}}{\partial Y}$ and $\frac{\partial \sigma_{YZ}}{\partial Z}$ are approximately zero due to the absence of lateral forces and in-plane distortion, respectively, $\frac{\partial \tau_{XY}}{\partial X}$ turns out to be zero from the elemental equilibrium condition in the Y direction:

$$\frac{\partial \tau_{YX}}{\partial X}+\frac{\partial \sigma_{YY}}{\partial Y}+\frac{\partial \sigma_{YZ}}{\partial Z}=0 \;\Rightarrow\; \frac{\partial \tau_{YX}}{\partial X}=0 \tag{5.23}$$

This result, along with Eq.(5.9), implies that κ_{Xd} remains constant with X. This, along with Eq.(5.22), implies that $\bar{U}'_X$ remains constant with X. This knowledge, along with the definition of $\bar{U}'_X$ in Eq.(5.13), yields the following relation:

$$\delta U'_X = -U'_Y \delta U'_Y - U'_Z \delta U'_Z \tag{5.24}$$

The value of $\delta U'_{XL}$ is now substituted back in Eq.(5.21), which reduces to:

$$\begin{aligned}
\delta\Theta_{XL} &= \delta\Theta_{XdL} - U'_{ZL}\delta U'_{YL} \\
\delta\Theta_{YL} &= -\delta U'_{ZL} - U'_{YL}U'_{ZL}\delta U'_{YL} + U'_{YL}\delta\Theta_{XdL} \\
\delta\Theta_{ZL} &= \delta U'_{YL} + U'_{ZL}\delta\Theta_{XdL}
\end{aligned} \tag{5.25}$$

This allows one to express all the terms on the right and left hand sides of Eq. (5.15) using the same set of six virtual end-displacements. Now, the respective coefficients of all the virtual displacements on both sides of this equation are compared and equated.

Comparing the coefficients of $\delta\Theta_{XdL}$ and $\delta\Theta_{Xd}$, we get

$$\left\{GJ\left(1+\frac{2EI}{GJ}\bar{U}'_X\right)\kappa_{Xd}\right\}\Big|_L = \boldsymbol{M_{XdL}} \text{ and } \quad \left\{\left(1+\frac{2EI}{GJ}\bar{U}'_X\right)\kappa_{Xd}\right\}' = 0$$

where $\boldsymbol{M_{XdL}} \triangleq \boldsymbol{M_{XL}} + U'_{YL}\boldsymbol{M_{YL}} + U'_{ZL}\boldsymbol{M_{ZL}}$

$$\Rightarrow \kappa_{Xd} = \left\{\Theta'_{Xd} - U''_Z\, U'_Y\right\} = \text{constant} = \frac{\boldsymbol{M_{XdL}}}{GJ}\left(1+\frac{2EI}{GJ}\bar{U}'_X\right)^{-1} \tag{5.26}$$

Since U'_{YL} and U'_{ZL} are equal to Θ_{ZL} and $-\Theta_{YL}$ respectively, $\boldsymbol{M_{XdL}}$ is simply the equivalent torsional moment expressed along the deformed centroidal axis at the free end of the beam. Equations (5.22) and (5.26) can now be solved simultaneously for $\bar{U}'_X$ and Θ_{Xd}. Since

these two quantities are of the order of 10^{-2} and 10^{-1}, respectively, second order approximations are made in arriving at the following two simplified relations.

$$U'_{XL} + \frac{1}{2}U'^{2}_{YL} + \frac{1}{2}U'^{2}_{ZL} \approx \frac{\boldsymbol{F_{XL}}}{EA} - \frac{I}{A}\cdot\frac{\boldsymbol{M^{2}_{XdL}}}{G^{2}J^{2}} \tag{5.27}$$

$$\Theta'_{Xd} - U''_{Z}\,U'_{Y} \approx \frac{\boldsymbol{M_{XdL}}}{GJ} - \frac{2I\boldsymbol{M_{XdL}F_{XL}}}{G^{2}J^{2}A} \tag{5.28}$$

Equations (5.27) and (5.28) are the governing differential equations associated with extension and torsion, respectively. Eq. (5.27) clearly captures beam arc-length conservation, which leads geometric coupling between the axial and two bending directions. Additionally, it also captures the weak coupling between axial and torsional directions, also known as the trapeze effect [59]. This coupling is also evident in the torsion Eq.(5.28), which additionally captures the geometric dependence of twisting angle on the two bending displacements.

Equating the coefficients of the remaining virtual displacements, δU_{YL}, δU_{Y}, δU_{ZL}, δU_{Z}, $\delta U'_{YL}$, and $\delta U'_{ZL}$, two more governing differential equations associated with bending in the XY and XZ planes are obtained, along with four natural boundary conditions at the beam end.

$$EIU^{iv}_{Y} - \boldsymbol{F_{XL}}U''_{Y} + \boldsymbol{M_{XdL}}U'''_{Z} = 0; \qquad EIU^{iv}_{Z} - \boldsymbol{F_{XL}}U''_{Z} - \boldsymbol{M_{XdL}}U'''_{Y} = 0 \tag{5.29}$$

$$\begin{aligned}
&\boldsymbol{F_{YL}} = \boldsymbol{F_{XL}}U'_{YL} - EIU'''_{YL} - \boldsymbol{M_{XdL}}U''_{ZL}\\
&\boldsymbol{F_{ZL}} = \boldsymbol{F_{XL}}U'_{ZL} - EIU'''_{ZL} + \boldsymbol{M_{XdL}}U''_{YL}\\
&\boldsymbol{M_{YL}} = -EIU''_{ZL} + \boldsymbol{M_{XdL}}U'_{YL}\\
&\left(1+U'^{2}_{ZL}\right)\boldsymbol{M_{ZL}} = EIU''_{YL} + \boldsymbol{M_{XdL}}U'_{ZL} \;\Rightarrow\; \boldsymbol{M_{ZL}} \approx EIU''_{YL} + \boldsymbol{M_{XdL}}U'_{ZL}
\end{aligned} \tag{5.30}$$

Eq. (5.29) captures the stiffening effect of axial force on the bending displacements and the coupling between the two bending directions due to the axial moment. The final approximation in the natural boundary condition, although not necessary, is made to maintain consistency with previous second order approximations. The beam governing differential equations (5.27)–(5.29) derived here are in agreement with previously derived non-linear beam models [36, 61] that contain more terms and are therefore mathematically more complex. When subjected to the same assumptions and second order approximations that have been made here, these previous models reduce to the results presented here. However, we have taken a more basic approach of deriving the governing equations from first principles, recognizing every assumption

and approximation made in the process, and highlighting the physical implications of these mathematical steps to avoid accidental elimination of relevant non-linear effects.

Although capturing the various non-linear coupling effects renders the governing equations of extension and torsion to be non-linear, the bending equations are still linear and coupled in U_Y and U_Z. This allows Eq.(5.29), along with associated boundary conditions (5.30), to be solved using linear algebra and then the results can be substituted in Eq. (5.27) and (5.28) to solve for U_X and θ_{Xd}, which provide the two geometric constraint conditions. The results may also be substituted in the strain energy term. This procedure is employed in the next section to obtain closed-form load-displacement relations, geometric constraint conditions, and strain energy expression for the slender, symmetric, spatial beam in terms of it end-displacements and end-loads.

5.4 Spatial Beam Constraint Model (SBCM) for a Symmetric Spatial Beam

At this point in the analysis, all the loads and displacements are normalized per the following scheme to make the equations and results compact:

$$\boldsymbol{m}_{z1} \triangleq \frac{\boldsymbol{M}_{ZL}L}{EI}, \quad \boldsymbol{m}_{y1} \triangleq \frac{\boldsymbol{M}_{YL}L}{EI}, \quad \boldsymbol{m}_{xd1} \triangleq \frac{\boldsymbol{M}_{XdL}L}{EI}, \quad \boldsymbol{f}_{z1} \triangleq \frac{\boldsymbol{F}_{ZL}L^2}{EI}, \quad \boldsymbol{f}_{y1} \triangleq \frac{\boldsymbol{F}_{YL}L^2}{EI}, \boldsymbol{f}_{x1} \triangleq \frac{\boldsymbol{F}_{XL}L^2}{EI},$$

$$v \triangleq \frac{VL}{EI}, \; u_y \triangleq \frac{U_Y}{L}, \; u_z \triangleq \frac{U_Z}{L}, \; u_{y1} \triangleq \frac{U_{YL}}{L}, \; u_{z1} \triangleq \frac{U_{ZL}}{L}, \; x \triangleq \frac{X}{L}, \; \theta_{xd} \triangleq \Theta_{Xd}, \; \theta_{xd1} \triangleq \Theta_{XdL}$$

Based on this, the beam governing differential equations (5.27)–(5.29), can be normalized as follows.

$$u_y^{iv} - \boldsymbol{f}_{x1}u_Y'' + \boldsymbol{m}_{xd1}u_z''' = 0; \qquad u_z^{iv} - \boldsymbol{f}_{x1}u_Z'' - \boldsymbol{m}_{xd1}u_y''' = 0 \tag{5.31}$$

$$u_{x1}' + \frac{1}{2}u_{y1}'^2 + \frac{1}{2}u_{z1}'^2 \approx \frac{\boldsymbol{f}_{x1}}{k_{33}} - \frac{2\boldsymbol{m}_{xd1}^2}{k_{33}k_{44}^2} \tag{5.32}$$

$$\left\{\theta_{xd}' - u_z'' \; u_y'\right\} \approx \frac{\boldsymbol{m}_{xd1}}{k_{44}} - \frac{2\boldsymbol{m}_{xd1}\boldsymbol{f}_{x1}}{k_{33}k_{44}^2} \tag{5.33}$$

where, $\quad k_{33} \triangleq \frac{12L^2}{T_Y^2}, \quad k_{44} \triangleq \frac{GJ}{EI}, \quad \boldsymbol{m}_{xd1} \triangleq \boldsymbol{m}_{x1} + u_{y1}'\boldsymbol{m}_{y1} + u_{z1}'\boldsymbol{m}_{z1}$

In spite of the non-linearity associated with $\boldsymbol{m}_{xd1}$, the two coupled bending equations (5.31) are linear with respect to the bending displacements u_y and u_z, and therefore can be readily solved for end loads and displacements using standard linear algebra and ordinary differential equation techniques [29].

Upon double differentiation, Eq.(5.31) may be expressed as a first order ordinary differential matrix equation:

$$\begin{Bmatrix} u_y''' \\ u_y'' \\ u_z''' \\ u_z'' \end{Bmatrix}' = \begin{bmatrix} 0 & \boldsymbol{f}_{x1} & -\boldsymbol{m}_{x1} & 0 \\ 1 & 0 & 0 & 0 \\ \boldsymbol{m}_{x1} & 0 & 0 & \boldsymbol{f}_{x1} \\ 0 & 0 & 1 & 0 \end{bmatrix} \begin{Bmatrix} u_y''' \\ u_y'' \\ u_z''' \\ u_z'' \end{Bmatrix} \tag{5.34}$$

The four scalar equations represented above can be solved by first decoupling them. This may be done via the eigen-values and eigen-vectors of the square matrix in the above equation.

E-values: $\boldsymbol{\lambda}_1 = \boldsymbol{\lambda}, \quad \boldsymbol{\lambda}_2 = -\boldsymbol{\lambda}, \quad \boldsymbol{\lambda}_3 = \dfrac{\boldsymbol{f}_{x1}}{\boldsymbol{\lambda}}, \quad \boldsymbol{\lambda}_4 = -\dfrac{\boldsymbol{f}_{x1}}{\boldsymbol{\lambda}}$

where, $\boldsymbol{\lambda} \triangleq \dfrac{1}{2}\sqrt{4\boldsymbol{f}_{x1} - 2\boldsymbol{m}_{x1}^{\,2} + 2\boldsymbol{m}_{x1}\sqrt{\boldsymbol{m}_{x1}^{\,2} - 4\boldsymbol{f}_{x1}}}$

E-vector matrix: $[Q] = \begin{bmatrix} -\boldsymbol{r} & -\boldsymbol{r} & -\dfrac{\boldsymbol{f}_{x1}}{\boldsymbol{r}} & -\dfrac{\boldsymbol{f}_{x1}}{\boldsymbol{r}} \\ -\dfrac{\boldsymbol{r}}{\boldsymbol{\lambda}_1} & -\dfrac{\boldsymbol{r}}{\boldsymbol{\lambda}_2} & -\dfrac{\boldsymbol{f}_{x1}}{\boldsymbol{\lambda}_3\boldsymbol{r}} & -\dfrac{\boldsymbol{f}_{x1}}{\boldsymbol{\lambda}_4\boldsymbol{r}} \\ \boldsymbol{\lambda}_1 & \boldsymbol{\lambda}_2 & \boldsymbol{\lambda}_3 & \boldsymbol{\lambda}_4 \\ 1 & 1 & 1 & 1 \end{bmatrix}$

where, $\boldsymbol{r} \triangleq \dfrac{1}{2}\left[\boldsymbol{m}_{x1} - \sqrt{\boldsymbol{m}_{x1}^{\,2} - 4\boldsymbol{f}_{x1}}\right]$

The eigen-values λ_1, λ_2, λ_3 and λ_4 are distinct for non-zero $\boldsymbol{f}_{x1}$ values implying that the equations can be decoupled for $\boldsymbol{f}_{x1}$ non-zero [15]†. The eigen-vectors are constitute the columns of the matrix [Q]. Using these eigen-values and eigen-vectors, the solution to Eq.(5.34) is simply given by:

† The case when $\boldsymbol{f}_{x1}$ is zero is trivial and is solved separately; however, details are not presented here since the final results are found to be consistent with the general solution for non-zero $\boldsymbol{f}_{x1}$.

$$\begin{Bmatrix} u_y''' \\ u_y'' \\ u_z''' \\ u_z'' \end{Bmatrix} = [Q] \begin{Bmatrix} c_1 e^{\lambda_1 x} \\ c_2 e^{\lambda_2 x} \\ c_3 e^{\lambda_3 x} \\ c_4 e^{\lambda_4 x} \end{Bmatrix} = \begin{bmatrix} -\boldsymbol{r} & -\boldsymbol{r} & -\dfrac{\boldsymbol{f_{x1}}}{\boldsymbol{r}} & -\dfrac{\boldsymbol{f_{x1}}}{\boldsymbol{r}} \\ -\dfrac{\boldsymbol{r}}{\boldsymbol{\lambda_1}} & -\dfrac{\boldsymbol{r}}{\boldsymbol{\lambda_2}} & -\dfrac{\boldsymbol{f_{x1}}}{\boldsymbol{\lambda_3 r}} & -\dfrac{\boldsymbol{f_{x1}}}{\boldsymbol{\lambda_4 r}} \\ \boldsymbol{\lambda_1} & \boldsymbol{\lambda_2} & \boldsymbol{\lambda_3} & \boldsymbol{\lambda_4} \\ 1 & 1 & 1 & 1 \end{bmatrix} \begin{Bmatrix} c_1 e^{\lambda_1 x} \\ c_2 e^{\lambda_2 x} \\ c_3 e^{\lambda_3 x} \\ c_4 e^{\lambda_4 x} \end{Bmatrix} \tag{5.35}$$

Here c_1, c_2, c_3 and c_4 are the constants of integration. From these four scalar equation, the general solution for the normalized transverse displacements u_y and u_z are given by:

$$\begin{aligned} u_y &= -\frac{\boldsymbol{r}}{\boldsymbol{\lambda_1}^3} c_1 e^{\lambda_1 x} - \frac{\boldsymbol{r}}{\boldsymbol{\lambda_2}^3} c_2 e^{\lambda_2 x} - \frac{\boldsymbol{f_{x1}}}{\boldsymbol{\lambda_3}^3 \boldsymbol{r}} c_3 e^{\lambda_3 x} - \frac{\boldsymbol{f_{x1}}}{\boldsymbol{\lambda_4}^3 \boldsymbol{r}} c_4 e^{\lambda_4 x} + c_5 x + c_6 \\ u_z &= \frac{c_1 e^{\lambda_1 x}}{\boldsymbol{\lambda_1}^2} + \frac{c_2 e^{\lambda_2 x}}{\boldsymbol{\lambda_2}^2} + \frac{c_3 e^{\lambda_3 x}}{\boldsymbol{\lambda_3}^2} + \frac{c_4 e^{\lambda_4 x}}{\boldsymbol{\lambda_4}^2} + c_7 x + c_8 \end{aligned} \tag{5.36}$$

The constants are solved in two steps. First the constants c_5, c_6, c_7 and c_8 are expressed in terms of c_1, c_2, c_3 and c_4 using the geometric boundary conditions arising from the spatial beam being rigidly fixed at one end:

$$u_y(0) = u_y'(0) = u_z(0) = u_z'(0) = 0 \quad \Rightarrow \begin{Bmatrix} c_5 \\ c_6 \\ c_7 \\ c_8 \end{Bmatrix} = \begin{bmatrix} \dfrac{\boldsymbol{r}}{\boldsymbol{\lambda_1}^2} & \dfrac{\boldsymbol{r}}{\boldsymbol{\lambda_2}^2} & \dfrac{\boldsymbol{f_{x1}}}{\boldsymbol{r}\boldsymbol{\lambda_3}^2} & \dfrac{\boldsymbol{f_{x1}}}{\boldsymbol{r}\boldsymbol{\lambda_4}^2} \\ \dfrac{\boldsymbol{r}}{\boldsymbol{\lambda_1}^3} & \dfrac{\boldsymbol{r}}{\boldsymbol{\lambda_2}^3} & \dfrac{\boldsymbol{f_{x1}}}{\boldsymbol{r}\boldsymbol{\lambda_3}^3} & \dfrac{\boldsymbol{f_{x1}}}{\boldsymbol{r}\boldsymbol{\lambda_4}^3} \\ -\dfrac{1}{\boldsymbol{\lambda_1}} & -\dfrac{1}{\boldsymbol{\lambda_2}} & -\dfrac{1}{\boldsymbol{\lambda_3}} & -\dfrac{1}{\boldsymbol{\lambda_4}} \\ -\dfrac{1}{\boldsymbol{\lambda_1}^2} & -\dfrac{1}{\boldsymbol{\lambda_2}^2} & -\dfrac{1}{\boldsymbol{\lambda_3}^2} & -\dfrac{1}{\boldsymbol{\lambda_4}^2} \end{bmatrix} \begin{Bmatrix} c_1 \\ c_2 \\ c_3 \\ c_4 \end{Bmatrix} \tag{5.37}$$

The remaining four constants are solved using the free-end displacement boundary conditions:

$u_y(1) = u_{y1}, \quad u_y'(1) = \theta_{z1}, \quad u_z(1) = u_{z1}, \quad u_z'(1) = -\theta_{y1} \quad \Rightarrow$

$\{c_1 \quad c_2 \quad c_3 \quad c_4\}^T = [C]\{u_{y1} \quad \theta_{z1} \quad u_{z1} \quad \theta_{y1}\}^T$, where

$$[C] \triangleq \begin{bmatrix} \frac{\boldsymbol{r}}{\boldsymbol{\lambda}_1^{\,3}}\boldsymbol{t}_{11} & \frac{\boldsymbol{r}}{\boldsymbol{\lambda}_2^{\,3}}\boldsymbol{t}_{12} & \frac{\boldsymbol{f}_{x1}}{\boldsymbol{r}\boldsymbol{\lambda}_3^{\,3}}\boldsymbol{t}_{13} & \frac{\boldsymbol{f}_{x1}}{\boldsymbol{r}\boldsymbol{\lambda}_4^{\,3}}\boldsymbol{t}_{14} \\ \frac{\boldsymbol{r}}{\boldsymbol{\lambda}_1^{\,2}}\boldsymbol{t}_{21} & \frac{\boldsymbol{r}}{\boldsymbol{\lambda}_2^{\,2}}\boldsymbol{t}_{22} & \frac{\boldsymbol{f}_{x1}}{\boldsymbol{r}\boldsymbol{\lambda}_3^{\,2}}\boldsymbol{t}_{23} & \frac{\boldsymbol{f}_{x1}}{\boldsymbol{r}\boldsymbol{\lambda}_4^{\,2}}\boldsymbol{t}_{24} \\ -\frac{1}{\boldsymbol{\lambda}_1^{\,2}}\boldsymbol{t}_{31} & -\frac{1}{\boldsymbol{\lambda}_2^{\,2}}\boldsymbol{t}_{32} & -\frac{1}{\boldsymbol{\lambda}_3^{\,2}}\boldsymbol{t}_{33} & -\frac{1}{\boldsymbol{\lambda}_4^{\,2}}\boldsymbol{t}_{34} \\ \frac{1}{\boldsymbol{\lambda}_1}\boldsymbol{t}_{41} & \frac{1}{\boldsymbol{\lambda}_2}\boldsymbol{t}_{42} & \frac{1}{\boldsymbol{\lambda}_3}\boldsymbol{t}_{43} & \frac{1}{\boldsymbol{\lambda}_4}\boldsymbol{t}_{44} \end{bmatrix}^{-1}$$

$$\boldsymbol{t}_{1i} = \boldsymbol{t}_{3i} \triangleq \left(1 + \boldsymbol{\lambda}_1 - e^{\boldsymbol{\lambda}_1}\right), \qquad \boldsymbol{t}_{2i} = \boldsymbol{t}_{3i} \triangleq \left(1 - e^{\boldsymbol{\lambda}_1}\right)$$

We next make use of the natural boundary conditions at the free end of the beam. Natural boundary conditions involve relations between loads and displacements that occur naturally because of the beam governing equation. The natural boundary conditions at $x = 1$ are

$$\begin{aligned} u_y''(1) &= -u_z'(1)\boldsymbol{m}_{x1} + \boldsymbol{m}_{z1} \\ u_y'''(1) &= -u_z''(1)\boldsymbol{m}_{x1} - \boldsymbol{f}_{y1} + \boldsymbol{f}_{x1}u_y'(1) \\ u_z''(1) &= u_y'(1)\boldsymbol{m}_{x1} - \boldsymbol{m}_{y1} \\ u_z'''(1) &= u_y''(1)\boldsymbol{m}_{x1} - \boldsymbol{f}_{z1} + \boldsymbol{f}_{x1}u_z'(1) \end{aligned} \tag{5.38}$$

The general solution for u_y and u_z, given by (5.36) is plugged into the above natural boundary conditions to relate the transverse loads $\boldsymbol{f}_{y1}$, $\boldsymbol{f}_{z1}$, $\boldsymbol{m}_{y1}$ and $\boldsymbol{m}_{z1}$ to the transverse displacements u_{y1}, u_{z1}, θ_{y1} and θ_{z1} by a stiffness matrix:

$$\begin{Bmatrix} \boldsymbol{f}_{y1} \\ \boldsymbol{m}_{z1} \\ \boldsymbol{f}_{z1} \\ \boldsymbol{m}_{y1} \end{Bmatrix} = [k] \begin{Bmatrix} u_{y1} \\ \theta_{z1} \\ u_{z1} \\ \theta_{y1} \end{Bmatrix}, \quad \text{where} \quad [k] \triangleq \{[A][B][C] + [D]\} \tag{5.39}$$

$$[A] \triangleq \begin{bmatrix} \boldsymbol{r} - \boldsymbol{m}_{x1} & \boldsymbol{r} - \boldsymbol{m}_{x1} & \frac{\boldsymbol{f}_{x1}}{\boldsymbol{r}} - \boldsymbol{m}_{x1} & \frac{\boldsymbol{f}_{x1}}{\boldsymbol{r}} - \boldsymbol{m}_{x1} \\ -\frac{\boldsymbol{r}}{\boldsymbol{\lambda}} & \frac{\boldsymbol{r}}{\boldsymbol{\lambda}} & -\frac{\boldsymbol{\lambda}}{\boldsymbol{r}} & \frac{\boldsymbol{\lambda}}{\boldsymbol{r}} \\ -\left(\boldsymbol{\lambda} + \frac{\boldsymbol{r}\boldsymbol{m}_{x1}}{\boldsymbol{\lambda}}\right) & \left(\boldsymbol{\lambda} + \frac{\boldsymbol{r}\boldsymbol{m}_{x1}}{\boldsymbol{\lambda}}\right) & -\left(\frac{\boldsymbol{f}_{x1}}{\boldsymbol{\lambda}} + \frac{\boldsymbol{\lambda}\boldsymbol{m}_{x1}}{\boldsymbol{r}}\right) & \left(\frac{\boldsymbol{f}_{x1}}{\boldsymbol{\lambda}} + \frac{\boldsymbol{\lambda}\boldsymbol{m}_{x1}}{\boldsymbol{r}}\right) \\ -1 & -1 & -1 & -1 \end{bmatrix}$$

$$[B] \triangleq \begin{bmatrix} e^{\lambda} & 0 & 0 & 0 \\ 0 & e^{\lambda} & 0 & 0 \\ 0 & 0 & e^{\frac{f_{x1}}{\lambda}} & 0 \\ 0 & 0 & 0 & e^{-\frac{f_{x1}}{\lambda}} \end{bmatrix} \quad , \quad [D] \triangleq \begin{bmatrix} 0 & \boldsymbol{f}_{x1} & 0 & 0 \\ 0 & 0 & 0 & -\boldsymbol{m}_{x1} \\ 0 & 0 & 0 & -\boldsymbol{f}_{x1} \\ 0 & \boldsymbol{m}_{x1} & 0 & 0 \end{bmatrix}$$

The above relations show that the transverse end-loads and transverse end-displacements are linearly related by a stiffness matrix. This is expected because the bending direction beam governing equations (5.31) were also linear in these loads and displacements. However, the transverse stiffness matrix does include the axial force $\boldsymbol{f}_{x1}$ and twisting moment $\boldsymbol{m}_{x1}$. The individual stiffness terms, when stated in an explicit form, turn out to be very complicated transcendental expressions in $\boldsymbol{f}_{x1}$ and $\boldsymbol{m}_{x1}$, making it impossible to gauge the influence of these loads on the transverse stiffness. Therefore, to gain better insight, we carry out the Taylor series expansion of these transcendental expressions in terms of $\boldsymbol{f}_{x1}$ and $\boldsymbol{m}_{x1}$, as follows:

$$[k] = \begin{bmatrix} k_{11} & k_{12} & k_{15} & k_{16} \\ k_{21} & k_{22} & k_{25} & k_{26} \\ k_{51} & k_{52} & k_{55} & k_{56} \\ k_{61} & k_{62} & k_{65} & k_{66} \end{bmatrix} \tag{5.40}$$

$$k_{11} = k_{55} = \left(12 - \frac{1}{5}\boldsymbol{m}_{x1}{}^2 + \cdots\right) + \frac{6}{5}\boldsymbol{f}_{x1}\left(1 + \frac{2\boldsymbol{m}_{x1}{}^2}{315} + \cdots\right) - \frac{1}{700}\boldsymbol{f}_{x1}{}^2\left(1 + \frac{31\boldsymbol{m}_{x1}{}^2}{34} + \cdots\right) + \cdots$$

$$k_{12} = k_{21} = -k_{56} = -k_{65} = \left(-6 + \frac{1}{10}\boldsymbol{m}_{x1}{}^2 + \cdots\right) - \frac{1}{10}\boldsymbol{f}_{x1}\left(1 + \frac{4\boldsymbol{m}_{x1}{}^2}{105} + \cdots\right) + \frac{1}{1400}\boldsymbol{f}_{x1}{}^2\left(1 + \frac{5\boldsymbol{m}_{x1}{}^2}{36} + \cdots\right) + \cdots$$

$$k_{22} = k_{66} = \left(4 - \frac{1}{20}\boldsymbol{m}_{x1}{}^2 + \cdots\right) + \frac{2}{15}\boldsymbol{f}_{x1}\left(1 + \frac{\boldsymbol{m}_{x1}{}^2}{70} + \cdots\right) - \frac{11}{6300}\boldsymbol{f}_{x1}{}^2\left(1 + \frac{\boldsymbol{m}_{x1}{}^2}{44} + \cdots\right) + \cdots$$

$$k_{15} = k_{51} = 0, \qquad k_{26} = -k_{62} = -\frac{1}{2}\boldsymbol{m}_{x1}$$

$$k_{16} = k_{61} = k_{25} = k_{52} = \boldsymbol{m}_{x1} - \frac{1}{60}\boldsymbol{f}_{x1}\boldsymbol{m}_{x1} + \cdots$$

In the stiffness matrix above, the subscripts 1 and 2 are related to the two end-displacements, u_{y1} and θ_{z1}, in the XY bending plane. Subscripts 5 and 6 are related to the two

end-displacements, u_{z1} and θ_{y1}, in the XZ bending plane. Subscripts 3 and 4 are reserved for the X direction displacements, u_{x1} and θ_{x1}, respectively.

The above series expansions the transverse direction stiffness terms indeed shed more light on the effects of the axial load and twisting moment. First , it may be verified that in the absence of $\boldsymbol{f_{x1}}$ and $\boldsymbol{m_{x1}}$, the stiffness matrix coefficients relating u_{y1} and θ_{z1} to loads $\boldsymbol{f_{z1}}$ and $\boldsymbol{m_{y1}}$ and those relating u_{z1} and θ_{y1} to loads $\boldsymbol{f_{y1}}$ and $\boldsymbol{m_{z1}}$ become zero, showing that the two bending directions are uncoupled, and the resulting stiffness matrix is same as one obtained from a purely linear analysis [6, 12]. Next we find that if $\boldsymbol{m_{x1}}$ is set to zero the two bending directions are still decoupled. Also, in each bending direction, the influence of the axial $\boldsymbol{f_{x1}}$ on transverse stiffness is identical to that seen in planar beams [5, 6], i.e. there is a prominent load-stiffening component associated with the first power of $\boldsymbol{f_{x1}}$.

Thus, it is clear that any coupling between the two bending directions arises solely from the twisting moment $\boldsymbol{m_{x1}}$. The displacement range of interest (u_y, u_z and $\theta_{Xd} \sim 0.1$) implies that the normalized twisting moment $\boldsymbol{m_{x1}}$ is also of the order of 0.1 (based on nominal linear twisting stiffness). In comparison, the normalized axial force $\boldsymbol{f_{x1}}$ can be of the order of 1 or greater since it is along a DoC (or load bearing) direction.

Given this magnitude of $\boldsymbol{m_{x1}}$, it may be seen that its contribution in the k_{11}, k_{12}, k_{22}, k_{55}, k_{56}, and k_{66} terms is less than 0.5%, and therefore $\boldsymbol{m_{x1}}$ terms may be dropped altogether in these cases. Similarly, the second power and higher terms in $\boldsymbol{m_{x1}}$ may be dropped in k_{16} and k_{25} terms as well. However, the first power of $\boldsymbol{m_{x1}}$ that shows up only in the k_{26}, k_{62}, k_{25}, and k_{52} terms cannot be ignored, being the sole or most important contributor in each of these stiffness terms. In fact, it is these latter stiffness terms that give rise to cross-axis coupling between the two bending directions. Even though the coupling is weak, it captures a behavior that is not identified in a purely linear analysis.

Next, it may be seen that given the larger magnitude of $\boldsymbol{f_{x1}}$, its contribution to the transverse stiffness is stronger. In the stiffness terms k_{11}, k_{12}, k_{22}, k_{55}, k_{56}, and k_{66}, the first power in $\boldsymbol{f_{x1}}$ represents the load-stiffening effect, identical to that seen in planar beams discussed in Chapter 2 and 3. The second and higher power $\boldsymbol{f_{x1}}$ terms have a negligible contribution over the load and displacement range of interest, and can be dropped. However, as shown via energy arguments, the second power term should be retained to maintain consistency with the X direction constraint relation. Based on the above rationale for truncating higher order terms in the

series expansions of expression (5.40), the final simplified form of transverse direction stiffness terms are summarized below:

$$
\begin{aligned}
k_{11} = k_{55} &\approx 12 + \frac{6}{5}\,\boldsymbol{f}_{x1} - \frac{1}{700}\,\boldsymbol{f}_{x1}^{\,2} \\
k_{12} = k_{21} = -k_{56} = -k_{65} &\approx -6 - \frac{1}{10}\,\boldsymbol{f}_{x1} + \frac{1}{1400}\,\boldsymbol{f}_{x1}^{\,2} \\
k_{22} = k_{66} &\approx 4 + \frac{2}{15}\,\boldsymbol{f}_{x1} - \frac{11}{6300}\,\boldsymbol{f}_{x1}^{\,2} \\
k_{15} = k_{51} = 0, \qquad k_{26} = -k_{62} &= -\frac{1}{2}\boldsymbol{m}_{x1} \\
k_{16} = k_{61} = k_{25} = k_{52} &\approx \boldsymbol{m}_{x1} - \frac{1}{60}\,\boldsymbol{f}_{x1}\boldsymbol{m}_{x1}
\end{aligned}
\tag{5.41}
$$

This engineering approximation (truncation error) of the transcendental terms in the stiffness matrix produces less that *1%* error, while making the transverse direction load-displacement relation more insightful and simpler to work with for a designer.

To express this result in a form that is mathematically concise and provides insight into the geometric effects and non-linearities that are relevant to constraint characterization, we carry out a Taylor series expansion of each stiffness element in terms of the axial and torsional loads, $\boldsymbol{f}_{x1}$ and $\boldsymbol{m}_{xd1}$ and drop third and higher power terms.

$$
\begin{aligned}
\left\{ \boldsymbol{f}_{y1} \quad \boldsymbol{m}_{z1} \quad \boldsymbol{f}_{z1} \quad \boldsymbol{m}_{y1} \right\}^T = \quad & [H_1]\left\{ u_{y1} \quad \theta_{z1} \quad u_{z1} \quad \theta_{y1} \right\}^T \\
& -\left[2\,\boldsymbol{f}_{x1} H_2 + \boldsymbol{m}_{xd1}\left(2H_3 + H_7\right) \right]\left\{ u_{y1} \quad \theta_{z1} \quad u_{z1} \quad \theta_{y1} \right\}^T \\
& -\left[\boldsymbol{f}_{x1}^{2} H_4 + \boldsymbol{m}_{xd1}\,\boldsymbol{f}_{x1} H_5 + \boldsymbol{m}_{xd1}^{2} H_6 \right]\left\{ u_{y1} \quad \theta_{z1} \quad u_{z1} \quad \theta_{y1} \right\}^T + \ldots
\end{aligned}
\tag{5.42}
$$

where

$$
H_1 \triangleq \begin{bmatrix} 12 & -6 & 0 & 0 \\ -6 & 4 & 0 & 0 \\ 0 & 0 & 12 & 6 \\ 0 & 0 & 6 & 4 \end{bmatrix},\ H_2 \triangleq \begin{bmatrix} -\frac{3}{5} & \frac{1}{20} & 0 & 0 \\ \frac{1}{20} & -\frac{1}{15} & 0 & 0 \\ 0 & 0 & -\frac{3}{5} & -\frac{1}{20} \\ 0 & 0 & -\frac{1}{20} & -\frac{1}{15} \end{bmatrix},\ H_3 \triangleq \frac{1}{4}\begin{bmatrix} 0 & 0 & 0 & -2 \\ 0 & 0 & -2 & -1 \\ 0 & -2 & 0 & 0 \\ -2 & -1 & 0 & 0 \end{bmatrix}
$$

$$H_4 \triangleq \begin{bmatrix} \frac{1}{700} & -\frac{1}{1400} & 0 & 0 \\ -\frac{1}{1400} & \frac{11}{6300} & 0 & 0 \\ 0 & 0 & \frac{1}{700} & \frac{1}{1400} \\ 0 & 0 & \frac{1}{1400} & \frac{11}{6300} \end{bmatrix}, \; H_5 \triangleq \frac{1}{60}\begin{bmatrix} 0 & 0 & 0 & 1 \\ 0 & 0 & 1 & 0 \\ 0 & 1 & 0 & 0 \\ 1 & 0 & 0 & 0 \end{bmatrix}, \; H_6 \triangleq \frac{1}{20}\begin{bmatrix} 4 & -2 & 0 & 0 \\ -2 & 1 & 0 & 0 \\ 0 & 0 & 4 & 2 \\ 0 & 0 & 2 & 1 \end{bmatrix}$$

$$H_7 \triangleq \begin{bmatrix} 0 & 0 & 0 & 0 \\ 0 & 0 & 0 & 1 \\ 0 & 0 & 0 & 0 \\ 0 & 0 & 0 & 0 \end{bmatrix}$$

Next, the $u_y(x)$ and $u_z(x)$ solutions to the bending equations (5.31) are substituted into Eqs. (5.32) and (5.33), which upon integration provide the solution for the axial extension and twisting, respectively. Once again, these solutions contain 4 x 4 matrices, each non-zero element of which is a transcendental function of the end loads $\boldsymbol{f_{x1}}$ and $\boldsymbol{m_{xd1}}$. A Taylor series expansion of each element, followed by truncation of higher order terms produces the following two constraint relations, expressed in terms of the end displacements and loads of the beam.

$$\begin{aligned} u_{x1} = {} & \frac{\boldsymbol{f_{x1}}}{k_{33}} - \frac{\boldsymbol{m_{xd1}^2}}{k_{44}^2 k_{33}} + \{u_{y1} \quad \theta_{z1} \quad u_{z1} \quad \theta_{y1}\} H_2 \{u_{y1} \quad \theta_{z1} \quad u_{z1} \quad \theta_{y1}\}^T \\ & + \{u_{y1} \quad \theta_{z1} \quad u_{z1} \quad \theta_{y1}\} \left[\boldsymbol{f_{x1}} H_4 + \frac{1}{2} \boldsymbol{m_{xd1}} H_5 \right] \{u_{y1} \quad \theta_{z1} \quad u_{z1} \quad \theta_{y1}\}^T + \ldots \end{aligned} \tag{5.43}$$

$$\begin{aligned} \theta_{xd1} = {} & \frac{\boldsymbol{m_{xd1}}}{k_{44}} - \frac{2\boldsymbol{m_{xd1}}\boldsymbol{f_{x1}}}{k_{33}k_{44}^2} + \{u_{y1} \quad \theta_{z1} \quad u_{z1} \quad \theta_{y1}\} H_3 \{u_{y1} \quad \theta_{z1} \quad u_{z1} \quad \theta_{y1}\}^T \\ & + \{u_{y1} \quad \theta_{z1} \quad u_{z1} \quad \theta_{y1}\} \left[\boldsymbol{m_{xd1}} H_6 + \frac{1}{2} \boldsymbol{f_{x1}} H_5 \right] \{u_{y1} \quad \theta_{z1} \quad u_{z1} \quad \theta_{y1}\}^T + \ldots \end{aligned} \tag{5.44}$$

The series truncations produce less than 1% loss of accuracy in each respective relation over an $\boldsymbol{f_{x1}}$ range of ±5 and an $\boldsymbol{m_{xd1}}$ range of ±0.1, while providing considerable mathematical simplicity and physical insight. The former represents a typical DoC direction bearing force, while the latter represents the normalized moment associated with a rotation of 0.1 along the Θ_x DoF. The $[H_1]$ matrix in relation (5.42) represents the linear elastic stiffness associated with the four transverse bending displacements. The $[H_2]$ matrix captures load stiffening in these directions in the presence of axial load $\boldsymbol{f_{x1}}$ (Eq.(5.42)) and a corresponding purely kinematic

contribution of bending displacements to the axial displacement (Eq.(5.43)). The [H_3] and [H_7] matrices captures load stiffening in the bending directions in the presence of torsional moment $\boldsymbol{m_{xd1}}$ (Eq.(5.42)) and reveals a coupling between the two bending planes in the presence of this moment. Corresponding to this, the [H_3] matrix also captures the purely kinematic contribution of bending displacements to the twisting angle (Eq.(5.44)). Although the [H_4], [H_5], and [H_6] matrices make a negligible contribution in Eq.(5.42), they capture the important elastokinematic effects in Eqs. (5.43) and (5.44). In the axial direction, [H_4] provides an additional compliance with respect to axial load $\boldsymbol{f_{x1}}$ and [H_5] provides an additional compliance with respect to axial moment $\boldsymbol{m_{xd1}}$, in the presence of transverse bending displacements. Similarly, in the twisting direction, [H_5] provides an additional compliance with respect to axial load $\boldsymbol{f_{x1}}$ and [H_6] provides an additional compliance with respect to axial moment $\boldsymbol{m_{xd1}}$, in the presence of transverse bending displacements. These relations also highlight the unique status of the twisting rotation θ_{dx1}. Based on physical intuition, this twisting direction appears to be a DoF, like the transverse displacements u_{y1}, θ_{y1}, u_{y1}, and θ_{z1}, because of its low stiffness. However, mathematically, it behaves more like the u_{x1} DoC and is dictated by the constraint relation (5.44), which is analogous to constraint relation (5.43). The [H_1] through [H_7] matrices are dimensionless and valid for any beam size and shape, as long as the beam is uniform, symmetric, and slender. Therefore, elements of these matrices are subsequently referred to as the *beam characteristic coefficients* for the spatial beam flexure.

Next, the strain energy expression (5.13) may be further simplified using Eqs. (5.32) and (5.33), and can be stated as follows after normalization:

$$v = \frac{1}{2}\int_0^1 \left(u_y''^2 + u_z''^2\right) dx + \frac{\boldsymbol{m}_{xd1}^2}{2k_{44}} + \frac{\boldsymbol{f}_{x1}^2}{2k_{33}} - \frac{2\boldsymbol{m}_{xd1}^2 \boldsymbol{f}_{x1}}{k_{33}k_{44}^2} \tag{5.45}$$

The $u_y(x)$ and $u_z(x)$ solutions to the bending equations (5.31) obtained previously can be substituted above to produce the total strain energy in terms of end-displacements u_{y1}, u_{z1}, θ_{y1}, and θ_{z1} and loads $\boldsymbol{m_{xd1}}$ and $\boldsymbol{f_{x1}}$ as follows:

$$\begin{aligned} v = \frac{1}{2}\begin{Bmatrix} u_{y1} & \theta_{z1} & u_{z1} & \theta_{y1} \end{Bmatrix} \left[H_1 + \frac{\boldsymbol{f}_{x1}^2}{2} H_4 + \frac{\boldsymbol{m}_{xd1}\boldsymbol{f}_{x1}}{2} H_5 + \frac{\boldsymbol{m}_{xd1}^2}{2} H_6 \right] \begin{Bmatrix} u_{y1} & \theta_{z1} & u_{z1} & \theta_{y1} \end{Bmatrix}^T \\ + \frac{\boldsymbol{m}_{xd1}^2}{2k_{44}} + \frac{\boldsymbol{f}_{x1}^2}{2k_{33}} - \frac{2\boldsymbol{m}_{xd1}^2 \boldsymbol{f}_{x1}}{k_{33}k_{44}^2} \end{aligned} \tag{5.46}$$

This strain energy expression allows a designer to treat the spatial beam as a single lumped entity, with all the relevant non-linearities captured, when analyzing a flexure mechanism consisting of multiple spatial beam flexures using energy methods. Overall, the transverse load-displacement relations (5.42), the geometric constraint relations in axial extension (5.43) and torsion (5.44), and the strain energy expression (5.46), collectively represent a closed-form, parametric, non-linear model that captures constraint characteristics of a slender, symmetric, spatial beam; this model is subsequently referred to as the spatial-beam constraint model (SBCM).

It is worthwhile to note the reoccurrence of matrices $[H_1]$ to $[H_7]$ in the force displacement relations (5.42)-(5.44) and strain energy expression in Eq.(5.46), which points to a connection between various terms in all these equations. Although, in the foregoing discussion, several physical effects were discussed to explain this connection, there isn't any mathematical proof yet to show that these connections are not coincidental for this particular cross-section but is true in a more general case. Such a proof is not obvious because matrices $[H_1]$ to $[H_7]$ are coefficients of the Taylor series of the actual beam solution and doesn't convey the full solution. This proof will be given in Chapter 6, which will not only cover the relation between the first few terms of the Taylor series expansion of the beam solution but all terms in the expansion.

5.5 Validation of SBCM

The results of the previous section are validated via non-linear FEA using ANSYS™. For these simulations, the beam dimensions were taken to be $L = 0.1$ m and $T_Y = T_Z = 0.0025$ m, and Young's modulus and Poisson's ratio were assumed to be *210* GPa and *0.3*, respectively. For each beam, 400 BEAM188 elements were used, with the *restrained warping*, *torsional shear*, and *large deformation* options turned on. To verify individual elements of $[H_1]$, three of the four displacements among u_{y1}, u_{z1}, θ_{y1} and θ_{z1} are set to zero, while the fourth displacement is varied from –0.1 to 0.1. When axial and torsional loads $\boldsymbol{f_{x1}}$ and $\boldsymbol{m_{xd1}}$ are set to zero, the reaction loads $\boldsymbol{f_{y1}}$, $\boldsymbol{m_{z1}}$, $\boldsymbol{f_{z1}}$ and $\boldsymbol{m_{y1}}$ provide the elements of $[H_1]$. In Figure 5.7(a), each non-zero (i, j) element of $[H_1]$ is plotted with respect to the respective transverse displacement that was varied, while keeping others zero, for its determination. The $[H_2]$ matrix is obtained by measuring the u_{x1} displacement for different values of u_{y1}, u_{z1}, θ_{y1} and θ_{z1} while setting $\boldsymbol{m_{xd1}}$ and $\boldsymbol{f_{x1}}$ to zero, as per Eq.(5.43). Similarly, the $[H_3]$ matrix is obtained by measuring the θ_{xd1} rotation for different

values of u_{y1}, u_{z1}, θ_{y1} and θ_{z1} while setting $\boldsymbol{m_{xd1}}$ and $\boldsymbol{f_{x1}}$ to zero, as per Eq.(5.44). Finally, as per Eq. (5.42), the $[H_7]$ matrix is verified by setting $\boldsymbol{m_{xd1}}$ and θ_{y1} to non-zero values and u_{y1}, u_{z1}, θ_{y1} and $\boldsymbol{f_{x1}}$ to zero, and measuring $\boldsymbol{m_{z1}}$. It should be noted that this will also capture the effect of $[H_1]$, which is separated out to obtain $[H_7]$. Non-zero elements of the $[H_2]$, $[H_3]$, and $[H_7]$ matrices are plotted in Figure 5.7(b). These results show that the elastic bending stiffness captured by the $[H_1]$ matrix, and load-stiffening and kinematic effects captured by the $[H_2]$, $[H_3]$, and $[H_7]$ in the BCM are accurate to within 1% with respect to FEA.

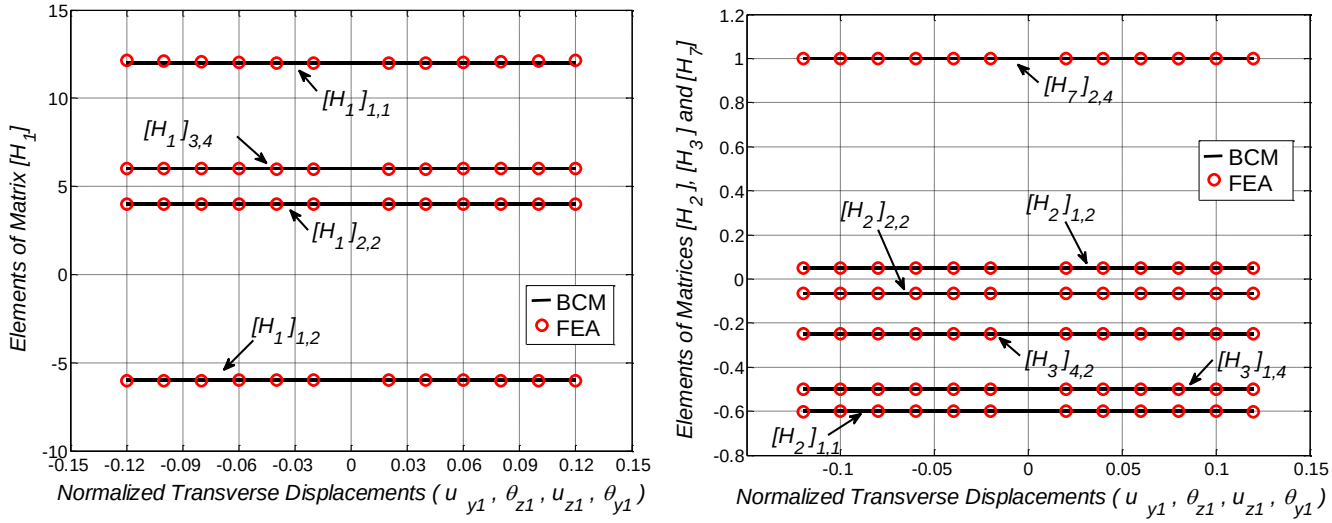

Figure 5.7: ***(a) Elastic Matrix*** **$[H_1]$,** ***(b) Kinematic Matrices*** **$[H_2]$, $[H_3]$, and $[H_7]$**

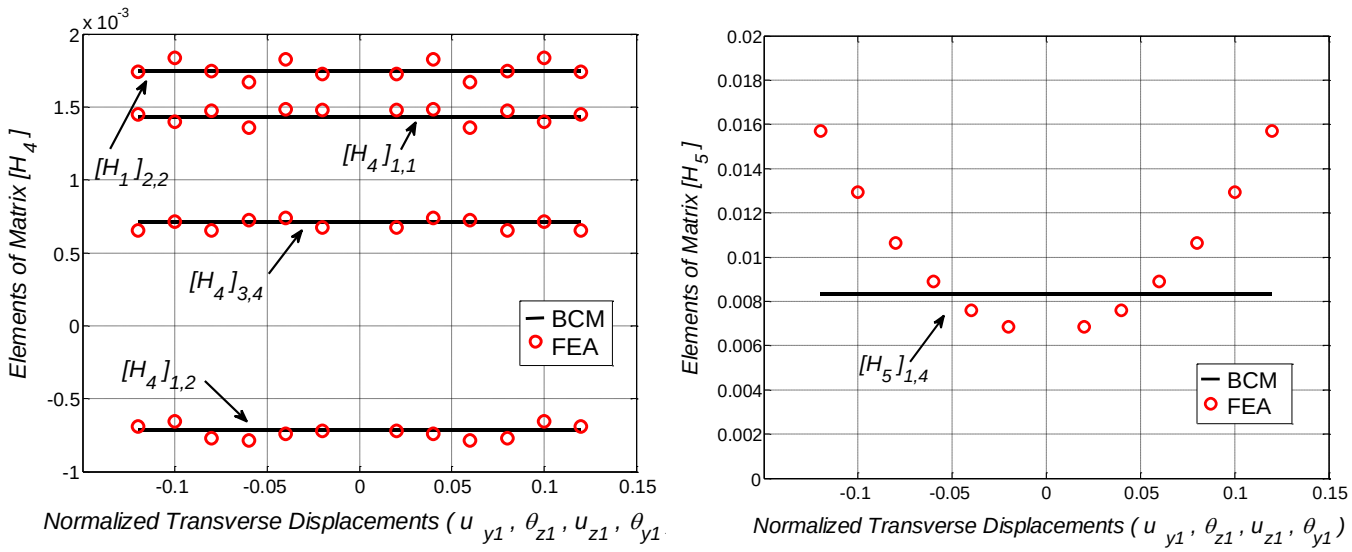

Figure 5.8: ***(a) Elastokinematic Matrix*** **[H_4]**, ***(b) Elastokinematic Matrix*** **[H_5]**

Matrices [H_4] and [H_5] capture the non-linear elastokinematic effects in the X direction and are obtained by measuring the u_{x1} for different values of u_{y1}, u_{z1}, θ_{y1} and θ_{z1} while setting $\boldsymbol{m_{xd1}}$ = 0 or $\boldsymbol{f_{x1}}$ = 0, one at a time. This calculation requires subtraction of the kinematic displacement component associated with [H_2], which has already been validated above. The non-zero elements of [H_4] and [H_5] are plotted in Figure 5.8 (a) and (b), respectively. Since the elastokinematic effects correspond to higher powers of $\boldsymbol{f_{x1}}$ and $\boldsymbol{m_{xd1}}$ in the load-displacement relations, their effect is relatively weak. Nevertheless, the [H_4] matrix, which contributes additional compliance in the X direction in the presence of transverse bending displacement, matches FEA results with less than 6% discrepancy. As seen in Fig.7, this discrepancy is much greater in the case of [H_5] – while the orders of magnitude are comparable between the BCM and FEA, the trends no longer agree. At this point, the second order assumption made throughout the derivation starts to become weak.

The elastokinematic effects captured by the [H_5] and [H_6] matrices in Eq.(5.44) contribute additional compliance in the Θ_x direction in the presence of transverse bending displacements. However, these effects are even smaller than those along the X direction, over the load and displacement range of interest. As a result, the [H_6] matrix is difficult to estimate and validate via FEA. In physical terms, these effects do not play a significant role in the constraint characteristics of the spatial beam. Since Θ_x is a DoF direction, it nominally exhibits a high

linear compliance ($1/k_{44}$); the small additional compliance due to these elastokinematic effects does not make much difference.

5.5 Discussion

While some spatial beam models exist, they are either too trivial to capture the non-linear effects that influence the constraint characteristics of spatial beams, or mathematically too complex to serve the goals of constraint-based flexure design, analysis, and optimization. In this chapter, we employed an existing beam mechanics formulation for a slender, spatial beam, but start from first principles to carefully make specific assumptions and approximations that are valid within an intermediate range of bending displacements and twisting angle (10% of beam length) and corresponding loads. This not only allows reduction of the mathematical complexity to a manageable level but also captures all the relevant non-linear effects in a compact, closed-form, parametric manner. The final model is based on the Euler's deformation assumption along with small out-of-plane cross-sectional warping, Green's strain measure, second order approximation of strain terms, partial linearization of curvature expressions, and truncation of higher power terms in axial and torsional loads.

This results in a new spatial-beam constraint model that comprises load-displacement relations in bending directions, geometric constraint relations in axial and torsional directions, and a strain energy expression – all in terms of the six end-loads and six end-displacements. These relations capture all the geometric nonlinearities that affect the constraint characteristics of the beam: load-stiffening in the bending directions in the presence of an axial load, coupling between the bending directions in the presence of a torsional moment, kinematic and elastokinematic components in the axial displacement and twisting angle due to transverse bending displacements, and the trapeze effect coupling between axial and torsional directions. These are all validated to be accurate within a few percent using non-linear FEA over the above-mentioned displacement and load range of interest, which is justified by typical material failure criteria in flexure mechanisms. Since no assumption, other than symmetry, is made for the beam cross-section, this model is applicable to beams with circular, square and other regular polygon shaped cross-sections. Furthermore, the model also reveals an interesting mathematical similarity

between the twisting angle and axial displacement, even though the former is generally recognized as a DoF and the latter as DoC.

With SBCM for symmetric spatial beam, a way to analyze any flexure mechanism comprised of symmetric spatial beam is now created. This model overcomes the restrictions of previous models for spatial beams of a very small displacement range, specific loading and displacement considerations or all of the above. Since SBCM capture the kinematic behavior of the spatial beam accurately it can be used to study the kinematics of a problem and parametric dependence on spacing and orientation of the beam. Furthermore, elastic properties of flexure mechanisms that are often challenging to find in a parametric relation due to geometric nonlinearities are easily available from SBCM via stiffness estimations. Finally the simplicity of SBCM should be noted. Not only does it separates out the various physical effects of deformation but also represents it in a manageable manner. It is estimated that the extensive knowledge of matrix algebra can be used, when integrating several SBCMs for a flexure mechanism with multiple spatial beam flexures.

Chapter 6

Energy Model for SBCM for a Spatial Beam Flexure With Symmetric Cross-section

6.1 Introduction

Nonlinear closed formed analysis of flexure mechanism with multiple (n) spatial beam flexure elements using free body diagrams is non-trivial because it requires solving 6n+6 variables (each leg contributes 6 internal load variables while the motion stage contributes 6 displacement variables) from 12n+6 nonlinear simultaneous equations (each leg contributes 6 load-displacement relations and 6 geometric compatibility relations, and the motion contributes 6 load-equilibrium relations). For example, consider the 3DoF table flexure, shown in Figure 6.1 with n-legs, that provides relatively high stiffness against out-of-plane translational displacements along X and out-of-plane rotational displacements about Y and Z while allowing in-plane translation motions along Y and Z and in-plane rotation about X. An analytical model of 3-legged table with vertical spatial beam flexures was derived using free body diagrams by Hao [60]. The analysis is highly complex because it involves solving of 24 variables. It is estimated that a similar analysis of a 4-legged table or n-legged table, by the same procedure will be very difficult. However, if an energy based approach such as PVW is used, the number of unknown variables reduces to 6 irrespectively of the number of legs of the table. This is because PVW requires the strain energy of the deformed table which may be expressed entirely in terms of displacement of the table and the spacing of the legs, thus eliminating the internal load variables. Furthermore, the derivation of the load displacement relations from the strain energy of the table is linear operation, making the complexity of the analysis exactly same for any n-legged table.

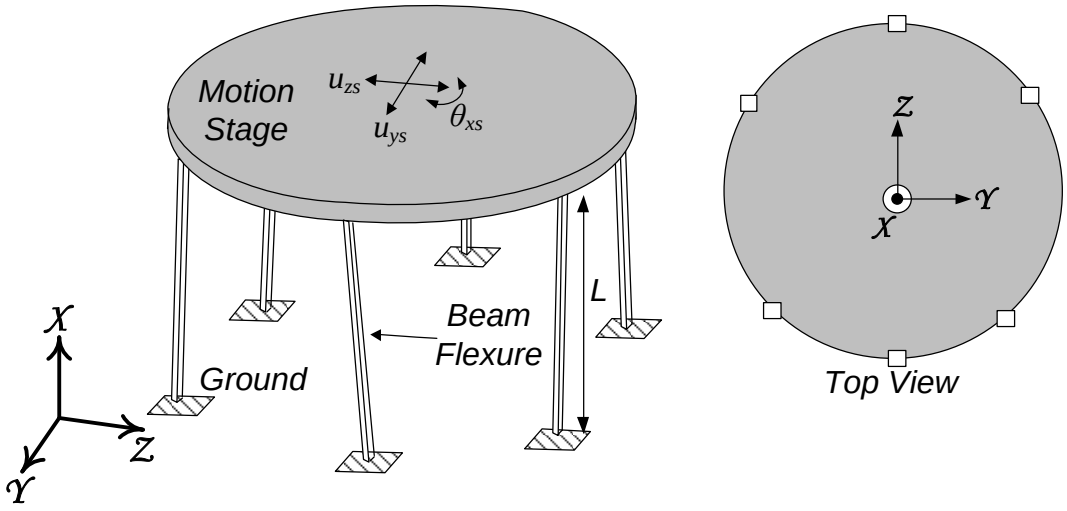

Figure 6.1: A 3-DoF Spatial Flexure Mechanism

Since the legs of the table may be tilted by design or due to manufacturing defects, we first derive the strain energy of symmetrical spatial beam with a small but otherwise arbitrary tilt in section 6.2. It should be noted that although a tilted spatial beam may be analyzed as a straight spatial beam by using an aligned local co-ordinate frame instead of the global co-ordinate frame, such a formulation leads to mathematical complexity when the local co-ordinate frame needs to be changed back to the global co-ordinate frame.

In order to provide additional designing flexibility, legs with spatial beam flexures with varying cross-section is also considered. By using the fundamental relations between the beam characteristic coefficients, shown in section 6.3, one may easily derive the strain energy of a non-prismatic straight spatial beam with a symmetric cross-section. This feature will allow the use of some typical beam shapes which has special characteristics. One example of such a beam is one that has a rigid section in the middle to change the distributed compliance of the beam to be lumped at the two corners [30]. Using the analysis of a tilted spatial beam and a non-prismatic spatial beam, a generalized n-legged table is analyzed in section 6.4. For verification, the analyses predictions for a 3-legged table with vertical legs are compared against the predictions of FEA. Finally, section 6.5 concludes this chapter with a brief discussion and future work.

6.2 Strain Energy Of A Bisymmetric Spatial Beam With Arbitrary Tilt

A slender beam with equal thickness along the two narrow dimensions and whose centroidal axis is not perfectly parallel with the X-axis of a reference co-ordinate frame X-Y-Z,

due to manufacturing/assembly defects or intentional design, is shown in Figure 6.2. The orientation of the undeformed beam may be described by rotating a beam, that is initially aligned with X, Y and Z, through a rotation of β about the Y axis and γ about the rotated Z axis. It is assumed that if the beam also has an initial twist α, the X-Y-Z co-ordinate axes is rotated by the same angle to align Y and Z with the principle axes of symmetry of the beam cross-section. After deformation, the arbitrary point P on the centroidal axis, translates U_X, U_Y and U_Z along the X, Y and Z axes respectively. To describe the orientation of the tangent of the centroidal axis at P, three Euler rotations, φ about the rotated Y axis followed by ψ about the rotated Z axis followed by Θ_{Xd} about the rotated X axis, is chosen. These three rotations occur after the rotation due to β and γ have taken place. These sequence of five rotations can also be approximately represented by three Euler rotations, φ-β about the rotated Y axis followed by $\psi+\gamma$ about the rotated Z axis followed by Θ_{Xd} about the rotated X axis as shown in Figure 6.2.

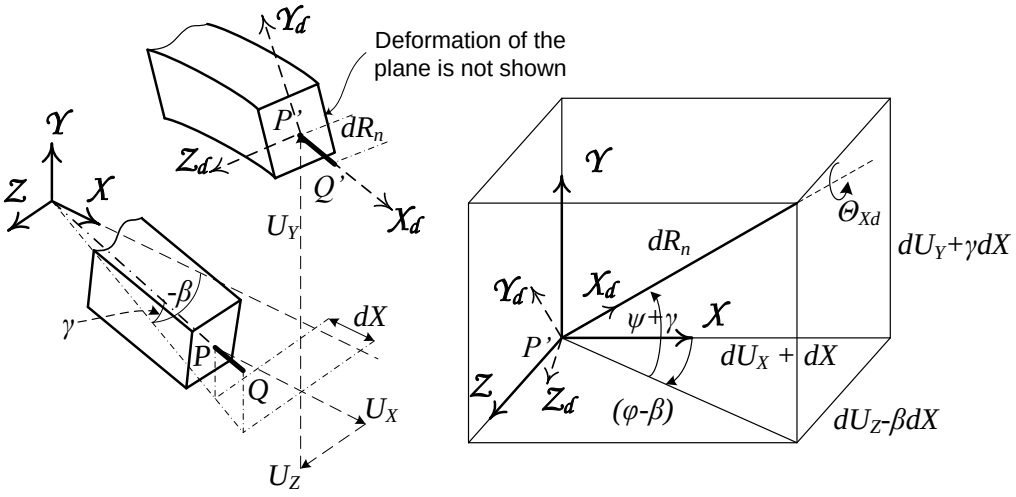

Figure 6.2: Tilted Spatial Beam deformation

The deformation any cross-section perpendicular to the undeformed centroidal axis is determined to be a rigid body translation and rotation followed by an out of plane warping. Using this deformation field, a new co-ordinate frame is defined in which X_d axis is defined along the tangent to the deformed centroidal axis while Y_d and Z_d are the axes of principle moment of area of the cross-section prior to warping. This deformation assumption is based on (i) Euler Bernoulli assumption which ignored shear effects due to shear forces $\boldsymbol{F_{YL}}$ and $\boldsymbol{F_{ZL}}$ in comparison to bending for slender beams with thickness/length ratio less than 1/20, and (ii) St.

Venant solution of slender prismatic beam that shows in-plane distortion to be absent. A more detailed analysis of the assumptions can be found the analysis of non-tilted uniform bisymmetric spatial beam in Chapter 5. Using this beam deformation, the strain at any general point before deformation with coordinate position (X, Y, Z) may be defined using Green's strain measure. Here $\vec{R}_0$ and $\vec{R}_d$ are the position vectors of this point before and after deformation.

$$d\vec{R}_d \bullet d\vec{R}_d - d\vec{R}_0 \bullet d\vec{R}_0 = 2\{dX \quad dY \quad dZ\}\begin{bmatrix} \varepsilon_{XX} & \varepsilon_{XY} & \varepsilon_{XZ} \\ \varepsilon_{YX} & \varepsilon_{YY} & \varepsilon_{YZ} \\ \varepsilon_{ZX} & \varepsilon_{ZY} & \varepsilon_{ZZ} \end{bmatrix}\begin{Bmatrix} dX \\ dY \\ dZ \end{Bmatrix} \tag{6.1}$$

Using Eq.(6.1), the final expression for non-linear strain, approximated to the second order, may be derived to be:

$$\varepsilon_{XX} \approx U'_X + \gamma U'_Y - \beta U'_Z + \frac{1}{2}U'^2_Y + \frac{1}{2}U'^2_Z - Y\kappa_{Zd} + Z\kappa_{Yd} + \frac{1}{2}\kappa_{Xd}{}^2\left(Y^2 + Z^2\right) \tag{6.2}$$

$$\gamma_{XY} \approx \kappa_{Xd}\left[Y - Y_W\right] \qquad \text{where } Y_W \triangleq \frac{d\lambda}{dZ} \tag{6.3}$$

$$\gamma_{XZ} \approx \kappa_{Xd}\left[Z - Z_W\right] \qquad \text{where } Z_W \triangleq \frac{d\lambda}{dY} \tag{6.4}$$

Points P and Q, the co-ordinates of which are (X, γX, βX) and ($X+dX$, $\gamma X+\gamma dX$, $\beta X+\beta dX$) respectively lie on the undeformed centroidal axis while points P' and Q', the coordinates of which are ($X+U_X$, $\gamma X+U_Y$, $\beta X+U_Z$) and ($X+dX+U_X+dU_X$, $\gamma X+\gamma dX+U_Y+dU_Y$, $\beta X+\beta dX+U_Z+dUZ$) respectively are the displaced position of P and Q before deformation due to out-of-plane warping. These co-ordinates maybe used to calculate the sides of cube shown in Figure 6.2 of which dR_n is the diagonal. The rate of twist angle, κ_{Xd}, and bending curvatures κ_{Yd} and κ_{Zd} can be expressed to the second order approximation, as follows:

$$\begin{aligned} &\kappa_{Xd} \approx \Theta'_{Xd} - U''_Z\left(U'_Y + \gamma\right); \qquad \kappa_{Yd} \approx \sin\left(\Theta_{Xd}\right)U''_Y - \cos\left(\Theta_{Xd}\right)U''_Z; \\ &\kappa_{Zd} \approx \cos\left(\Theta_{Xd}\right)U''_Y + \sin\left(\Theta_{Xd}\right)U''_Z \end{aligned} \tag{6.5}$$

The out-of-plane warping along X_d is estimated to be $\lambda \cdot \kappa_{Xd}$, where λ is a warping function dependent on only the local cross-sectional coordinates Y_d and Z_d and independent of coordinate X.

The strain energy for the initially tilted spatial beam flexure is expressed below by assuming linear material properties. It should be noted that for a slender beam stresses along Y

and Z axes may be approximated to be zero and hence strains ε_{YY} and ε_{ZZ} do not appear in the calculation of the strain energy.

$$V = \frac{E}{2}\int_{vol} \varepsilon_{xx}^2 dAdX + \frac{G}{2}\int_{vol} \left(\gamma_{xy}^2 + \gamma_{xz}^2\right) dAdX \tag{6.6}$$

This strain energy expression may be expanded using the strain expressions from Eqs.(6.2), (6.3) and (6.4) as follows:

$$\begin{aligned}
V = {} & \frac{E}{2}\int_{vol}\left(U_X' + \gamma U_Y' - \beta U_Z' + \frac{1}{2}U_Y'^2 + \frac{1}{2}U_Z'^2\right)^2 dAdX \\
& + \frac{E}{2}\int_{vol} 2\left(U_X' + \gamma U_Y' - \beta U_Z' + \frac{1}{2}U_Y'^2 + \frac{1}{2}U_Z'^2\right)\left(-Y\kappa_{Zd} + Z\kappa_{Yd}\right) dAdX \\
& + \frac{E}{2}\int_{vol}\left\{\kappa_{Xd}{}^2\left(Y^2 + Z^2\right)\right\}\left(-Y\kappa_{Zd} + Z\kappa_{Yd}\right) dAdX + \frac{E}{2}\int_{v}\left(-Y\kappa_{Zd} + Z\kappa_{Yd}\right)^2 dAdX \\
& + \frac{E}{2}\int_{vol}\left(U_X' + \gamma U_Y' - \beta U_Z' + \frac{1}{2}U_Y'^2 + \frac{1}{2}U_Z'^2\right)\left[\kappa_{Xd}{}^2\left(Y^2 + Z^2\right)\right] dAdX \\
& + \frac{E}{8}\int_{vol}\left\{\kappa_{Xd}{}^2\left(Y^2 + Z^2\right)\right\}^2 dAdX + \frac{G}{2}\int_{vol}\kappa_{Xd}{}^2\left\{\left(Y - Y_W\right)^2 + \left(Z - Z_W\right)^2\right\} dAdX \\
\triangleq {} & I_1 + I_2 + I_3 + I_4 + I_5 + I_6 + I_7
\end{aligned}$$

Several simplifications on the seven individual integrals, denoted by I_1 through I_7, can be done to simplify the strain energy, V. Of these, the integrals I_2 and I_3 are identically zero by the definition of the centroidal axis. For a slender beam with total twisting angle Θ_{Xd} limited to ±0.1, it may be shown that integral I_6 is at least four orders of magnitude smaller than integral I_1, and is therefore dropped. Next, the strain energy expression is simplified by recognizing that the beam curvatures, given in Eq.(6.5), are only dependent on the axial coordinate X. Thus, each volume integral can be decomposed into two integrals: a double integral over the cross-section and a single integral over X. This leads to:

$$V = \frac{EA}{2}\int_0^L \left(\bar{U}_X'\right)^2 dX \; + \; \frac{EI}{2}\int_0^L \left(U_Y''^2 + U_Z''^2\right) dX \; + \; EI\int_0^L \left(\bar{U}_X'\right)\kappa_{Xd}^2 dX \; + \; \frac{GJ}{2}\int_0^L \kappa_{Xd}^2 dX$$

$$\text{where} \quad \bar{U}_X' \triangleq U_X' + \gamma U_Y' - \beta U_Z' + \frac{1}{2}U_Y'^2 + \frac{1}{2}U_Z'^2, \quad \int_A Y^2 dA = \int_A Z^2 dA \triangleq I, \quad \int_A YZ dA = 0 \tag{6.7}$$

$$\int_A \left(Y^2 + Z^2\right) dA = 2I, \quad \int_A \left\{\left(Y - Y_W\right)^2 + \left(Z - Z_W\right)^2\right\} dA \triangleq J$$

Once the total strain energy for the spatial beam has been obtained, the Principle of Virtual Work (PVW) may be applied to generate the beam differential equations and boundary conditions.

U_X, U_Y, U_Z, Θ_{Xd}, U'_Y and U'_Z may be chosen as the six generalized coordinates which, along with their boundary conditions, completely define the deformation and strain energy of the beam.

$$\delta V = \delta I_1 + \delta I_4 + \delta I_5 + I_7 \tag{6.8}$$

The variation of the strain energy is expressed in terms of the six generalized virtual displacements δU_X, δU_Y, δU_Z, $\delta\Theta_{Xd}$, $\delta U'_Y$ and $\delta U'_Z$, all variables in the X coordinate, and their boundary values at the fixed and free ends of the beam.

At the fixed end, i.e., X = *0*

$$\delta U_X = 0;\ \delta U_Y = 0;\ \delta U_Z = 0;\ \delta\Theta_{Xd} = 0;\ \delta U'_Z = 0;\ \delta U'_Y = 0 \tag{6.9}$$

At the free end i.e. X = *L*

$$\delta U_X = \delta U_{XL};\ \delta U_Y = \delta U_{YL};\ \delta U_Z = \delta U_{ZL};\ \ \delta\Theta_{Xd} = \delta\Theta_{XdL};\ \delta U'_Z = \delta U'_{ZL};\ \delta U'_Y = \delta U'_{YL} \tag{6.10}$$

Next, the virtual work done by external loads $\boldsymbol{F_{XL}}$, $\boldsymbol{F_{YL}}$, $\boldsymbol{F_{ZL}}$, $\boldsymbol{M_{XL}}$, $\boldsymbol{M_{YL}}$ and $\boldsymbol{M_{ZL}}$ may be expressed as:

$$\delta W = \boldsymbol{F_{XL}}\delta U_{XL} + \boldsymbol{F_{YL}}\delta U_{YL} + \boldsymbol{F_{ZL}}\delta U_{ZL} + \boldsymbol{M_{XL}}\delta\Theta_{XL} + \boldsymbol{M_{YL}}\delta\Theta_{YL} + \boldsymbol{M_{ZL}}\delta\Theta_{ZL} \tag{6.11}$$

where δU_{XL}, δU_{YL}, δU_{ZL}, $\delta\Theta_{XL}$, $\delta\Theta_{YL}$ and $\delta\Theta_{ZL}$ represent a slightly different set of six independent virtual displacements at the beam end in the respective directions of the six external loads. These six virtual end-displacements have to be expressed in terms of the previous set of six virtual end-displacements that are used in the variation of the strain energy in Eq.(6.8) so that coefficients of the same virtual end-displacements on both sides of PVW may be equated. Specifically, this requires expressing virtual rotations $\delta\Theta_{XL}$, $\delta\Theta_{YL}$ and $\delta\Theta_{ZL}$ as functions of δU_{XL}, δU_{YL}, δU_{ZL}, $\delta\Theta_{XdL}$, $\delta U'_{YL}$ and $\delta U'_{ZL}$. Since virtual rotations can be chosen to be arbitrarily small, they can be represented as vectors. Therefore, the virtual rotations at the beam end may be expressed as variations of the corresponding Euler angles (Figure 6.2):

$$\delta\Theta_{XL}\hat{i}+\delta\Theta_{YL}\hat{j}+\delta\Theta_{ZL}\hat{k} = -\delta\varphi\hat{j}\Big|_L+\left\{\cos(\varphi-\beta)\hat{k}-\sin(\varphi-\beta)\hat{i}\right\}\delta\psi\Big|_L + \left\{\frac{1+U'_X}{1+\bar{U}'_X}\hat{i}+\frac{U'_Y+\gamma}{1+\bar{U}'_X}\hat{j}+\frac{U'_Z-\beta}{1+\bar{U}'_X}\hat{k}\right\}\delta\Theta_{Xd}\Big|_L \tag{6.12}$$

where $\delta\varphi=-\dfrac{\delta U'_Z}{1+U'_X}+\dfrac{(U'_Z-\beta)\delta U'_X}{(1+U'_X)^2}$

and $\delta\psi=\dfrac{\delta U'_Y}{1-\dfrac{\gamma^2}{2}+U'_X+\dfrac{1}{2}U'^2_Z-\beta U'_z}-\dfrac{(U'_Y+\gamma)\left(\delta U'_X+(U'_Z-\beta)\delta U'_Z\right)}{\left(1+U'_X+\dfrac{1}{2}U'^2_Z\right)^2}$

For the range of end displacements considered, $\bar{U}'_{XL}$, U'_{XL}, U'_{YL}, and U'_{ZL} are of the order of 10^{-3}, 10^{-2}, 10^{-1} and 10^{-1}, respectively. Therefore, second order approximations are made to simplify Eq.(6.12) to yield:

$$\begin{aligned}
\delta\Theta_{XL} &\approx \delta\Theta_{XdL}-(U'_{ZL}-\beta)\delta U'_{YL}+(U'_{ZL}-\beta)(U'_Y+\gamma)\left(\delta U'_{XL}+(U'_{ZL}-\beta)\delta U'_{ZL}\right)\\
\delta\Theta_{YL} &\approx -\delta U'_{ZL}+(U'_{ZL}-\beta)\delta U'_{XL}+(U'_Y+\gamma)\delta\Theta_{XdL}\\
\delta\Theta_{ZL} &\approx \delta U'_{YL}-(U'_Y+\gamma)\left(\delta U'_{XL}+(U'_{ZL}-\beta)\delta U'_{ZL}\right)+(U'_{ZL}-\beta)\delta\Theta_{XdL}
\end{aligned} \tag{6.13}$$

Using Eq.(6.13), the δW can be expressed in terms of $\delta U_{XL}, \delta U_{YL}, \delta U_{ZL}, \delta\Theta_{XdL}, \delta U'_{XL}, \delta U'_{YL}$ and $\delta U'_{ZL}$. The only remaining dependent displacement variable now is $\delta U'_{XL}$. Although its dependence on the other virtual displacements is not known at this stage, we know that it is mathematically independent of δU_{XL}. Therefore, the coefficients of δU_{XL} and δU_X on both sides of PVW can be respectively compared and equated.

$\left(EA\bar{U}'_X+EI\kappa^2_{Xd}\right)\Big|_L=\boldsymbol{F_{XL}}$, and $\left(EA\bar{U}'_X+EI\kappa^2_{Xd}\right)'=0$

These two relations imply that

$$EA\bar{U}'_X+EI\kappa^2_{Xd}=\text{constant}=\boldsymbol{F_{XL}} \tag{6.14}$$

This relation may now be used to derive the geometric dependence of U'_{XL} on the other displacement variables. Since $\dfrac{\partial\sigma_{YY}}{\partial Y}$ and $\dfrac{\partial\sigma_{YZ}}{\partial Z}$ are approximately zero due to the absence of lateral forces and in-plane distortion, respectively, $\dfrac{\partial\tau_{XY}}{\partial X}$ turns out to be zero from the elemental equilibrium condition in the Y direction:

$$\frac{\partial \tau_{YX}}{\partial X}+\frac{\partial \sigma_{YY}}{\partial Y}+\frac{\partial \tau_{YZ}}{\partial Z}=0 \;\Rightarrow\; \frac{\partial \tau_{YX}}{\partial X}=0 \;\Rightarrow\; G\left[Y-Y_W\right]\frac{\partial \kappa_{Xd}}{\partial X}=0 \tag{6.15}$$

Since κ_{Xd} remains constant with X it implies from Eq.(6.14) that $\bar{U}'_X$ also remains constant with X. This knowledge, along with the definition of $\bar{U}'_X$ in Eq., yields the following relation:

$$\delta U'_X=-\left(U'_Y+\gamma\right)\delta U'_Y-\left(U'_Z-\beta\right)\delta U'_Z \tag{6.16}$$

The value of $\delta U'_{XL}$ is now substituted back in Eq., which reduces to:

$$\begin{aligned}
\delta\Theta_{XL}&=\delta\Theta_{XdL}-\left(U'_{ZL}-\beta\right)\delta U'_{YL}\\
\delta\Theta_{YL}&=-\delta U'_{ZL}-\left(U'_Y+\gamma\right)\left(U'_{ZL}-\beta\right)\delta U'_{YL}+\left(U'_Y+\gamma\right)\delta\Theta_{XdL}\\
\delta\Theta_{ZL}&=\delta U'_{YL}+\left(U'_{ZL}-\beta\right)\delta\Theta_{XdL}
\end{aligned} \tag{6.17}$$

The geometric relations in Eq.(6.17) allows one to express all the terms on the right and left hand sides of PVW using the same set of six virtual end-displacements. Now, the respective coefficients of all the virtual displacements on both sides of this equation are compared and equated. Equating the coefficients of the remaining virtual displacements, δU_{YL}, δU_Y, δU_{ZL}, δU_Z, $\delta U'_{YL}$, $\delta U'_{ZL}$, $\delta\Theta_{Xd}$ and $\delta\Theta_{XdL}$, three more governing differential equations associated with bending in the XY and XZ planes and torsion are obtained, along with four natural boundary conditions at the beam end. The final set of beam governing equations and natural boundary conditions are given in Eq.(6.18) and Eq.(6.19) respectively.

$$\begin{aligned}
&EIU_Y^{iv}-\boldsymbol{F_{XL}}U''_Y+\boldsymbol{M_{XdL}}U'''_Z=0\\
&EIU_Z^{iv}-\boldsymbol{F_{XL}}U''_Z-\boldsymbol{M_{XdL}}U'''_Y=0\\
&U'_{XL}+\gamma U'_Y-\beta U'_Z+\frac{1}{2}U'^2_{YL}+\frac{1}{2}U'^2_{ZL}=\frac{\boldsymbol{F_{XL}}}{EA}-\frac{I}{A}\cdot\frac{\boldsymbol{M}^{\boldsymbol{2}}_{\boldsymbol{XdL}}}{G^2J^2}\\
&\Theta'_{Xd}-U''_Z\left(U'_Y+\gamma\right)=\frac{\boldsymbol{M_{XdL}}}{GJ}-\frac{2I\boldsymbol{M_{XdL}}\boldsymbol{F_{XL}}}{G^2J^2A}
\end{aligned} \tag{6.18}$$

$$\begin{aligned}
&\boldsymbol{F_{YL}}=\boldsymbol{F_{XL}}\left(U'_{YL}+\gamma\right)-EIU'''_{YL}-\boldsymbol{M_{XdL}}U''_{ZL}\\
&\boldsymbol{F_{ZL}}=\boldsymbol{F_{XL}}\left(U'_{ZL}-\beta\right)-EIU'''_{ZL}+\boldsymbol{M_{XdL}}U''_{YL}\\
&\boldsymbol{M_{YL}}=-EIU''_{ZL}+\boldsymbol{M_{XdL}}\left(U'_{YL}+\gamma\right)\\
&\boldsymbol{M_{ZL}}\approx EIU''_{YL}+\boldsymbol{M_{XdL}}\left(U'_{ZL}-\beta\right)
\end{aligned} \tag{6.19}$$

where $\boldsymbol{M_{XdL}}\triangleq\boldsymbol{M_{XL}}+\left(U'_{YL}+\gamma\right)\boldsymbol{M_{YL}}+\left(U'_{ZL}-\beta\right)\boldsymbol{M_{ZL}}$

Since $U'_{YL}+\gamma$ and $U'_{ZL}-\beta$ are approximately equal to rotations about Z and Y axes respectively, $\boldsymbol{M}_{XdL}$ is simply the equivalent torsional moment expressed along the deformed centroidal axis at the free end of the beam. The geometric boundary conditions are

$$U_Y(0)=0\ ;\ U_Z(0)=0\ ;\ U'_Y(0)=0\ ;\ U'_Z(0)=0$$

At this point in the analysis, all the loads and displacements are normalized per the following scheme to make the equations and results compact:

$$\boldsymbol{m}_{z1}\triangleq\frac{\boldsymbol{M}_{ZL}L}{EI},\quad \boldsymbol{m}_{y1}\triangleq\frac{\boldsymbol{M}_{YL}L}{EI},\quad \boldsymbol{m}_{xd1}\triangleq\frac{\boldsymbol{M}_{XdL}L}{EI},\quad \boldsymbol{f}_{z1}\triangleq\frac{\boldsymbol{F}_{ZL}L^2}{EI},\quad \boldsymbol{f}_{y1}\triangleq\frac{\boldsymbol{F}_{YL}L^2}{EI},\ \boldsymbol{f}_{x1}\triangleq\frac{\boldsymbol{F}_{XL}L^2}{EI},$$

$$v\triangleq\frac{VL}{EI},\ u_y\triangleq\frac{U_Y}{L},\ u_z\triangleq\frac{U_Z}{L},\ u_{y1}\triangleq\frac{U_{YL}}{L},\ u_{z1}\triangleq\frac{U_{ZL}}{L},\ x\triangleq\frac{X}{L},\ \theta_{xd}\triangleq\Theta_{Xd},\ \theta_{xd1}\triangleq\Theta_{XdL}$$

Based on the normalization scheme, the beam governing differential equations (6.18) and natural and geometric boundary conditions(6.19), can be normalized as follows.

$$\begin{aligned}
&u_y^{iv}-\boldsymbol{f}_{x1}u''_Y+\boldsymbol{m}_{xd1}u'''_z=0\\
&u_z^{iv}-\boldsymbol{f}_{x1}u''_Z-\boldsymbol{m}_{xd1}u'''_y=0\\
&u'_x+\gamma u'_y-\beta u'_z+\frac{1}{2}u'^2_y+\frac{1}{2}u'^2_z=\frac{\boldsymbol{f}_{x1}}{k_{33}}-\frac{2\boldsymbol{m}^2_{xd1}}{k_{33}k_{44}^2}\\
&\left\{\theta'_{xd}-u''_z\left(u'_y+\gamma\right)\right\}=\frac{\boldsymbol{m}_{xd1}}{k_{44}}-\frac{2\boldsymbol{m}_{xd1}\boldsymbol{f}_{x1}}{k_{33}k_{44}^2}
\end{aligned}\qquad(6.20)$$

where, $k_{33}\triangleq\frac{12L^2}{T_Y^2},\quad k_{44}\triangleq\frac{GJ}{EI},\quad \boldsymbol{m}_{xd1}\triangleq\boldsymbol{m}_{x1}+\left(u'_y+\gamma\right)\boldsymbol{m}_{y1}+\left(u'_{z1}-\beta\right)\boldsymbol{m}_{z1}$

$$\begin{aligned}
&\boldsymbol{f}_{y1}=\boldsymbol{f}_{x1}\left(u'_y+\gamma\right)-u'''_{y1}-\boldsymbol{m}_{xd1}u''_{z1};\qquad \boldsymbol{f}_{z1}=\boldsymbol{f}_{x1}\left(u'_{z1}-\beta\right)-u'''_{z1}+\boldsymbol{m}_{xd1}u''_{y1}\\
&\boldsymbol{m}_{y1}=-u''_{z1}+\boldsymbol{m}_{xd1}\left(u'_y+\gamma\right);\qquad \boldsymbol{m}_{z1}=u''_{y1}+\boldsymbol{m}_{xd1}\left(u'_{z1}-\beta\right)\\
&u_y(0)=0\ ;\ u_z(0)=0\ ;\ u'_y(0)=0\ ;\ u'_z(0)=0
\end{aligned}\qquad(6.21)$$

The strain energy expression may be further simplified using Eqs.(6.20) and can be stated compactly as follows after normalization:

$$v=\frac{1}{2}\int_0^1\left(u''^2_y+u''^2_z\right)dx+\frac{\boldsymbol{m}^2_{xd1}}{2k_{44}}+\frac{\boldsymbol{f}^2_{x1}}{2k_{33}}-\frac{2\boldsymbol{m}^2_{xd1}\boldsymbol{f}_{x1}}{k_{33}k_{44}^2}\qquad(6.22)$$

Although capturing the various non-linear coupling effects renders the governing equations of extension and torsion non-linear, the bending equations are still linear and albeit coupled in U_Y and U_Z. This allows the first two equations of Eq. (6.20), along with associated

boundary conditions , to be solved using linear algebra techniques and then the results can be substituted in last two equations of Eq. (6.20) to solve for U_X and θ_{Xd}, which provide the two geometric constraint conditions. The results may also be substituted in the strain energy term.

To express this result in a form that is mathematically concise and provides insight into the geometric effects and non-linearities that are relevant to constraint characterization, we carry out a Taylor series expansion of the solution of $\boldsymbol{f_{y1}}$, $\boldsymbol{f_{z1}}$, $\boldsymbol{m_{y1}}$, and $\boldsymbol{m_{z1}}$ in terms of the axial and torsional loads, $\boldsymbol{f_{x1}}$ and $\boldsymbol{m_{xd1}}$ and drop third and higher power terms. Since the co-efficients of $\boldsymbol{f_{x1}}$ and $\boldsymbol{m_{xd1}}$ diminish quickly with increasing powers, the truncation results in less 1% error in the displacement and load range of interest. Similarly Taylor series expansion of the solutions of $\boldsymbol{u_{x1}}$ and $\boldsymbol{\theta_{xd1}}$ in term of $\boldsymbol{f_{x1}}$ and $\boldsymbol{m_{xd1}}$ are carried out and second and higher power terms are dropped. Error due to truncation in this case is less than 5% for $\boldsymbol{f_{x1}}$ and $\boldsymbol{m_{xd1}}$ less than 5.

$$\{\boldsymbol{l_b}\} = [H_1]\{d_b\} + \boldsymbol{m_{xd1}}\{0 \quad -\beta \quad 0 \quad \gamma\}^T + \boldsymbol{f_{x1}}\{\gamma \quad 0 \quad -\beta \quad 0\}^T$$
$$-\left(2\boldsymbol{f_{x1}}[H_2] + \boldsymbol{m_{xd1}}\left(2[H_3] + [H_7]\right)\right)\{d_b\} - \left(\boldsymbol{f_{x1}^2}[H_4] + \boldsymbol{m_{xd1}}\boldsymbol{f_{x1}}[H_5] + \boldsymbol{m_{xd1}^2}[H_6]\right)\{d_b\} \quad (6.23)$$

$$u_{x1} = \frac{\boldsymbol{f_{x1}}}{k_{33}} - \frac{\boldsymbol{m_{xd1}^2}}{k_{44}^2 k_{33}} + \{d_b\}^T[H_2]\{d_b\} - \gamma u_{y1} + \beta u_{z1} + \{d_b\}^T\left(\boldsymbol{f_{x1}}[H_4] + \frac{1}{2}\boldsymbol{m_{xd1}}[H_5]\right)\{d_b\} \quad (6.24)$$

$$\theta_{xd1} = \frac{\boldsymbol{m_{xd1}}}{k_{44}} - \frac{2\boldsymbol{m_{xd1}}\boldsymbol{f_{x1}}}{k_{33}k_{44}^2} + \{d_b\}^T[H_3]\{d_b\} + u'_{z1}\gamma + \{d_b\}^T\left(\boldsymbol{m_{xd1}}[H_6] + \frac{1}{2}\boldsymbol{f_{x1}}[H_5]\right)\{d_b\} \quad (6.25)$$

$$v = \frac{\boldsymbol{m_{xd1}^2}}{2k_{44}} + \frac{\boldsymbol{f_{x1}^2}}{2k_{33}} - \frac{2\boldsymbol{m_{xd1}^2}\boldsymbol{f_{x1}}}{k_{33}k_{44}^2} + \frac{1}{2}\{d_b\}^T\left([H_1] + \frac{\boldsymbol{f_{x1}^2}}{2}[H_4] + \frac{\boldsymbol{m_{xd1}}\boldsymbol{f_{x1}}}{2}[H_5] + \frac{\boldsymbol{m_{xd1}^2}}{2}[H_6]\right)\{d_b\} \quad (6.26)$$

where

$$\{\boldsymbol{l_b}\} \triangleq \{\boldsymbol{f_{y1}} \quad \boldsymbol{m_{z1}} \quad \boldsymbol{f_{z1}} \quad \boldsymbol{m_{y1}}\}^T, \qquad \{d_b\} \triangleq \{u_{y1} \quad u'_{y1} \quad u_{z1} \quad -u'_{z1}\}^T$$

$$[H_1] \triangleq \begin{bmatrix} 12 & -6 & 0 & 0 \\ -6 & 4 & 0 & 0 \\ 0 & 0 & 12 & 6 \\ 0 & 0 & 6 & 4 \end{bmatrix}, \quad [H_2] \triangleq \begin{bmatrix} -\frac{3}{5} & \frac{1}{20} & 0 & 0 \\ \frac{1}{20} & -\frac{1}{15} & 0 & 0 \\ 0 & 0 & -\frac{3}{5} & -\frac{1}{20} \\ 0 & 0 & -\frac{1}{20} & -\frac{1}{15} \end{bmatrix}, \quad [H_3] \triangleq \frac{1}{4}\begin{bmatrix} 0 & 0 & 0 & -2 \\ 0 & 0 & -2 & -1 \\ 0 & -2 & 0 & 0 \\ -2 & -1 & 0 & 0 \end{bmatrix}$$

$$[H_4] \triangleq \begin{bmatrix} \frac{1}{700} & -\frac{1}{1400} & 0 & 0 \\ -\frac{1}{1400} & \frac{11}{6300} & 0 & 0 \\ 0 & 0 & \frac{1}{700} & \frac{1}{1400} \\ 0 & 0 & \frac{1}{1400} & \frac{11}{6300} \end{bmatrix}, \quad [H_5] \triangleq \frac{1}{60}\begin{bmatrix} 0 & 0 & 0 & 1 \\ 0 & 0 & 1 & 0 \\ 0 & 1 & 0 & 0 \\ 1 & 0 & 0 & 0 \end{bmatrix}, \quad [H_6] \triangleq \frac{1}{20}\begin{bmatrix} 4 & -2 & 0 & 0 \\ -2 & 1 & 0 & 0 \\ 0 & 0 & 4 & 2 \\ 0 & 0 & 2 & 1 \end{bmatrix}$$

$$[H_7] \triangleq \begin{bmatrix} 0 & 0 & 0 & 0 \\ 0 & 0 & 0 & 1 \\ 0 & 0 & 0 & 0 \\ 0 & 0 & 0 & 0 \end{bmatrix}$$

All nonlinear effects, that are significant when the translational and angular displacement range of the beam end is limited to 0.1L and 0.1 radians, respectively, are captured in Eqs. (6.23) -(6.26). Equation(6.23), known as transverse load-displacement relation, expresses bending loads $\{\boldsymbol{l_b}\}$ as a product of bending stiffness values and bending displacement [23]. It should be noted that $-u'_{z1}$ and u_{y1} may be approximated as the rotational displacements θ_{y1} and θ_{z1}.

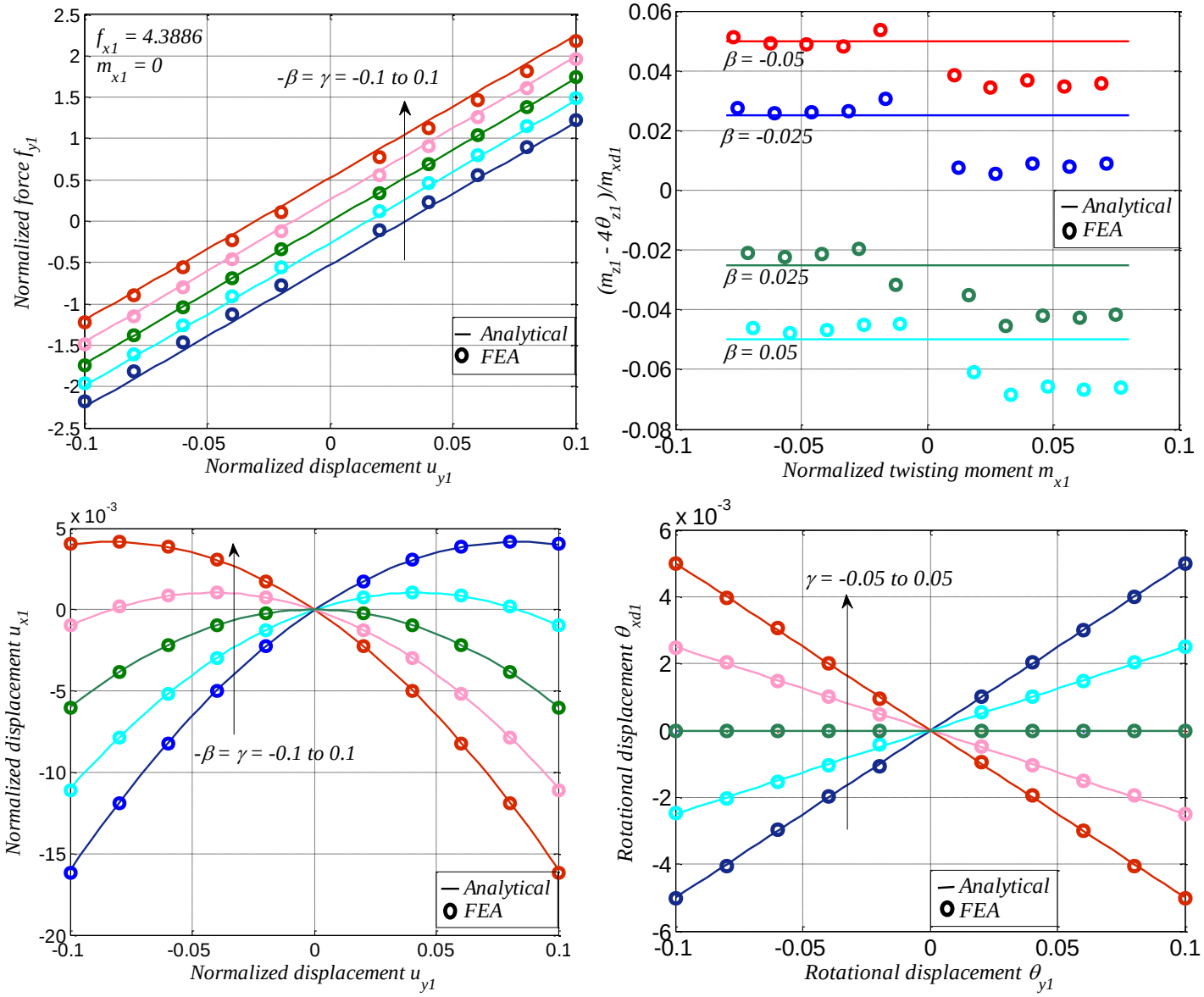

Figure 6.3:(i) Normalized force f_{y1} vs normalized displacement u_{y1} for varying tilt angle β and γ (ii) Normalized $(m_{z1}-4\theta_{z1})/m_{xd1}$ vs normalized moment m_{x1} at θ_{y1}=0 and θ_{z1}=0.02 radians for varying tilt angle β (iii) Normalized displacement u_{x1} vs normalized displacement u_{y1} for varying β and γ (iv) Rotational displacement θ_{xd1} vs Rotational displacement θ_{y1} for varying γ

The first and second powers of $\boldsymbol{f_{x1}}$ and $\boldsymbol{m_{xd1}}$ in the bending stiffness values parametrically capture the variation in bending stiffnesses due to axial loads. In particular, the stiffness terms with single power of $\boldsymbol{f_{x1}}$ and $\boldsymbol{m_{xd1}}$ are a result of the geometric arc length conservation and are call load stiffening terms. The terms quadratic in $\boldsymbol{f_{x1}}$ and $\boldsymbol{m_{xd1}}$ are relatively less significant than the load stiffening terms but are retained to maintain truncation consistency with Eqs.(6.24)

and(6.25). Due to the tilt the load displacement curves shift while maintaining the stiffness values. This curve shift is more significant for the transverse force ($\boldsymbol{f_{y1}}$ or $\boldsymbol{f_{z1}}$) vs transverse displacement (u_{y1} or u_{z1}) as shown in Figure 6.3(i). For the transverse moment vs. transverse rotation curve, the shifts due to tilt angles β and γ (i.e. $-\boldsymbol{m_{xd1}}\theta_{y1}$ in $\boldsymbol{m_{y1}}$ vs. θ_{y1}, and $-\boldsymbol{m_{xd1}}\theta_{z1}$ in $\boldsymbol{m_{z1}}$ vs. θ_{z1}) are much smaller due to the limited range of θ_{y1} and θ_{z1}. However, this shift becomes crucial for an accurate determination of bending moments, $\boldsymbol{m_{y1}}$ and $\boldsymbol{m_{z1}}$, at small bending angles. For a small angle, θ_{z1} = 0.02 rad, Figure 6.3(ii) plots this curve shift divided by $\boldsymbol{m_{xd1}}$ for varying $\boldsymbol{m_{x1}}$. Noticeable fluctuations are seen in the FEA validation results, indicating that this term is of the order of other second approximations made during model derivation.

Equation (6.24), which quantifies the axial displacement u_{x1}, is known as a constraint equation because of the inherit high stiffness in the axial stretching direction with respect to the bending direction. The first two terms in Eq. (6.24) represent the elastic stretching of the beam due to $\boldsymbol{f_{x1}}$ and $\boldsymbol{m_{xd1}}$. The stretching due to $\boldsymbol{m_{xd1}}$ is the well-known trapeze effect which occurs due to the addition axial stresses developed during torsion by unequal contraction of fibers parallel to but at different distance from the centroidal axis of the beam. The third term in Eq. (6.24), that is dependent only on transverse displacements due to bending, [23], represents the shortening of the projection of the beam on the X-axis due to the geometric arc length conservation. The fourth and the fifth terms represent additional kinematic relation between the bending displacements and axial displacement u_{x1}. This kinematic behavior is shown in Figure 6.3(iii). Essentially due to the tilt, the parabola u_{x1} vs u_{y1} gets shift vertically as well as horizontally. The fourth term in Eq. (6.24), which is dependent on both displacements [23] and loads, $\boldsymbol{f_{x1}}$ and $\boldsymbol{m_{xd1}}$, represents a variation in the amount of shortening of the projection of the beam on the X-axis as $\boldsymbol{f_{x1}}$ and $\boldsymbol{m_{xd1}}$ change the shape of a bent beam by producing additional bending moments. From a different point of view, this term quantifies the softening of the stiffness in X direction of a bent beam with respect to a straight beam. Since this term is non-zero only in the presence of both loads and displacements, it is called an elastokinematic effect. It should be noted that tilt angles β and γ have no significant impact on the axial stiffness.

Equation (6.25) parametrically quantifies the dependence of the twist θ_{xd1} on the axial and torsional loads $\boldsymbol{f_{x1}}$ and $\boldsymbol{m_{xd1}}$ and transverse bending displacements [23]. Similar to Eq.(6.24), elastic, kinematic/geometric and elastokinematic terms are present. The only difference is that the trapeze effect can only vary stiffness rather than produce an independent twist displacement

as in the case of Eq. (6.24). Tilt angle γ give rise to an additional kinematic dependence of twist θ_{xd1} on bending displacements [23]. This relation is verified using FEA in Figure 6.3(iv). It is not surprising that tilt angle β does not affect twist θ_{xd1}, because the definition of the Euler angles itself introduces non-symmetry in the problem. Because of the mathematical similarity with Eq.(6.24), Eq. (6.25) will be also called a constraint equation in spite of having a relatively low stiffness.

Equation (6.26) represents the total strain energy stored in the beam due to end displacements [23], u_{x1} and θ_{xd1}. The first third terms really functions of displacement, they are written in terms of axial loads, $\boldsymbol{f}_{x1}$ and $\boldsymbol{m}_{xd1}$, for the convenience of representation. Terms with single powers of $\boldsymbol{f}_{x1}$ and $\boldsymbol{m}_{xd1}$ in Eq.(6.23) -(6.25) are all kinematic effect and hence have no contribution to the strain energy. However, the strain energy due to elastokinematic terms are captured in the terms with quadratic powers $\boldsymbol{f}_{x1}$ and $\boldsymbol{m}_{xd1}$. It should be noted that there is no term of α, β and γ in the strain energy because they represent the undeformed state, rather than any deformation.

6.3 Fundamental Relations Between Beam Characteristic Coefficients

We proceed to show that the format of Eqs. (5.27)- (5.30) accommodates any general beam shape and not just a uniform-thickness beam. The beam deformation, end loading, and end displacement representations for the variable cross-section beam remain the same as in Figure 5.6. The modeling assumptions are also the same as earlier, except that the beam thickness in Y and Z direction is now a function of X: $T_Y = T_Z = T(X) = T_0\xi(X)$, where T_0 is the nominal beam thickness at the beam root and $\xi(X)$ represents the beam shape variation. Thus, the second moment of area becomes $I_{YY}(X) = I_{ZZ}(X) = I_0\xi^4(X)$. Similarly the area and the torsion constant become $A_0\xi^2(X)$ and $J_0\xi^4(X)$ respectively. The normalization scheme remains the same as earlier, with the exception that I_0 is now used in place of I. Following a PVW procedure analogous to the one outlined in Sec. 2, one may derive the following normalized governing equations and natural boundary conditions for this case:

$$\left\{\xi^4(x)u_y''\right\}'' - \boldsymbol{f}_{x1}u_y'' + \boldsymbol{m}_{xd1}u_z''' = 0; \qquad \left\{\xi^4(x)u_z''\right\}'' - \boldsymbol{f}_{x1}u_z'' - \boldsymbol{m}_{xd1}u_y''' = 0 \tag{6.27}$$

$$u_x' + \frac{1}{2}u_y'^2 + \frac{1}{2}u_z'^2 = \frac{\boldsymbol{f}_{x1}}{k_{33}\xi^2(x)} - \frac{\boldsymbol{m}_{xd1}^2}{k_{33}k_{44}^2\xi^6(x)}; \quad \theta_{xd}' - u_z''\,u_y' \approx \frac{\boldsymbol{m}_{xd1}}{k_{44}\xi^4(x)} - \frac{2\boldsymbol{m}_{xd1}\boldsymbol{f}_{x1}}{k_{33}k_{44}^2\xi^6(x)} \tag{6.28}$$

$$\begin{aligned}
&\boldsymbol{f}_{y1} = \boldsymbol{f}_{x1}u'_{y1} - \xi^4(x)u'''_{y1} - \boldsymbol{m}_{xd1}u''_{z1}; \quad \boldsymbol{f}_{z1} = \boldsymbol{f}_{x1}u'_{z1} - \xi^4(x)u'''_{z1} + \boldsymbol{m}_{xd1}u''_{y1} \\
&\boldsymbol{m}_{y1} = -\xi^4(x)u''_{z1} + \boldsymbol{m}_{xd1}u'_{y1}; \quad \boldsymbol{m}_{z1} = \xi^4(x)u''_{y1} + \boldsymbol{m}_{xd1}u'_{z1}
\end{aligned} \tag{6.29}$$

Given the arbitrary choice of $\xi(X)$, a closed-form solution to this ordinary differential equation with variable coefficients (Eq.(6.27)) is no longer possible. Nevertheless, the equation and associated boundary conditions remain linear in the transverse loads $(\boldsymbol{F}_{YL}, \boldsymbol{F}_{ZL}, \boldsymbol{M}_{YL}, \text{ and } \boldsymbol{M}_{ZL})$ and transverse displacements (U_{YL} and U_{ZL} and its derivatives). This implies that the resulting normalized relation between the transverse end loads and end displacement also has to be linear, of the form

$$\{\boldsymbol{l}_b\} = \left[k\left(\boldsymbol{f}_{x1}; \boldsymbol{m}_{xd1}; \xi(x)\right)\right]\{d_b\} \qquad \text{where } [k] = \begin{bmatrix} k_{11} & k_{12} & k_{13} & k_{14} \\ k_{21} & k_{22} & k_{23} & k_{24} \\ k_{31} & k_{32} & k_{33} & k_{34} \\ k_{41} & k_{42} & k_{43} & k_{44} \end{bmatrix}$$

The effective stiffness terms (k's) will now be some functions of the axial loads $\boldsymbol{f}_{x1}$ and $\boldsymbol{m}_{xd1}$, dictated by the beam shape $\xi(X)$ and might be difficult or impossible to determine in closed form. Nevertheless, these functions may certainly be expanded as a generic infinite series in $\boldsymbol{f}_{x1}$ and $\boldsymbol{m}_{xd1}$,

$$\begin{aligned}
\{\boldsymbol{l}_b\} = &\begin{bmatrix} k_{11}^{(0,0)} & k_{12}^{(0,0)} & k_{13}^{(0,0)} & k_{14}^{(0,0)} \\ k_{21}^{(0,0)} & k_{22}^{(0,0)} & k_{23}^{(0,0)} & k_{24}^{(0,0)} \\ k_{31}^{(0,0)} & k_{32}^{(0,0)} & k_{33}^{(0,0)} & k_{34}^{(0,0)} \\ k_{41}^{(0,0)} & k_{42}^{(0,0)} & k_{43}^{(0,0)} & k_{44}^{(0,0)} \end{bmatrix}\{d_b\} + \boldsymbol{f}_{x1}\begin{bmatrix} k_{11}^{(1,0)} & k_{12}^{(1,0)} & k_{13}^{(1,0)} & k_{14}^{(1,0)} \\ k_{21}^{(1,0)} & k_{22}^{(1,0)} & k_{23}^{(1,0)} & k_{24}^{(1,0)} \\ k_{31}^{(1,0)} & k_{32}^{(1,0)} & k_{33}^{(1,0)} & k_{34}^{(1,0)} \\ k_{41}^{(1,0)} & k_{42}^{(1,0)} & k_{43}^{(1,0)} & k_{44}^{(1,0)} \end{bmatrix}\{d_b\} \\
&+ \boldsymbol{m}_{xd1}\begin{bmatrix} k_{11}^{(0,1)} & k_{12}^{(0,1)} & k_{13}^{(0,1)} & k_{14}^{(0,1)} \\ k_{21}^{(0,1)} & k_{22}^{(0,1)} & k_{23}^{(0,1)} & k_{24}^{(0,1)} \\ k_{31}^{(0,1)} & k_{32}^{(0,1)} & k_{33}^{(0,1)} & k_{34}^{(0,1)} \\ k_{41}^{(0,1)} & k_{42}^{(0,1)} & k_{43}^{(0,1)} & k_{44}^{(0,1)} \end{bmatrix}\{d_b\} + \ldots = \sum_{n=0}^{\infty}\sum_{i=0}^{n} \boldsymbol{f}_{x1}^{n-i}\boldsymbol{m}_{xd1}^{i}\left[k^{(n-i,i)}\right]\{d_b\}
\end{aligned} \tag{6.30}$$

Similarly, it may be shown that irrespective of the beam shape, solution to the constraint equations (6.28) will be quadratic in [23] and therefore may be expanded as

$$u_{x1} = \frac{\boldsymbol{f}_{x1}}{k_{33}}\int_0^1 \frac{dx}{\xi^2(x)} - \frac{\boldsymbol{m}_{xd1}^2}{k_{44}^2 k_{33}}\int_0^1 \frac{dx}{\xi^6(x)} + \sum_{n=0}^{\infty}\sum_{i=0}^{n} \boldsymbol{f}_{x1}^{n-i}\boldsymbol{m}_{x1}^{i}\{d_b\}^T\left[g^{(n-i,i)}\right]\{d_b\} \tag{6.31}$$

$$\theta_{xd1} = \frac{\boldsymbol{m}_{xd1}}{k_{44}}\int_0^1 \frac{dx}{\xi^4(x)} - \frac{2\boldsymbol{m}_{xd1}\boldsymbol{f}_{x1}}{k_{33}k_{44}^2}\int_0^1 \frac{dx}{\xi^6(x)} + \sum_{n=0}^{\infty}\sum_{i=0}^{n} \boldsymbol{f}_{x1}^{n-i}\boldsymbol{m}_{x1}^{i}\{d_b\}^T\left[e^{(n-i,i)}\right]\{d_b\} \tag{6.32}$$

Here $[g^{(n-i,i)}]$ and $[e^{(n-i,i)}]$ are 4×4 matrices similar to $[k^{(n-i,i)}]$.

Along the same lines, the strain energy for a variable cross-section beam may be shown to be quadratic in the transverse displacements u_{y1}, u_{z1}, θ_{y1} and θ_{z1}, and some unknown function of the loads $\boldsymbol{f_{x1}}$ and $\boldsymbol{m_{xd1}}$. This expression may be expanded as follows:

$$v = \frac{\boldsymbol{m}_{xd1}^2}{2k_{44}}\int_0^1 \frac{dx}{\xi^4(x)} + \frac{\boldsymbol{f}_{x1}^2}{2k_{33}}\int_0^1 \frac{dx}{\xi^2(x)} - \frac{2\boldsymbol{m}_{xd1}^2\boldsymbol{f}_{x1}}{k_{33}k_{44}^2}\int_0^1 \frac{dx}{\xi^6(x)} + \frac{1}{2}\sum_{n=0}^{\infty}\sum_{i=0}^{n} \boldsymbol{f}_{x1}^{n-i}\boldsymbol{m}_{xd1}^{i}\{d_b\}^T\left[v^{(n-i,i)}\right]\{d_b\} \quad (6.33)$$

The 4×4 matrices in equations (6.30) - (6.33), $[k^{(n-i,i)}]$, $[g^{(n-i,i)}]$, $[e^{(n-i,i)}]$ and $[v^{(n-i,i)}]$, are constants dependent only on the shape of the beam, that is on $\xi(X)$, but independent of loads and end-displacements. Here on they will be referred to as beam characteristic coefficients.

The first three terms of Eq.(6.33) represent the energy due to elastic stretching and elastic twisting given by the first two terms of Eqs.(6.31) and (6.32). Although these energy terms should ideally be represented using displacement variables, in this case there are expressed in terms of loads for simplicity of representation. The fourth term in Eq. (6.33) represents the energy due to bending. Ideally this energy term should consist of only bending displacements, [23]. However, due to geometric nonlinearity, the actual beam shape is dependent on the axial loads $\boldsymbol{f_{x1}}$ and $\boldsymbol{m_{xd1}}$. As a result, $\boldsymbol{f_{x1}}$ and $\boldsymbol{m_{xd1}}$ appear in strain energy due to bending, as parameters in the same capacity as beam shape parameters and beam characteristic coefficients.

Next, we take a variation of the strain energy, keeping in mind that as loads are kept constant while virtual displacements are applied. Therefore, the loads $\boldsymbol{f_{x1}}$ and $\boldsymbol{m_{xd1}}$ in the strain energy due to bending do not produce $\delta\boldsymbol{f_{x1}}$ and $\delta\boldsymbol{m_{xd1}}$. On the other hand, since $\boldsymbol{f_{x1}}$ and $\boldsymbol{m_{xd1}}$ in the stretching and twisting energy terms are representative of displacements u_{x1} and θ_{xd1}, $\delta\boldsymbol{f_{x1}}$ and $\delta\boldsymbol{m_{xd1}}$ is retained from these terms. Next, PVW is applied in order to relate [k] matrices of the load displacement relation to the [g], [e] and [v] matrices of the constraint relations and strain energy expression.

The PVW for the normalized displacement co-ordinates of δu_{x1}, δu_{y1}, δu_{z1}, $\delta\theta_{xd1}$, $\delta u'_{y1}$ and $\delta u'_{z1}$ and normalized loads $\boldsymbol{f_{x1}}$, $\boldsymbol{f_{y1}}$, $\boldsymbol{f_{z1}}$, $\boldsymbol{m_{xd1}}$, $\boldsymbol{m_{y1}}$ and $\boldsymbol{m_{z1}}$ can be obtained using Eq.(6.13) by setting the tilt angles β and γ as zero.

$$\delta v = \boldsymbol{f_{x1}}\delta u_{x1} + \boldsymbol{f_{y1}}\delta u_{y1} + \boldsymbol{f_{z1}}\delta u_{z1} + \boldsymbol{m_{xd1}}\delta\theta_{xd1} - \boldsymbol{m_{y1}}\delta u'_{z1} + \left(\boldsymbol{m_{z1}} - \boldsymbol{m_{xd1}}u'_{z1}\right)\delta u'_{y1} \quad (6.34)$$

Comparing coefficients between the right and left hand sides of the above equation, the relations between [k], [g], [e] and [v] are found to be as follows:

$$
\begin{aligned}
&\left[k^{(0,0)}\right]=\left[v^{(0,0)}\right] \\
&\left[k^{(a,0)}\right]=\left[v^{(a,0)}\right]-2\left[g^{(a-1,0)}\right] && \forall\ a=1,2,3,.... \\
&\left[k^{(0,1)}\right]+\left[H_7\right]=\left[v^{(0,1)}\right]-2\left[e^{(0,0)}\right] && (6.35) \\
&\left[k^{(0,b)}\right]=\left[v^{(0,b)}\right]-2\left[e^{(0,b-1)}\right] && \forall\ b=2,3,.... \\
&\left[k^{(a,b)}\right]=\left[v^{(a,b)}\right]-2\left[g^{(a-1,b)}\right]-2\left[e^{(a,b-1)}\right] && \forall\ a,b=1,2,3,....
\end{aligned}
$$

The above relations may be readily verified for the case of a simple spatial beam using known results; however, it should be noted that these are valid for any general beam shape, as proven above.

Using conservation of energy yet another fundamental relation between the beam characteristic coefficients can be found. Since a given set of end loads $\boldsymbol{f_{x1}}$, $\boldsymbol{f_{y1}}$, $\boldsymbol{f_{z1}}$, $\boldsymbol{m_{xd1}}$, $\boldsymbol{m_{y1}}$ and $\boldsymbol{m_{z1}}$ produces a unique set of end displacements u_{x1}, u_{y1}, u_{z1}, θ_{xd1}, u'_{y1} and u'_{z1}, the resulting strain energy stored in the deformed beam remains the same irrespective of the order in which the loading is carried out. Therefore, we consider a case where the loading is performed in three steps: (1) End loads $\bar{\boldsymbol{f}}_{\boldsymbol{y1}}$, $\bar{\boldsymbol{f}}_{\boldsymbol{z1}}$, $\bar{\boldsymbol{m}}_{\boldsymbol{y1}}$ and $\bar{\boldsymbol{m}}_{\boldsymbol{z1}}$ are applied to produce end-displacements $\bar{u}_{x1}, u_{y1}, u_{z1}, \bar{\theta}_{xd1}, u'_{z1}$, and u'_{y1}. (2) While holding the end displacements u_{y1}, u_{z1}, u'_{z1}, and u'_{y1} fixed, end load $\boldsymbol{f_{x1}}$ is applied to change the axial displacement from $\bar{u}_{x1}$ to $\bar{\bar{u}}_{x1}$. Due to $\boldsymbol{f_{x1}}$, $\bar{\theta}_{xd1}$ changes to $\bar{\bar{\theta}}_{xd1}$. (3) While holding the end displacements u_{y1}, u_{z1}, u'_{z1}, and u'_{y1} and end load $\boldsymbol{f_{x1}}$ fixed, end load $\boldsymbol{m_{xd1}}$ is applied to change the axial displacement from $\bar{\bar{\theta}}_{xd1}$ to θ_{xd1}. Due to end load $\boldsymbol{m_{xd1}}$, end displacement $\bar{\bar{u}}_{x1}$ changes to u_{x1}. Also, with $\boldsymbol{f_{x1}}$ and $\boldsymbol{m_{xd1}}$ applied end loads $\bar{\boldsymbol{f}}_{\boldsymbol{y1}}$, $\bar{\boldsymbol{f}}_{\boldsymbol{z1}}$, $\bar{\boldsymbol{m}}_{\boldsymbol{y1}}$ and $\bar{\boldsymbol{m}}_{\boldsymbol{z1}}$ will change to $\boldsymbol{f_{y1}}$, $\boldsymbol{f_{z1}}$, $\boldsymbol{m_{y1}}$ and $\boldsymbol{m_{z1}}$ in order to maintain u_{y1}, u_{z1}, u'_{z1}, and u'_{y1}.

The sum of energy added to the beam in these three steps should be equal to the final strain energy given by Eq. (6.33). Energy stored in step 1 is simply obtained by setting $\boldsymbol{f_{x1}}$ and $\boldsymbol{m_{xd1}}$=0 in Eq.(6.33).

$$v_1=\frac{1}{2}\{d_b\}^T\left[v^{(0,0)}\right]\{d_b\} \tag{6.36}$$

The axial displacement and rotation at the end of step 1 is given by

$$\bar{u}_{x1}=\{d_b\}^T\left[g^{(0,0)}\right]\{d_b\} \tag{6.37}$$

$$\bar{\theta}_{xd1} = \{d_b\}^T \left[e^{(0,0)} \right] \{d_b\} \tag{6.38}$$

Next, assuming a conservative system, the energy added to the beam in step 2 may simply be determined by calculating the work done on the system when force $\boldsymbol{f_{x1}}$ causes the beam end to move from $\bar{u}_{x1}$ to $\bar{\bar{u}}_{x1}$ in the axial direction. End-displacement $\bar{\bar{u}}_{x1}$ can be easily calculated by setting $\boldsymbol{m_{xd1}}$=0 in Eq.(6.31).

$$\bar{\bar{u}}_{x1} = \frac{\boldsymbol{f_{x1}}}{k_{33}} \int_0^1 \frac{dx}{\xi^2(x)} + \sum_{n=0}^{\infty} \boldsymbol{f}_{\boldsymbol{x1}}^n \{d_b\}^T \left[g^{(n,0)} \right] \{d_b\} \tag{6.39}$$

An integral needs to be carried out since the relation between $\boldsymbol{f_{x1}}$ and u_{x1} is nonlinear. However, since inverting Eq.(6.39), which provides displacement in terms of force, is not trivial, determining the work done in this fashion is difficult if not impossible. Therefore, instead we choose to determine the complementary energy, which is readily derived using Eq.(6.37) and(6.39):

$$v_2^*(\boldsymbol{f_{x1}}) = \int_0^{f_{x1}} (\bar{\bar{u}}_{x1} - \bar{u}_{x1}) . d\boldsymbol{f_{x1}} \tag{6.40}$$

This result is then used to calculate the strain energy stored in the beam during step 2 as follows:

$$\begin{aligned} v_2(\boldsymbol{f_{x1}}) &= (\bar{\bar{u}}_{x1} - \bar{u}_{x1}) . \boldsymbol{f_{x1}} - v_2^*(\boldsymbol{f_{x1}}) \\ &= \boldsymbol{f_{x1}} \frac{\boldsymbol{f_{x1}}}{k_{33}} \int_0^1 \frac{dx}{\xi^2(x)} + \boldsymbol{f_{x1}} \sum_{n=1}^{\infty} \boldsymbol{f}_{\boldsymbol{x1}}^n \{d_b\}^T \left[g^{(n,0)} \right] \{d_b\} - \int_0^{f_{x1}} \left\{ \frac{\boldsymbol{f_{x1}}}{k_{33}} \int_0^1 \frac{dx}{\xi^2(x)} + \sum_{n=1}^{\infty} \boldsymbol{f}_{\boldsymbol{x1}}^n \{d_b\}^T \left[g^{(n,0)} \right] \{d_b\} \right\} . d\boldsymbol{f_{x1}} \\ &= \frac{\boldsymbol{f}_{\boldsymbol{x1}}^2}{k_{33}} \int_0^1 \frac{dx}{\xi^2(x)} + \sum_{n=1}^{\infty} \boldsymbol{f}_{\boldsymbol{x1}}^{n+1} \{d_b\}^T \left[g^{(n,0)} \right] \{d_b\} - \frac{\boldsymbol{f}_{\boldsymbol{x1}}^2}{2k_{33}} \int_0^1 \frac{dx}{\xi^2(x)} - \sum_{n=1}^{\infty} \frac{\boldsymbol{f}_{\boldsymbol{x1}}^{n+1}}{n+1} \{d_b\}^T \left[g^{(n,0)} \right] \{d_b\} \\ &= \frac{\boldsymbol{f}_{\boldsymbol{x1}}^2}{2k_{33}} \int_0^1 \frac{dx}{\xi^2(x)} + \sum_{n=1}^{\infty} \frac{n\boldsymbol{f}_{\boldsymbol{x1}}^{n+1}}{n+1} \{d_b\}^T \left[g^{(n,0)} \right] \{d_b\} = \frac{\boldsymbol{f}_{\boldsymbol{x1}}^2}{2k_{33}} \int_0^1 \frac{dx}{\xi^2(x)} + \sum_{n=0}^{\infty} \frac{(n-1)\boldsymbol{f}_{\boldsymbol{x1}}^n}{n} \{d_b\}^T \left[g^{(n-1,0)} \right] \{d_b\} \end{aligned}$$

The twisting angle $\bar{\bar{\theta}}_{xd1}$ can be calculated by setting $\boldsymbol{m_{xd1}}$=0 in Eq.(6.32).

$$\bar{\bar{\theta}}_{xd1} = \sum_{n=0}^{\infty} \boldsymbol{f}_{\boldsymbol{x1}}^n \{d_b\}^T \left[g^{(n,0)} \right] \{d_b\} \tag{6.41}$$

Next, the energy added to the beam in step 3 may simply be determined by calculating the sum of work done on the system when moment $\boldsymbol{m_{xd1}}$ causes the beam end to twist from $\bar{\bar{\theta}}_{xd1}$ to θ_{xd1}, denoted as $v_{31}(\boldsymbol{m_{xd1}})$, and work done when the beam end moves $\bar{\bar{u}}_{x1}$ to u_{x1} against

constant force $\boldsymbol{f_{x1}}$, denoted as $v_{32}\left(\boldsymbol{m_{xd1}}\right)$. The first term, $v_{31}\left(\boldsymbol{m_{xd1}}\right)$, is calculated in the same way as done in step 2.

$$
\begin{aligned}
v_{31}\left(\boldsymbol{m_{xd1}}\right) &= \left(\theta_{xd1} - \bar{\bar{\theta}}_{xd1}\right).\boldsymbol{m_{xd1}} - v_3^*\left(\boldsymbol{m_{xd1}}\right) \\
&= \frac{\boldsymbol{m}_{xd1}^2}{k_{44}}\int_0^1 \frac{dx}{\xi^4(x)} - \frac{2\boldsymbol{m}_{xd1}^2\boldsymbol{f}_{x1}}{k_{33}k_{44}^2}\int_0^1 \frac{dx}{\xi^6(x)} + \sum_{n=0}^{\infty}\sum_{i=1}^{n} \boldsymbol{f}_{x1}^{n-i}\boldsymbol{m}_{x1}^{i+1}\{d_b\}^T\left[e^{(n-i,i)}\right]\{d_b\} \\
&\quad - \int_0^{\boldsymbol{m}_{xd1}} \left\{ \frac{\boldsymbol{m}_{xd1}}{k_{44}}\int_0^1 \frac{dx}{\xi^4(x)} - \frac{2\boldsymbol{m}_{xd1}\boldsymbol{f}_{x1}}{k_{33}k_{44}^2}\int_0^1 \frac{dx}{\xi^6(x)} + \sum_{n=0}^{\infty}\sum_{i=1}^{n} \boldsymbol{f}_{x1}^{n-i}\boldsymbol{m}_{x1}^{i}\{d_b\}^T\left[e^{(n-i,i)}\right]\{d_b\} \right\}.d\boldsymbol{m}_{xd1} \\
&= \frac{\boldsymbol{m}_{xd1}^2}{2k_{44}}\int_0^1 \frac{dx}{\xi^4(x)} - \frac{\boldsymbol{m}_{xd1}^2\boldsymbol{f}_{x1}}{k_{33}k_{44}^2}\int_0^1 \frac{dx}{\xi^6(x)} + \sum_{n=0}^{\infty}\sum_{i=1}^{n} \frac{i\boldsymbol{f}_{x1}^{n-i}\boldsymbol{m}_{x1}^{i+1}}{i+1}\{d_b\}^T\left[e^{(n-i,i)}\right]\{d_b\}
\end{aligned}
\tag{6.42}
$$

The second portion energy term $v_{32}\left(\boldsymbol{m_{xd1}}\right)$ in step 3 is given by

$$
v_{32}\left(\boldsymbol{f_{x1}}\right) = \left(u_{x1} - \bar{\bar{u}}_{xd1}\right).\boldsymbol{f_{x1}} = -\frac{\boldsymbol{m}_{xd1}^2\boldsymbol{f}_{x1}}{k_{44}^2k_{33}}\int_0^1 \frac{dx}{\xi^6(x)} + \sum_{n=0}^{\infty}\sum_{i=1}^{n} \boldsymbol{f}_{x1}^{n-i+1}\boldsymbol{m}_{x1}^{i}\{d_b\}^T\left[g^{(n-i,i)}\right]\{d_b\} \tag{6.43}
$$

Therefore the total strain energy in the beam due to the application of $\boldsymbol{f_{x1}}$, $\boldsymbol{f_{y1}}$, $\boldsymbol{f_{z1}}$, $\boldsymbol{m_{x1}}$, $\boldsymbol{m_{y1}}$ and $\boldsymbol{m_{z1}}$ resulting in end displacements, u_{x1}, u_{y1}, u_{z1}, θ_{xd1}, u'_{y1} and u'_{z1}, calculated using step 1, 2 and 3 is

$$
\begin{aligned}
v &= \frac{\boldsymbol{f}_{x1}^2}{2k_{33}}\int_0^1 \frac{dx}{\xi^2(x)} + \frac{\boldsymbol{m}_{xd1}^2}{2k_{44}}\int_0^1 \frac{dx}{\xi^4(x)} - \frac{2\boldsymbol{m}_{xd1}^2\boldsymbol{f}_{x1}}{k_{33}k_{44}^2}\int_0^1 \frac{dx}{\xi^6(x)} + \frac{1}{2}\{d_b\}^T\left[v^{(0,0)}\right]\{d_b\} \\
&\quad + \sum_{n=1}^{\infty}\frac{(n-1)\,\boldsymbol{f}_{x1}^n}{n}\{d_b\}^T\left[g^{(n-1,0)}\right]\{d_b\} + \sum_{n=1}^{\infty}\sum_{i=1}^{n}\frac{i\boldsymbol{f}_{x1}^{n-i}\boldsymbol{m}_{x1}^{i+1}}{i+1}\{d_b\}^T\left[e^{(n-i,i)}\right]\{d_b\} \\
&\quad + \sum_{n=1}^{\infty}\sum_{i=1}^{n} \boldsymbol{f}_{x1}^{n-i+1}\boldsymbol{m}_{x1}^{i}\{d_b\}^T\left[g^{(n-i,i)}\right]\{d_b\}
\end{aligned}
\tag{6.44}
$$

Comparing Eqs.(6.33) and (6.44), we obtain the following relations between the beam characteristic equations.

$$
\begin{aligned}
&\frac{1}{2}\left[v^{(a,0)}\right] = \frac{a-1}{a}\left[g^{(a-1,0)}\right] \qquad \forall\ a = 1,2,3,.. \\
&\frac{1}{2}\left[v^{(0,b)}\right] = \frac{b-1}{b}\left[e^{(0,b-1)}\right] \qquad \forall\ \mathrm{b} = 1,2,3,.. \\
&\frac{1}{2}\left[v^{(a,b)}\right] = \left[g^{(a-1,b)}\right] + \frac{b-1}{b}\left[e^{(a,b-1)}\right] \qquad \forall\ a,b = 1,2,3,..
\end{aligned}
\tag{6.45}
$$

Alternatively the conservation of energy could have also been applied while interchanging steps 2 and 3. In that case the u_{x1} and θ_{xd1} displacement at the end of steps 2 would have been as follows:

$$\overline{\overline{\overline{u}}}_{x1} = -\frac{\boldsymbol{m}_{xd1}^{2}}{k_{44}^{2}k_{33}}\int_{0}^{1}\frac{dx}{\xi^{6}(x)} + \sum_{n=0}^{\infty}\boldsymbol{m}_{x1}^{n}\{d_b\}^{T}\left[g^{(0,n)}\right]\{d_b\} \tag{6.46}$$

$$\overline{\overline{\overline{\theta}}}_{xd1} = \frac{\boldsymbol{m}_{xd1}}{k_{44}}\int_{0}^{1}\frac{dx}{\xi^{4}(x)} + \sum_{n=0}^{\infty}\boldsymbol{m}_{x1}^{n}\{d_b\}^{T}\left[e^{(0,n)}\right]\{d_b\} \tag{6.47}$$

The total strain energy in this case will be

$$\begin{aligned} v = {} & \frac{\boldsymbol{f}_{x1}^{2}}{2k_{33}}\int_{0}^{1}\frac{dx}{\xi^{2}(x)} + \frac{\boldsymbol{m}_{xd1}^{2}}{2k_{44}}\int_{0}^{1}\frac{dx}{\xi^{4}(x)} - \frac{2\boldsymbol{m}_{xd1}^{2}\boldsymbol{f}_{x1}}{k_{33}k_{44}^{2}}\int_{0}^{1}\frac{dx}{\xi^{6}(x)} + \frac{1}{2}\{d_b\}^{T}\left[v^{(0,0)}\right]\{d_b\} + \sum_{n=1}^{\infty}\frac{n\boldsymbol{m}_{xd1}^{n+1}}{n+1}\{d_b\}^{T}\left[e^{(0,n)}\right]\{d_b\} \\ & + \sum_{n=0}^{\infty}\sum_{i=0}^{n-1}\frac{(n-i)\,\boldsymbol{f}_{x1}^{n-i+1}\boldsymbol{m}_{xd1}^{i}}{n-i+1}\{d_b\}^{T}\left[g^{(n-i,i)}\right]\{d_b\} + \sum_{n=0}^{\infty}\sum_{i=0}^{n-1}\boldsymbol{f}_{x1}^{n-i}\boldsymbol{m}_{xd1}^{i+1}\{d_b\}^{T}\left[e^{(n-i,i)}\right]\{d_b\} \end{aligned} \tag{6.48}$$

Comparing Eqs. (6.33) and (6.48), we obtain the following relations between the beam characteristic equations.

$$\begin{aligned} &\frac{1}{2}\left[v^{(a,0)}\right] = \frac{a-1}{a}\left[g^{(a-1,0)}\right] \qquad \forall\ a = 1,2,3,.. \\ &\frac{1}{2}\left[v^{(0,b)}\right] = \frac{b-1}{b}\left[e^{(0,b-1)}\right] \qquad \forall\ \mathrm{b} = 1,2,3,.. \\ &\frac{1}{2}\left[v^{(a,b)}\right] = \left[e^{(a,b-1)}\right] + \frac{a-1}{a}\left[g^{(a-1,b)}\right] \qquad \forall\ a,b = 1,2,3,.. \end{aligned} \tag{6.49}$$

Equations (6.45) and (6.49) has to be identical. This implies the following relation must exist between the [e] and [g] matrices.

$$\frac{1}{b}\left[e^{(a,b-1)}\right] = \frac{1}{a}\left[g^{(a-1,b)}\right] \qquad \forall\ a,b = 1,2,3,.. \tag{6.50}$$

Equation (6.50) physically means that when $\boldsymbol{f}_{x1}$ and $\boldsymbol{m}_{xd1}$ are applied together on the spatial beam, the work done by $\boldsymbol{f}_{x1}$ due to the u_x displacement produced by $\boldsymbol{m}_{xd1}$ is equal to the work done by $\boldsymbol{m}_{xd1}$ due to the θ_{xd1} displacement produced by $\boldsymbol{f}_{x1}$. This is nothing but manifestation Maxwell's reciprocity theorem.

Using Eqs. (6.35), (6.45) and (6.50) matrices [$g^{(a,b)}$], [$e^{(a,b)}$] and [$v^{(a,b)}$] can be expressed in terms of [$k^{(a,b)}$].

$$
\begin{aligned}
&\left[v^{(a,b)}\right]=(1-a-b)\left[k^{(a,b)}\right] \qquad \forall\ a,b=0,1,2,3,....\\
&\left[g^{(a,b)}\right]=-\frac{a+1}{2}\left[k^{(a+1,b)}\right] \qquad \forall\ a,b=0,1,2,3,....\\
&\left[e^{(a,b)}\right]=-\frac{b+1}{2}\left[k^{(a,b+1)}\right] \qquad \forall\ a,b=0,1,2,3,.... \text{ except } a=b=0\\
&\left[e^{(0,0)}\right]=-\frac{1}{2}\left(\left[k^{(0,1)}\right]+\left[H_7\right]\right)
\end{aligned}
\tag{6.51}
$$

Equation (6.51) forms the fundamental relations between the beam characteristic coefficients and shows that all the beam characteristic coefficients can be easily obtained from the solution of the bending load displacement equation, Eq.(6.30). Therefore for any beam shape, as long as it is slender and its cross-section is bisymmetric, one only needs to solve the differential equation related to bending, Eq.(6.27), which is relatively easier than having to solve the torsion and the axial extension equation as well.

The formulation of an initially tilted spatial beam flexure and variable cross-section spatial beam flexure can be combined, by noticing that the effect of the initial tilt is purely geometric in nature. As a result, the tilt angles β and γ, do not appear in the strain energy expression, Eq.(6.26). Therefore the load displacement and constraint relation for a tilt spatial beam with variable but bisymmetric cross-section can be written as:

$$
\{\boldsymbol{l_b}\}=\sum_{n=0}^{\infty}\sum_{i=0}^{n}\boldsymbol{f}_{x1}^{\,n-i}\boldsymbol{m}_{xd1}^{\,i}\left[k^{(n-i,i)}\right]\{d_b\}+\boldsymbol{m}_{xd1}\{0\quad -\beta\quad 0\quad \gamma\}^T+\boldsymbol{f}_{x1}\{\gamma\quad 0\quad -\beta\quad 0\}^T \tag{6.52}
$$

$$
u_{x1}=-\gamma u_{y1}+\beta u_{z1}+\frac{\boldsymbol{f}_{x1}}{k_{33}}\int_0^1\frac{dx}{\xi^2(x)}-\frac{\boldsymbol{m}_{xd1}^{\boldsymbol{2}}}{k_{44}^2k_{33}}\int_0^1\frac{dx}{\xi^6(x)}-\sum_{n=0}^{\infty}\sum_{i=0}^{n}\frac{n-i+1}{2}\boldsymbol{f}_{x1}^{\,n-i}\boldsymbol{m}_{x1}^{\,i}\{d_b\}^T\left[k^{(n-i+1,i)}\right]\{d_b\} \tag{6.53}
$$

$$
\begin{aligned}
\theta_{xd1}=u_{z1}'\gamma&+\frac{\boldsymbol{m}_{xd1}}{k_{44}}\int_0^1\frac{dx}{\xi^4(x)}-\frac{2\boldsymbol{m}_{xd1}\boldsymbol{f}_{x1}}{k_{33}k_{44}^2}\int_0^1\frac{dx}{\xi^6(x)}-\frac{1}{2}\{d_b\}^T\left[H_7\right]\{d_b\}\\
&-\sum_{n=0}^{\infty}\sum_{i=0}^{n}\frac{i+1}{2}\boldsymbol{f}_{x1}^{\,n-i}\boldsymbol{m}_{x1}^{\,i}\{d_b\}^T\left[k^{(n-i,i+1)}\right]\{d_b\}
\end{aligned}
\tag{6.54}
$$

The corresponding strain energy is

$$
\begin{aligned}
v=&\frac{\boldsymbol{m}_{xd1}^{\boldsymbol{2}}}{2k_{44}}\int_0^1\frac{dx}{\xi^4(x)}+\frac{\boldsymbol{f}_{x1}^{\boldsymbol{2}}}{2k_{33}}\int_0^1\frac{dx}{\xi^2(x)}-\frac{2\boldsymbol{m}_{xd1}^{\boldsymbol{2}}\boldsymbol{f}_{x1}}{k_{33}k_{44}^2}\int_0^1\frac{dx}{\xi^6(x)}+\frac{1}{2}\{d_b\}^T\left[k^{(0,0)}\right]\{d_b\}\\
&+\frac{1}{2}\sum_{n=1}^{\infty}\sum_{i=0}^{n}(1-n-2i)\,\boldsymbol{f}_{x1}^{\,n-i}\boldsymbol{m}_{xd1}^{\,i}\{d_b\}^T\left[k^{(n-i,i)}\right]\{d_b\}
\end{aligned}
\tag{6.55}
$$

6.4 Case-Study: Multi-Beam Table Flexure Mechanism

In this section, using the strain energy of the initially-tilted, general shaped, spatial beam flexure derived in the previous section in terms of its end displacements, the principle of virtual work will be used to formulate the parametric closed-form nonlinear load-displacement relations of an n-legged table flexure mechanism, shown in Figure 6.1. An initially horizontal rigid stage is connected to the ground via identical beams, not necessarily uniform in thickness or perfectly parallel, numbered 1 through *n*. The location of the i^{th} beam is given by the normalized (with respect to *L*) co-ordinates (y_i, z_i) in the X-Y-Z co-ordinate system shown in Figure 6.1. Using the same co-ordinate system, the final normalized displacement of the motion stage is described by $\{u_{xs},\ u_{ys},\ u_{zs},\ \theta_{xs},\ \theta_{ys}$ and $\theta_{zs}\}$. Preliminary FEA experiments show that for the normalized planar translation and rotation of *0.1* and *0.1* radians, respectively, out of plane translation u_{xs} is of the order of 0.01 primarily cause by geometric arc length conservation while the out-of-plane rotations, θ_{ys} and θ_{zs}, are of the order of 0.001 when 3 or more beams are used. The out-of-plane rotations depend on the rotations of the individual beam flexures as well as the axial stretching of the beam flexures due to elastic and elastokinematic effect. From preliminary FEA experiments, the stiffness of rotation about the X axis is found to increase in a quadratic manner as the spacing between the beams increase. In this case, the maximum distance between any two beams in the YZ plane which is assumed to be no greater than the length of the beam. This ensures a reasonably low stiffness of rotation about the X axis. Also for simplicity, it is assumed that each of the principle axes of moment of area of all the cross-sections align with the global coordinate axis. If this was not the case, the kinematic relation between the displacement of the stage and displacement of each beam flexure would be slightly different, requiring coordinate transformations. Although, such a case can be readily dealt with a few additional mathematical steps, it is not considered here.

In the displacement range of interest, the individual end displacement of each beam can be approximately expressed in terms of the stage displacement as given in Eq.(6.56). The kinematics of the problem constrains the rotation of all the beams to be equal to that of the motion stage.

$$u_{x,i} \approx u_{xs} - y_i\left(\theta_{zs} - \theta_{xs}\theta_{ys}\right) + z_i\left(\theta_{ys} + \theta_{xs}\theta_{zs}\right), \qquad u_{y,i} \approx u_{ys} - \frac{1}{2}y_i\theta_{xs}^2 - z_i\theta_{xs},$$
$$u_{z,i} \approx u_{zs} - \frac{1}{2}z_i\theta_{xs}^2 + y_i\theta_{xs}, \qquad \theta_{x,i} = \theta_{xs},\ \theta_{y,i} = \theta_{ys},\ \theta_{z,i} = \theta_{zs} \tag{6.56}$$

The truncated strain energy and constraint equations of the tilted spatial beam model, used in this case, are given in Eq.(6.57)-(6.59). The trapeze effect is dropped here assuming that $\boldsymbol{f_{xs}}$ is of the same order as the $\boldsymbol{f_{ys}}$ needed to produce a u_{ys} of 0.1, and $\boldsymbol{m_{xs}}$ in limited to a value corresponding to a θ_{xs} value of 0.1. Furthermore the terms with product of $\boldsymbol{f_{x1}}$ and $\boldsymbol{m_{xd1}}$ have also small coefficients and are dropped in this analysis. Finally elastokinematic effect in torsion is dropped because the torsional stiffness of the stage is dominated by the elastic torsional stiffness and spacing of the beams. This model captures the linear elastic effect, and the nonlinear kinematic and elastokinematic effects in the respective axial stretching directions of all the individual beams.

$$v_i = \frac{\boldsymbol{m_{xd1,i}^2}}{2k_{44}^e} + \frac{\boldsymbol{f_{x1,i}^2}}{2k_{33}^e} + \frac{1}{2}\left\{d_{b,i}\right\}^T\left[k^{(0,0)}\right]\left\{d_{b,i}\right\} - \frac{1}{2}\boldsymbol{f_{x1}^2}\left\{d_{b,i}\right\}^T\left[k^{(2,0)}\right]\left\{d_{b,i}\right\} \tag{6.57}$$

$$u_{x1,i} = -\gamma_i u_{y1,i} + \beta_i u_{z1,i} + \frac{\boldsymbol{f_{x1,i}}}{k_{33}^e} - \frac{1}{2}\left\{d_{b,i}\right\}^T\left[k^{(1,0)}\right]\left\{d_{b,i}\right\} - \boldsymbol{f_{x1,i}}\left\{d_{b,i}\right\}^T\left[k^{(2,0)}\right]\left\{d_{b,i}\right\} \tag{6.58}$$

$$\theta_{xd1,i} = -\theta_{y,i}\gamma_i + \frac{\boldsymbol{m_{xd1,i}}}{k_{44}^e} - \frac{1}{2}\left\{d_{b,i}\right\}^T\left(\left[k^{(0,1)}\right] + \left[H_7\right]\right)\left\{d_{b,i}\right\} \tag{6.59}$$

where $k_{33}^e \triangleq \dfrac{k_{33}}{\int_0^1 \dfrac{dx}{\xi^2(x)}}$, $k_{44}^e \triangleq \dfrac{k_{44}}{\int_0^1 \dfrac{dx}{\xi^4(x)}}$, $\left\{d_{b,i}\right\} \triangleq \left\{u_{y1,i} \quad \theta_{z1,i} \quad u_{z1,i} \quad \theta_{y1,i}\right\}^T$

The values of $\boldsymbol{f_{x,i}}$ and $\boldsymbol{m_{xd,i}}$ are solved from Eq.(6.58) and (6.59) and substituted in the strain energy expression given in Eq.(6.57). The total strain energy, obtained by summing the strain energy for all the beams, is given below in terms of the displacements of the rigid stage.

$$v = \sum_i v_i = \frac{1}{2}\sum_i \left\{d_{b,i}\right\}^T\left[k^{0,0}\right]\left\{d_{b,i}\right\} + \frac{1}{2}\sum_i \frac{\left\{u_{x,i} + \gamma_i u_{y,i} - \beta_i u_{z,i} + \frac{1}{2}\left\{d_{b,i}\right\}^T\left[k^{1,0}\right]\left\{d_{b,i}\right\}\right\}^2}{\left(\frac{1}{k_{33}^e} - \left\{d_{b,i}\right\}^T\left[k^{2,0}\right]\left\{d_{b,i}\right\}\right)}$$
$$+ \frac{1}{2}k_{44}^e\sum_i\left\{\theta_{xds} + \gamma_i\theta_{ys} + \frac{1}{2}\left\{d_{b,i}\right\}^T\left(\left[k^{0,1}\right] + \left[H_7\right]\right)\left\{d_{b,i}\right\}\right\}^2 \tag{6.60}$$

The principle of virtual work applied to the multi-beam table flexure system, may be stated as:

$$\delta v = \boldsymbol{f_{xs}}\delta u_{xs} + \boldsymbol{f_{ys}}\delta u_{ys} + \boldsymbol{f_{zs}}\delta u_{zs} + \boldsymbol{m_{xds}}\delta\theta_{xds} + \boldsymbol{m_{ys}}\delta\theta_{ys} + \left(\boldsymbol{m_{zs}} + \boldsymbol{m_{xds}}\theta_{ys}\right)\delta\theta_{zs} \tag{6.61}$$

where $\boldsymbol{m_{xds}} \triangleq \boldsymbol{m_{xs}} + \theta_{zs}\boldsymbol{m_{ys}} - \theta_{ys}\boldsymbol{m_{zs}}$

The virtual displacements δu_{xs}, δu_{ys}, δu_{zs}, $\delta\theta_{xds}$, $\delta\theta_{ys}$, $\delta\theta_{zs}$ are arbitrary quantities and hence their respective coefficients from both sides of Eq.(6.61) should be identical.

Using the above relations the force displacement relations can be derived and are as follows:

$$\begin{Bmatrix} \boldsymbol{f_{ys}} \\ \boldsymbol{m_{zs}} \\ \boldsymbol{f_{zs}} \\ \boldsymbol{m_{ys}} \end{Bmatrix} = \left(n\left[k^{0,0}\right] + \left[k^{1,0}\right]\boldsymbol{f_{xs}} - \boldsymbol{m_{xds}}\left[H_7\right]\right)\left\{d_{b,s}\right\} + n\sum_i\left[k^{0,0}\right]\left\{r_i\right\} + \sum_i\left[k^{1,0}\right]\frac{\left\{a_i\right\}}{\left\{b_i\right\}}\left\{r_i\right\}$$

$$+\sum_i\left[k^{2,0}\right]\frac{\left\{a_i\right\}^2}{\left\{b_i\right\}^2}\left(\left\{d_{b,s}\right\}+\left\{r_i\right\}\right) + k_{44}^e\sum_i\left(\left[k^{0,1}\right]+\left[H_7\right]\right)\left\{c_i\right\}\left(\left\{d_{b,s}\right\}+\left\{r_i\right\}\right) + \begin{Bmatrix} \sum_i\frac{\left\{a_i\right\}\gamma_i}{\left\{b_i\right\}} \\ \sum_i\frac{\left\{a_i\right\}\left(-y_i+\theta_{xs}z_i\right)}{\left\{b_i\right\}} \\ -\sum_i\frac{\left\{a_i\right\}\beta_i}{\left\{b_i\right\}} \\ \sum_i\gamma_i\left\{c_i\right\}+\frac{\left\{a_i\right\}\left(z_i+\theta_{xs}y_i\right)}{\left\{b_i\right\}} \end{Bmatrix}$$

(6.62)

$$\boldsymbol{f_{xs}} = \sum_i\frac{\left\{a_i\right\}}{\left\{b_i\right\}} \tag{6.63}$$

$$\begin{aligned}\boldsymbol{m_{xds}} = {} & k_{44}^e\sum_i\left\{c_i\right\}\left[1+\left\{s_i\right\}\left(\left[k^{0,1}\right]+\left[H_7\right]\right)\left(\left\{d_{b,s}\right\}+\left\{r_i\right\}\right)\right] + \sum_i\left\{s_i\right\}\left[k^{0,0}\right]\left(\left\{d_{b,s}\right\}+\left\{r_i\right\}\right) \\ & + \sum_i\frac{\left\{a_i\right\}}{\left\{b_i\right\}}\left[y_i\theta_{ys}+z_i\theta_{zs}+\left\{s_i\right\}\left[k^{1,0}\right]\left(\left\{d_{b,s}\right\}+\left\{r_i\right\}\right)-\gamma_i\left(y_i\theta_{xs}+z_i\right)+\beta_i\left(z_i\theta_{xs}-y_i\right)\right] \\ & + \sum_i\frac{\left\{a_i\right\}^2}{\left\{b_i\right\}^2}\left\{s_i\right\}\left[k^{2,0}\right]\left(\left\{d_{b,s}\right\}+\left\{r_i\right\}\right)\end{aligned} \tag{6.64}$$

where $\{d_{b,s}\} \triangleq \{u_{ys} \quad \theta_{zs} \quad u_{zs} \quad \theta_{ys}\}^T$, $\{a_i\} \triangleq \left\{u_{x,i} + \gamma_i u_{y,i} - \beta_i u_{z,i} + \frac{1}{2}\{d_{b,i}\}^T \left[k^{1,0}\right]\{d_{b,i}\}\right\}$,

$\{b_i\} \triangleq \left(\frac{1}{k_{33}^e} - \{d_{b,i}\}^T \left[k^{2,0}\right]\{d_{b,i}\}\right)$, $\{c_i\} \triangleq \left\{\theta_{xds} + \gamma_i \theta_{ys} + \frac{1}{2}\{d_{b,i}\}^T \left(\left[k^{0,1}\right] + \left[H_7\right]\right)\{d_{b,i}\}\right\}$

$\{r_i\} \triangleq \left\{-\frac{1}{2} y_i \theta_{xs}^2 - z_i \theta_{xs} \quad 0 \quad -\frac{1}{2} z_i \theta_{xs}^2 + y_i \theta_{xs} \quad 0\right\}^T$, $\{s_i\} \triangleq \{-y_i \theta_{xs} - z_i \quad 0 \quad -z_i \theta_{xs} + y_i \quad 0\}^T$

Equations (6.62)-(6.64) express the externally applied loads completely in terms of the displacements of the motion stage. This analytical model is valid for any number of beams, any beam spacing and arbitrary small and independent tilts at each beam for a displacement range of u_{ys}, u_{zs}, θ_{xds} within ± 0.1 and u_{zs}, θ_{ys}, θ_{zs} within ±0.01. For validation using finite elements analysis, a specific case of the n-legged table is considered with all the beam flexures perfectly vertical and placed symmetrically about the center axis on a circle of radius $p \times L$. This implies the following summations are zero.

$$\sum_i y_i = \sum_i z_i = \sum_i y_i z_i = 0 \tag{6.65}$$

Given that the diameter of the table is of the order of the length of the beam, several second order approximations can be made without any significant loss of accuracy. Also the maximum axial force in each beam $\boldsymbol{f_{x,i}}$ is restricted to half the buckling load which is $\pi^2/2$.

$$\boldsymbol{f_{ys}} \approx n\left(12 + k_{44}^e \theta_{xs}\right) u_{ys} + \frac{6}{5} \boldsymbol{f_{xs}} u_{ys} - \frac{3\theta_{xs}^2}{5} A - \frac{6\theta_{xs}}{5} B \tag{6.66}$$

$$\boldsymbol{f_{zs}} \approx n\left(12 + k_{44}^e \theta_{xs}\right) u_{zs} + \frac{6}{5} \boldsymbol{f_{xs}} u_{zs} - \frac{3\theta_{xs}^2}{5} B + \frac{6\theta_{xs}}{5} A \tag{6.67}$$

$$\boldsymbol{m_{xs}} \approx \left(nk_{44}^e + 12np^2 + \frac{6}{5} p^2 \boldsymbol{f_{xs}}\right)\theta_{xs} - \frac{6}{5}\left(u_{ys}\theta_{xs} - u_{zs}\right) A - \frac{6}{5}\left(u_{zs}\theta_{xs} + u_{ys}\right) B \tag{6.68}$$

$$\boldsymbol{f_{xs}} = \sum_i \frac{\left\{u_{x,i} + \frac{3}{5}\left(u_{y,i}^2 + u_{z,i}^2\right)\right\}}{\left(\frac{1}{700}\left(u_{y,i}^2 + u_{z,i}^2\right) + \frac{1}{k_{33}^e}\right)} \tag{6.69}$$

$$\boldsymbol{m_{ys}} \approx \left(6n + \frac{1}{10} \boldsymbol{f_{xs}}\right) u_{zs} + \left(4n + \frac{2}{15} \boldsymbol{f_{xs}} + k_{44}^e \theta_{xs}^2 \sum_i y_i^2\right)\theta_{ys} + nk_{44}^e \theta_{xs} u_{ys} + B + \frac{11\theta_{xs}}{10} A \tag{6.70}$$

$$\boldsymbol{m}_{zs}+\boldsymbol{m}_{xs}\theta_{ys}\approx-\left(6n+\frac{1}{10}\boldsymbol{f}_{xs}\right)u_{ys}+\left(4n+\frac{2}{15}\boldsymbol{f}_{xs}+k_{44}^{e}\theta_{xs}^{2}\sum_{i}z_{i}^{2}\right)\theta_{zs}+nk_{44}^{e}\theta_{xs}u_{zs}-A+\frac{11\theta_{xs}}{10}B \quad (6.71)$$

where $A\triangleq\sum_{i}\dfrac{y_{i}\left\{u_{x,i}+\frac{3}{5}\left(u_{y,i}^{2}+u_{z,i}^{2}\right)\right\}}{\left(\frac{1}{700}\left(u_{y,i}^{2}+u_{z,i}^{2}\right)+\frac{1}{k_{33}^{e}}\right)}$, $B\triangleq\sum_{i}\dfrac{z_{i}\left\{u_{x,i}+\frac{3}{5}\left(u_{y,i}^{2}+u_{z,i}^{2}\right)\right\}}{\left(\frac{1}{700}\left(u_{y,i}^{2}+u_{z,i}^{2}\right)+\frac{1}{k_{33}^{e}}\right)}$

The load-displacement equations, approximated to the second order, are given in Eqs.(6.66) - (6.71). The variables, *A* and *B*, are total moments about Z and Y axis respectively by the internal axial forces $\boldsymbol{f}_{x,i}$ for each beam. They are solved using Eqs.(6.70) and (6.71).

$$\begin{aligned}
A\approx{}&\frac{11\theta_{xs}}{10}\left[\boldsymbol{m}_{ys}-\left\{\left(6n+\frac{1}{10}\boldsymbol{f}_{xs}\right)u_{zs}+\left(4n+\frac{2}{15}\boldsymbol{f}_{xs}+k_{44}^{e}\theta_{xs}^{2}\sum_{i}z_{i}^{2}\right)\theta_{ys}+nk_{44}^{e}\theta_{xs}u_{ys}\right\}\right]\\
&-\left[\boldsymbol{m}_{zs}+\boldsymbol{m}_{xds}\theta_{ys}-\left\{-\left(6n+\frac{1}{10}\boldsymbol{f}_{xs}\right)u_{ys}+\left(4n+\frac{2}{15}\boldsymbol{f}_{xs}+k_{44}^{e}\theta_{xs}^{2}\sum_{i}y_{i}^{2}\right)\theta_{zs}+nk_{44}^{e}\theta_{xs}u_{zs}\right\}\right]\\
B\approx{}&\left[\boldsymbol{m}_{ys}-\left\{\left(6n+\frac{1}{10}\boldsymbol{f}_{xs}\right)u_{zs}+\left(4n+\frac{2}{15}\boldsymbol{f}_{xs}+k_{44}^{e}\theta_{xs}^{2}\sum_{i}z_{i}^{2}\right)\theta_{ys}+nk_{44}^{e}\theta_{xs}u_{ys}\right\}\right]\\
&+\frac{11\theta_{xs}}{10}\left[\boldsymbol{m}_{zs}+\boldsymbol{m}_{xds}\theta_{ys}-\left\{-\left(6n+\frac{1}{10}\boldsymbol{f}_{xs}\right)u_{ys}+\left(4n+\frac{2}{15}\boldsymbol{f}_{xs}+k_{44}^{e}\theta_{xs}^{2}\sum_{i}y_{i}^{2}\right)\theta_{zs}+nk_{44}^{e}\theta_{xs}u_{zs}\right\}\right]
\end{aligned} \quad (6.72)$$

Using the values of A and B, the load-displacement relations for in-plane displacement can be further simplified.

$$\boldsymbol{f}_{ys}\approx\left(12n+\frac{6}{5}\boldsymbol{f}_{xs}\right)u_{ys}-\frac{18\theta_{xs}^{2}}{25}\boldsymbol{m}_{zs}-\frac{6\theta_{xs}}{5}\boldsymbol{m}_{ys} \quad (6.73)$$

$$\boldsymbol{f}_{zs}\approx\left(12n+\frac{6}{5}\boldsymbol{f}_{xs}\right)u_{zs}+\frac{18\theta_{xs}^{2}}{25}\boldsymbol{m}_{ys}-\frac{6\theta_{xs}}{5}\boldsymbol{m}_{zs} \quad (6.74)$$

$$\begin{aligned}
\boldsymbol{m}_{xs}\approx{}&\left(nk_{44}^{e}+12np^{2}+\frac{6}{5}p^{2}\boldsymbol{f}_{xs}+\frac{3}{25}\left(\boldsymbol{m}_{ys}u_{zs}-\boldsymbol{m}_{zs}u_{ys}\right)\right)\theta_{xs}\\
&-\frac{6u_{ys}}{5}\left[\boldsymbol{m}_{ys}-\left(6n+\frac{1}{10}\boldsymbol{f}_{xs}\right)u_{zs}\right]-\frac{6u_{zs}}{5}\left[\boldsymbol{m}_{zs}+\left(6n+\frac{1}{10}\boldsymbol{f}_{xs}\right)u_{ys}\right]
\end{aligned} \quad (6.75)$$

Equations (6.73)-(6.75) capture the nonlinear stiffness variation in the in-plane displacement direction and rotation. Furthermore it also captures the coupling between in-plane translations and in-plane rotations. Given the constraint loads $\boldsymbol{f}_{xs}$, $\boldsymbol{m}_{ys}$ and $\boldsymbol{m}_{zs}$, the DoF

displacements can be found in terms of DoF loads or vice-versa. Using nonlinear finite element analysis in ANSYS, Eqs. (6.73)-(6.75) are verified in Figure 6.4.

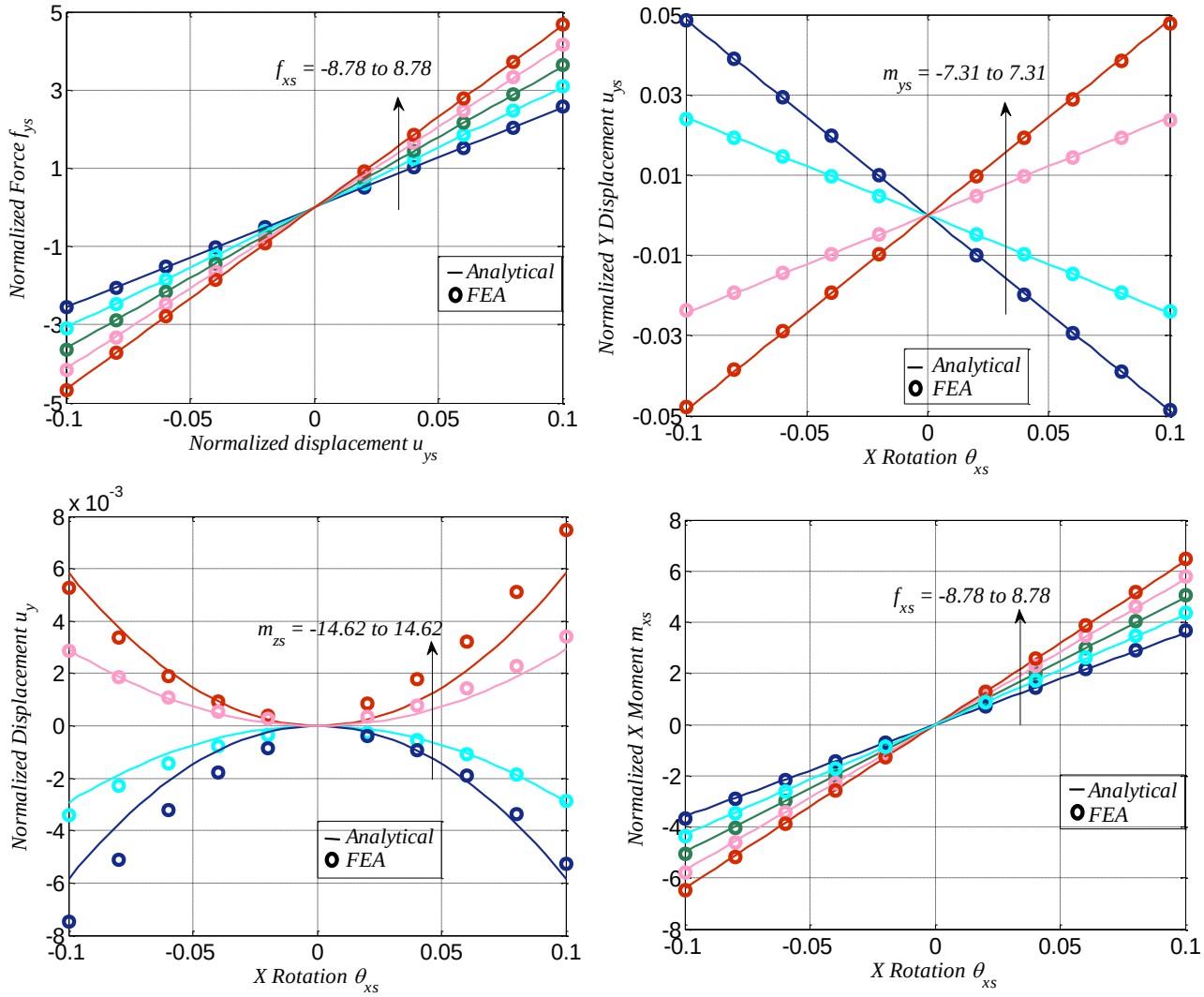

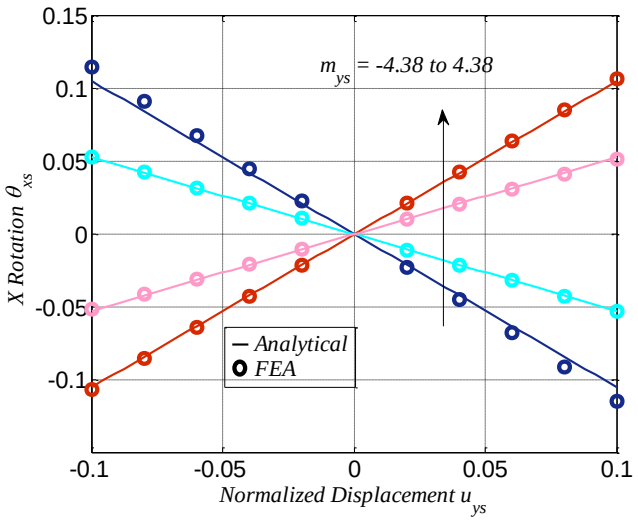

Figure 6.4:(a) Load stiffening during in-plane translation along y, (b) In-plane translation along y due to in-plane rotation in the presence of $\mathbf{m}_{ys}$*, (c) In-plane translation along y due to in-plane rotation in the presence of* $\mathbf{m}_{zs}$*,(d) Load stiffening during in-plane rotation due to x, (e) In-plane rotation due to in-plane translation along y in the presence of* $\mathbf{m}_{ys}$

With the DoF displacement are known, Eqs.(6.69)-(6.71) become three linear equations in u_{xs}, θ_{ys} and θ_{zs}, which can be solved using linear algebra.

$$\begin{Bmatrix} u_{xs}+\frac{3}{5}\left(u_{ys}^2+u_{zs}^2+p^2\theta_{xs}^2\right) \\ \theta_{ys} \\ \theta_{zs} \end{Bmatrix}$$

$$= \begin{bmatrix} N & p(C+\theta_{xs}S) & -p(S-\theta_{xs}C) \\ p\left(C+1.1\theta_{xs}S\right) & 4n+\frac{2}{15}\boldsymbol{f_{xs}}+p^2\begin{pmatrix} C2+\theta_{xs}SC+ \\ 1.1\theta_{xs}\left(SC+\theta_{xs}S2\right)\end{pmatrix} & -p^2\left(SC-\theta_{xs}C2+1.1\theta_{xs}\left(S2-\theta_{xs}SC\right)\right) \\ p\left(-S+1.1\theta_{xs}C\right) & -p^2\left(SC+\theta_{xs}S2-1.1\theta_{xs}\left(C2+\theta_{xs}SC\right)\right) & 4n+\frac{2}{15}\boldsymbol{f_{xs}}+p^2\begin{pmatrix} S2-\theta_{xs}SC \\ -1.1\theta_{xs}\left(SC-\theta_{xs}C2\right)\end{pmatrix} \end{bmatrix}^{-1}$$

$$\times \begin{Bmatrix} f_{xs}+\frac{6}{5}p\theta_{xs}\sqrt{u_{ys}^2+u_{zs}^2}D \\ m_{ys}-\left(6n+\frac{1}{10}\boldsymbol{f_{xs}}\right)u_{zs}-nk_{44}^e\theta_{xs}u_{ys}+\frac{6}{5}p\theta_{xs}\sqrt{u_{ys}^2+u_{zs}^2}E \\ m_{zs}+\left(6n+\frac{1}{10}\boldsymbol{f_{xs}}\right)u_{ys}-nk_{44}^e\theta_{xs}u_{zs}+\frac{6}{5}p\theta_{xs}\sqrt{u_{ys}^2+u_{zs}^2}F \end{Bmatrix}$$

$$N \triangleq \sum_i \frac{1}{H_i}, \quad S \triangleq \sum_i \frac{\sin(\phi_i)}{H_i}, \quad C \triangleq \sum_i \frac{\cos(\phi_i)}{H_i}, \quad SC \triangleq \sum_i \frac{\sin(\phi_i)\cos(\phi_i)}{H_i}$$

$$S2 \triangleq \sum_i \frac{\sin^2(\phi_i)}{H_i}, \quad C2 \triangleq \sum_i \frac{\cos^2(\phi_i)}{H_i}, \quad \psi_i \triangleq \tan^{-1}\left(\frac{u_{zs}}{u_{ys}}\right)+\frac{\theta_{xs}}{2}-\phi_i$$

$$D \triangleq \sum_i \frac{\cos(\psi_i)}{H_i}, \quad E \triangleq \sum_i \frac{\sin(\phi_i)\cos(\psi_i)}{H_i}, \quad F \triangleq \sum_i \frac{\cos(\phi_i)\cos(\psi_i)}{H_i}$$

$$H_i \triangleq \frac{1}{k_{33}^e}+\frac{1}{700}\left(u_{ys}^2+u_{zs}^2+p^2\theta_{xs}^2-2p\theta_{xs}\sqrt{u_{ys}^2+u_{zs}^2}\cos(\psi_i)\right)$$

(6.76)

In eq.(6.76), for simple representation, the normalized co-ordinates of any beam is taken to be $\left(p\sin(\phi_i), p\cos(\phi_i)\right)$. This follows that assumption that the beams are arranged along the circumference of a circle with normalized radius *p*. In the cases, when either in-plane rotation is zero ($\theta_{xs}=0$) or in-plane translation is zero ($u_{ys}=u_{zs}=0$), then eq.(6.76) may be simplified a great deal as the denominator H_i becomes constant while $S = C = SC = 0$.

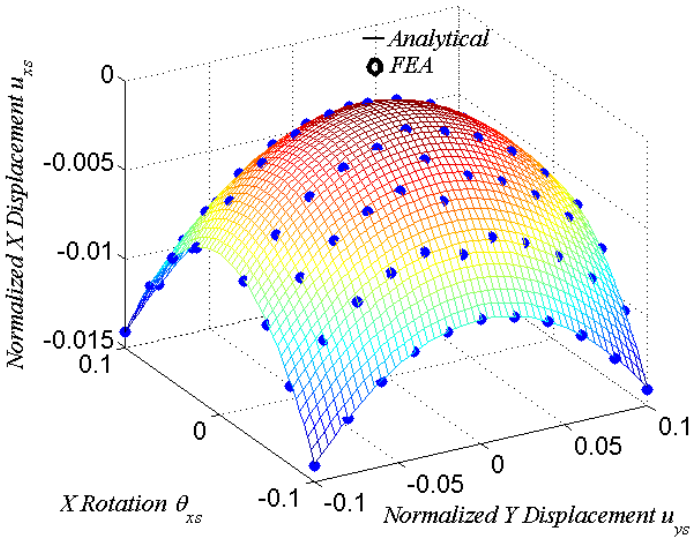

Figure 6.5: Parasitic Error motion in u_{xs} due to u_{ys} and θ_{xs}

Validation of parasitic u_{xs} motion due to in-plane translation u_{ys} and in-plane rotation θ_{xs} is shown in Figure 6.5. Clearly u_{xs} has a quadratic dependence on both in-plane translation u_{ys} and u_{zs} as well as on in-plane rotation θ_{xs}. Furthermore the stiffness in u_{xs} also drops quadratically with u_{ys}, u_{zs} and θ_{xs} due the elastokinematic effect.

6.5 Discussion

This chapter provides a generalized, closed-form and parametric mathematical model of tilted spatial beam flexure with bisymmetric cross-section, which accurately captures the constraint characteristics of the spatial beam for intermediate range of end-displacements. Several pertinent nonlinear effects such as load stiffening effect of axial force and torsional moment, kinematic effect of axial and torsional displacements, elastokinematic effect in the softening the axial and torsional stiffness and the trapeze effect were captured. Although the trapeze effect turned out to very small, in the presence of normal axial forces, it is retained for the sake of completeness.

For beams that have varying cross-sections, solving the beam governing differential equations, especially the nonlinear axial displacement and torsion equation is extremely difficult. The fundamental relations between beam characteristic coefficients were represented which showed that the load-displacement relation, constraint relations and strain energy expression are not independent. By employing these relations and a numerical computation technique similar to

Chapter 2 Section 2.4.2, the linear bending equation can be used to generate the entire BCM model for the spatial beam flexures with varying cross-section. This allows for a relatively easy route to expand the library of usable spatial beam flexures.

The ability of the generalized BCM to enable the use of energy methods, such as the principle of virtual work, was also illustrated with the case study of a multi-legged table flexure mechanism. Not only did this approach show the ability of handling any number of legs of the flexure mechanism, but also the ability of account for arbitrary and independent tilt and shape variation of the individual legs.

Chapter 7

Conclusion and Future Work

7.1 Conclusion

Flexure mechanisms, also known as compliant mechanisms, provide repeatable guided motion via elastic deformation. Its output motion is often characterized by dividing the entire motion into directions along with stiffness is relatively low and other independent directions along which stiffness is relatively high. These directions are known as degrees of freedom or DoFs and degrees of constraints or DoCs, respectively. Constraint based design recognizes the presence of DoCs and DoFs at the level of flexure elements, the building blocks of flexure mechanisms and, by arranging the flexure elements, it attempts to regenerate the DoCs and DoFs of the entire mechanisms. One of the major limitations of the constraint based design methodology is that it assumes the flexure elements to produce ideal DoCs and DoFs. Because of this assumption constraint based design is generally suitable for the synthesis of small motions. In this dissertation, this limitation is removed to analytically quantify the non-ideal constraint behavior of flexure elements. The challenge of modeling constraint characteristics for large displacements is overcome by recognizing properties of beam geometries rather than restricting them. Additionally, provision for characterizing common geometric effects and using energy methods are provided. A more details discussion on each of the analyzed flexure element is given below.

7.1.1 Planar Beams

Planar beams are a commonly used flexure element for planar mechanisms that has several applications in macro-scale and MEMS devices. Although it has been analyzed several

times in literature, a strain energy expression in terms of end-displacement that is accurate over intermediate displacements is not present. Such an expression will be useful for analyzing complex flexure mechanisms using energy methods. In this dissertation, a generalized Planar Beam Constant Model (PBCM) for the planar flexure strip with generalized shape is formulated that provides a strain energy expression along with end load-displacement characteristics in term of end-displacements. This lumped parameter model allows the flexure elements to be represented via a lumped stiffness and geometric parameters. It is illustrated how misalignment of flexure elements with the global co-ordinate axes can be easily tackled using the derived strain energy expression.

Furthermore fundamental relations within the beam characteristic coefficients of the PBCM are determined. These relations showed that even for varying thickness, the basic behavior of planar flexure strips does not change. In other words, the nature of relationship (linear, quadratic etc.) of the end-displacements with the end-loads remains the same while the proportionality constants given the beam characteristic coefficient change. The main utility of these relations is in expanding the library of available flexure elements that can be used in designing flexure mechanisms by generating models with same capabilities without dealing with most the complexity associated with varying cross-section.

7.1.2 Flexure Strip with Spatial Loading

Several examples of flexure mechanism exist where flexure strip are used in such a manner that planar analysis to determine the motion characteristics is insufficient. Since, under spatial loading, stresses are significant in more than one direction, beam theory is generally unsuited for these analyses. Therefore, plate theory is used for the analysis of the flexure strips. However, obtaining closed form models using nonlinear plate theory is difficult and often computational methods like finite element analysis are used. The beam characteristic differential equations that will lead to a closed-form model which can not only take generalized loading into consideration but also be accurate over intermediate displacements of about 10% of the length of the flexure strip is given in this dissertation.

The key assumption of this analysis is the estimation of the transverse stress along the width of the flexure strip which leads to the anticlastic curvature. This stress is estimated to be proportional to the stress along the neutral axis of the beam. The constant of proportionality is

determined as a function of the width and the length of the beam. Another key challenge was to overcome the analytical complexity brought about by torsion. When the ends of a flexure strip are kept straight, the torsional stiffness varies nonlinearly due to the Wagner's effect. Normally, this nonlinearity cannot be dropped. However when the geometry of the flexure strip has an aspect ratio of $Width^2/(Length \times Thickness)$ less than 15, this nonlinearity in torsion becomes negligible. Further simplification was done by recognizing that the kinematic arc-length conservation is insignificant in the plane of the flexure strip when the width of the flexure strip is at least 10 times the thickness. Dropping the associated kinematic nonlinear effects, a set of four solvable differential equations can be found. Three of the four governing differential equations are linear with varying coefficients and are potentially solvable, while the last nonlinear equation which determines the axial displacement, can be solved using the solutions of the first three differential equations.

7.1.3 Symmetric Spatial Beam Flexure

The third flexure element that was analyzed was the symmetric spatial beam flexure. This element, also known as the wire flexure, is also an extensively used flexure element. Although the nonlinear mechanics in the case of wire flexure is complex, it was identified that a closed-form model can be obtained if the area moments of inertia associated with bending in two mutually perpendicular planes are equal. By choosing the co-ordinate such that this condition is satisfied, closed form model of wire flexure that captures all the pertinent nonlinearities for a intermediate range of displacements.

The key nonlinearities that was captured were 1) The kinematic coupling between the bending planes in the presence of torsional moment 2) The variation of axial, transverse and torsional stiffness due to bending displacements 3) The kinematic axial displacement and torsional rotation caused by the bending displacement 4) A elastic stiffening of the torsional direction in the presence of axial tension forces.

Similar to the models for planar loading of flexure strips, the Spatial Beam Constraint Model (SBCM) for wire flexure is generalized in terms of both loads and displacements. It is also capable of handling small tilts with the global co-ordinate frame due to manufacturing defects without using co-ordinate transformations. Furthermore, fundamental relations between

the beam characteristic coefficients of the SBCM are also derived. These relations show a similar pattern to those derived for the flexure strips with planar loading. As in the case of flexure strip, the fundamental relations between the beam characteristic coefficients ensure the easy addition of various wire flexures with varying cross-sections to the library of flexure elements for the analysis of flexure mechanisms.

7.2 Future work

Although the differential equations of flexure strip with spatial loading are linear, solving them is challenging due to the presence of varying coefficients,. While a numerical solution, using standard mathematical software such as Matlab, can easily predict the constraint characteristics of a flexure strip, a closed-form model will be useful in quantifying design insights. Although a simple application of perturbation methods does not yield a closed form solution, more sophisticated application of perturbation methods like homotopy perturbation method may be tried out to obtain a solution to the given set of differential equations.

Using the derived models of various flexure elements, the next logical step is to refine the constraint based synthesis approach of flexure mechanisms. Given the accuracy of the BCM over finite displacement, a nonlinear constraint based synthesis that can generate mechanisms for producing finite motion paths should be the next step.

The closed-form representation of the BCM can also be leveraged in formulating optimization routines for flexure elements. Increasing number of flexure elements can add robustness against failure. Given, the availability of the strain energy expression, analyzing multiple flexure elements is no longer computationally challenging and can be easily done in closed-form. Hence, the number of flexure elements to be used and determining the optimal spacing between them can be easily computed by standard optimization techniques.

The BCM can also give valuable insight into the nonlinear dynamics of flexure mechanisms of the first resonant frequency. In several mechanisms, used in positioning devices, the first resonant frequency change with large displacements. Analysis using BCM can give insight into the nonlinear variation of the stiffness values in different displacement directions. Although, BCM does not give any insight into the higher frequency dynamics of flexure mechanics, the insights that are available can be used as a starting point for understanding the dynamics of a complex flexure mechanism.

REFERENCES

[1] G. Dai, F. Pohlenz, H.-U. Danzebrink, M. Xu, K. Hasche, and G. Wilkening, 2004, "Metrological large range scanning probe microscope," *Metrological large range scanning probe microscope,* vol. 75, pp. 962-969.

[2] A. Sinno, P. Ruaux, L. Chassagne, S. Topcu, and Y. Alayli, 2007, "Enlarged Atomic Force Microscopy Scanning Scope: Novel Sample-holder Device with Millimeter Range," *Review of Scientific Instruments,* vol. 78, pp. 1-7.

[3] A. Weckenmann and J. Hoffmann, 2007, "Long Range 3D Scanning Tunnelling Microscopy," *CIRP Annals - Manufacturing Technology,* vol. 56, pp. 525-528.

[4] X. Zhang, F. S. Chau, C. Quan, Y. L. Lam, and A. Q. Liu, 2001, "A study of the static characteristics of a torsional micromirror," *Sensors and Actuators A,* vol. 90, pp. 73-81.

[5] V. Jaecklin, C. Linder, N. D. Rooij, and J. M. Moret, 1993, "Comb actuators for xy-microstages," *Sensors & Actuators: A. Physical,* vol. 39, pp. 83-89.

[6] N. Sarkar, A. Geisberger, Matthew, and D. Ellis, "Fully Released MEMS XYZ Flexure Stage with Integrated Capacitive Feedback," United States Patent, 2004.

[7] M. V. D. Moosdijk, E. V. D. Brink, K. Simon, A. Friz, G. Phillipps, R. Travers, and E. Raaymakers, 2002, "Collinearity and stitching performance on an ASML stepper," in *Society of Photographic Instrumentation Engineers,* Santa Clara, CA, 4688, pp. 858-866.

[8] L. Hongzhong, L. Bingheng, D. Yucheng, T. Yiping, and L. Dichen, 2003, "A motor-piezo actuator for nano-scale positioning based on dual servo loop and nonlinearity compensation," *Journal of Micromechanics and Microengineering,* vol. 13, pp. 295-299.

[9] C. A. Mirkin, 2001, "Dip-Pen Nanolithography: Automated Fabrication of Custom Multicomponent, Sub-100-Nanometer Surface Architectures," *MRS Bulletin,* vol. 26, pp. 535-538.

[10] K. Salaita, Y. H. Wang, and C. A. Mirkin, 2007, "Applications of Dip-Pen Nanolithography," *Nature Nanotechnology,* vol. 2, pp. 145-155.

[11] G.-y. Liu and S. Xu. (1999). *Nanometer Scale Fabrication of Self-Assembled Monolayers: Nanoshaving and Nanografting*.

[12] J. A. Kramar, 2005, "Nanometre Resolution Metrology with the Molecular Measuring Machine," *Nanometre Resolution Metrology with the Molecular Measuring Machine*, vol. 16, pp. 2121-2128.

[13] A. Sebastian, A. Pantazi, H. Pozidis, and E. Eleftheriou, 2008, "Nanopositioning for probe-based data storage [Applications of Control]," *IEEE Control Systems Magazine*, vol. 28, pp. 26-35.

[14] E. Pernette, S. Henein, I. Magnani, and R. Clavel, 1997, "Design of parallel robots in microrobotics," *Cambridge Journals,* vol. 15, pp. 417-420.

[15] H.-H. Pham, H.-C. Yeh, and I.-M. Chen, 2006, "Micromanipulation System Design Based on Selective Actuation Mechanisms," *The International Journal of Robotics Research,* vol. 25, pp. 171-186.

[16] A. Eisinberg, A. Menciassi, S. Micera, D. Campolo, M. C. Carrozza, and P. Dario, 2001, "PI force control of a microgripper for assembling biomedical microdevices," *IEE Proceedings -Circuits Devices System,* vol. 148, pp. 348-352.
[17] P. H. Hoang and V. D. T. Thang, "Design and simulation of flexure-based planar force/torque sensor," presented at the Conference on Robotics, Automation and Mechatronics, 2010.
[18] S. E. Alper, K. M. Silay, and T. Atkin, 2006, "A low-cost rate-grade nickel microgyroscope," *Sensors and Actuators A,* vol. 132, pp. 171-181.
[19] H. Liu and W. S. a. F.-t. Zhang, 2011, "A resonant accelerometer based on electrostatic stiffness and its closed-loop control method," *Sensor Review,* vol. 31, pp. 58-64.
[20] Y.-M. Moon, 2006, "Bio-mimetic design of finger mechanism with contact aided compliant mechanism," *Mechanism and Machine Theory,* vol. 42, pp. 600-611.
[21] J. M. Huang, A. Q. Liu, Z. L. Deng, Q. X. Z. J. Ahn, and A. Asundi, 2004, "An approach to the coupling effect between torsion and bending for electrostatic torsional micromirrors," *Sensors and Actuators A,* vol. 115, pp. 159-166.
[22] D.-M. Sun, W. Dong, C.-X. Liu, W.-Y. Chen, and M. Kraft, 2007, "Analysis of the dynamic behavior of a torsional micro-mirror," *Microsystem Technology,* vol. 13, pp. 61-70.
[23] R. Andosca, G. McDonald, V. Genova, S. Rosenberg, J. Keating, C. Benedixen, and J. Wu, 2012, "Experimental and theoretical studies on MEMS piezoelectric vibrational energy harvesters with mass loading," *Sensors & Actuators: A,* vol. 178, pp. 76-87.
[24] S. Awtar, 2004, "Analysis and Synthesis of Planer Kinematic XY Mechanisms," Sc. D., Massachusetts Institute of Technology, Cambridge, MA.
[25] S. Timoshenko and J. N. Goodier, 1969, *Theory of Elastisity*. New York, NY: McGraw-Hill.
[26] C. Truesdell, W. Noll, and S. Antman, 2004, *The Non-Linear Field Theories of Mechanics,* 3 ed.: Springer.
[27] A. E. H. Love, 1892, *A Treatise on the Mathematical Theory of Elasticity*: C. J. Clay and Sons, Cambridge University Press.
[28] L. S. Srinath, 1982, *Advance Mechanics of Solids*. India: Tata McGraw Hill.
[29] S. H. Crandall, N. C. Dahl, and T. J. Lardner, 1972, *An Introduction to the Mechanics of Solids*. New York, NY: McGraw-Hill Book Company.
[30] S. Awtar, A. H. Slocum, and E. Sevincer, 2006, "Characteristics of Beam-based Flexure Modules," *Journal of Mechanical Design,* vol. 129, pp. 625-639.
[31] S. Awtar, S. Sood, and M. Olfatnia, 2012, "A large-stroke electrostatic comb-drive actuator based on a novel flexure mechanism," in *IDETC*, Chicago.
[32] S. Timoshenko. (1921) On the correction factor for shear of the differential equation for transverse vibrations of bars of uniform cross-section. *Philosophical Magazine*. 744.
[33] S. Awtar and S. Sen, 2010, "A Generalized Constraint Model for Two-dimensional Beam Flexures: Non-linear Load-Displacement Formulation," *ASME Journal of Mechanical Design,* vol. 132, pp. 0810091-08100911.
[34] ANSYS, "Theory Reference."
[35] D. H. Hodges, 1984, "Proper Definition of Curvature in Nonlinear Beam Kinematics," *AIAA Journal,* vol. 22, pp. 1825-1827.

[36] M. R. M. C. DaSilva, 1988, "Non-Linear Flexural-flexural-torsional-Extensional Dynamics of Beams-I. Formulation," *International Journal of Solid Structures*, vol. 24, pp. 1225-1234.
[37] T. R. Tauchert, 1974, *Energy Principles in Structural Mechanics*. New York, NY: McGraw-Hill.
[38] S. Awtar, K. Shimotsu, and S. Sen, 2010, " Elastic Averaging in Flexure Mechanisms: A Three-Beam Parallelogram Flexure Case Study," *ASME Journal of Mechanisms and Robotics*, vol. 2,
[39] I. Todhunter and K. Pearson, 1886, *A History of the Theory of Elasticity and of the Strength of Materials: Galilei to Saint-Venant*: Univerisity Press.
[40] R. Hooke, 1678, *Lectures De Potentia Restitutiva*: John Martyn Printer.
[41] E. Mariotte, 1686, *Traité du mouvement des eaux*.
[42] D. Bernoulli, ed, 1742.
[43] L. Euler, 1744, *Methodus inveniendi lineas curvas maximi minimive proprietate gaudentes*. Lausanne.
[44] J. Bernoulli, 1744, *Veritable Hypothése de la Résistance des Solides, avec la demonstration de la courbure des qui font resort, Bernoulli's collected works* vol. II. Geneva.
[45] C. A. D. Coulomb, 1776, "Essai sur une application des règles de Maximis et Minimis à quelques Problèmes de Statique, relatifs à l'Architecture," *Mém…par divers savans,* pp. 350-354.
[46] J. Murray, 1855, *Miscellaneous works of the late Thomas Young*: W. Clowes and Sons.
[47] B. A. L. Cauchy. (1827) De la pression ou tension dans un corps solide *Exercices de Mathématiques*.
[48] B. A. L. Cauchy. (1827) Sur la condensation et la dilatation des corps solides. *Exercices de Mathématiques*.
[49] B. A. L. Cauchy. (1828) Sur quelques theorems relatifs à la condensation ou à dilatation des corps. *Exercices de Mathématiques*.
[50] G. Lame, 1833, "Mémoir sue l'équilibre intérieur des corps solides homogènes," *Mém…par divers savans,*
[51] G. Green, "On the Laws of Reflexion and Refraction of Light at the common surface of two non-crystallized media," presented at the Camb. Phil. Soc, 1837.
[52] S. Venant, 1837-38, "Lecons de Mécanique appliquée," *Comptes rendus*, vol. 24,
[53] S. Venant, 1847, "Mémoir sue l'équilibre intérieur des corps solides," *Comptes rendus*, vol. 24,
[54] C. Truesdell, Ed., *Continuum Mechanics* (International science review series. Gordon and Breach, 1965, p.^pp. Pages.
[55] K. E. Bisshop and D. C. Drucker, 1945, "Large deflections of cantilever beams," *Quarterly of Applied Mathematics*, pp. 272-275.
[56] L. Howell, 2002, *Compliant Mechanisms*. New York: John Wiley & Sons, Inc.
[57] I. A. Ramirez and C. Lusk, 2011, "Spatial-beam large-deflection equations and pseudo-rigid body model for axisymmetric cantilever beams," in *Proc. IDETC/CIE 2011*, Washington D. C., Paper # 47389.
[58] A. N. Krylov, 1931, *Calculation of Beams on Elastic Foundation*. St. Petersburg: Russian Academy of Sciences.

[59] B. Popescu and D. H. Hodges, 1999, "Asymptotic treatment of the trapeze effect in Þnite element cross-sectional analysis of composite beams," *International Journal of Non-Linear Mechanics,* vol. 34, pp. 709-721.
[60] G. Hao, X. Kong, and R. L. Reuben, 2011, "A nonlinear analysis of spatial compliant parallel modules: Multi-beam modules," *Mechanism and Machine Theory,* vol. 46, pp. 680-706.
[61] D. H. Hodges and E. H. Dowell, 1974, "Nonlinear equations of motion for the elastic bending and torsion of twisted non-uniform rotor blades," *NASA Technical Note D-7818,* pp. D-7818.
[62] D. K. Blanding, 1999, *Exact Constraint: Machine Design Using Kinematic Principles*. New York, NY: ASME Press.
[63] S. T. Smith, 2000, *Flexures: Elements of Elastic Mechanisms*. New York, NY: Gordon and Breach Science Publishers.
[64] J. S. Przemieniecki, 1968, *Theory of Matrix Structural Analysis*. New York: McGraw-Hill.
[65] J. Mayo and J. Dominguez, 1992, "Geometrically Nonlinear Coupling between Axial and Flexural Modes of Deformation of Multibody Systems," in *Winter Annual Meeting of ASME,* Anaheim, CA, pp. 95-103.
[66] W. A. Bonin, "Microactuator Suspension with Multiple Narrow Beams," US Patent, 2001.
[67] B. Trease, Y. Moon, and S. Kota, 2005, " Design Of Large-Displacement Compliant Joints," *ASME Transactions, Journal of Mechanical Design,* vol. 127,
[68] S. Awtar., T. T. Trutna, J. M. Nielsen, R. Abani, and J. D. Geiger, 2010, "FlexDex: A Minimally Invasive Surgical Tool with Enhanced Dexterity and Intuitive Actuation," *ASME Journal of Medical Devices,* vol. 4,
[69] S. Awtar and S. Alexander H, 2007, "Constraint-based design of parallel kinematic XY flexure mechanisms," *ASME Journal of Mechanical Design,* vol. 129, pp. 816-830.
[70] S. Awtar, J. Ustick, and S. Sen, 2011, "An XYZ Parallel Kinematic Flexure Mechanism with Geometrically Decoupled Degrees of Freedom," in *IDETC/CIE,* Washington D.C., p. Paper No. 47713.
[71] N. S. Trahair, "Wagner's beam cycle," presented at the Structural Stability Research Council Annual Stability Conference, 2011.
[72] E. Reissner, 1957, "Finite Twisting and Bending of Thin Rectangular Elastic Plates," *The Journal of Applied Mechanics,* vol. 24, pp. 391-396.
[73] D. M. Brouwer, J. P. Meijaard, and J. B. Jonker, 2013, "Large deflection stiffness analysis of parallel prismatic leaf-spring flexures," *Precision Engineering,* vol. Accepted,
[74] D. G. Ashwell, 1950, "Anticlastic Curvature of Rectangular Beams and Plates," *Journal of Royal Aeronautical Society,* vol. 54, p. 708.
[75] I. H. Shames and C. L. Dym, 1985, *Energy and finite element methods in structural mechanics*. New York, NY: Taylor and Francis.
[76] N. S. Trahair, Ed., *Flexural-Torsional Buckling of Structures*. Boca Raton, Florida: CRC Press, 1993, p.^pp. Pages.
[77] J.-H. He, 2003, "Homotopy perturbation method: a new nonlinear analytical technique," *Applied Mathematics and Computation,* vol. 135, pp. 73-79.
[78] K. J. Freitag, 2007, "Neural Network and Differential Equations," Masters, Department of Mathematics, San Jose State University, San Jose.

[79] K. S. Chen, D. L. Trumper, and S. T. Smith, 2002, "Design and control for an electromagnetically driven X–Y–θ stage," *Precision Engineering,* vol. 26, pp. 355-369.
[80] H. D. Samuel and N. S. Sergio, "Compliant assembly system," US Patent, 1979.
[81] X. L. Ding and J. S. Dai, 2006, "Characteristic Equation-Based Dynamics Analysis of Vibratory Bowl Feeders with Three Spatial Compliant Legs," *IEEE Transactions on Robotics and Automation,* vol. 5, pp. 164-175.
[82] H. J. Su and H. Tari, 2010, "Realizing orthogonal motions with wire flexures connected in parallel," *ASME Journal of Mechanism Design,* vol. 132, p. 121002.
[83] I. S. Sokolnikoff, 1956, *Mathematical Theory of Elasticity*: McGraw-Hill, NY.
[84] R. Frisch-Fay, 1962, *Flexible Bars*. London: Butterworth & Co. Ltd.
[85] E. Dokumaci, 1987, "An Exact Solution for Coupled Bending and Torsion Vibrations of Uniform Beams having a Single Cross-Sectional Symmetry," *Journal of Sound and Vibration,* vol. 131, pp. 443-449.
[86] K. V. Avramov, C. Pierre, and N. Shyriaieva, 2007, "Flexural-flexural-torsional Nonlinear Vibrations of Pretwisted Rotating Beams with Asymmetric Cross-sections," *Journal of Vibration and Control,* vol. 13, pp. 329-364.